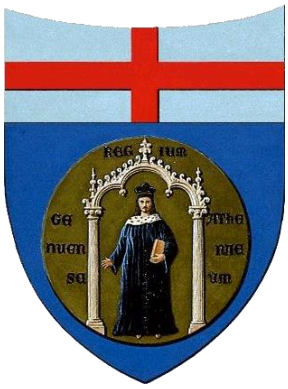

UNIVERSITA' DEGLI STUDI DI GENOVA

Scuola di Scienze Matematiche Fisiche Naturali

Dipartimento di Scienze della Terra, dell'Ambiente e della Vita (DISTAV)

XXXII Course of sciences and technologies for the environment and the territory (STAT)

Curriculum: Biology applied to agriculture and the environment (code 6206)

Evaluation of the effects of natural and synthetic compounds on lipid accumulation and inflammation in hepatocytes, endotheliocytes and adipocytes.

Dott.ssa Francesca Baldini

Supervisor: Prof. Laura Vergani and Prof. Adriana Voci

List of abbreviations

Ac	Cell contact area
ADRP	Adipose differentiation related protein
AOX	Peroxisomes by acyl-CoA oxidase
APE1	Apurinic/apyrimidinic (AP) endonuclease 1
AQP9	Aquaporin 9
ATG7	Autophagy related protein 7
BCA	Bicinchoninic acid
BSA	Bovine albumin serum
CAT	Catalase
COX	Cytochrome c oxidase
CPT-1	Carnitine palmitoyltransferase 1
Cr	Radius of curvature
CS	Citrate Synthase
CVDs	Cardiovascular diseases
CYP2E1	Cytochrome P450 2E1
DAPI	4',6-diamidino-2-phenylindole
DCF	Dichlorofluorescein
DCF-DA	Dichlorofluorescein diacetate
DEX	Dexamethasone
DFIT	Direct fit
DMEM	Dulbecco's modified Eagle medium
DMSO	Dimethyl sulfoxide
DNL	*De novo* hepatic lipogenesis
DTT	Dithiothreitol
ECACC	European Collection of Authenticated Cell Cultures
EDTA	Ethylenediaminetetraacetic acid
eNOS	Endothelial NO synthase
ER	Endoplasmic reticulum
ETS	Electron Transport System
FA	free fatty acids
FAME	Fatty acid methyl ester
FAS	Fatty acid synthase
FBS	Foetal Bovine Serum

FCCP	Cyanide-4-(trifluoromethoxy)phenylhydrazone
FDA	Food and Drug Administration
FIEL	Force Integration to Equal Limits
FITC	Fluorescein- isothiocyanate
Fru	Fructose
GAPDH	Glyceraldehyde 3-phosphate dehydrogenase
GSH	Glutathione
H2O2	Hydrogen peroxide
Hc	Cell height
HCC	Hepatocellular carcinoma
HECV	Human endothelial cell line
HSP60	Heat shock protein 60
IBMX	3-isobuthyl-1-methylxanthine
ICAM	Intercellular adhesion molecule
IKBip	Inhibitor of nuclear factor kappa-B kinase-interacting protein
IL1	Interleukin 1
IL-1b	Interleukin-1b
IL6	Interleukin 6
LA	Linoleic acid
LC3	Microtubule-associated proteins 1A/1B light chain 3B
LCFA	Long chain fatty acids
LDLR	Low-density lipoprotein receptor
LDs	lipid droplets
MA	Myristic acid
MDA	Malondialdehyde
miRNAs	MicroRNAs
mTOR	Mammalian target of rapamycin
MTs	Metallothioneins
MTT	3-(4,5-dimethylthiazol-2-yl)-2,5-diphenyltetrazolium bromide
MUFAs	Monounsaturated fatty acids
MULV	RevertAid H Minus Reverse Trancriptase
NAFL	Non-alcoholic fatty liver
NAFLD	Non-alcoholic fatty liver disease
$NaNO_2$	Sodium nitrite
NASH	Non-alcoholic steatohepatitis
NEFAs	Non-esterified fatty acids

NF-κB	Nuclear factor kappa-B
NO	Nitric oxide
NR	Nile Red
O2K	Oxygraph 2 k
OA	Oleic acid
ORO	Oil-RedO
PA	Palmitic acid
PBS	Phosphate buffer saline
PCSK9	Proprotein convertase subtilisin/kexin type 9
PMSF	Phenylmethanesulfonyl fluoride
PMSF	Phenylmethylsulfonyl fluoride
POLG	DNA polymerase subunit gamma
PPARs	Peroxisome proliferator-activated receptors
qPCR	Quantitative real time PCR
QPM	Quantitative Phase Microscopy
Rc	Cell roughness
ROD	Relative Optical Density
ROS	Reactive oxygen species
SA	Stearic acid
SAMe	S-adenosylmethionine
SCD1	Stearoyl-CoA desaturase
SCFS	Single Cell Force Spectroscopy
SD	Standard deviation
SDS-PAGE	Sodium dodecyl sulfate polyacrylamide gel electrophoresis
Se	Surface extension
SFA	Saturated fatty acid
SH	Steatohepatitis
Sil	Silybin
SREBP-1c	Sterol regulatory element- binding protein-1c
SS	Simple steatosis
T2DM	Type 2 diabetes
TBA	Thiobarbituric acid
TBARS	Thiobarbituric acid reactive substances
TG	Triglycerides
TMRE	Tetramethylrhodamine ethyl ester

TNFα	Tumor necrosis factor
UCP2	Uncoupling protein 2
UFA	Unsaturated fatty acid
ULK1	UNC51-like kinase 1
VLCAD	Very long-chain acyl- CoA dehydrogenase
VLDL	Very low-density lipoproteins
WAT	White Adipose Tissue
WHO	World Health Organization

List of figures

1.Riassunto della tesi

L'obesità è una condizione caratterizzata da un eccessivo accumulo di grasso corporeo, soprattutto a livello viscerale, che determina gravi danni alla salute. L'obesità è causata, nella maggior parte dei casi, da stili di vita scorretti (da una parte, un'alimentazione ipercalorica, e dall'altra, ridotta o nulla attività fisica). Dal punto di vista eziologico l'obesità è una patologia multifattoriale associata a diverse condizioni patologiche quali insulino-resistenza, diabete mellito di tipo 2, ipertensione, aterosclerosi e steatosi epatica da cause non alcolica (NAFLD). L'obesità è, attualmente, uno dei più importanti problemi di salute pubblica nel mondo, giacché la sua prevalenza è in costante aumento. L'obesità rappresenta, pertanto, una delle principali sfide nel campo della ricerca che, da un lato, studia i meccanismi cellulari/tissutali coinvolti nello sviluppo e nella progressione della patologia a livello dei diversi organi, dall'altro, cerca di identificare composti naturali e sintetici per il trattamento di questa condizione, da associare alla dieta e ad una adeguata attività fisica.

La presente Tesi di Dottorato si inserisce in tale contesto, proponendosi di studiare, dapprima i meccanismi molecolari associati ad un eccessivo accumulo di grasso in diversi tipi cellulari rappresentativi dei tessuti coinvolti nell'obesità, successivamente di identificare e studiare composti naturali (di origine vegetale o comunque endogeni) che possano esercitare effetti benefici sui modelli cellulari messi a punto. A tale scopo si sono sviluppati e utilizzati i seguenti modelli cellulari di NAFLD, ipertrofia del tessuto adiposo (obesità) e disfunzione endoteliale (aterosclerosi):

- Un modello *in vitro* di NAFLD che consiste di cellule di epatoma di ratto trattate con diversi agenti steatogeni in modo da mimare *in vitro* gli step che accompagnano la progressione della NAFLD *in vivo* da semplice steatosi a steatoepatite.
- Un modello *in vitro* di aterosclerosi che consiste di cellule endoteliali vascolari umane esposte ad una miscela di acidi grassi.
- Un modello *in vitro* di ipertrofia adipocitaria, rappresentato da pre-adipociti di topo trattati con una miscela di sostanza adipogeniche e, successivamente con acidi grassi a catena lunga per indurre un quadro di ipertrofia *in vitro*.

Partendo dai diversi modelli cellulari sopra citati, l'attività di ricerca si è concentrata sullo studio

dei possibili effetti benefici di diversi composti:

- La silibina, molecola di origine naturale che rappresenta il principale componente della silimarina, un estratto del cardo mariano (*Silybum marianum).* Partendo da precedenti studi, sia clinici che su animali, che suggerivano un potenziale effetto benefico della silibina a livello epatico, questa tesi ha indagato gli effetti ed i meccanismi molecolari del trattamento con silibina nel modello *in vitro* di NAFLD.
- La S-Adenosilmetionina (SAMe), una molecola endogena che agisce come principale donatore di gruppi metile a livello cellulare. Precedenti studi avevano osservato che bassi livelli epatici di SAMe sono correlati a condizioni patologiche a carico del fegato. In questa tesi si è andati a valutare se e con quali meccanismi molecolari il SAMe potesse migliorare una condizione di steatosi epatica e di disfunzione endoteliale utilizzando i due modelli *in vitro*.

I risultati hanno dimostrato: *(i)* che i tre sistemi cellulari *in vitro* messi a punto rappresentano un buon modello delle diverse condizioni fisio-patologiche di interesse, ovvero steatosi epatica (NAFLD), disfunzione endoteliale (aterosclerosi) ed ipertrofia adipocitaria (obesità); *(ii)* che sia la silibina che il SAMe hanno significative proprietà benefiche. In particolare entrambi i composti hanno dimostrato un effetto anti-steatosico ed antiossidante nel modello *in vitro* di steatosi epatica. Il SAMe ha mostrato anche una significativa attività antiossidante e citoprotettiva su cellule endoteliali disfunzionali.

In conclusione, possiamo affermare che i tre modelli messi a punto ed utilizzati in questa tesi rappresentano un buon modello sperimentale *in vitro* per lo studio dei meccanismi molecolari e biochimici coinvolti in condizioni patologiche complesse e che possono essere efficacemente impiegati per lo studio di possibili composti naturali da usare come nutraceutici.

2.Summary of the thesis

Obesity is a condition characterized by an excessive accumulation of body fat, especially at the visceral level, which causes serious damage to health. Obesity is caused, in most cases, by unhealthy lifestyles (on the one hand, a high-calorie diet, and on the other, reduced or no physical activity). From an etiological point of view obesity is a multifactorial disease associated with various pathological conditions such as insulin resistance, type 2 diabetes mellitus, hypertension, atherosclerosis and non-alcoholic liver steatosis (NAFLD).

Obesity is currently one of the most important public health problems in the world, as its prevalence is constantly increasing. Obesity therefore represents one of the main challenges in the field of research which, on one side, studies the cellular/tissutal mechanisms involved in the development and progression of the disease at the level of the different organs and, on the other side, tries to identify natural and synthetic compounds for the treatment of this condition, to be associated with diet and adequate physical activity.

This PhD thesis is part of this context, with the aim of studying, first, the molecular mechanisms associated with excessive fat accumulation in different cell types representative of the tissues involved in obesity, then to identify and study natural compounds (of plant origin or otherwise endogenous) that may have beneficial effects on the cellular models developed.

For this purpose, the following cellular models of NAFLD, adipose tissue hypertrophy (obesity) and endothelial dysfunction (atherosclerosis) have been developed and used:

- An in vitro model of NAFLD consisting of rat hepatoma cells treated with different steatogenic agents in order to mimic *in vitro* the steps of the progression of NAFLD *in vivo* from simple steatosis to steatohepatitis.
- An *in vitro* model of atherosclerosis, consisting of human umbilical vein endothelial cells exposed to a mixture of fatty acids.
- An *in vitro* model of adipocytic hypertrophy, represented by mouse pre-adipocytes treated with a mixture of adipogenic substances and then with long chain fatty acids to induce a picture of hypertrophy *in vitro*.

Starting from the different cellular models mentioned above, the research activity has been focused on the study of the possible beneficial effects of different compounds:

- Silybin, a natural molecule, that represents the main component of silymarin, an extract from *Silybum marianum*. Starting from previous studies, both clinical and animal, which suggested a potential beneficial effect of silybin on the liver, this thesis investigated the effects and molecular mechanisms of this molecule treatment in the in vitro model of NAFLD.
- S-Adenosylmethionine (SAMe), an endogenous molecule that acts as the main donor of methyl groups at the cellular level. Previous studies had observed that low levels of SAMe in the liver are related to pathological organ conditions. In this thesis it was evaluated whether and by what molecular mechanisms SAMe could improve a condition of liver steatosis and endothelial dysfunction using the two *in vitro* models.

The results have shown that: *(i)* the three *in vitro* cellular systems developed duing this thesis work represent a good model of the different physio-pathological conditions of interest, liver steatosis (NAFLD), endothelial dysfunction (atherosclerosis) and adipocytic hypertrophy (obesity); (ii) both silybin and SAMe have significant beneficial properties. In particular, both compounds have demonstrated an anti-steatotic and antioxidant effect in the *in vitro* model of liver steatosis. SAMe also showed significant antioxidant and cytoprotective activity on dysfunctional endothelial cells.

In conclusion, we can say that the three models developed and used in this thesis represent a good *in vitro* experimental model for the study of molecular and biochemical mechanisms involved in complex pathological conditions and that they can be effectively used for the study of possible natural compounds to be used as nutraceuticals.

3.Aim of the study

Nowadays, obesity represents one of the main global health problems and the prevalence of this condition is continuously increasing in industrialized societies and also in developing countries. The present thesis is aimed at studying the molecular mechanisms associated with an excessive accumulation of fat in different cell types representative of the main tissues involved in obesity, and then to identify and study natural compounds (of plant origin or otherwise endogenous) that may have beneficial effects on the cellular models developed and that could be employed as nutraceuticals.

Our interest has been focused, in particular, on liver, vascular endothelium and adipose tissue, as these tissues/organs cooperate in onset and progression of obesity and obesity-related disorders. For this aim, I developed and employed different cellular models mimicking *in vitro* hepatosteatosis (NAFLD), endothelial dysfunction (atherosclerosis) and adipocyte hypertrophy (obesity). The *in vitro* model of NAFLD consists of rat hepatoma cells treated with different steatogenic agents to mimic *in vitro* the progression of NAFLD from simple steatosis to steatohepatitis. A human umbilical vein endothelial cell line exposed to a mixture of fatty acids has been used to mimic *in vitro* atherosclerosis. A mouse pre-adipocyte cell line treated with an adipogenic mixture and with long chain fatty acids represent the model of hypertrophy *in vitro*.

Starting from these well consolidated cell models, the second part of my activity investigated the possible beneficial effects of two natural compounds that might find application as nutraceuticals: silybin, the main component of *Silybum marianum*, and SAMe, an endogenous molecule being the main donor of methyl groups at the cellular level.

4.Introduction

The epidemic of overweight and obesity –"globesity"– in the developed world is continuously increasing and represents a major challenge in term of chronic disease prevention and health across the life. Obesity is one of today's main public health problems, paradoxically coexisting with undernutrition. Fueled by economic growth, industrialization, sedentary lifestyle and a nutritional transition to processed foods and high calorie diets over the last 30 years, in many countries the prevalence of obesity is double, and even quadruple. However, the obesity epidemic is not restricted to industrialized societies: in developing countries over 115 million people suffer from obesity-related problems. According to the World Health Organization (WHO), the worldwide prevalence of obesity nearly tripled between 1975 and 2016 and, overall, about the 13% of the world's adult population (11% of men and 15% of women) were obese in 2016.

Obesity is a complex multifactorial disease which is generally defined as a medical condition in which excess body fat has accumulated to an extent that it may have a negative effect on health. Obesity is commonly caused by a combination of excessive food intake, lack of physical activity and genetic susceptibility.

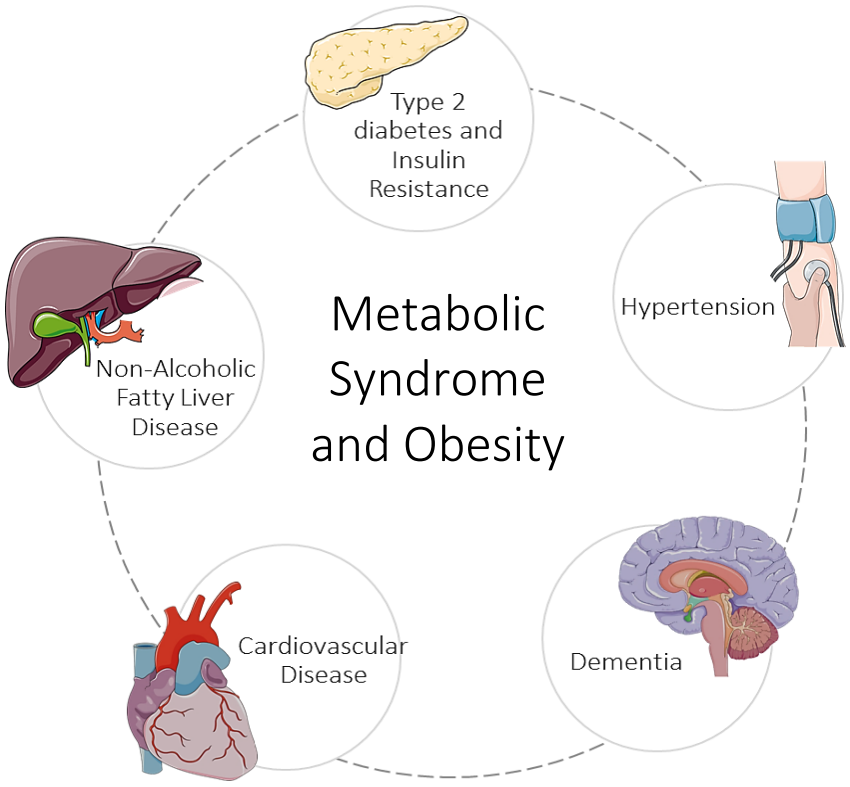

Figure 1. Metabolic syndrome and obesity: scheme of the metabolic syndrome and related disorders

Obesity, abdominal obesity especially, is one of the first features of the metabolic syndrome, which refers to the co-occurrence of several known pathological conditions, including insulin resistance, obesity, non-alcoholic fatty liver disease (NAFLD), atherogenic dyslipidemia and hypertension. These conditions are interrelated and share underlying mediators, mechanisms and pathways.

As the prevalence of obesity increases, so does the burden of its associated co-morbidities: obesity greatly increases risk of chronic disease morbidity, such as type 2 diabetes, cardiovascular disease, certain cancers.

4.1 Non-alcoholic fatty liver disease

Nonalcoholic fatty liver disease (NAFLD) is the hepatic manifestation of the metabolic syndrome. It is defined by excess fat accumulation in the form of triglycerides (TG) in the hepatocytes, due to causes other than significant alcohol consumption or other medical conditions. NAFLD encompasses the simple steatosis (NAFL, non-alcoholic fatty liver) to larger steatosis with associated inflammation (NASH, non-alcoholic steatohepatitis), fibrosis, cirrhosis, and in some cases hepatocellular carcinoma (HCC). Despite its high prevalence, only a small minority of patients with steatosis develops inflammation and subsequent fibrosis and chronic liver disease.

Steatosis is histologically defined by the visible accumulation of macro- and/or micro- vesicular lipid droplets (LDs) in cytosol of more than 5% of hepatocytes; when the capacity of hepatocytes to safely store excess TG in LDs is exceeded, hepatic injury may occur (Vergani, 2019).

At the molecular level, hepatic steatosis develops when uptake and/or *de novo* synthesis of free fatty acids (FA) in the liver exceed oxidation and/or secretion. Therefore, the excess FA triggering steatosis may derive from different sources: (*i*) the plasma FA delivered by adipose tissue (pathway 1); (*ii*) *de novo* hepatic lipogenesis (DNL) (pathway 2); (*iii*) dietary FA transported as intestinally-derived chylomicron (pathway 3) (Rinella, 2015; Bradbury and Berk, 2004).

The etiopathogenesis of NAFLD is rather complex and multifactorial. In the past, the two-hit model of NAFLD development was widely accepted, with the first hit consisting in hepatic lipid accumulation depending on different causes, followed by a second hit activating pro-inflammatory events (Day and James, 1998). As it has evidently emerged that (*i*) accumulation of triglycerides in hepatocytes may be a protective mechanism from liver damage, and (*ii*) hepatic inflammation can precede the simple hepatic steatosis and can also be a cause of steatosis, it has been suggested that many "hit" factors may act simultaneously leading to the development of NAFLD (Tilg and Moschen, 2010). The multiple-hit hypothesis proposes that many hit factors can interact with each other, forming a vicious circle. Among them there are dietary habits, environmental and genetic factors that can lead to development of insulin resistance, obesity with adipocyte proliferation and hypertrophy, and changes in gut microbiome. Insulin resistance is one of the key factors in the development of NAFLD and results in increased hepatic *de novo* lipogenesis and impaired inhibition of adipose tissue lipolysis, with consequent increased flux of fatty acids to the liver. At the liver level, fatty acids overflow may result in endoplasmic reticulum stress and mitochondrial dysfunction and consequent activation of inflammatory responses. Furthermore, genetic factors might explain certain more progressive disease courses in NAFLD.

4.2 In vitro models of NAFLD progression

NAFLD represents the hepatic manifestation of metabolic syndrome associated to obesity and it is the most common chronic liver disease in Western countries (Loomba and Sanyal, 2013). NAFLD is a growing challenge in term of prevention and treatment. In the light of that, the full understanding of the mechanisms underlying the onset and progression of NAFLD is of extreme importance: despite the new findings in this field, knowledge on the pathogenesis of NAFLD is still incomplete.

In the last decades, cellular models have been developed to elucidate the molecular mechanisms involved in the progression of NAFLD. Hepatocytes exposed to high concentrations of FA *in vitro* result in lipid overload which is similar to the steatosis observed in both patients and animal models with NAFLD. In the present study, we aimed to develop an *in vitro* model of NAFLD progression to study the molecular mechanisms sustaining pathogenesis and development of liver steatosis/steatohepatitis.

For this purpose, we employed the rat hepatoma cell line FaO (European Collection of Cell Cultures, Sigma-Aldrich Corp., Milan, Italy). FaO cells maintain many hepatocytes specific markers and were exposed to different steatogenic agents to mimic what happens *in vivo* during NAFLD. Cells were exposed to:

- Oleate and palmitate mixture for 3 hours (2:1 molar ratio, final concentration of 0.75 mM). High levels of circulating FA provide the main source for the hepatic TG synthesis: in patients with NAFLD approximately 60% of hepatic TG is synthesized from FA deriving from adipose tissue, 26% from DNL, and 15% from the diet (Donnelly et al., 2005). A critical point for *in vitro* NAFLD model is the choice of exogenous FA to be used, since FA have different steatotic and toxic activity. In normal and in NAFLD subjects, the most abundant FA are oleic acid (18:1) and palmitic acid (16:0). The treatment with a mixture of these two FA in FaO cells well mimic an *in vitro* mild steatosis.
- Fructose for 24 hours (final concentration 5.5 mM). The fructose is a monosaccharide and in the past, was considered a beneficial dietary component since it does not stimulate insulin secretion. Sucrose and high fructose corn syrup are increasingly present in our food as alimentary additive. However, the harmful effects of fructose have recently gained mainstream attention. Recent studies have reported that high fructose intake stimulates *de novo* lipogenesis (Hudging et al, 2011), and mice fed with a diet of fats and high-fructose corn syrup developed equally severe NAFLD (Tetri et al., 2008): high fructose in the diet induces: leptin resistance, insulin resistance, and increases the blood level of triglycerides.
- Tumor necrosis factor (TNFα) for 24 hours (final concentration 10 ng/ml). Oxidative stress and release of pro-inflammatory cytokines are major consequences of hepatic lipid overload. TNFα is a pro-inflammatory cytokine which is associated with insulin resistance and systemic inflammatory responses and has a main role in NAFLD progression. Therefore, high serum levels of TNFα have been found in patients with NASH compared with healthy subjects (Crespo et al., 2001). TNFα plasma levels correlate positively with the grade of liver fibrosis in patients with advanced stages of NAFLD. For this reason, we choose TNFα as a hit to mimic *in vitro* NAFLD progression.

4.3 Atherosclerosis and endothelial dysfunction

Visceral obesity and insulin resistance are associated to chronic inflammation and it depends mainly on the overproduction of many adipokines such as TNFα, interleukin 1 (IL1), IL6, leptin, and adiponectin. These pro-inflammatory molecules act on different systems and tissue types, including endothelial cells where can induce a chronic, subclinical vascular inflammation which may result in atherosclerosis.

Endothelium is a semi-permeable barrier between the blood and the tissues and acts as a metabolically active organ regulating vascular homeostasis. Endothelial dysfunction/activation is the early step in the atherosclerosis, a progressive disease characterized by the accumulation of lipids and fibrous elements in arteries (Marchesini et al., 1999; Cortez-Pinto et al., 1999; Villanova et al., 2005). Hepatic steatosis and insulin resistance trigger vascular endothelial dysfunction leading to a decrease in synthesis/release of NO (Liao, 2013).

Both ROS generation and nitric oxide (NO) release are involved in the endothelial dysfunction in atherosclerosis. NO plays cardio-protective effects acting as vasodilator and inhibitor of platelets aggregation; some reports described NO-induced abnormal vasodilation in patients with IR (Williams et al., 1996), other ones showed a reduced vasodilation in hypertensive patients with liver steatosis (Sciacqua et al., 2011). In endothelial plasma membrane, ICAM-1, an immunoglobulin that mediates cell-cell adhesion (Heiska et al., 1998; Kevil et al., 2003), is over-expressed as a response to ROS and pro- inflammatory cytokines. ICAM-1 seems to be involved in endothelial cell migration, and in endothelial NO synthase (eNOS) activation. In atherosclerotic patients, ICAM-1 over- expression in endothelial cells of coronary plaques has been reported (Boyle et al., 2000). In mouse, endothelial dysfunction is associated to impaired endothelial autophagy which protects cells from oxidative stress resulting in liver fibrosis (Ruart et al., 2019).

During my thesis work, I aimed to develop an *in vitro* model of atherosclerosis to study the molecular effects of synthetic compounds that can improve the condition of oxidative stress and counteract the atherogenic factors. For this purpose, we employed the human endothelial cell line (HECV) isolated from umbilical vein (Cell Bank and Culture, GMP-IST, Genoa, Italy). As for FaO cells, HECV cells were exposed to an oleate and palmitate mixture for 3 hours (2:1 molar ratio, final concentration of 0.75 mM). The treatment with a mixture of these two FA in

HECV cells mimic an *in vitro* atherosclerosis, by increasing intracellular lipid content and oxidative stress.

4.4 Adipocyte hypertrophy

The metabolic syndrome is a complex network which correlates with NAFLD, endothelial dysfunction and adipocyte hypertrophy. During adipogenesis, fibroblast-like pre-adipocytes differentiate into mature adipocytes through a rearrangement of the molecular machinery where lipogenic processes are promoted and fatty acid uptake and triglyceride accumulation are increased. Mature adipocytes strictly regulate the balance between lipogenesis and lipolysis, and produce a panel of adipokines such as leptin, resistin, adiponectin, tumor necrosis factor-a (TNF-α), interleukin-1b (IL-1b) that modulate metabolism of the other tissues (Rajala and Scherer, 2003).

Enlarged adipocytes are associated with insulin resistance and are an independent predictor of type 2 diabetes. To understand the molecular link between adipocyte hypertrophy and metabolic diseases we developed a procedure for inducing hypertrophy. To do this we used an in vitro model in which mature 3T3-L1 adipocytes were loaded with oleate/palmitate mixture, resulting in artificially hypertrophied mature adipocytes.

During my thesis work, I aimed to develop an *in vitro* model of adipocyte hypertrophy to assess differences between mature and hypertrophic adipocytes. For this purpose, we employed the mouse fibroblast cell line 3T3L1 from the American Type Culture Collection (Manassas, VA, USA). In order to induce adipocyte differentiation, cells were at 2-day post confluence, cells were treated with the differentiation mixture containing 1µM insulin, 1µM dexamethasone (DEX), and 500µM 3-isobuthyl-1-methylxanthine (IBMX) to the culture medium for 2 days. Then, cells were incubated with 100nM insulin for 7 days, changing the medium every 2–3 days. In all experiments, more than 90% of the cells were mature adipocytes after 10 days of incubation. Adipogenic differentiation was monitored at different days by lipid staining. To induce cellular hypertrophy, mature adipocytes were exposed to oleate and palmitate mixture (1 mM) for 2 days.

4.5 Effects of natural and synthetic compounds on lipid accumulation and inflammation in hepatocytes and

endotheliocytes

Definitive treatments for NAFLD and obesity are lacking so far and there are no medications approved by the U.S. Food and Drug Administration (FDA) or European Medicine Agency. Dietary intervention, regular exercise, and weight loss could improve some of the metabolic factors and potentially offset the development of NAFLD.

In the light of that, in recent years, the increase in cases of NAFLD and NASH has stimulated the scientific community to identify compounds that can improve the condition of oxidative stress and counteract the atherogenic factors. These molecules could be useful in the treatment of these pathological conditions and prevent or slow down the progression in fibrosis and/or cirrhosis: this represents one of the most important challenges for the scientific community in the coming years.

4.6 Silybin (from *Silybum marianum*)

As an important category of phytochemicals, natural polyphenols have attracted increasing attention as potential agents for the prevention and treatment of liver diseases. Polyphenols are phenolic compounds containing benzene rings attached with one or more hydroxyl groups. Based on their chemical structure, polyphenols are classified into two major groups: flavonoids and non-flavonoids. Flavonoids are composed of two aromatic rings connected by a three-carbon bridge; they include subgroups of flavonols, flavones, flavan-3-ols, flavanones, isoflavones, and anthocyanidins. In nature, the majority of flavonoids are present as glycosides so that they have increased structural stability. Non-flavonoids encompass the rest of polyphenols, such as stilbenes (resveratrol), lignans, and phenolic acids.

Silymarin is an extract of the milk thistle seeds (*Silybum marianum* L. Gaertner, Compositae) containing a mixture of flavonolignans (silybin, isosilybin, silycristin, silydianin and others). Silybin, which is the major active constituent of silymarin and represents the 70% of the total composition of the mixture, has been demonstrated to exert antioxidant, anti-inflammatory and antifibrotic properties (Gazak et al., 2007; Loguercio et al., 2012).

These compounds exhibit a number of pharmacological effects, particularly in the liver: many studies demonstrated that silybin ameliorate liver damage and diabetes in animal models of

NASH and in patients with diabetes (Serviddio et al., 2010; Di Sario et al., 2005). Recent studies from our group demonstrate that silybin exerts an antisteatotic and antioxidant effect also in *in vitro* models of NAFLD and NASH (Vecchione et al., 2016).

Research conducted so far explained only partially the mechanisms through which the silybin exerts its effects. The aim of this project was to clarify the mechanism of action of the silybin by using the *in vitro* model of steatosis explained before.

4.7 S-adenosylmethionine (SAMe)

S-adenosylmethionine (SAMe) is an endogenous and pleiotropic common substrate involved in many crucial biochemical pathways, including biosynthesis of hormones and neurotransmitters (Cantoni, 1985; Bottiglieri, 2001). Although these anabolic reactions occur throughout the body, most SAM-e is synthesized and consumed in the liver or distributed throughout the body. SAMe is the main methyl donor in mammalian cells, where it transfers a methyl group to an acceptor molecule such as DNA, proteins and phospholipids, modifying their structure and function. Indeed, DNA methylation switch on/off the gene transcription, protein methylation regulates the enzyme activity, phospholipid methylation modulates membrane fluidity. Moreover, SAMe is precursor for cysteine, one of the amino acids of glutathione, the major physiological defence against reactive oxygen species (ROS), thus it acts also as protection against oxidative stress.

SAMe has been reported to be involved in many liver diseases (Lu and Mato, 2012; Mato, 2013). Reduced hepatic SAMe levels were described in patients with alcoholic hepatitis resulting in decreased hepatic GSH levels (Lee et al., 2004), and SAMe administration has been shown to normalize the GSH levels (Vendemiale et al., 1989). Many studies done mostly in alcoholic liver disease, cholestasis of pregnancy, and primary biliary cirrhosis have shown significant improvement in liver test abnormalities during therapy with SAMe (Anstee and Day, 2012).

Part of the present project was to investigate if SAMe might improve fatty liver disease in rat hepatoma cells representing a reliable in vitro model for hepatic steatosis. As FAs seem to play also direct effects on oxidative stress of vascular endothelium (Zhou et al., 2009), we used also human endothelial HECV cells exposed to FA mimicking the in vivo atherosclerosis, as

endothelial damage is typically observed in metabolic syndrome.

4.8 Cellular models

Three different cell lines have been employed:

- FaO cells, a rat hepatoma cell line, to mimic NAFLD onset and progression. The FaO rat hepatoma cells were supplied by European Collection of Cell Cultures, (ECCC-Sigma-Aldrich Corp.). They express a broad array of liver-specific mRNAs and maintain the ability to assemble and secrete VLDL as well as to respond to *stimuli* that activate transcription factors such as PPARs (Grasselli et al., 2017; Clayton et al., 1985; Lauris et al., 1986). Therefore, this cell line is a good and widely employed cellular system maintaining the main features of rat hepatocytes.

  In our experiment, FaO cells at 70-80% confluence were incubated in starvation medium (F12 Coon's modified medium supplemented with 0.25% BSA) with different steatogenic agents. It is noteworthy that basal lipid content of FaO cells is much lower than that of primary hepatocytes, thus, steatogenic treatments resulted in a more rapid and pronounced triglyceride accumulation with respect to primary cultured hepatocytes. The exposure to different steatogenic agents alone or in combination, led to a marked increase in number and size of cytosolic lipid droplets. These observations candidate lipid-loaded FaO cells as a reliable and convenient *in vitro* model of NAFLD (Grasselli et al., 2011).

- HECV cells, a human endothelial vascular cell line, to mimic human endothelium dysfunction. The human endothelial cell line (HECV) was supplied by Cell Bank and Culture (GMP-IST- Genoa, Italy). These cells were isolated from human umbilical vein and maintain a good number of endothelium function; indeed, they are widely employed for *in vitro* studies. Cells were grown in Dulbecco's modified Eagle's medium high glucose (D-MEM) supplemented with L-glutamine and 10% FCS. For treatments, cells were grown until 80% confluence and, to mimic in vitro the effect of high fat diet, were treated with a mixture of long-chain fatty acids (Vergani et al., 2018). The exposure to oleate and palmitate led to a marked fat accumulation into cells, thus suggesting lipid loaded HECV cells represents a reliable *in vitro* model of

endothelial disfunction.

- 3T3L1 cells, a mouse pre-adipocyte cell line. 3T3-L1 mouse fibroblasts were purchased from the American Type Culture Collection (Manassas, VA, USA). The 3T3-L1 cells are well-established murine preadipocytes displaying a fibroblast-like morphology that, under appropriate conditions, progress towards an adipocyte-like phenotype (Green and Meuth, 1974). A large body of articles have employed 3T3-L1 cells to investigate adipogenesis and obesity-related characteristics. One of the main advantages of this cell line is that provides a homogenous and reproducible system (Poulos et al., 2010). Cells were maintained in Dulbecco's modified Eagle medium (D-MEM) containing 25 mmol/l glucose and 10% Foetal Bovine Serum (FBS, Euroclone, Milan, Italy). Adipogenesis was induced by adding the differentiation mixture (1µM insulin, 12µM dexamethasone and 500µM 3-isobuthyl-1-methylxanthine) to the culture medium for 2 days. Then, cells were incubated with 1µM insulin for 7 days. More than 90% of the cells were mature adipocytes after 10 days of incubation. To induce cellular hypertrophy, mature adipocytes were exposed to oleate/palmitate mixture (1 mM) for 2 days.

5.Silybin counteracts lipid excess and oxidative stress in cultured steatotic hepatic cells

Vecchione G[1], Grasselli E[1], Voci A[1], Baldini F[1], Grattagliano I[2], Wang DQ[3], Portincasa P[2], Vergani L[1].

[1]DISTAV, Department of Earth, Environment and Life Sciences, University of Genova, 16132 Genova, Italy; [2] Department of Biomedical Sciences and Human Oncology, University School of Medicine, 70124 Bari, Italy; [3]Department of Internal Medicine, Division of Gastroenterology and Hepatology, Saint Louis, University School of Medicine, St. Louis, MO 63104, United States

World J Gastroenterol. 2016 Jul 14;22(26):6016-26. doi: 10.3748/wjg.v22.i26.6016.

ABSTRACT

AIM: To investigate *in vitro* the therapeutic effect and mechanisms of silybin in a cellular model of hepatic steatosis.

METHODS: Rat hepatoma FaO cells were loaded with lipids by exposure to 0.75 mmol/L oleate/palmitate for 3 h to mimic liver steatosis. Then, the steatotic cells were incubated for 24 h with different concentrations (25 to 100 μmol/L) of silybin as phytosome complex with vitamin E. The effects of silybin on lipid accumulation and metabolism, and on indices of oxidative stress were evaluated by absorption and fluorescence microscopy, quantitative real-time PCR, Western blot, spectrophotometric and fluorimetric assays.

RESULTS: Lipid-loading resulted in intracellular triglyceride (TG) accumulation inside lipid droplets, whose number and size increased. TG accumulation was mediated by increased levels of peroxisome proliferator-activated receptors (PPARs) and sterol regulatory element-binding protein-1c (SREBP-1c). The lipid imbalance was associated with higher production of reactive oxygen species (ROS) resulting in increased lipid peroxidation, stimulation of catalase activity and activation of nuclear factor kappa-B (NF-κB). Incubation of steatotic cells with silybin 50 µmol/L significantly reduced TG accumulation likely by promoting lipid catabolism

and by inhibiting lipogenic pathways, as suggested by the changes in carnitine palmitoyltransferase 1 (CPT-1), PPAR and SREBP-1c levels. The reduction in fat accumulation exerted by silybin in the steatotic cells was associated with the improvement of the oxidative imbalance caused by lipid excess as demonstrated by the reduction in ROS content, lipid peroxidation, catalase activity and NF-*κ*B activation.

CONCLUSION: We demonstrated the direct anti- steatotic and anti-oxidant effects of silybin in steatotic cells, thus elucidating at a cellular level the encouraging results demonstrated in clinical and animal studies.

Key words: Non-alcoholic fatty liver disease; Steatotic hepatocytes; Silybin; Lipid metabolism; Oxidative stress; Lipid droplets; Mitochondrial β-oxidation

INTRODUCTION

Non-alcoholic fatty liver disease (NAFLD) is characterized by excess fat accumulation, mainly in the form of triglycerides (TGs), in hepatocytes of subjects who do not consume excess alcohol. NAFLD definition encompasses a large spectrum of liver abnormalities which range from the simple steatosis, to nonalcoholic steatohepatitis (NASH), till to cirrhosis and hepatocellular carcinoma (Brunt et al., 2015; Rinella, 2015). NAFLD is the most common cause of abnormal liver function tests in Western countries, and evidences substantiate a strong association between NAFLD and metabolic abnormalities such as obesity, insulin resistance, and metabolic syndrome (Portincasa et al., 2004).

In the hepatocyte, TGs (Alkhouri et al., 2009) are synthesized from fatty acids (FAs) deriving from three major sources: plasmatic non-esterified fatty acids (NEFAs) from adipose tissue, de novo lipogenesis, and dietary FAs (Donnelly et al., 2005). Uptake of FAs by hepatocytes is related to their serum concentrations and is mediated by different classes of fatty acid transport proteins (Nakamura et al., 2014). In the liver, FAs follow three different destinations: (1) oxidation, mainly in mitochondria, but also in extra-mitochondrial organelles such as peroxisomes; (2) assembly and export as very low-density lipoproteins (VLDL); and (3) storing as TGs within lipid droplets (LDs).

Storing of excess TGs in LDs is a protective mechanism against FA-induced toxicity that is mainly related to FA oxidation. Most FAs are metabolized through β-oxidation in mitochondria which is primarily regulated by carnitine palmitoyltransferase 1 (CPT-1) required for transport of long-chain fatty acids into mitochondria (Ramsay et al., 2001). Over-active FA oxidation leads to over- production of reactive oxygen species (ROS) with consequent oxidative stress (Fromenty and Pessayre, 1995; Seifert et al., 2010). Excess ROS as well as pro-inflammatory cytokines can activate inflammatory signaling such as that sustained by the transcription factor nuclear kappa-B (NF-κB) which is implicated in the response to oxidative stress (Cnop et al., 2012).

In light of these considerations, a reduction in liver steatosis through a stimulation of lipolytic pathways may potentially expose hepatocytes to the damaging effect of excess free FAs (Yamaguchi et al., 2007) and this point has to be considered when anti-steatotic molecules are tested for therapeutic applications.

Medicinal plants have become popular as the source of dietary supplements (Chang, 2000). Flavonoids, a large class of polyphenolic products, are well-known antioxidants and free radical scavengers (Kandaswami and Middleton, 1994). Silymarin, the standardized extract from milk thistle (*Sylibum marianum*), and its major active compound silybin, have been used for a long time as a hepatoprotective agents for the treatment of acute and chronic liver diseases (Saller et al., 2001). Previous clinical findings evidenced the efficacy of silybin on insulin resistance and liver injury in patients with NAFLD (Federico et al., 2006). Moreover, in a recent study on sixty four patients with NASH, silymarin helped to lower the hepatic enzymes, particularly ALT (Solhi et al., 2014). The improvement of liver histology after silybin treatment was recently reported in a multicenter randomized controlled trial (Loguercio et al., 2012). However, the molecular mechanisms associated with the hepatoprotective activity of silybin remain to be elucidated.

The hepatic lipid metabolism is governed by two main families of transcription factors, the peroxisome proliferator-activated receptors (PPARs) that regulate both lipogenic and lipolytic pathways (Huang et al., 2012), and the sterol regulatory element-binding proteins (SREBPs) that stimulate sterol and fatty acid biosynthesis (Ferrè and Foufelle, 2010; Shimano, 2001). FAs are endogenous ligands of all PPAR isoforms (Nakamura et al., 2014); uptake of FAs into hepatocytes and their oxidation is regulated mainly by PPARα, while their esterification and conversion to TGs by PPARγ and SREBP-1, whose expression typically increases in NAFLD (Eberlè et al., 2004). Moreover, macroautophagy, a process that leads to the degradation of cellular constituents through lysosomes (Mizsushima et al., 2002), participates in lipid metabolism through the breakdown of LDs (lipophagy). A decreased autophagic function may promote the development of hepatic steatosis and the progression of steatosis to NASH (Komatsu et al., 2005). The autophagy-related protein 7 (Atg7) is considered essential for this process in mammalian cells (Komatsu et al., 2005).

This study aimed to clarify whether silybin as phytosome complex with vitamin E may favorably affect lipid and radical homeostasis using an in vitro model of NAFLD induced by the exposure of hepatoma FaO cells to exogenous FAs. Changes in expression of PPARs and SREBP-1c, the main regulators of lipid metabolism, as well as of CPT1, the master controller of mitochondrial FA oxidation, and Atg7, a key autophagy-promoting gene, have been assessed to investigate the pathways possibly activated by silybin. In parallel, the stimulation of defense systems against oxidative stress, such as catalase and NF-κB, were evaluated to assess the potential

protective effects of silybin.

MATERIALS AND METHODS

Chemicals

All chemicals, unless otherwise indicated, were of analytical grade and were supplied by Sigma-Aldrich Corp. (Milan, Italy).

Cell treatments

Rat hepatoma FaO cells (European Collection of Cell Cultures, Sigma-Aldrich Corp., Milan, Italy) are a liver cell line maintaining hepatocyte specific markers (Clayton et al., 1985). Cells were grown in Coon's modified Ham's F12 with 10% fetal bovine serum (FBS). For treatments, cells were grown until 80% confluence, then incubated overnight in high-glucose medium with 0.25% bovine serum albumin (BSA). Steatosis was induced by exposing cells for 3 h to an oleate/palmitate mixture (2:1 molar ratio, final concentration 0.75 mmol/L). Thereafter, steatotic cells were incubated for 24 h with 0 to 100 μmol/L (final concentration) of silybin (S) as phytosome complex with vitamin E (Realsil®, Istituto Biochimico Italiano, Lorenzini S.p.a, Italy). Silybin stock (10 mmol/L) was prepared in dimethyl sulfoxide (DMSO) and then diluted with the culture medium to a final concentration 0.3 mmol/L.

The viability of FaO cells upon exposure to FAs or silybin, both as single agents or combined, was determined by the MTT [3-(4,5-dimethylthiazol-2-yl)-2,5-diphenyltetrazolium bromide] and measured spectrophotometrically (Grasselli et al., 2013).

Quantification of triglycerides

For determination of intracellular TG content, at the end of each treatment cells were scraped and centrifuged at 14000 × *g* for 3 min. After cell lysis, obtained by passing cell suspension through 25 gauge needle, lipids were extracted using the chloroform/methanol (2:1) method (Grasselli et al., 2010) and TG content was measured by spectrophotometric analysis ("Triglycerides liquid" kit, Sentinel, Milan, Italy). Values were normalized to protein content as determined by the bicinchoninic acid (BCA) method using BSA as a standard (Wiechelman et al., 1988). In parallel, TG content was determined in the culture medium. Data are expressed as percent TG content relative to controls.

Lipid droplet analysis

Cells were grown on collagen-coated glass slides (Falcon, BD, Milan, Italy); neutral lipids were visualized using the selective Oil-RedO (ORO) dye. Briefly, after fixing in 4% paraformaldehyde, cells were washed with PBS, stained with ORO 1% in triethyl phosphate 60% for 20 min and washed (Trunkey, 1990). Slides were examined by Leica DMRB light microscope equipped with a Leica CCD camera DFC420C (Leica, Wetzlar, Germany). In parallel, the LD abundance inside the cells was assessed fluorimetrically using Nile Red (NR), a vital lipophilic dye. At the end of each treatment, cells were incubated with 0.3 µmol/L NR solution (from a stock solution of 100 µg/mL in PBS) for 30 min at 37 °C. After washing with PBS the NR fluorescence was measured by LS-50B spectrofluorimeter (Perkin Elmer, United States) at λex = 580 nm and λem = 630 nm and slit width set to 5.0 (Greenspan et al., 1985). All measurements were performed at 25 °C using a water-thermostated cuvette holder.

ROS production and lipid peroxidation measurement

The oxidation of the cell-permeant 2'-7' dichlorofluorescin diacetate (DCF-DA, Fluka, Germany) to 2'-7' dichlorofluorescein (DCF) is extensively used for quantifying *in situ* the production of H2O2 and other ROS (Halliwell and Whiteman, 2004). Stock solution of DCF- DA (10 mmol/L in DMSO) was prepared and stored at -20 °C in the dark. At the end of each treatment, cells were scraped and gently spun down (600 × *g* for 10 min at 4 °C). After washing, cells were loaded with 10 µmol/L DCF-DA in PBS for 30 min at 37 °C in the dark, centrifuged and suspended in PBS. The DCF fluorescence was measured fluorometrically at λex = 495 nm and λem = 525 nm using. All measurements were performed at 25 °C using a water-thermostated cuvette holder.

In parallel, H2O2 production was assessed directly on cells grown on collagen-coated glass slides. After treatment, cells were incubated with 100 µmol/L DCF-DA for 1 h (Okuda et al., 1996). Slides were examined by Leica DMRB light microscope equipped with a Leica CCD camera DFC420C. Lipid peroxidation was determined spectrophotometrically through the thiobarbituric acid reactive substances (TBARS) assay which is based on the reaction of malondialdehyde (MDA; 1,1,3,3-tetramethoxypropane) with thiobarbituric acid (TBA) (Iguchi et al., 1993). Briefly, 1 vol. of cell suspension was incubated for 45 min at 95 °C with 2 vol. of TBA solution (0.375% TBA, 15% trichloroacetic acid, 0.25 mol/L HCl. Then, 1 vol. of N-butanol was added and the organic phase was read using a Varian Cary50 spectrophotometer at 532 nm. Results were expressed as pmol MDA/mL per milligram protein.

Determination of catalase activity

Catalase (CAT, EC 1.11.16) activity was evaluated in both 12000 × *g* supernatant and pellet of cell lysates following the consumption of H2O2 at 25 °C according to (Aebi, 1984). Enzyme activity (as the sum of both pellet and supernatant) was expressed as µmoles of decomposed H2O2 per min/mg protein. Protein content was determined by BCA method. All measurements were performed at 25 °C using a water-thermostated cuvette holder.

RNA extraction and quantitative real-time PCR

RNA was isolated using the Trizol reagent, cDNA was synthesized and quantitative real-time PCR (qPCR) was performed in quadruplicate using 1 × IQTM SybrGreen SuperMix and Chromo4TM System apparatus (Biorad, Milan, Italy) (Grasselli et al., 2014). The relative quantity of target mRNA was calculated by the comparative Cq method using glyceraldehyde 3-phosphate dehydrogenase (GAPDH) as housekeeping gene, and expressed as fold induction with respect to controls (Pfaffl, 2001). Primer pairs were designed *ad hoc* starting from the coding sequences of *Rattus norvegicus* available on the GenBank database (http://www.ncbi.nlm.nih.gov/Genbank/GenbankSearch.html) and synthesized by TibMolBiol custom oligosynthesis service (Genova, Italy). Primers are listed in Table 1.

Table 1 Characteristics of the primer pairs used for reverse transcription-quantitative real-time PCR analysis

Primer name	Primer sequence (5′→3′)	Annealing temperature (℃)	Product lenght (bp)	Accession ID
GAPDH-F	GACCCCTTCATTGACCTCAAC	60	136	DQ403053
GAPDH- R	CGCTCCTGGAAGATGGTGATGGG			
PPARα-F	CCCCACTTGAAGCAGATGACC	60	139	NM_013196
PPARα-R	CCCTAAGTACTGGTAGTCCGC			
PPARδ-F	AATGCCTACCTGAAAAACTTCAAC	60	96	AJ306400 .1
PPARδ-R	TGCCTGCCACAGCGTCTCAAT			
PPARγ-F	CGGAGTCCTCCCAGCTGTTCGCC	60	116	Y12882
PPARγ-R	GGCTCATATCTGTCTCCGTCTTC			
CPT1-F	CCGCTCATGGTCAACAGCA	60	105	NM_031559
CPT1-R	CAGCAGTATGGCGTGGATGG			
Atg7-F	CCTCAGCGGATGTATGGACC	60	160	NM_001012097.1
Atg7-R	AGCCACATTACACCCCAAGG			

F: Forward sequence; R: Reverse sequence.

Western blotting

Both cellular and nuclear homogenates were processed by Western blot analysis to assess the protein levels of SREBP1-c and NF-κB/p65, respectively. In fact, activation of the NF-κB transcription factor is associated with its phosphorylation and nuclear translocation of the p65 component of the complex. Cells were lysed on ice in lysis buffer (NaCl 150 mmol/L, Tris HCl pH 7.4, 50 mmol/L, SDS 0.33%) as described elsewhere[34]. For nuclear extraction, the cellular pellet was suspended in 400 µL ice-cold Buffer A (20 mmol/L Tris HCl pH 7.8, 50 mmol/L KCl, 10 µg/mL Leupeptin, 0.1 mmol/L Dithiothreitol-DTT, 1 mmol/L phenylmethanesulfonyl fluoride-PMSF); then 400 µL Buffer B (Buffer A plus 1.2% Nonindet P40) was added. The suspension was vortex-mixed for 10 sec; after centrifugation (14000× g for 30 s, 4 °C) the supernatant was discarded and the nuclear pellet was washed with 400 µL Buffer A and centrifuged. Next, the nuclear pellet was suspended in 100 µL Buffer B, mixed thoroughly in ice for 15 min and finally centrifuged (14000 × g for 20 min, 4 °C). The supernatant containing the nuclear extracts was collected and the protein content was measured by BCA method. About 30-50 µg proteins were electrophoresed on sodium dodecyl sulfate polyacrylamide gel electrophoresis (SDS-PAGE) (Laemmli, 1970). Membrane was blocked for 1 h in 5% fat-free milk/PBS (pH 7.4) and probed using mouse anti–human SREBP-1 (SC-13551) or rabbit anti-human NF-κB p65 (SC-109) antibodies supplied by Santa Cruz Biotechnology (DBA, Milan, Italy). Membranes were incubated overnight at 4 °C with primary antibody in PBST buffer (PBS with 0.1% Tween 20) (Towbin et al., 1979), washed and incubated with horseradish peroxidase (HRP)-conjugated rabbit anti-mouse IgG (Sigma- Aldrich), as a secondary antibody in PBST for 1 h at room temperature. Immune complexes were visualized using an enhanced chemiluminescence Western blotting analysis system (Bio-Rad ChemiDoc XRS System). Films

were digitized and band optical densities were quantified against the actin band using a computerized imaging system and expressed as Relative Optical Density (ROD, arbitrary units). ROD of each band was expressed as percentage respect to control.

Statistical analysis

RNA and protein data are expressed as mean ± SD of at least four independent experiments in triplicate. Statistical analysis was performed using ANOVA with Tukey's post-test (GraphPad Software, Inc., San Diego, CA, United States).

RESULTS

Effects of silybin on lipid accumulation

Lipid accumulation was visualized *in situ* by optical microscopy of ORO-stained cells in control (C) and steatotic hepatocytes incubated for 24 h in the absence (SC) or in the presence (SC + S) of increasing concentrations of silybin (25, 50, and 100 μmol/L). The number and size of LDs increased markedly in steatotic cells, and decreased dose- dependently with silybin incubation (Fig. 1A). Also TG content was significantly higher in teatotic than in control cells (+113%; $P \leq 0.001$) (Fig. 1B). Incubation with silybin 50 μmol/L and 100 μmol/L decreased significantly the TG content by -33% and by -38%, respectively, ($P \leq 0.001$ for both doses *vs* untreated steatotic cells). Silybin did not affect the lipid content of control cells (data not shown).

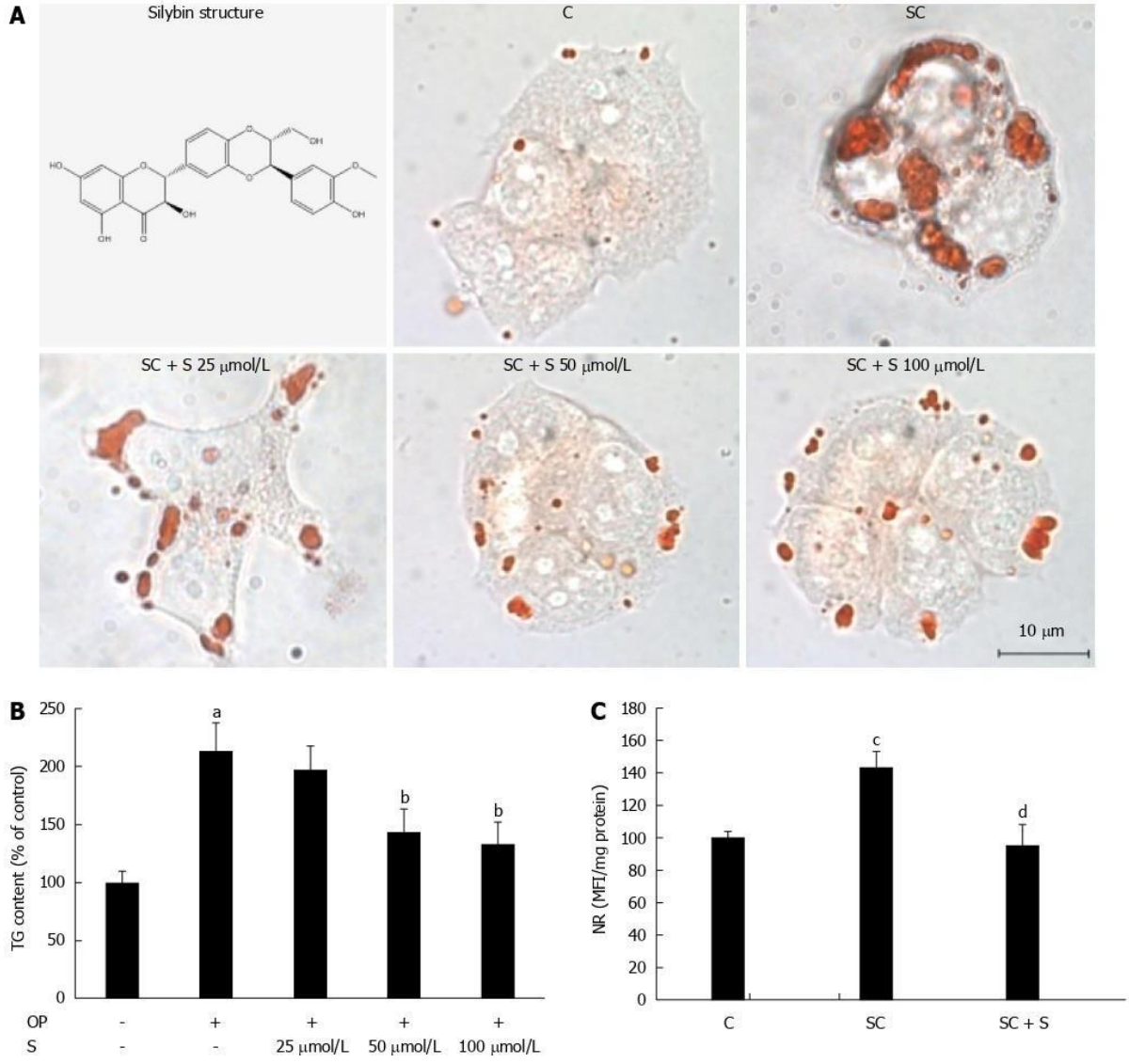

Figure 2. Lipid-lowering effects of silybin in steatotic FaO cells

(A) Neutral lipids were visualized in situ by ORO-staining in control (C) and steatotic FaO cells incubated in the absence (SC) or in the presence (SC + S) of the silybin at different doses (silybin 25; 50; 100 µmol/L) (magnification × 40; Bar: 10 µm). Silybin structure is also shown; **(B)** On the same samples TG content was quantified by spectrophotometric assay; data are expressed as percent TG content relative to control and normalized for total proteins; **(C)** LD accumulation was evaluated by NR-staining in control and steatotic FaO cells incubated in the absence or in the presence of 50 µmol/L silybin; data are expressed as percent mean fluorescence intensity (MFI) relative to control and normalized for total proteins. Values are mean ± SD from a least three independent experiments. ANOVA followed by Tukey's test was used to assess the statistical significance between groups. Significant differences are denoted by symbols: aP ≤0.001, cP ≤0.01 C vs OP and bP ≤ 0.001, dP ≤ 0.01 OP vs silybin.

Following these pilot experiments, silybin at a concentration of 50 µmol/L was used for all further experiments. Using NR fluorescence we measured LD accumulation as a function of the treatments. The average content of LDs increased significantly by +43% ($P \leq 0.01$) in steatotic cells compared to control, and decreased by -33% ($P \leq 0.01$) with silybin 50 µmol/L compared to steatotic cells (Fig 1 C). Cell viability was not significantly affected by FA and/or silybin treatments as single agents or combined (data not shown).

Effects of silybin on lipid metabolism pathways

Lipid metabolism pathways are controlled by PPARS, a family of FA-regulated transcription factors. In rat hepatocytes, we have previously showed the following abundance of the three PPAR transcripts: PPARα > PPARδ > PPARγ [38]. The present results show that expression of PPARα mRNA was 1.7 fold higher in steatotic cells compared to control ($P \leq 0.05$), and increased further upon incubation with silybin 50 µmol/L (+54% with respect to steatotic cells; $P \leq 0.01$) (Fig. 2A). A significant increase was also observed in PPARγ mRNA expression upon lipid-loading (2.8 fold induction with respect to control; $P \leq 0.01$), but, in in this case, silybin 50 µmol/L reduced the up-regulation (-34% with respect to steatotic cells, $P \leq 0.05$) (Fig. 2A). By contrast, mRNA expression of PPARδ decreased upon lipid-loading (about 0.55 fold induction with respect to control; $P \leq 0.05$) and silybin 50 µmol/L restored PPARδ expression to values similar to control (+115% compared to steatotic cells, $P \leq 0.01$) (Fig. 2A).

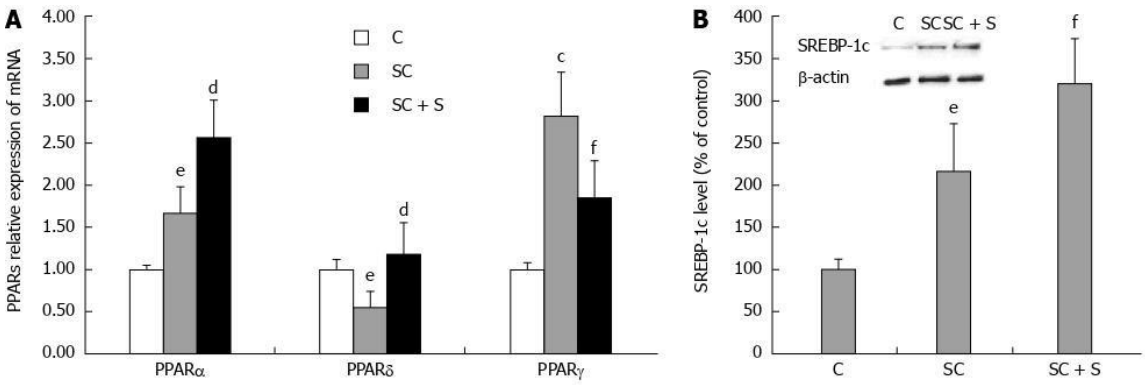

Figure 3. Effects of silybin on transcription factors regulating lipid metabolism

In control (C) and steatotic FaO cells incubated in the absence (SC) or in the presence (SC + S) of silybin 50 µmol/L we assessed. (A) mRNA expression of PPARa, PPARd and PPARγ by qPCR; GAPDH was used as the internal control for quantifying gene expression; data expressed as fold induction with respect to controls; (B) Densitometric analysis of SREBP- 1c by Western blotting; b-actin was the protein loading control used as housekeeping gene for normalization; data are expressed as percentage values with respect to controls. Values are mean ± SD from at least three independent experiments. ANOVA followed by Tukey's test was used to assess the statistical significance between groups Significant differences are denoted by symbols: cP ≤ 0.01, eP ≤ 0.05 C vs OP and dP ≤ 0.01, fP ≤ 0.05 OP vs Silybin.

SREBP-1c is a PPARα-target gene which regulates expression of lipogenic enzymes. Activation of SREBP-1c increased in steatotic hepatocytes (+116%; $P \leq 0.05$) with respect to control and further increased upon exposure to silybin 50 µmol/L (+48% compared to steatotic cells; $P \leq 0.05$) (Fig. 2B).

A reduced TG accumulation in hepatocytes might be sustained by both stimulation of oxidative and/or secretory pathways. CPT-1, the main regulator of mitochondrial β-oxidation of FAs, is significantly up-regulated in steatotic cells upon incubation with silybin 50 µmol/L (+217% with respect to steatotic cells; $P \leq 0.001$) (Fig. 3A). At the same time, the mRNA expression of *Atg7*, an autophagy-promoting gene in hepatocytes, was significantly increased in steatotic cells (1.45 fold induction with respect to control; $P \leq 0.05$), but it did not change upon treatment with silybin 50 µmol/L (Fig. 3B). On the other hand, steatotic cells showed an increased TG secretion into the culture medium compared to control cells (+57%; $P \leq 0.001$), but incubation with silybin 50 µmol/L did not further stimulate TG secretion as compared to steatotic cells (Fig. 3C).

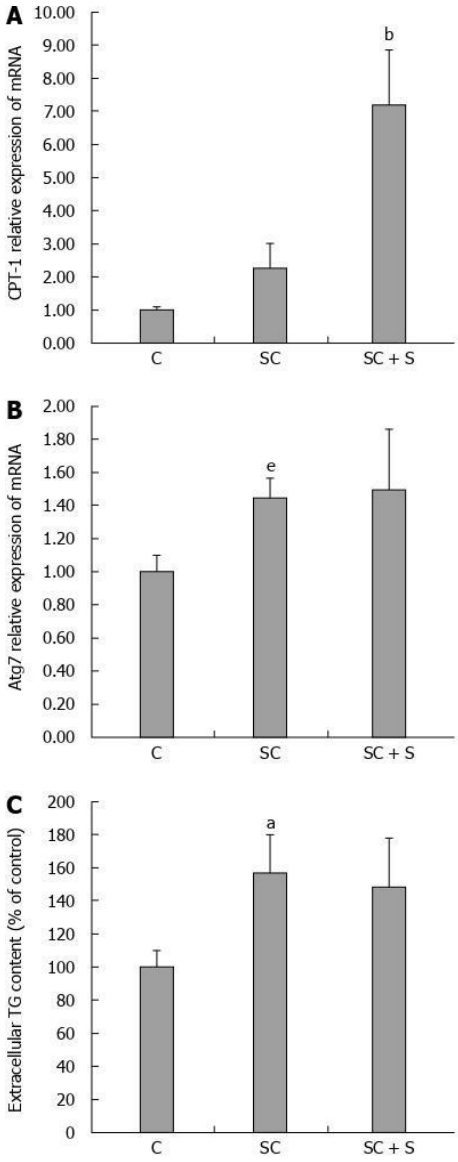

Figure 4. Effects of silybin on lipid catabolism pathways

In control (C) and steatotic FaO cells incubated in the absence (SC) or in the presence (SC + S) of silybin 50 µmol/L we assessed: mRNA expression of CPT-1 **(A)** and of Atg7 **(B)** by qPCR; GAPDH was used as the internal control for quantifying gene expression and data expressed as fold induction with respect to controls; extracellular TG content quantified in the medium by spectrophotometric assay **(C)**; data are expressed as percent TG content relative to control and normalized for total proteins; Values are mean ± SD from at least three independent experiments. ANOVA followed by Tukey's test was used to assess the statistical significance between groups Significant differences are denoted by symbols: aP ≤ 0.001, eP ≤ C vs OP and bP ≤ 0.001, dP ≤ 0.01 OP vs Silybin.

Effects of silybin on oxidative stress

The intracellular production of ROS, mainly hydrogen peroxide (H_2O_2), was visualized *in situ* by fluorescence microscopy of DCF-stained cells (Fig.4). Higher and diffuse DCF fluorescence was observed in steatotic cells (Fig. 4C, D) and it was lower in cells treated with silybin 50 µmol/L (Fig. 4E, F). DCF fluorescence was almost null in control cells (Fig. 4A). These changes were quantified by spectrofluorometer readings (Fig. 4B) that showed a significant DCF decrease (-45%; $P \leq 0.001$) in silybin-treated cells with respect to steatotic cells used as control.

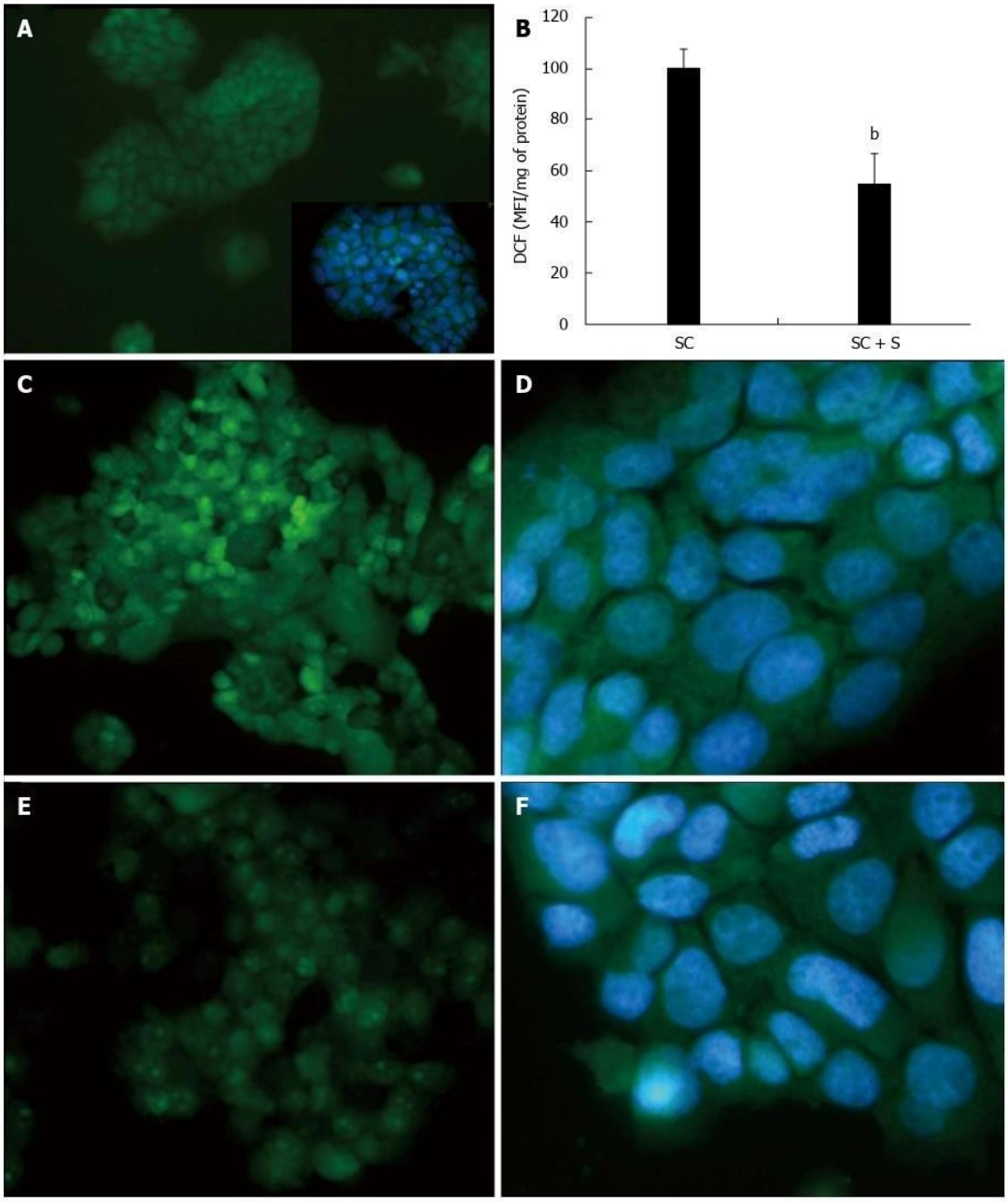

Figure 5. Effects of silybin on reactive oxygen species production

The intracellular level of reactive oxygen species (ROS), mainly hydrogen peroxide, was visualized in situ by optical microscopy in control **(A and inset)** and steatotic FaO cells incubated in the absence **(C-D)** or in the presence **(E-F)** of silybin 50 µmol/L. The ROS level were also quantified by spectrofluorimeter assay of DCF-stained cells **(B)** and data are expressed as percent mean fluorescence intensity (MFI) relative to steatotic cells and normalized for total proteins. DCF: 2'-7' dichlorofluorescein. bP < 0.001 SC vs SC + S.

Also MDA level was greater in steatotic than in control cells (+100%; $P \leq 0.001$) and decreased with silybin 50 µmol/L (-57% with respect to steatotic cells; $P \leq 0.001$) (Fig. 5A). The analyses of antioxidant defence mechanisms showed increased catalase activity in steatotic cells with respect to control (+45% *vs* control, $P \leq 0.01$) that decreased with silybin 50 µmol/L (-38% with respect to steatotic cells, $P \leq 0.01$) (Fig. 5B). Also NF-κB activation showed a trend to an increase in steatotic cells and a significant reduction upon exposure to silybin 50 µmol/L (-29% with respect to steatotic cells; $P \leq 0.05$) (Figure 5C).

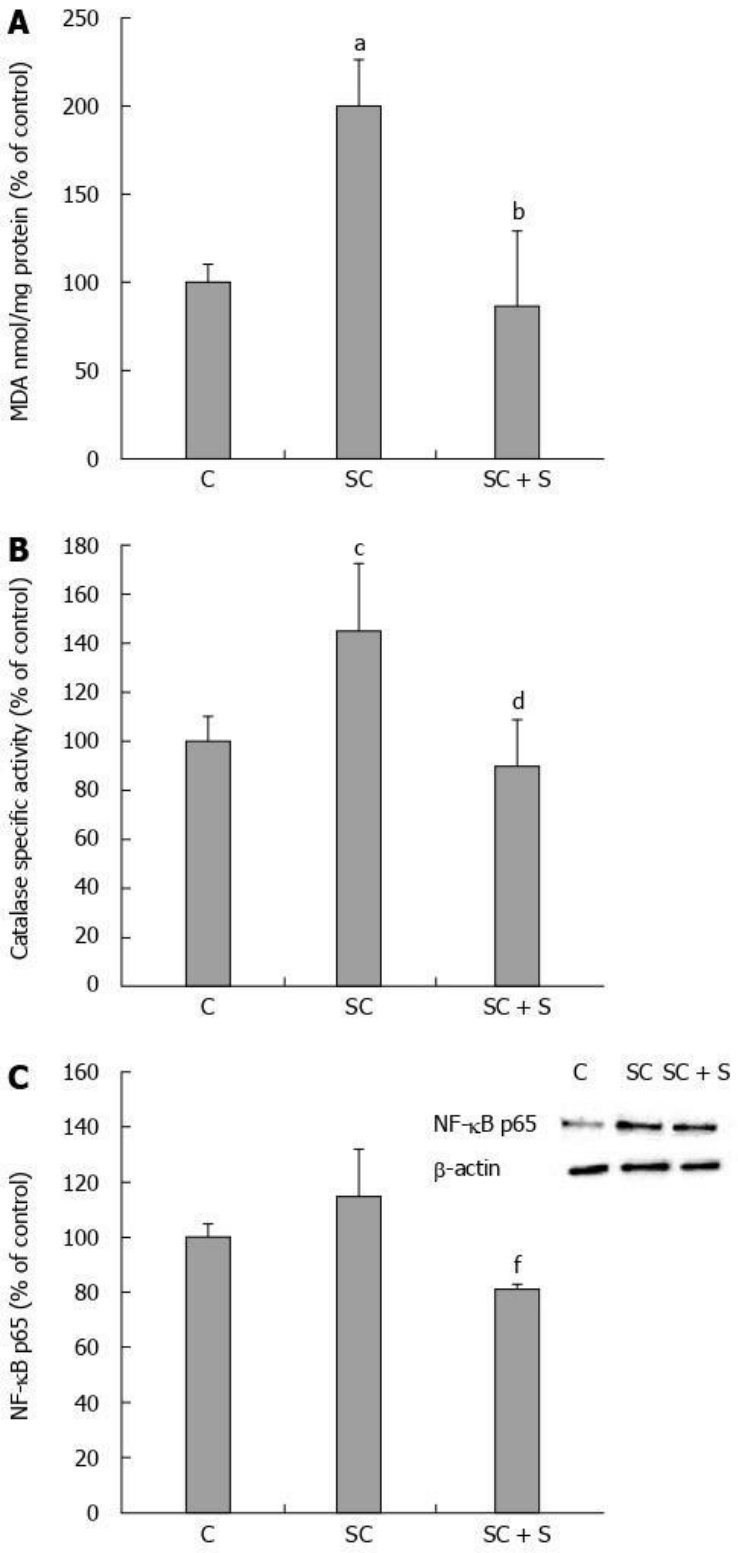

Figure 6. Effects of silybin on oxidative stress markers

In control and steatotic FaO cells incubated in the absence or in the presence of silybin 50 µmol/L we assessed. **(A)** The intracellular level of MDA (pmol MDA/mL x mg of sample protein) quantified by TBARS assay data are expressed as percentage values with respect to controls and normalized for total proteins; **(B)** Catalase specific activity (micromoles of decomposed H2O2 per min/mg of sample protein) evaluated by spectrophotometric assay, data are expressed as percentage values with respect to controls and normalized for total proteins. **(C)** Densitometric analysis of nuclear NF- κB/p65 evaluated by Western blotting; b-actin was the protein loading control used as housekeeping gene for normalization; data are expressed as

percentage values with respect to controls. Values are mean ± SD from at least three independent experiments. ANOVA followed by Tukey's test was used to assess the statistical significance between groups Significant differences are denoted by symbols: aP ≤ 0.001, cP ≤ 0.01 C vs OP and bP ≤ 0.001; dP ≤ 0.01; fP ≤ 0.05 OP vs silybin.

DISCUSSION

The burden of nonalcoholic liver steatosis is rapidly increasing worldwide and is exposing the populations to the risk of liver-related complications (Brunt et al., 2015). Ultimate therapeutic approaches are lacking so far, besides diet and physical exercise. The nutraceutic silybin has shown preliminary encouraging results either in clinical and animal studies (Reina and Martinez, 2015; Rosso et al., 2015) The present study provides a deeper characterization of some pathophysiologically relevant mechanisms of action of silybin administered as phytosome complex with vitamin E directly to fatty hepatocytes mimicking a steatosis condition *in vitro*. In this study, silybin disclosed direct anti-steatotic and anti-oxidant properties in steatotic cells, thus extending previous observations carried out by our group in studies with patients suffering with liver steatosis (Loguercio et al., 2012), and in animal models fed a steatogenic diet (Grattagliano et al., 2013).

Accumulation of LDs within hepatocytes is the first step in the development of NAFLD (Vanni et al., 2010), while oxidative stress causing membrane lipid peroxidation and necro-inflammatory changes represents the second step leading to NASH (Aragno et al., 2009; Day, 2002). The exposure of hepatoma cells to exogenous FAs mimicked the first “hit” of NAFLD and led to TG accumulation within large cytosolic LDs that we observed by microscopic, fluorimetric and spectrophotometric analyses.

At the molecular level, TG accumulation in LDs seems to be sustained by the up-regulation of PPARα that promotes FA transportation inside the cells, and by a larger up-regulation of PPARγ, the lipogenic isoform that promotes TG synthesis from FAs. It has to be underlined that, although PPARα is mostly known for its ability to induce FA oxidation, growing evidence points to its role in regulation of lipogenesis. In fact, PPARα regulates many aspects of hepatic lipid metabolism including FA uptake through membranes, intracellular FA trafficking and oxidation, TG storage and lipolysis. In the present study, the changes in PPARα mRNA expression are paralleled by those in the protein levels of SREBP-1c, that in fact is a PPARα target gene (Fernández-Alvarez et al., 2011). Moreover, PPARα up-regulation can explain both the increase in lipophagy, TG secretion and in CPT-1 expression observed in steatotic cells. In fact, PPARα typically promotes lipid mobilization from the cytosolic stores by stimulating both LD autophagy, lipid secretion and FA oxidation in mitochondria.

The activation of all these pathways represents an attempt of the cell to reduce excess fat accumulation, but are usually accompanied by increased ROS production. Indeed, the present data show that excess fat accumulation is accompanied by increased oxidative stress. To assess cellular oxidative stress, we measured: (1) content of ROS and hydrogen peroxide and activity of catalase, the main scavenger of H_2O_2; (2) lipid peroxidation, one of the most common indicators of free radical formation and a key indicator of oxidative stress; and (3) activation of NF-κB, the master transcription factor in the control of molecular pathways related to oxidative stress. All these indices were increased in steatotic cells.

Incubation of steatotic cells with silybin 50 µmol/L significantly reduces TG accumulation likely by promoting lipid catabolism pathways, as suggested by the up-regulation of PPARα and PPARδ, and by inhibiting lipogenic pathways, as suggested by the down-regulation of PPARγ. In fact, PPARα and PPARδ stimulation is known to promote hepatic fatty acid oxidation, and one of the strategies for improving lipid metabolism in metabolic diseases is to use a molecule which can simultaneously activate these two PPARs (Arment et al., 2016), action that seems to be played by silybin. The stimulation of mitochondrial catabolism of FAs by silybin is also indicated by the marked up-regulation of CPT-1, which is the first component and rate-limiting step of mitochondrial β-oxidation as it allows long chain fatty acids (LCFA) to enter the mitochondria. Many studies indeed indicate that the activity of CPT1 determines the rate of LCFA oxidation and that over-expression of CPT1a in cultured cells increases fatty acid oxidation (Eaton, 2002; Rubí et al., 2002). On the other hand, silybin- dependent TG reduction occurred without a significant stimulation of lipophagic pathways and of TG release into the culture medium, as indicated by the unaltered levels of *Atg7* transcripts and extracellular TG content. It is noteworthy that this fact could be important for possible therapeutic applications.

In general, when TG storage inside LDs is inhibited, the extent of liver steatosis decreases, but liver damage might even increase due to excess of reactive free FAs produced by fat oxidation reactions. In fact, Teissier et al. (2004) found that PPAR agonists induce ROS production by stimulating NADPH oxidase activity. By contrast, in our study, the reduction in fat accumulation exerted by silybin in the steatotic hepatocytes is associated with the improvement of the oxidative unbalance caused by lipid excess as demonstrated by the reduction in lipid peroxidation (MDA levels, namely), catalase activity and NF-κB activation.

Taken together, our results suggest that the antioxidant capacity of silybin effectively counteracts the possible damaging effects of a high rate of fat catabolism which is stimulated in the attempt to reduce excess FA accumulation. This step occurs by neutralizing the free radicals produced by fat oxidation reactions, thus rendering unnecessary the TG synthesis as a protection against toxic and proapoptotic effects of excess FAs (Ricchi et al., 2009).

In conclusion, the present study points to the cellular modulatory and protective effect of silybin with respect to lipid accumulation, expression of lipid metabolism genes, TG secretion, and FA-driven oxidative stress. This study fits with prior studies investigating the beneficial effects of silybin on liver steatosis in animal models (Grattagliano et al., 2013), on inflammation and fibrosis in human hepatic stellate cells (Trappoliere et al., 2009) and in patients with NAFLD and metabolic disorders (Loguercio et al., 2012). Therefore silybin could represent a promising molecule for therapy of NAFLD and maybe of NASH. The prosecution of our work will be focused on testing the possible efficacy of silybin in NASH.

6.The nutraceutic silybin counteracts excess lipid accumulation and ongoing oxidative stress in an in vitro model of non-alcoholic fatty liver disease progression

Giulia Vecchione[1], Elena Grasselli[1], Federica Cioffi[2], Francesca Baldini[1], Paulo J. Oliveira[3], Vilma A. Sardão[3], Katia Cortese[4], Antonia Lanni[2], Adriana Voci[1], Piero Portincasa[5] and Laura Vergani[1]

[1] DISTAV, Department of Earth, Environment and Life Sciences, University of Genova, Genoa, Italy, [2] Department of Science and Technology, University of Sannio, Benevento, Italy, [3] Center for Neuroscience and Cellular Biology (CNC), University of Coimbra, Coimbra, Portugal, [4] Department of Experimental Medicine (DIMES), University of Genova, Genoa, Italy, [5] Department of Biomedical Sciences and Human Oncology, University of Bari Medical School, Bari, Italy

Front Nutr. 2017 Sep 19;4:42. doi: 10.3389/fnut.2017.00042. eCollection 2017.

ABSTRACT

Non-alcoholic fatty liver disease (NAFLD) is a major cause of liver-related morbidity and mortality. Oxidative stress and release of pro-inflammatory cytokines, such as tumor necrosis factor α (TNFα), are major consequences of hepatic lipid overload, which can contribute to progression of NAFLD to non-alcoholic steatohepatitis (NASH). Also, mitochondria are involved in the NAFLD pathogenesis for their role in hepatic lipid metabolism. Definitive treatments for NAFLD/NASH are lacking so far. Silybin, the extract of the milk thistle seeds, has previously shown beneficial effects in NAFLD. Sequential exposure of hepatocytes to high concentrations of fatty acids (FAs) and TNFα resulted in fat overload and oxidative stress, which mimic in vitro the progression of NAFLD from simple steatosis (SS) to steatohepatitis (SH). The exposure to 50 μM silybin for 24 h reduced fat accumulation in the model of NAFLD progression. The in vitro progression of NAFLD from SS to SH resulted in reduced hepatocyte viability, increased

apoptosis and oxidative stress, reduction in lipid droplet size, and up- regulation of IκB kinase β-interacting protein and adipose triglyceride lipase expressions. The direct action of silybin on SS or SH cells and the underlying mechanisms were assessed. Beneficial action of silybin was sustained by changes in expression/activity of peroxisome proliferator-activated receptors and enzymes for FA oxidation. Moreover, silybin counteracted the FA-induced mitochondrial damage by acting on complementary pathways: (i) increased the mitochondrial size and improved the mitochondrial cristae organization; (ii) stimulated mitochondrial FA oxidation; (iii) reduced basal and maximal respiration and ATP production in SH cells; (iv) stimulated ATP production in SS cells; and (v) rescued the FA- induced apoptotic signals and oxidative stress in SH cells. We provide new insights about the direct protective effects of the nutraceutic silybin on hepatocytes mimicking *in vitro* NAFLD progression.

Keywords: non-alcoholic fatty liver disease, non-alcoholic steatohepatitis, FaO hepatoma cells, lipid metabolism, oxidative stress, silybin

INTRODUCTION

Hepatic steatosis is defined as the accumulation of triglycerides (TGs) exceeding 5% of liver weight. Without excess alcohol consumption, the simple steatosis (SS) is named non-alcoholic fatty liver, which may progress to more severe conditions, such as non-alcoholic fatty liver disease (NAFLD), non-alcoholic steatohepatitis (NASH) with hepatocyte injury and lobular and portal inflammation, and non-alcoholic liver cirrhosis with massive fibrosis and vascular remodeling (Brunt et al., 2015), up to hepatocellular carcinoma (Nagaya et al., 2008; Baffy et al., 2012). Patients with NAFLD exhibit peculiar metabolic abnormalities, which include insulin resistance (IR), overweight, and obesity (Yki-Järvinen, 2014). Following the epidemics of obesity, NAFLD has become the leading cause of liver disease in developed countries.

Excess TG deposition in the liver occurs when hepatic availability of fatty acids (FAs) from plasma and/or *de novo* synthesis exceeds hepatic FA disposal by oxidation and TG export as very low-density lipoprotein (Vergani, 2014). TG synthesis is an adaptive, beneficial response in hepatocytes exposed to potentially toxic concentrations of FAs or their metabolites. FAs and cholesterol, especially when accumulated in the mitochondria, are “aggressive” lipids leading to tumor necrosis factor α (TNFα) and reactive oxygen species (ROS) production and acting as early “inflammatory” hits (Berlanga et al., 2014), which contribute to promote NASH (Tilg and Moschen, 2010).

Excess TGs are stored in lipid droplets (LDs), a protective mechanism against FA lipotoxicity. LDs consist of a core of neutral lipids covered by phospholipids and proteins. Adipose differentiation-related protein (ADRP) is the major LD-associated protein, which promotes FA uptake and LD formation (Gao and Serrero, 1999). In fact, the absence of ADRP reduces LD formation and protects against the development of steatosis (Paul et al., 2008). LDs also regulate lipid metabolism and trafficking through a network of molecules localized at the LD surface including the adipose triglyceride lipase (ATGL), which catalyzes the first reaction of TG hydrolysis (Zimmermann et al., 2009). The master regulators of hepatic lipid metabolism are the peroxisome proliferator-activated receptors (PPARs), a family of transcription factors controlling both lipogenic and lipolytic pathways (Huang et al., 2013). FAs are endogenous ligands of all PPAR isofoms (Nakamura et al., 2014); uptake and oxidation of FAs are regulated

mainly by PPARα, while their esterification and conversion to TGs by PPARγ whose expression typically increases in NAFLD (Eberlé et al., 2004).

Mitochondria are the main site for β-oxidation of FAs, which is primarily regulated by carnitine palmitoyltransferase 1 (CPT-1), an enzyme required for transport of long-chain FAs inside mitochondria (Serviddio et al., 2011). Mitochondria play an important role in the pathogenesis and progression of NAFLD, which has been proposed as a mitochondrial disease (Pessayre and Fromenty, 2005). Mitochondrial defects may underlie NAFLD process by altering energetic homeostasis and stimulating ROS production with consequent oxidative stress and impairment of fat oxidation processes (Begriche et al., 2011). In addition to mitochondria, FAs are oxidized in peroxisomes by acyl-CoA oxidase (AOX) and in endoplasmic reticulum (ER) by CYP2E1; both processes lead to the overproduction of ROS and consequent oxidative stress, which triggers progression of steatosis toward NASH (Fromenty and Pessayre, 1995; Seifert et al., 2010).

Moreover, excess lipid accumulation disturbs the ER function, thereby generating ER stress. In the ER, we find the IκB kinase β (IKBKB)-interacting protein (IkBip), a serine kinase that plays a role in the nuclear factor kappa-B (NF-κB) signaling, which is activated by multiple stimuli such as inflammatory cytokines, DNA damages, and other cellular stresses (Choi et al., 2016). NF-kB activation was observed in the livers of obese mice where it causes liver inflammation and apoptosis and increases local and circulating levels of interleukins (Cnop et al., 2012). In contrast, IkBip is associated with the progression of SS to steatohepatitis (SH) as it links steatosis with the activation of apoptotic pathways (Hennig et al., 2014).

While the knowledge of the complex pathophysiological mechanisms involved in the onset and progression of livers steatosis has increased exponentially, a definitive therapy is still missing in NAFLD/NASH patients. Medicinal plants are largely employed as the source of dietary supplements (Baselga-Escudero et al., 2017). Silymarin, the extract from milk thistle (*Silybum marianum*), and its major active compound silybin are hepatoprotective agents for the treatment of liver diseases (Saller et al., 2001). Previous clinical findings evidenced the efficacy of silybin on improving IR and liver injury in patients with NAFLD (Federico et al., 2006) and in lowering some hepatic enzymes in patients with NASH (Solhi et al., 2014). Moreover, silybin improved liver histology in a multicenter randomized controlled trial

(Loguercio et al., 2012). However, the direct hepatoprotective activity of silybin in both non-alcoholic steatosis and SH remains to be elucidated and the possible mechanisms involving a potential anti-inflammatory effect require deeper investigations.

The present study aimed to clarify whether silybin may favorably affect lipid and radical homeostasis in *in vitro* model of NAFLD progression induced by sequential exposure of hepatoma FaO cells to high concentrations of FAs and TNFα. The experimental protocol mimics what occurs *in vivo* where chronically elevated levels of FAs induce IR in many organs and fat accumulation in the liver. In the adipose tissue, IR enhances lipolysis and increases the delivery of adipose-derived FAs to the liver. In contrast, in adipocytes FA excess increases TNFα production, which act on the liver by promoting inflammation and oxidative stress (Berlanga et al., 2014). Therefore, TNFα is the first inflammatory molecule linked with IR (Lang et al., 1992) and high serum levels of TNFα have been found in patients with NASH compared with healthy subjects (Crespo et al., 2001). TNFα plasma levels correlate positively with the grade of liver fibrosis assessed by ultrasound-guided liver biopsy in patients with advanced stages of NAFLD (Lesmana et al., 2009). For this reason, we choose TNFα as the second hit to model *in vitro* NAFLD progression.

Our results show that silybin reduced excess TG accumulation in the *in vitro* models of both steatosis and SH. Changes in the expression of transcription factors such as PPARs and of enzymes for mitochondrial, peroxisomial, and ER oxidations of FAs have been evidenced. In particular, silybin rescued the FA-induced mitochondrial dysfunction as well as apoptotic signals and oxidative stress characteristic of SH condition.

MATERIALS AND METHODS

Cell Treatments

Rat hepatoma FaO cells (European Collection of Cell Cultures, Sigma-Aldrich Corp.) (Clayton et al., 1985) were grown in Coon's modified Ham's F12 with 10% fetal bovine serum. Cells were grown until 80% confluence, incubated in high-glucose medium with 0.25% bovine serum albumin (BSA) to increase stability and solubility of FFA (Joshi-Barve et al., 2007). A condition mimicking human steatosis (SS) was induced by incubating FaO cells for 3 h with oleate/palmitate mixture (2:1 M ratio, final concentration 0.75 mM). A SH condition was mimicked by incubating SS cells for 24 h with 10 ng/mL TNFα (Zhang et al., 2010). After replacing the medium, both SS and SH cells were treated for 24 h with 50 µM silybin (S) [Istituto Biochimico Italiano (IBI), Lorenzini, Italy]. Silybin stock (10 mM) was prepared in dimethyl sulfoxide.

Cell Viability and Apoptosis

For both resazurin and sulforhodamine B (SRB) assays 1.5×10^4 cells/well were seeded in 96-well plates. For resazurin assay, after treatment, the medium was removed and cells were incubated for 30 min with medium supplemented with 10 µg/mL resazurin. The reduction of resazurin to resorufin, indicative of metabolic activity, was measured fluorimetrically (λ_{exc} 570 nm; λ_{em} 600 nm) in Biotek-Cytation 3 reader (Biotek Instruments, Winooski, VT, USA) (Voytik-Harbin et al., 1998). For SRB assay, cells were fixed with ice-cold methanol containing 1% acetic acid for 30 min and then incubated with 0.5% SRB in 1% acetic acid for 1 h at 37°C. The unbound dye was removed with 1% acetic acid solution. The dye bound to proteins was extracted with 10 mM Tris-base solution pH 10, and absorbance was measured at 540 nm (Vichai et al., 2006).

For apoptosis assessment, cells were collected and the pellet resuspended in 20 mM HEPES/NaOH pH 7.5, 250 mM sucrose, 10 mM KCl, 2 mM $MgCl_2$, 1 mM EDTA, 2 mM dithiothreitol (DTT), and 100 µM phenylmethylsulfonyl fluoride (PMSF), a protease-inhibitor cocktail (1 µg/mL of leupeptin, antipain, chymostatin, and pepstatin A). Caspase 3-like activity was measured in cell extracts containing 25 µg protein determined by the bicinchoninic acid method using BSA as a standard (Wiechelman et al., 1988). For calibration, known concentrations of p-nitroanilide (pNA) were measured. Cell extracts were incubated

for 1 h at 37°C in 25 mM Hepes pH 7.5, 10% sucrose, 10 mM DTT, 0.1% CHAPS, and 100 µM caspase substrate Ac-DEVD-pNA; the pNA released after cleavage from the substrate was measured. The results are expressed as amount of nanomoles of pNA released per microgram of protein (Moreira et al., 2014).

TG Content

Cells were scraped and lysed. Lipids were extracted using the chloroform/methanol (2:1) method (Grasselli et al., 2010). TG content was quantified spectrophotometrically by using "Triglycerides liquid" kit (Sentinel, Milan, Italy) in a Varian Cary-50Bio spectrophotometer (Agilent, Milan, Italy). Values were normalized to protein content. Data are expressed as percent TG content relative to controls.

LD Imaging

Cells grown on coverslips were rinsed with phosphate-buffered saline (PBS) pH 7.4 and fixed with 4% paraformaldehyde for 20 min at room temperature. Slides were incubated with 1 µg/mL BODIPY 493/503 (Molecular Probes, Life technologies, Monza, Italy) in PBS for 30 min (Grandl and Schmitz, 2010). After washing and mounting with 4',6-diamidino-2- phenylindole (DAPI) (ProLong Gold medium with DAPI; Invitrogen) slides were examined by Nikon Eclipse E80i light microscope (Nikon, Tokyo, Japan) equipped with the standard epifluorescence filter set up. Images were captured under oil with a 100× plan apochromat objective. Analyses were performed on two independent experiments measuring at least 40 cells for each treatment using the ImageJ software.

Mitochondria Imaging

Cells grown on µ-slides eight-well ibiTreat (Ibidi, Germany) were incubated with 50 nM tetramethylrhodamine ethyl ester (TMRE) and 1 µg/µL Hoechst for 30 min at 37°C in the dark. A lower concentration of $TMRM^+$ was maintained in the medium to avoid leakage from mitochondria. Cells were observed under a Nikon Eclipse Ti-S microscope. Images were obtained through LSM Image Browser (Scaduto and Grotyohann, 1999).

Electron Microscopy

Cells grown on glass chamber slides (Lab-Tek, Nunc, 177380) were washed in 0.1 M

cacodylate buffer and fixed in 0.1 M cacodylate buffer containing 2.5% glutaraldehyde for 1 h at room temperature. Cells were post-fixed in osmium tetroxide for 2 h and 1% uranyl acetate for 1 h. Samples were dehydrated through a graded ethanol series and flat embedded in resin (Poly-Bed; Polysciences, Inc., Warrington, PA, USA) for 24 h at 60°C. Ultrathin sections (50 nm) were cut parallel to the substrate until reaching the apical surface, stained with 5% uranyl acetate in 50% ethanol, and observed with CM10 electron microscope (Philips, Eindhoven, the Netherlands), images were taken with a Megaview 3 camera. Mitochondrial number and size were assessed in 12 randomly taken images at 25k magnification for each treatment. The mitochondrial length (major axis) and width (minor axis) were measured with iTEM software package (Olympus-SYS). Statistical analysis for mitochondrial diameter was performed using the Mann–Whitney test. The total number of mitochondria and mitochondrial cristae was manually scored. Statistical analysis was performed with Student's *t*-test.

Catalase Activity

Catalase activity was evaluated spectrophotometrically in both 12,000 × *g* of supernatant and pellet of hepatocyte lysates (Aebi, 1984). Catalase specific activity was expressed as micromoles of decomposed H_2O_2 per minute per milligram of sample protein. Data are expressed as percent relative to controls.

Lipid Peroxidation

Lipid peroxidation was determined through the thiobarbituric acid reactive substances assay based on the reaction of malondialdehyde (MDA; 1,1,3,3-tetramethoxypropane) with thiobarbituric acid (TBA) (Iguchi et al., 1993). Briefly, 1 vol of cell suspension was incubated for 45 min at 95°C with 2 vol of TBA solution (0.375% TBA, 15% trichloroacetic acid, 0.25 N HCl) and, then, 1 vol of *N*-butanol was added and the absorbance of the organic phase was measured spectrophotometrically. Results were expressed as picomoles MDA per milliliter/milligram protein. Data are expressed as percent relative to controls.

8-Hydroxy-2-Deoxy Guanosine (8-OHdG) Release

The 8-OHdG excreted into the medium after DNA repair/turnover was quantified using DNA/RNA Oxidative Damage ELISA kit (Cayman Chemical Company, MI, USA). Samples were

analyzed in duplicate. Standard 8-OHdG was assayed over a concentration range of 10.3–3,000 pg/mL (Chen et al., 1996). Results were expressed as picogram 8-OHdG per milliliter

RNA Extraction and Real-time Quantitative PCR (qPCR)

RNA was isolated using Trizol reagent, cDNA was synthesized, and real-time qPCR performed in quadruplicate using 1× IQ™SybrGreen SuperMix and Chromo4™ System apparatus (Bio-Rad, Milan, Italy) (Grasselli et al., 2014). The relative quantity of target mRNA was calculated by the comparative Cq method using glyceraldehyde 3-phosphate dehydrogenase (GAPDH) as housekeeping gene and expressed as fold induction with respect to controls (Pfaffl, 2001). Primer pairs designed *ad hoc* starting from the coding sequences of *Rattus norvegicus* and synthesized by TibMolBiol (Genova, Italy) are listed in Table 1.

TABLE 1 | Primer sequences table.

Primer name	Primer sequence (5′→3′)	Annealing temperature (°C)	Accession ID
Adipose differentiation-related protein (ADRP) Fwd	CCGAGCGTGGTGACGAGGG	64	AAH85861
ADRP Rev	GAGGTCACGGTCCTCACTCCC		
Glyceraldehyde 3-phosphate dehydrogenase (GAPDH) Fwd	GACCCCTTCATTGACCTCAAC	60	DQ403053
GAPDH Rev	CGCTCCTGGGAAGATGGTGATGGG		
IκB kinase β-interacting protein (IkBip) Fwd	CAGAACAGTGAGCAGGCAAG	60	NM_001009430.2
IkBip Rev	ACGGCATTCTCTATGGTTGG		
Peroxisome proliferator-activated receptor (PPAR)α Fwd	CCCCACTTGAAGCAGATGACC	60	NM_013196
PPARα Rev	CCCTAAGTACTGGTAGTCCGC		
PPARγ Fwd	CGGAGTCCTCCCAGCTGTTCGCC	60	Y12882
PPARγ Rev	GGCTCATATCTGTCTCCGTCTTC		
PPARδ Fwd	AATGCCTACCTGAAAAACTTCAAC	60	AJ306400.1
PPARδRev	TGCCTGCCACAGCGTCTCAAT		
Carnitine palmitoyltransferase 1 (CPT-1) Fwd	CCGCTCATGGTCAACAGCA	60	NM_031559
CPT-1 Rev	CAGCAGTATGGCGTGGATGG		
CYP2E1 Fwd	ACCTTCAGTCACTGGACATCAA	60	BC081774
CYP2E1 Rev	AGGATCAGGAGCCCATATCTC		
Adipose triglyceride lipase (ATGL) Fwd	CGGTGGATGAAGGAGCAGACA	60	NM_001108509
ATGL Rev	TGGCACAGACGGCAGAGACT		
APE1 Fwd	CAGATCAGAAAACGTCAGCCAG	60	NM_024148.1
APE1 Rev	GGTCTCTTGGAGGCACAAGATG		
POLG Fwd	GAAGAGCGTTACTCTTGGACCAG	62	NM_053528.1
POLG Rev	AACATTGTGCCCCACCACTAAC		
COII Fwd	TGAGCCATCCCTTCACTAGG	60	X14848.1
COII Rev	TGAGCCGCAAATTTCAGAG		
β-Actin Fwd	CTGCTCTTTCCCAGATGAGG	60	NM_031144.2
β-Actin Rev	CCACAGCACTGTAGGGGTTT		

mtDNA Copy Number

DNA extracted using Genomic-tip 20/G kit (Qiagen, Valencia, CA, USA) was quantified using the PicoGreen dsDNA reagent (Invitrogen, Milan, Italy). Relative mtDNA copy numbers were measured by qPCR using iQ5 System Apparatus (Bio-Rad) and corrected by simultaneous measurement of nuclear DNA. Amplification of mitochondrial cytochrome *c* oxidase subunit

II (COII, mitochondrial-encoded gene) and β-actin (nuclear-encoded gene) was performed using the primers listed in Table 1. The mtDNA content was calculated using ΔCt = average Ctnuclear DNA − average CtmtDNA and, then, was obtained using the formula mtDNA content = 2(2ΔCt).

Western Blotting

In nuclear homogenates, NF-kB/p65 was detected by Western blot. Cellular pellet was suspended in 400 µL ice-cold Buffer A (20 mM Tris-HCl pH 7.8, 50 mM KCl, 10 µg/mL Leupeptin, 0.1 mM DTT, 1 mM PMSF) and 400 µL Buffer B (Buffer A plus 1.2% Non-indet P40). After vortex and centrifugation (14,000 × *g* for 30 s, 4°C) the nuclear pellet was washed with 400 µL Buffer A, resuspended in 100 µL Buffer B, mixed in ice for 15 min, and centrifuged (14,000 × *g* for 20 min, 4°C). The supernatant containing nuclei was collected, and 30–50 µg proteins were electrophoresed on SDS polyacrylamide gel electrophoresis (Laemmli, 1970). Membrane was blocked for 1 h in 5% fat-free milk/PBS (pH 7.4), probed overnight using rabbit anti-human NF-kB p65 (SC-109; Santa Cruz Biotechnology, DBA, Milan, Italy) in PBST buffer (PBS 0.1% Tween 20) at 4°C (Towbin et al., 1979), and then washed and incubated with horseradish peroxidase-conjugated rabbit anti-mouse IgG (Sigma-Aldrich) in PBST for 1 h at room temperature. Immune complexes were visualized using chemiluminescence western blotting analysis system (Bio-Rad ChemiDoc XRS System). Films were digitized and band optical densities were quantified against the actin band and expressed as Relative Optical Density (ROD, arbitrary units). ROD of each band was expressed as percentage respect to control.

Oxygen Consumption

Oxygen consumption was measured at 37°C using Seahorse XFe96 Extracellular Flux Analyzer (Seahorse Bioscience, Germany). About 2×10^4 cells/well were seeded in 96-well plates. In parallel, an XFe96 sensor cartridge for each cell plate was placed in a 96-well calibration plate containing 200 µL/well calibration buffer and left to hydrate overnight at 37°C. Medium was replaced with 200 µL/well of low-buffered serum-free medium pH 7.4 left at 37°C for 1 h without CO_2 to allow de-gassing the plate. A final concentration of 3 µM oligomycin, 1 µM carbonyl cyanide-4-(trifluoromethoxy)phenylhydrazone (FCCP), and a mixture of 1 µM rotenone and 1 µM antimycin were added sequentially to cells from prot A, B, and C,

respectively. A total of 25 µM of each compound was pre-loaded into the ports of each well in the XFe96 sensor cartridge. The sensor cartridge and the calibration plate were loaded into the XFe96 Extracellular Flux Analyzer for calibration, and then, the calibration plate was replaced with the study plate. Three baseline rate measurements of oxygen consumption rate (OCR) were made using a 3 min mix and 3 min measure cycle. The compounds were injected pneumatically by the XFe96-Analyzer into each well, mixed, OCR measurements made using the 3 min mix and 3 min measure cycle (Deus et al., 2015).

Statistical Analysis

Data are expressed as mean ± SD of at least three independent experiments in triplicate. Statistical analysis was performed using ANOVA with Tukey's post-test (GraphPad Software, Inc., San Diego, CA, USA).

RESULTS

Effects of Silybin on Intracellular Fat Overload

Intracellular TG content increased significantly and to a similar extent in steatotic (SS) (+109%; $p \leq 0.001$) and in SH (+90%; $p \leq 0.001$) cells compared to control (Fig. 1A). Exposure to silybin 50 µM did not affect the TG content of control cells (data not shown) but significantly decreased to a similar extent the TG content in both SS and SH cells (−38 and −30%, respectively; $p \leq 0.001$ *vs* their counterpart).

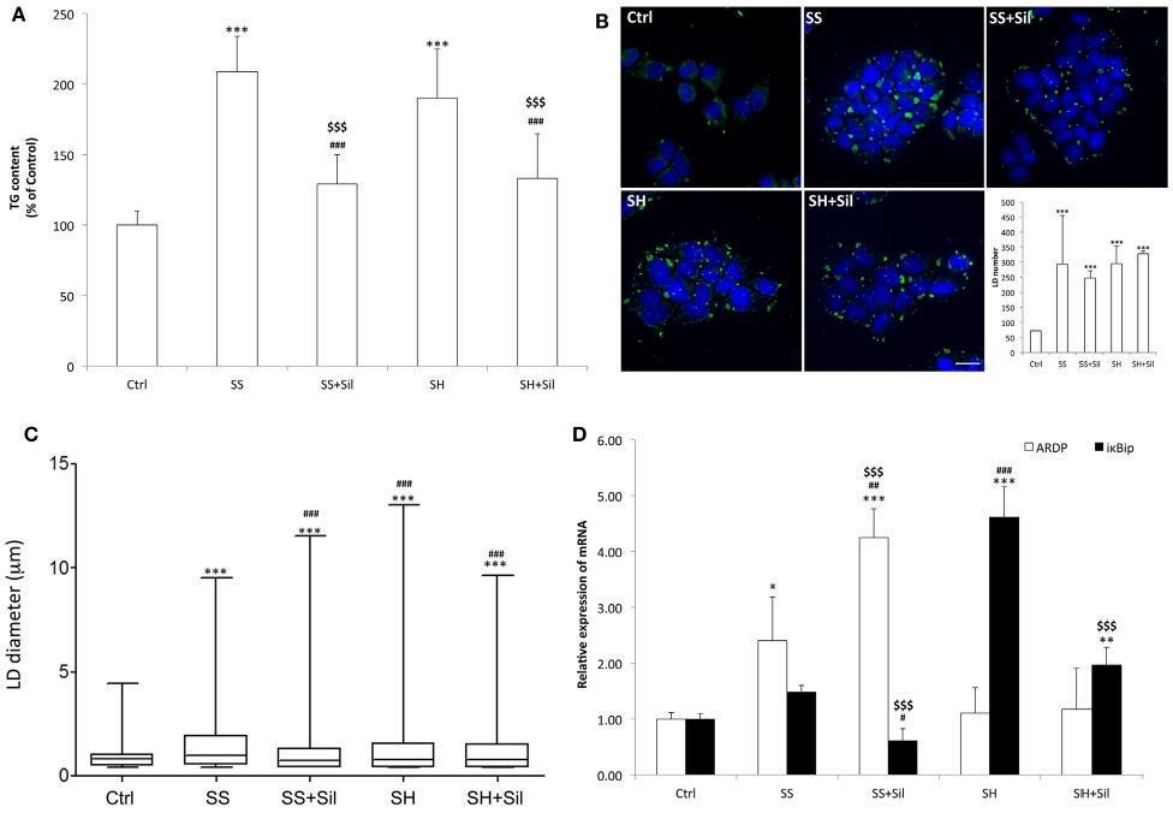

Figure 7. Effect of silybin on lipid accumulation

Lipid accumulation parameters were measured in FaO cells incubated in the absence (Ctrl) or in the presence of fatty acids [simple steatosis (SS)] or fatty acids and tumor necrosis factor α (TNFα) [steatohepatitis (SH)] and subsequently treated with 50 µM silybin (SS + Sil or SH + Sil, respectively). **(A)** Intracellular triglyceride (TG) content quantified by spectrophotometric assay. Data are expressed as percent TG content relative to control and normalized for total proteins determined with bicinchoninic acid (BCA). Values are mean ± SD from at least three independent experiments. **(B)** Lipid droplets (LDs) visualized by fluorescence microscopy using BODIPY 493/503 (green fluorescence) and nuclei visualized by 4',6-diamidino-2- phenylindole (DAPI) (blue fluorescence) (magnification 100×; scale bar: 10 µm). Representative images and the average LD number for all the experimental conditions were also shown. **(C)** Average LD size measured on two independent

experiments (40 cells per treatment for each experiment) by using Huygens professional suite software. The results were plotted as box-and-whisker plot, showing the interquartile range, the median as horizontal bar and the whiskers are the minimum and maximum values. **(D)** The mRNA expression of adipose differentiation-related protein (ADRP) and IκB kinase β-interacting protein (IkBip) evaluated by quantitative PCR (qPCR); glyceraldehyde 3-phosphate dehydrogenase (GAPDH) was used as the internal control and data expressed as fold induction with respect to controls. ANOVA followed by Tukey's test was used to assess the statistical significance between groups. Significant differences are denoted by symbols: Ctrl vs all treatments ***p ≤ 0.001, **p ≤ 0.01, *p ≤ 0.05; simple steatosis (SS) vs all treatments ###p ≤ 0.001, ##p ≤ 0.01, #p ≤ 0.05; steatohepatitis (SH) vs all treatments $$$p ≤ 0.001.

Lipid accumulation was associated to increased number and size of LDs, as visualized by BODIPY staining. At fluorescence microscopy, control cells showed few (about 72 LDs/cell) and small (0.9 μm average diameter) LDs, which were dispersed in the cytosol (Fig. 1B, C). In SS, we observed an increase in both number (294 LDs/cell) and size (1.5 μm) of LDs, with average diameter increasing of about +67% ($p \leq 0.001$) compared to controls, and sylibin reduced the LD diameter to a value similar to controls (1.1 μm; $p \leq 0.001$) (Fig. 1B, C). In contrast, SH cells displayed a LD number similar to that of SS cells but a LD size slightly lower (1.3 μm) (Fig. 1B, C); silybin did not affect LD size.

The mRNA levels of ADRP and IkBip, two markers of LDs and NAFLD progression, respectively, were analyzed by qPCR (Fig. 1D). Excess lipid accumulation in SS cells resulted in up-regulation of ADRP expression (2.4-fold induction vs control; $p \leq 0.05$) that was further stimulated by silybin (4.2-fold induction compared to control; +77% vs SS; $p \leq 0.01$). In SH cells, ADRP expression was at a level similar to control and it was unaffected by silybin. In regard to IkBip expression, we observed only a small, non-significant up-regulation in SS cells, while it was dramatically up-regulate in SH cells (4.6-fold induction compared to control; $p \leq 0.001$). Exposure to silybin greatly and comparably reduced IkBip expression in both SS (−59% with respect to SS; $p \leq 0.05$) and SH (−57% with respect to SH; $p \leq 0.001$) cells. Sylibin did not affect ADRP and IkBip expression in control cells (data not shown).

Effects of Silybin on Lipid Metabolism

Lipid metabolism is regulated by PPARs, the main transcription factors for lipolytic and lipogenic genes (48). The mRNA level of PPARs was assessed by qPCR (Figure (Figure2A).2A). As compared to control cells, SS cells showed a significant increase in expression of PPARα and PPARγ (1.29-fold induction, p ≤ 0.05; 2.8-fold induction, p ≤ 0.001, respectively), and a

down-regulation of PPARδ (about 0.55-fold induction; $p \leq 0.05$). The lipid-lowering action of silybin was sustained by increased expression of PPARα (2.6-fold induction compared to controls; +99% compared to SS, $p \leq 0.01$), decreased expression of PPARγ (1.6-fold induction compared to controls, −42% compared to SS; $p \leq 0.05$), and increased expression of PPARδ (1.6-fold induction compared to controls; +193% compared to SS, $p \leq 0.001$). In SH hepatocytes, the profile of PPARα and PPARγ expression was similar to SS, whereas PPARδ expression showed values similar to controls. Exposure of SH cells to silybin reduced transcription of both PPARα (1.1-fold induction compared to controls; −39% compared to SH, $p \leq 0.05$) and PPARγ (1.5-fold induction compared to controls; −48% compared to SH, $p \leq 0.01$), without affecting PPARδ expression.

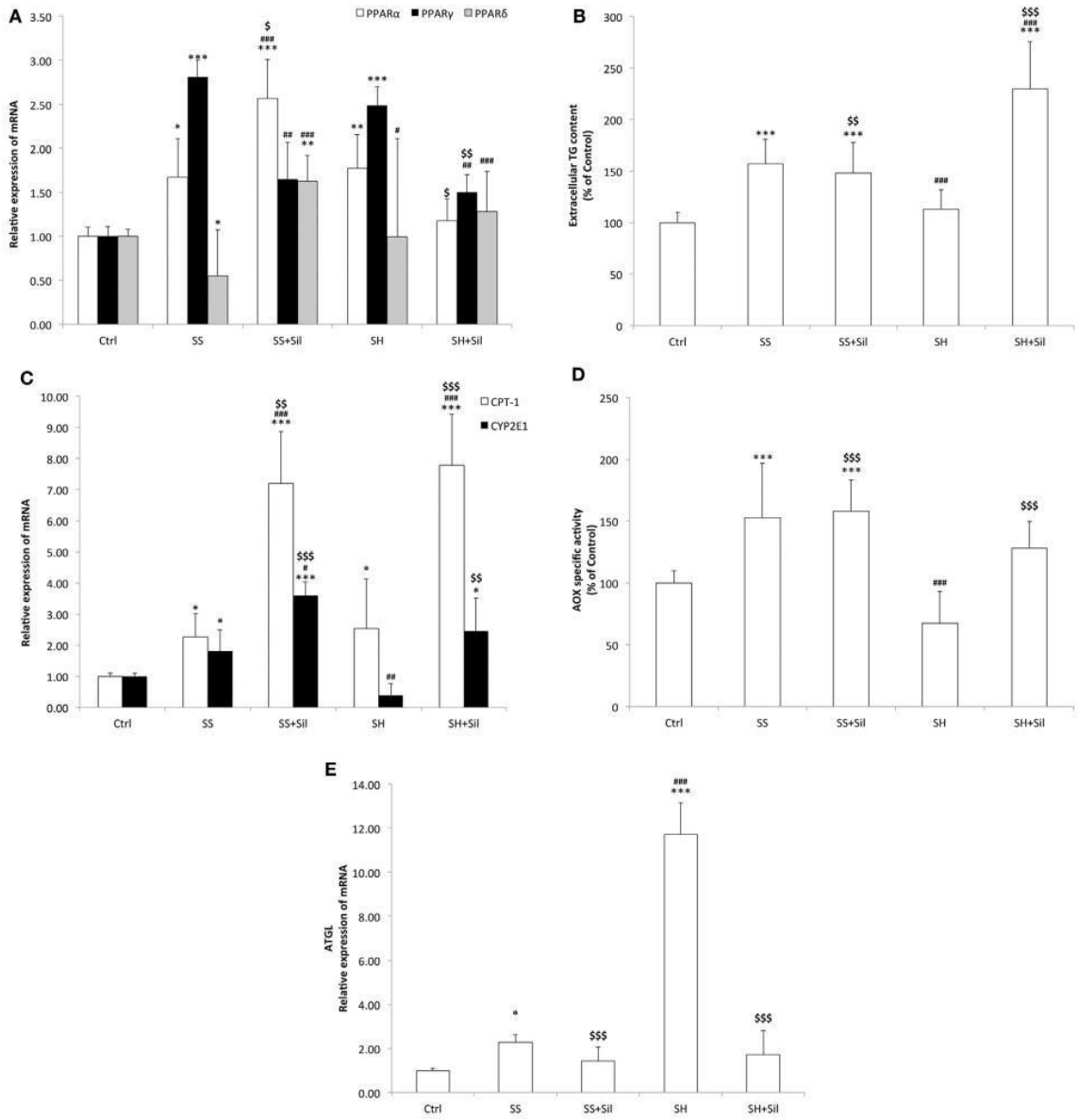

Figure 8. Effect of Silybin on lipid metabolism

In FaO cells treated as described above the following parameters were evaluated: **(A)** The mRNA expression of peroxisome proliferator-activated receptor (PPAR) α, PPARγ, and PPARδ by quantitative PCR (qPCR). **(B)** The extracellular triglyceride (TG) content by spectrophotometric analysis. **(C)** The mRNA expression of carnitine palmitoyltransferase 1 (CPT-1) and CYP2E1 by qPCR. **(D)** The enzymatic activity of peroxisomial acyl CoA oxidase (AOX) (nmol H2O2/min/mg protein) by using spectrophotometric assay. Data are expressed as percentage values with respect to controls and normalized for total proteins. **(E)** The mRNA expression of adipose triglyceride lipase (ATGL) by quantitative PCR (qPCR). For qPCR experiments, glyceraldehyde 3-phosphate dehydrogenase (GAPDH) was used as the internal control and data were expressed as fold induction with respect to controls. Values are mean ± SD from at least three independent experiments. ANOVA followed by Tukey's test was used to assess the statistical significance between groups. Significant differences are denoted by symbols: Ctrl vs all treatments ***p ≤ 0.001, **p ≤ 0.01, *p ≤ 0.05; simple steatosis (SS) vs all treatments ###p ≤ 0.001, ##p ≤ 0.01, #p ≤ 0.05; steatohepatitis (SH) vs all treatments $$$p ≤ 0.001, $$p ≤ 0.01, and $p ≤ 0.05.

The lipid-lowering action of silybin could be sustained by increased TG secretion, since SS cells released more TGs into culture medium than controls (+157%; $p \leq 0.001$). The addition of silybin 50 μM did not modify this picture. In SH cells, a significant reduction in TG secretion was observed compared to SS (−28%; $p \leq 0.001$). The addition of silybin counteracted this condition as TG secretion was stimulated (+103% with respect to SH; $p \leq 0.001$) (Fig. 2B).

In contrast, TG accumulation might be also reduced by stimulation of oxidative pathways taking place in mitochondria, peroxisomes, and ER (Grasselli et al., 2014). Thus, mitochondrial CPT-1 and peroxisomal AOX for β-oxidation and microsomal cytochrome P450 (CYP) 2E1 for ω-oxidation were assessed. The mRNA levels of CPT-1 were significantly up-regulated in both SS and SH cells (2.44- and 2.91-fold inductions, respectively; $p \leq 0.05$) and further increased upon incubation with silybin (+199% and +164 with respect to SS and SH cells, respectively; $p \leq 0.001$) (Fig. 2C). CYP2E1 expression was up-regulated in SS cells (2.20-fold induction; $p \leq 0.001$) and was further increased upon incubation with silybin (+63% with respect to SS; $p \leq 0.001$), whereas in SH hepatocytes, CYP2E1 expression was at basal level and it was markedly increased by silybin (+518 with respect to SH cells; $p \leq 0.01$) (Fig. 2C). In peroxisomes, AOX activity was stimulated in SS cells (+53%, $p < 0.001$ compared to controls), while silybin did not change it. We observed a decrease in AOX activity in SH cells compared to SS (−56% with respect to SS; $p < 0.001$) and an increase upon silybin treatment (+90% with respect to SH cells; $p < 0.001$) (Fig. 2D).

Up-stream of FA oxidation there is ATGL, a lipase controlling lipid mobilization from LDs. A significant increase in ATGL transcripts was observed in SS cells (2.29-fold induction with respect to control; $p \leq 0.05$) and a larger increase in SH cells (11.7-fold induction with respect to controls; $p \leq 0.001$) (Fig. 2E). ATGL mRNA expression was reduced after incubation of SH cells with silybin (−85% compared to SH; $p \leq 0.001$).

Hepatoprotective Effects of Silybin

We observed no significant changes in cell viability in SS cells, whereas a reduced viability was observed in SH cells (−24% compared to control; $p \leq 0.001$) and silybin did not counteract this effect (Fig. 3A). Similar results were supplied by cell density analysis: no significant decrease in cell density occurred in SS cells, while cell density was reduced in SH cells (−26%, compared to control; $p \leq 0.001$) and silybin did not counteract this effect (Fig. 3A). In regard to apoptosis, we observed an increase in the caspase 3-like activity in SS cells (+126% compared to control; $p \leq 0.001$) and a larger increase in SH cells (+219% compared to control; $p \leq 0.001$). Of note, incubation of both SS and SH cells with silybin significantly reduced caspase 3-like activity (−68 and 158%, respectively, in SS + sil and SH + sil; $p \leq 0.01$ and $p \leq 0.001$) (Fig. 3B).

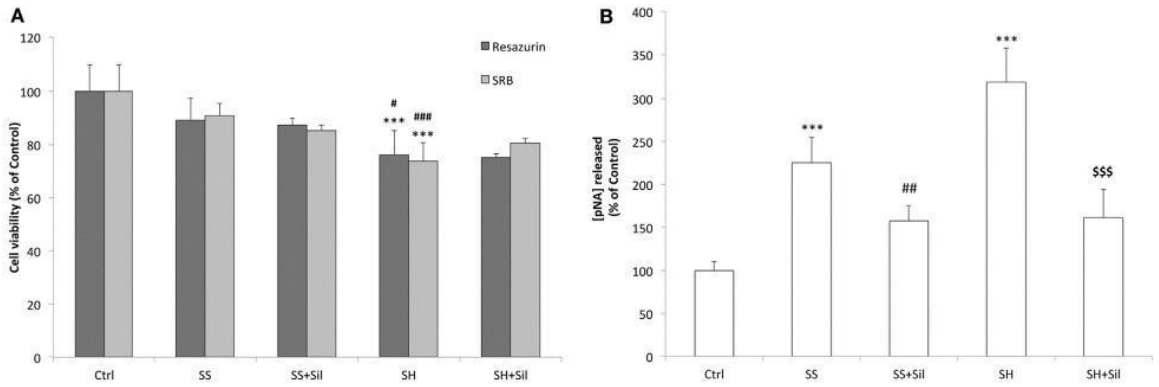

Figure 9. Effect of silybin on cell proliferation and apoptosis

Under the conditions of Figure 1, the following parameters were measured: **(A)** The metabolic activity and the cell mass by resazurin and sulforhodamine B (SRB) assay, respectively. Data are expressed as percentage values with respect to controls. **(B)** The activity of effector caspase 3, measured as p-nitroanilide (pNA) released after cleavage from the substrate (nmoles of pNA released/µg protein). Calibration was done using known concentrations of pNA. Values are mean ± SD from at least three independent experiments. ANOVA followed by Tukey's test was used to assess the statistical significance between groups. Significant differences are denoted by symbols: Ctrl vs all treatments ***p ≤ 0.001; simple steatosis (SS) vs all treatments ###p ≤ 0.001, ##p ≤ 0.01, #p ≤ 0.05; steatohepatitis (SH) vs all treatments $$$p ≤ 0.001.

Effects of Silybin on Mitochondrial Activity and Damage

Mitochondrial respiration was analyzed by using the Seahorse Extracellular Flux Analyzer (Fig. 4). Basal respiration remained unchanged across control, SS, and SH cells; silybin did not affect basal respiration of SS cells, but significantly reduced that of SH cells (−47% with respect to control; $p \leq 0.001$) (Fig. 4A). The proton leak was significantly reduced in both SS and SH cells with respect to controls (−42% and −31%, respectively; $p \leq 0.001$ and $p \leq 0.05$), and silybin did not influence this picture (Fig. 4B). Maximal respiration remained unchanged between control, SS cells, and SS cells exposed to sylibin, but it was significantly increased in SH cells (+12% respect to control, $p \leq 0.05$) and silybin dramatically reduced it (−70%, compared to SH; $p \leq 0.001$) (Fig. 4C). Also, the oxygen consumption associated with ATP production did not change in SS cells, while it increased in SH cells (+20% respect to control; $p \leq 0.05$). Silybin exerted an opposite effect by increasing ATP production in SS cells (+20% respect to SS; $p \leq 0.05$) and decreasing it in SH cells (−56% respect to SH cells; $p \leq 0.001$) (Fig. 4D).

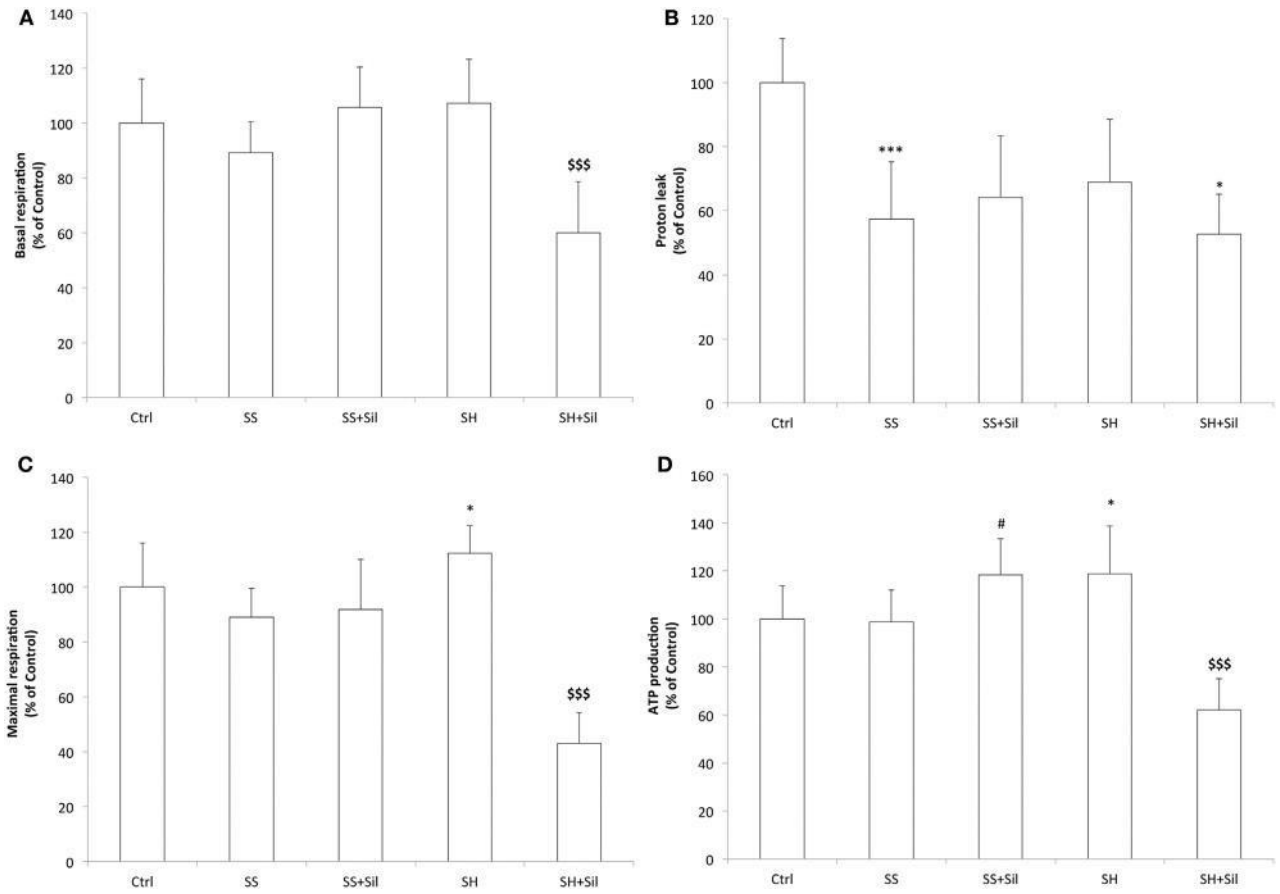

Figure 10. Effect of silybin on mitochondrial oxygen consumption rates (OCRs)

Under the conditions of Figure 1, we measured the cellular OCR by using Seahorse XFe96 Extracellular Flux Analyzer. The following respiratory parameters were evaluated: **(A)** Cell basal respiration (OCR pmol/min/SRB labeling). **(B)** Proton leak (OCR pmol/min/SRB labeling). **(C)** Cell maximal respiration (OCR pmol/min/SRB labeling); **(D)** ATP production (OCR pmol/min/SRB labeling). Data are expressed as mean ± SD of 14 separate experiments. ANOVA followed by Tukey's test was used to assess the statistical significance between groups. Significant differences are denoted by symbols: Ctrl vs all treatments ***p ≤ 0.001, *p ≤ 0.05; SS vs all treatments, #p ≤ 0.05; SH vs all treatments $$$p ≤ 0.001.

To assess possible mitochondria damage, we evaluated the mtDNA copy number and expression of the two main genes involved in mtDNA repair by qPCR (Fig. 5). The mtDNA copy number did not change in SS cells, but it was reduced in SH cells (−43% respect to control; $p \leq 0.05$), and silybin was not able to rescue this damage (Fig. 5A). With regard to the enzymes for DNA repair, SH cells exhibited an increase in mRNA expression of both APE1 (1.50-fold induction compared to control; +68% with respect to SS, $p \leq 0.001$) and POLG (1.45-fold induction compared to control; +75% with respect to control, $p \leq 0.001$), and silybin counteracted this effect (−30% for APE1 and −48% for POLG respect to SH; $p \leq 0.001$) (Fig. 5B).

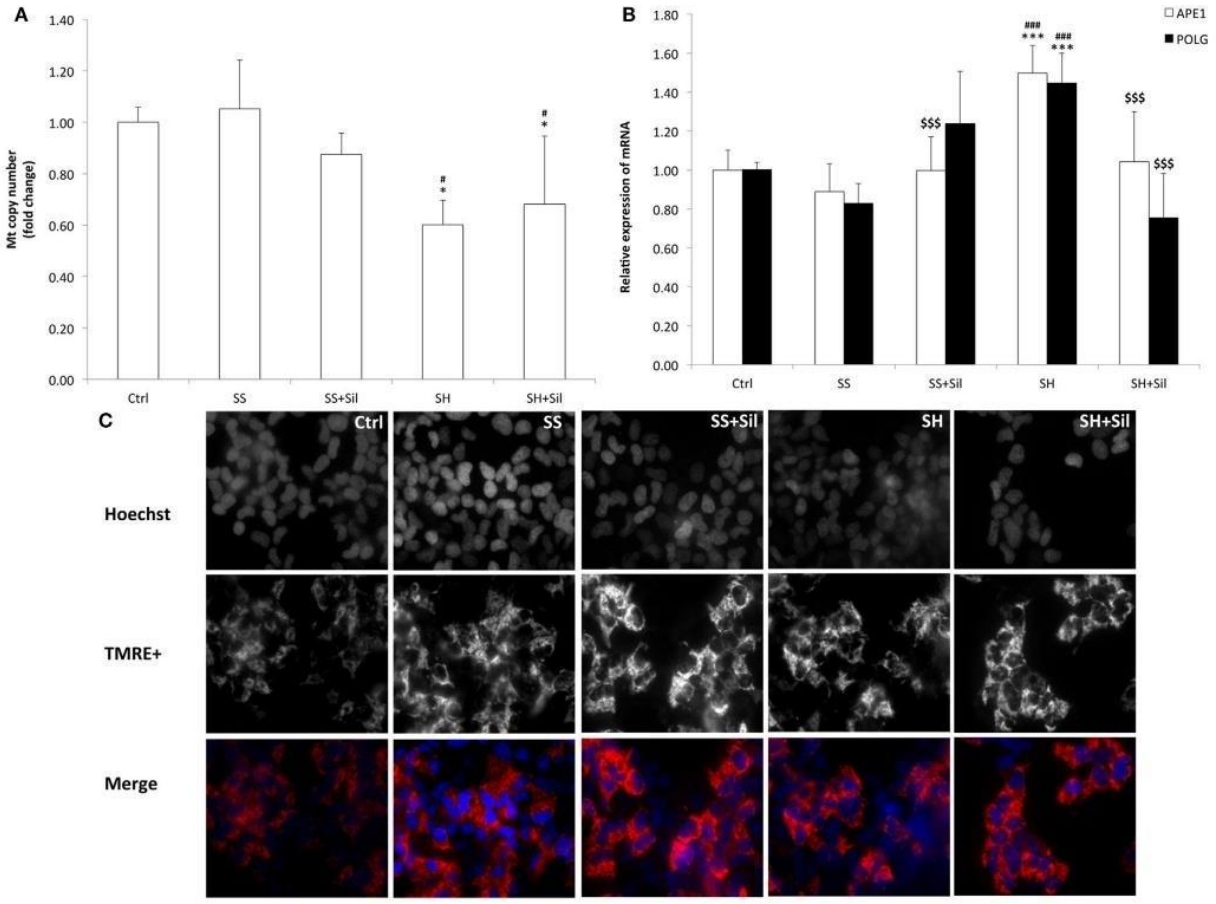

Figure 11. Effect of silybin on mitochondrial DNA (mtDNA) copy number and membrane polarization

Under the conditions of Figure 1, the following parameters were measured: **(A)** mtDNA copy number by quantitative PCR (qPCR) using primer for COII. The nuclear gene β-actin was used as the internal control; data were expressed as fold induction with respect to controls. **(B)** The mRNA expression of APE1 and POLG genes related to mtDNA repair; β-actin was used as the internal control and data were expressed as fold induction with respect to controls. **(C)** The mitochondrial polarization through cell vital staining with TMRE (mitochondria, red fluorescence) and Hoechst33342 (nuclei, blue fluorescence). Representative images for all the experimental conditions are reported separately for each staining (black/white) and then merged in colors. Images were acquired using 40× objective (scale bar 35 μm). Values are mean ± SD from at least three independent experiments. ANOVA followed by Tukey's test was used to assess the statistical significance between groups. Significant differences are denoted by symbols: Ctrl vs all treatments ***p ≤ 0.001, *p ≤ 0.05; simple steatosis (SS) vs all treatments ###p ≤ 0.001, #p ≤ 0.05; steatohepatitis (SH) vs all treatments $$$p ≤ 0.001.

In contrast, fluorescence microscopy of TMRE-stained mitochondria was performed to assess the potential of mitochondrial inner membrane (Fig. 5C). We observed a higher fluorescent signal in SS cells than in control cells, and fluorescence was reduced and less organized in SH cells where it appeared rather diffuse and irregular. Treatment of both SS and SH cells with silybin increased TMRE signal with cells appearing more brilliant compared to untreated counterparts.

Ultrastructural morphology of mitochondria was assessed by EM analysis to measure mitochondrial number, major and minor axe diameters, number, and organization of cristae (Fig. 6A-C). Our results showed that both mitochondrial morphometry and cristae number did not change in SS cells. Upon treatment of SS cells with silybin mitochondria showed a significant increase in size (both major and minor axes, $p \leq 0.001$) and the mitochondrial cristae increased in number and were better organized and parallel to each other's (Fig. 6A-C). In SH cells, mitochondrial size did not change (Fig. 6A, B) and the mitochondrial cristae were largely disorganized and significantly reduced in number compared to SS cells ($p \leq 0.05$) (Fig. 6C). Interestingly, in SH cells, treatment with silybin rescued both the number ($p \leq 0.001$) and the parallel organization of mitochondrial cristae compared to SS cells (Fig. 6C).

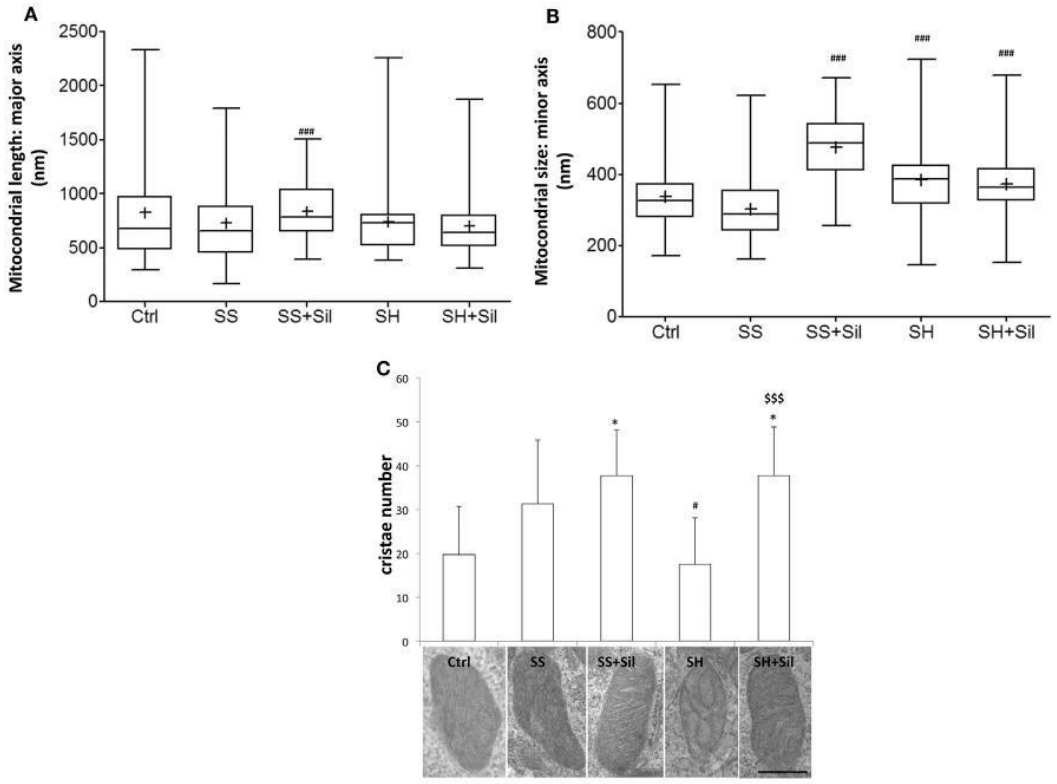

Figure 12. Effect of silybin on mitochondrial shape

Under the conditions of Figure 1, cells were analyzed by electron microscopy and the following parameters were assessed: **(A)** mitochondrial length (major axis) and mitochondrial size (minor axis) **(B)** were measured. The results were plotted as box-and-whisker plot, showing the interquartile range, the median as horizontal bar and the whiskers are the minimum and maximum values. **(C)** Cristae number was also evaluated. Values are mean ± SD from all mitochondria scored in 20 images for each experimental condition. Representative electron micrographs of randomly selected mitochondria from each experimental condition are also shown. (magnification 25k; scale bar: 0.5 μm). Significant differences are denoted by symbols: Ctrl vs all treatments, *p ≤ 0.05; simple steatosis (SS) vs all treatments ###p ≤ 0.001 and #p ≤ 0.05; steatohepatitis (SH) vs all treatments

$$$p ≤ 0.001.

Effects of Silybin on Oxidative Stress

Increased fat oxidation produces excess of ROS, which react with cellular structures leading to lipid peroxidation and DNA oxidative damage, which are classical markers for cellular oxidative stress (Seifert et al., 2010). By measuring lipid peroxidation, we found increased MDA levels in both SS and SH cells with respect to controls (+195 and +255%, respectively; $p \leq 0.001$), which decreased upon incubation with silybin (−49 and −52% with respect to SS and SH cells, respectively; $p \leq 0.001$) (Fig. 7A). When extracellular levels of 8- OHdG were measured as a marker for oxidative DNA damage, a slight but no significant increase was observed in both SH and SS cells, and silybin reduced 8-OHdG levels in both conditions (−49% in SS and −50% in SH cells with respect to their counterparts; $p \leq 0.05$) (Fig. 7B).

The ability of silybin in protecting cells from fat-induced oxidative stress was confirmed by measuring the activity of the antioxidant enzyme catalase and expression of the transcription factor NF-κB, which is activated by oxidative stress. Catalase activity increased in both SS and SH cells with respect to control (+145% and +140%, respectively; $p \leq 0.01$) and decreased upon incubation with silybin (−38% and −65% with respect to SS and SH cells, respectively; $p \leq 0.01$ and $p \leq 0.001$) (Fig. 7C). NF-κB activation did not change significantly in SS and SH cells with respect to controls, but a significant reduction was observed upon exposure to silybin (−29% and −31% with respect to SS and SH cells, respectively; $p \leq 0.05$) (Fig.7D).

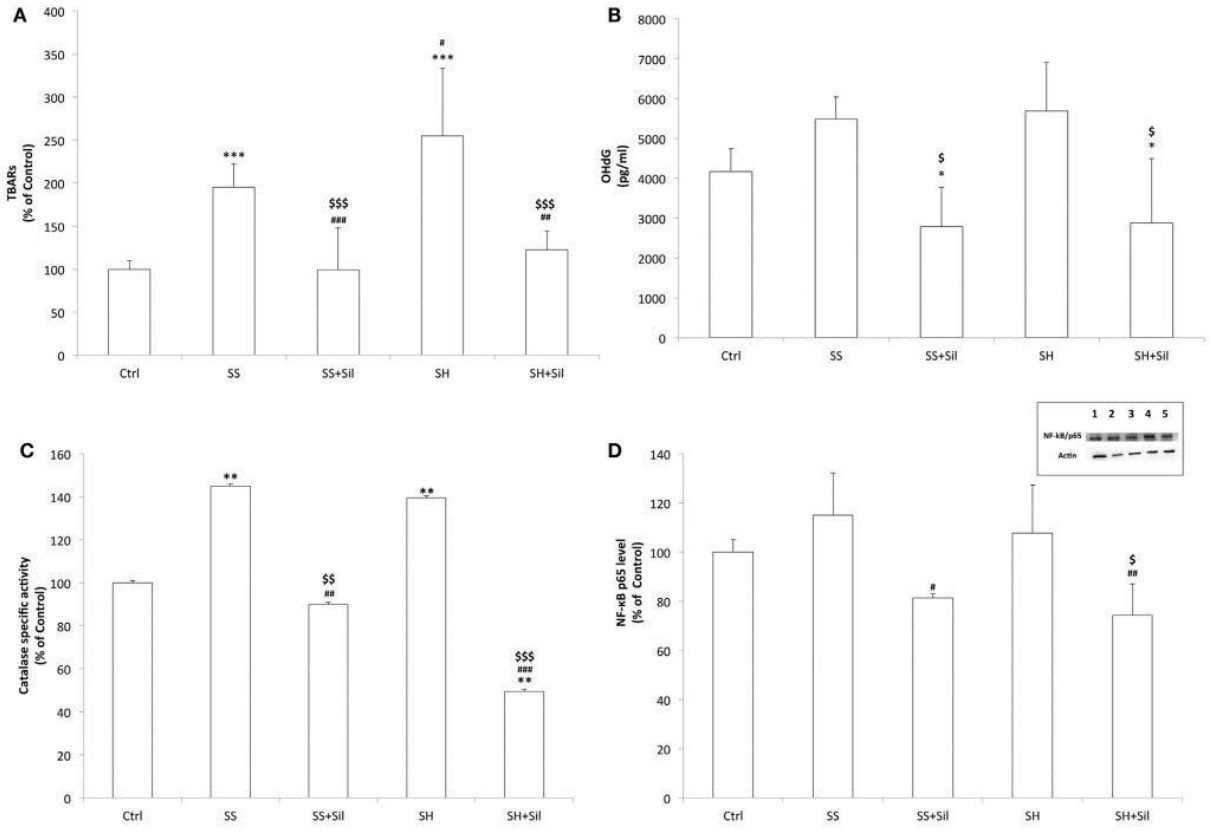

Figure13. Effect of silybin on oxidative stress end-points

Oxidative stress end-points were determined in FaO cells treated under the conditions described in Figure 1: **(A)** the intracellular level of MDA (pmol MDA/mL/mg of proteins) by spectrophotometric thiobarbituric acid reactive substances (TBARS) assay. Data are expressed as percentage values with respect to controls and normalized for total proteins. **(B)** Levels of 8-hydroxy-2-deoxy guanosine (8-OHdG) (pg/mL) released into the culture medium measured by competitive ELISA. **(C)** Catalase enzymatic activity (µmoles of decomposed H2O2/min/mg of proteins) by spectrophotometric assay. Data are expressed as percentage values with respect to controls and normalized for total proteins. **(D)** Densitometric analysis of nuclear nuclear factor kappa-B (NF-κB)/p65 evaluated by Western blotting. Data are expressed as percentage values with respect to controls and normalized for β-actin. Immune complexes were visualized using an enhanced chemiluminescence, quantified using a computerized imaging system (Biorad Quantity One 1-D Analysis Software) and expressed as relative optical density (ROD, arbitrary units). Inset: representative image of NF-κB/p65 immunoreactive bands: control (lane 1), simple steatosis (SS) (lane 2), SS + Sil (lane 3), steatohepatitis (SH) (lane 4), and SH + Sil (lane 5).Values are mean ± SD from at least three independent experiments. ANOVA followed by Tukey's test was used to assess the statistical significance between groups. Significant differences are denoted by symbols: Ctrl vs all treatments ***p ≤ 0.001, **p ≤ 0.01, *p ≤ 0.05; SS vs all treatments ###p ≤ 0.001, ##p ≤ 0.01, #p ≤ 0.05; SH vs all treatments $$$p ≤ 0.001, $$p ≤ 0.01, $p ≤ 0.05.

DISCUSSION

By using a novel cellular model mimicking initiation and progression of NAFLD in vivo, we demonstrated that silybin provides important protective and anti-steatotic effects involving crucial pathways, especially at mitochondrial level. Our model paves the way to simultaneous assessment of morphological and functional characteristics of hepatocytes exposed to the steatogenic and pro-inflammatory hits, thus resulting an optimal and reliable system to test the beneficial and direct effects of silybin, a bioactive compound known for its vague "hepatoprotective" features.

Chronic caloric overload initiates an inflammatory response originating from the adipose tissue with production of cytokines, such as TNFα, that impairs lipid metabolism in remote tissues such as the liver thus promoting the progression of SS to SH (Hotamisligil et al., 1995). Therefore, in our model, we induced a condition mimicking NAFLD progression by exposing SS cell to TNFα for 24 h. NAFLD progression was ascertained by assessing: (i) cell viability, which was not altered in SS cells but was significantly reduced in SH cells; (ii) IkBip expression, a classical liver damage marker, which increased in SS cells and further increased in SH cells; and (iii) caspase activity, a marker of apoptosis, which was stimulated in SS cells and further stimulated in SH cells.

A first result of our study is that TG accumulation did not increase when our SS cells progressed to SH cells, thus suggesting that this experimental system might mimic the so-called burned-out NASH, a NASH sub-type in, which hepatic TG accumulation does not increase with the progression of disease (Nagaya et al., 2010). Interestingly, the progression of SS cells to SH cells was associated to a slightly reduction in LD size and these changes of LD morphometry were paralleled by alterations of ADRP, the main LD-associated protein, which promotes FA uptake and LD enlargement. In fact, ADRP expression increased in SS cells, but it was reduced in SH hepatocytes. Therefore, we can suggest that the worsening of hepatocyte condition in our in vitro model of NAFLD progression may depend on a fragmentation of LDs rather than on an increased fat content per se. Increased LD surface may facilitate the traffic of FAs across LDs and the intracellular environment. In line with this result, ATGL expression showed a very large increase in SH cells; this indicates a high rate of lipid mobilization in SH cells with harmful potentials. According to expectations, we observed

a stimulation of TG secretion in SS cells, a likely attempt to protect cells from excess TG accumulation, while TG secretion was reduced in SH cells, and this impair in lipid release might worsen the damage in lipid homeostasis.

To limit excess fat accumulation, in both SS and SH cells, the systems involved in the mitochondrial oxidation of FAs were stimulated (CPT-1 expression), whereas microsomal (CYP2E1 expression) and peroxisomial (AOX activity) oxidation of FAs were stimulated only in SS cells. Over-active FA oxidation increases production of ROS with consequent oxidative stress, one of the key mechanisms responsible for NAFLD progression (Fromenty and Pessayre, 1995; Seifert et al.,2010). Indeed, in both SS and SH cells, we found a condition of oxidative stress as indicated by the increase in (i) the cellular level of MDA, marker of lipid peroxidation; (ii) the extracellular level of 8-OHdG, marker of oxidative damage, which is increased in patients with NASH with respect to SS and it was related to grade of inflammation; and (iii) the specific activity of catalase, the main antioxidant enzyme.

Impaired mitochondrial structure and function are reported to be a crucial event during progression of NAFLD. Ultrastructural analysis by EM showed that mitochondrial size was not significantly altered in both SS and SH cells compared to control cells. However, the mitochondrial cristae were largely disorganized and reduced in number in SH cells, and analysis of TMRE-stained mitochondria showed a reduced inner membrane polarization in SH cells, a further sign of damage (Aharoni-Simon et al., 2011). We observed a loss of mitochondria during progression from SS to SH, which was indicated by the marked reduction in the mtDNA copy number in SH cells. Also, the expression of APE1 and POLG, two main genes for mtDNA repair, was stimulated in SH cells. All these facts clearly indicate that mitochondria structure and number are largely damaged in our in vitro model of NAFLD progression.

Mitochondrial respiration parameters were assessed by using the Seahorse XF Analyzer. We did not observe significant differences in basal respiration in both SS and SH cells with respect to control, but the proton leak was significantly reduced in both SS and SH cells with respect to controls. This observation could indicate a decrease in mitochondrial uncoupling, possibly resulting from mitochondrial membrane alterations, which made it more impermeable to protons. In contrast, maximal respiration and ATP production did not change in SS cells, but

they increased in SH cells, which is an expected finding since mitochondrial function would be expected to be damaged in NASH (García-Ruiz et al., 2015). Finally, in response to protonophore addiction (FCCP), SH cells showed increased respiration, indirectly suggesting higher activity of the respiratory chain. We wish to emphasize that progression from increased to deteriorated mitochondrial function has been also observed in the context of fatty liver disease (Koliaki et al., 2015). Our present biological model may recapitulate the up-regulation of mitochondrial function observed in the initial stages of the disease. This probably indicates that SH cells were more damaged than SS cells. Taken together, our data parallel previous studies conducted in patients with simple liver steatosis and biopsy-proven SH undergoing functional breath tests with stable isotope to assess mitochondrial function in vivo and showing that indeed SH is the worst functional scenario (Portincasa et al., 2006).

The nutraceutic silybin has shown preliminary encouraging results for NAFLD either in clinical and animal studies (Reina and Martínez, 2015). The present study aimed to verify and better understand the molecular mechanisms sustaining the beneficial action of silybin on the hepatocyte. A key finding is that silybin exerts hepatoprotective effects on both SS and SH cells, at different levels depending on the NAFLD grade. First of all, silybin was able to reduce the apoptosis observed in SS and SH cells, although it did not improve the viability compromised in SH cells. More specifically, in our cellular models of NAFLD progression we observed a significant anti-steatotic action of silybin. In particular, silybin treatment led to (i) marked reduction of excess TGs accumulated in both SS and SH cells and (ii) down-regulation of IkBip expression that resulted increased passing from control to SS till to SH cells. The lipid-lowering action of silybin in SS cells was associated to a decrease in LD size but not in LD number.

The lipid-lowering effect of silybin was sustained by a transcripitonal modulation of PPARs, the master regulators of lipogenic and lipolytic pathways (Varga et al., 2011). In both SS and SH cells, silybin reduced expression of PPARγ, the lipogenic isoform promoting esterification of FAs. PPARγ expression typically increases in NAFLD; indeed, it was up-regulated in both SS and SH cells. Regarding PPARα, an activator of mitochondrial and peroxisomal β-oxidation of FAs, it was only slightly up-regulated in SS and SH cells and silybin played different effects depending on the extension of cell damage. In SS cells, silybin increased PPARα expression, whereas in SH cells, it reduced it. Further studies need to clarify if such results imply distinct

effects of silybin at different levels of steatogenic damage and play a role also in vivo.

The lipid-lowering effect of silybin was not supported by increased TG secretion, but by stimulation of FA oxidation. Expression of both mitochondrial CPT-1 and microsomal CYP2E1 was significantly up-regulated by silybin in both SS and SH cells. By contrast, the peroxisomial oxidation played by AOX was stimulated by silybin only in SH cells. The action of silybin appeared to be mainly dependent on its effects at the mitochondrial level, with different mechanisms depending on the NAFLD grade. In fact, at mitochondrial level, although silybin did not rescue the loss of mitochondria observed in SH cells, in both SS and SH cells, it led to a significant increase in mitochondria size (both major and minor axes), improved the organization of mitochondrial cristae, which became more evident and parallel to each other's, and increased the polarization of the inner membrane of mitochondria as indicated by the increased and better defined TMRE signal. Moreover, silybin increased expression of the DNA repair enzymes APE1 and POLG and reduced both basal and maximal respiration only in SH cells, where their rates were increased, and this may stem from different factors including modulation of mitochondrial substrate import or decreased ATP production. Interestingly, silybin stimulated ATP production in SS cells but decreased it in SH cells, where the ATP production rate was already higher, and these changes paralleled those observed for PPARα expression. In contrast, silybin did not counteract the reduction of proton leak observed in both SS and SH cells. Although more work needs to be performed, silybin appears to act as an inhibitor of mitochondrial function under diseased conditions (especially in SH cells), which may have beneficial effects as observed previously with other agents (Jenkins et al., 2013). The apparent increased oxidative metabolism in SH cells may be justified by increasing anabolic pathways, as previously described (Satapati et al., 2015).

Oxidative stress was observed in both SS and SH cells. Interestingly, the increased ROS generation following intracellular FA accumulation was almost completed blunted by co-treating the cells with silybin. In fact silybin was able to counteract the FA-dependent increase in (i) the lipid peroxidation measured as production of MDA; (ii) the oxidative DNA damage measured as extracellular levels of 8-OHdG; and (iii) the catalase activity. Excess ROS as well as pro-inflammatory cytokines can activate inflammatory signaling such as that sustained by the transcription factor NF-κB, which is widely implicated in the response to oxidative stress (Cnop et al., 2012). The ability of silybin in protecting cells from fat-induced

oxidative stress was confirmed by analyzing NF-κB activation, which was reduced upon exposure to silybin.

In conclusion, the present study provides new insights about the protective effects of silybin administered directly to hepatocytes mimicking in vitro the NAFLD progression. Further studies are on the way to translate such promising results into long-term beneficial effects, in the hope that onset, progression and worsening of NAFLD/NASH will be prevented/delayed in human being by using more natural nutraceutic approaches.

7.Aquaporin-9 is involved in the lipid-lowering activity of the nutraceutical silybin on hepatocytes through modulation of autophagy and lipid droplets composition

Francesca Baldini[1], Piero Portincasa[2], Elena Grasselli[1], Gianluca Damonte[3], Annalisa Salis[1], Michela Bonomo[4], Marilina Florio[4], Nadia Serale[1], Adriana Voci[1], Patrizia Gena[4], Laura Vergani[1],&,* and Giuseppe Calamita[4,]&,

[1]DISTAV, Dept. of Earth, Environment and Life Sciences; [2]Clinica Medica "A. Murri", Dept. of Biomedical Sciences and Human Oncology, Medical School, University of Bari "Aldo Moro", Italy; [3]Dept. of Experimental Medicine, University of Genova, Italy; [4]Dept. of Biosciences, Biotechnologies and Biopharmaceutics, University of Bari "Aldo Moro", Italy.

&Equally contributed

Biochim Biophys Acta Mol Cell Biol Lipids 2020 Mar;1865(3):158586. doi: 10.1016/j.bbalip.2019.158586. Epub 2019 Dec 6.

ABSTRACT

Hepatic steatosis is the hallmark of non-alcoholic fatty liver disease (NAFLD), the hepatic manifestation of the metabolic syndrome and insulin resistance with potential evolution towards non-alcoholic steatohepatitis (NASH), cirrhosis and hepatocellular carcinoma. Key roles of autophagy and oxidative stress in hepatic lipid accumulation and NAFLD progression are recognized. Here, we employed a rat hepatoma cell model of NAFLD progression made of FaO cells exposed to oleate/palmitate followed or not by TNFα treatment to investigate the molecular mechanisms through which silybin, a lipid-lowering nutraceutical, may improve hepatic lipid dyshomeostasis. The beneficial effect of silybin was found to involve amelioration of the fatty acids profile of lipid droplets, stimulation of the mitochondrial oxidation and upregulation of a microRNA of pivotal relevance in hepatic fat metabolism, miR-122. Silybin was

also found to restore the levels of Aquaporin-9 (AQP9) and glycerol permeability while reducing the activation of the oxidative stress-dependent transcription factor NF-κB, and autophagy turnover. In conclusion, silybin was shown to have molecular effects on signaling pathways that were previously unknown and potentially protect the hepatocyte. These actions intersect TG metabolism, fat-induced autophagy and AQP9- mediated glycerol transport in hepatocytes.

Key words: Steatosis, steatohepatitis, silybin, aquaglyceroporins, hepatic glycerol, mono-unsaturated and saturated fatty acids, autophagy

INTRODUCTION

Non-alcoholic fatty liver disease (NAFLD) is accompanying the growing epidemics of obesity, type 2 diabetes, and metabolic syndrome worldwide (Krawczyk et al., 2010). In this context, hepatic steatosis is the response to high levels of fatty acids (FA) from diet and adipose tissue, as well as from intrahepatic *de novo* lipogenesis and defective export as very low-density lipoproteins (VLDL) (Vergani, 2019). FA entering the hepatocytes are mainly esterified with glycerol to originate triglycerides (TG). The saturated palmitic acid (PA, 16:0) and the monounsaturated oleic acid (OA, 9-cis 18:1) are the most abundant FA in both diet and serum, and they show different lipotoxicity. In rodent hepatocytes cultured *in vitro,* excess PA induces apoptosis, whereas OA prevents cell death and promotes TG secretion (Ricchi et al., 2009). The formation of monounsaturated fatty acids (MUFAs) from saturated fatty acids (SFAs) is catalyzed mainly by the stearoyl-CoA desaturase (SCD-1) (Paton & Ntambi, 2009). In hepatocytes, TG are either packed as lipid droplets (LD) for storing, or as VLDL for secretion (Donnel et al., 2005).

The proprotein convertase subtilisin/kexin type 9 (PCSK9) is a hepatic protease that degrades the low-density lipoprotein receptor (LDLR) thereby elevating plasma LDL cholesterol levels (Lagace et al., 2006). Moreover, PCSK9 is involved in TG metabolism by acting on degradation of CD36, a major receptor involved in transport of long-chain FA and TG storage (Demers et al., 2015).

Although storing of lipids inside LD is beneficial, excess hepatocyte enlargement may result in cell dysfunction (Yamahguchi et al., 2007; Baldini et al., 2019), and benign hepatic steatosis can progress to non-alcoholic steatohepatitis (NASH), cirrhosis and hepatocellular carcinoma (Eckel et al., 2010). Adipokines, interleukins and Tumor Necrosis Factor α (TNFα) are known mediators of NAFLD progression (Bekaert et al., 2016). As a defense mechanism, excess TG accumulation promotes autophagy of LD (lipophagy) (Wang, 2016). Conventional autophagy is driven by a concerted action of a suite of “autophagy-related” molecules (Atg). The Atg8/MAP1LC3 (microtubule associated protein 1 light-chain 3, hereafter referred to as LC3) acts in elongation and maturation of the autophagosome, while Atg7 mediates the conversion of LC3-I to the active form LC3-II (Choi et al., 2013). Autophagy dysfunction has been linked to development of NAFLD (Kwanten et al., 2016).

The mobilization of lipids from LD results in excess FA entering oxidation pathways (Vergani, 2019). The long chain FA are oxidized mainly in mitochondria, where the very long-chain acyl-CoA dehydrogenase (VLCAD) catalyzes the first step of oxidation (Primassin et al., 2011), the cytochrome c oxidase (COX) in the respiratory chain converts molecular oxygen to water (Vecchione et al., 2017), and the uncoupling protein 2 (UCP2) in the inner membrane dissipates excess energy by separating oxidative phosphorylation from ATP synthesis (Baffy, 2005).

Stimulation of fat oxidation induces oxidative stress that promotes increased production of TNFα in adipose tissue and in the liver, which, in turn, may induce mitochondrial dysfunction. On the other hand, oxidative stress and stimulated autophagy activate the transcription factor NF-κB which regulates the expression of a broad range of anti-oxidants genes (Criollo et al., 2012), plays anti-apoptotic and pro-inflammatory functions and inhibits autophagy (Schlottmann et al., 2008).

MicroRNAs (miRNAs) are non-protein-coding, small single-stranded RNA, that bind to the 3′-UTR of the nucleotide sequence leading to inhibition of translation or mRNA degradation (Ambros, 2004). Dysregulation of miRNA expression has been observed in rodent models of NAFLD, often aligning with the changes observed in patients with steatosis and NASH (Cheung et al., 2008; Kong et al., 2011). In the liver, miR-122 represents about 70% of total miRNA and its down- or up-regulation can modify FA and cholesterol metabolism (Jin et al., 2014).

Aquaporin-9 (AQP9) belongs to *Aquaglyceroporins*, a branch of the *Aquaporin* family of membrane channels allowing permeation of glycerol and, to a lesser extent, water, hydrogen peroxide, urea and ammonia (Bernardino et al., 2016; Tesse et al., 2018). In liver, AQP9 represents the major route through which hepatocytes import glycerol (Jelen et al, 2011; Calamita et al., 2012; Calamita et al., 2015; Gena et al., 2017). Reduction in hepatic AQP9 levels resulting in reduced glycerol permeability decreases substrate availability for the TG synthesis in the cell (Portincasa et al., 2008; Calamita et al., 2015). Hepatic AQP9 is regulated by insulin and leptin (Rodriguez et al., 2011), and its pathophysiological relevance was shown in both cell and animal models of NAFLD, and in liver biopsies of obese patients with NAFLD (Gena et al., 2013; Rodriguez et al., 2014; Rodriguez et al., 2015a; Rodriguez et al., 2015b).

Male rats fed a high-fat diet (HFD) show reduction in liver steatosis after knock-down of liver *Aqp9* at disease onset (Cai et al., 2013). Leptin-deficient mice, an animal model of NAFLD, have decreased levels of hepatic AQP9 (Gena et al., 2013). Therefore, AQP9 might become an additional therapeutic target for treatment of NAFLD/NASH (Calamita & Portincasa, 2007; Calamita et al., 2018). The possible correlation between AQP9 and autophagy in hepatic lipid metabolism needs to be investigated (Kwanten et al., 2016), as changes in AQP9 may prevent or reduce TG accumulation through autophagy (Calamita et al., 2018).

So far, therapeutic options in NAFLD and NASH are lacking, and currently the best approach is limited to changes of lifestyles (i.e. balanced diet, regular physical exercise, and reduction of overweight) (Molina-Molina et al., 2018). As oxidative stress seems to have a central role in hepatic cell injury in the context of NASH, the influence of several antioxidants such as the phytochemical silybin and other compounds are being actively investigated. Silybin is the most relevant flavonolignan of silymarin, the extract of milk thistle seed (*Silybum marianum)*. Silybin has antioxidant, anti-inflammatory and cytoprotective actions and it has been used in patients with NAFLD with some beneficial effects (Loguercio & Festi, 2011; Loguercio et al., 2012). Here, in addition to a significant amelioration of the lipid profile of LD, we report involvement of AQP9 in the lipid-lowering activity of silybin on a hepatocyte model of NAFLD through modulation of autophagy.

MATERIALS AND METHODS

Chemicals

All chemicals, unless otherwise indicated, were supplied by Sigma-Aldrich Corp. (Milan, Italy).

Cell Treatments

Rat hepatoma FaO cells [The European Collection of Authenticated Cell Cultures (ECACC)], (Clayton et al., 1985) were grown in Coon's modified Ham's F12 with 10% foetal bovine serum (FBS). Cells grown until 80% confluence were incubated in high-glucose medium with 0.25% bovine serum albumin (BSA) to increase stability and solubility of FA (Vergani et al., 2018). A condition mimicking human steatosis (SS) was induced by incubating FaO cells for 3 h with an oleate/palmitate mixture (2:1 molar ratio, final concentration 0.75 mM). A steatohepatitis (SH) condition was mimicked by incubating SS cells for 24 h with 10 ng/mL TNFα (Zhang et al., 2010). After replacing the medium, both SS and SH cells were treated for 24 h with 50 µM silybin (Sil) (Istituto Biochimico Italiano, Lorenzini SpA, Italy) (Vecchione et al., 2016). Silybin stock (10 mM) was prepared in dimethyl sulfoxide (DMSO).

Lipid Droplet imaging

Cells grown on coverslips were rinsed with PBS and neutral lipids were visualized by optical microscopy using the selective Oil-Red-O (ORO) dye (Koopman et al., 2001). Briefly, after fixing in 4% paraformaldehyde for 20 min at room temperature, cells were washed with PBS, stained for 30 min with 0.3% ORO solution in isopropanol 60%. After fixation and washing, cells were mounted with 4',6-diamidino-2-phenylindole (DAPI). Images were obtained using a Leica DMRB light microscope equipped with a Leica CCD camera DFC420C (Leica, Wetzlar, Germany). A first image was obtained by acquiring the ORO-stained LD with bright field set-up, then a second image of the DAPI stained nuclei was acquired with fluorescence set-up. Images were captured with 40x objective and merged (Khalil et al., 2019). Both the average size and the number of LD/cell were evaluated on acquired images using the open source image processing program ImageJ free software (http://imagej.nih.gov/ij/). At least five images from random fields in each sample were acquired for each experiment set, and at least forty cells for each image were analyzed. Values were expressed as mean ± S.D. from at least three independent experiments.

Lipid Droplet isolation and composition

Lipid droplets were isolated from cells following a standard protocol with minor modifications (Atshaves et al., 2001). FaO cells were scraped from the dishes. Cell suspension (about $40x10^6$ cells/sample) was homogenized with a glass dounce homogenizer on ice, and centrifuged at 800xg for 10 min at 4 °C. The supernatant was centrifuged at 5,000xg for 20 min. Then the supernatant was further centrifuged at 43,000 rpm in SW55 rotor (230,000xg) for 2 h at 4 °C. The LD fraction forming a distinct white band on the surface of the preparation was collected. Lipids were then extracted from isolated LD using the method of Folch et al. (Folch et al., 1957) as previously described (Grasselli et al., 2014). Briefly, the lipid phase was saponified with methanolic KOH (3 M) and the non-saponifiable lipids were extracted by diethylether, and the aqueous phase was acidified and extracted with n-hexane. The hexane phases containing NEFAs were collected, the solvent evaporated, and the residue derivatized by acid-catalyzed esterification (Morrison & Smith, 1964). Then, samples resuspended in hexane were injected in a HP5890 series II gas chromatograph coupled to a HP5970 mass spectrometer equipped with an electron impact ionization source (Agilent). Separation was performed on a DB5MS capillary column (Phenomenex, 0.25 mm × 30 m); the helium gas flow was 1 mL/min. The oven temperature gradient was as follows: initial temperature of 100 °C, isothermal at 100 °C for 3 min, 100 to 300 °C (rate, 15 °C/min) and isothermal at 300 °C for 5 min. The MS analysis was performed in full-scan mode. FAME (fatty acid methyl ester) quantification was performed using a calibration curve obtained injecting different FAME standards referring to selected ions. The most abundant and specific ions were used for the quantification of FAMEs: m/z 74 was used for saturated FAMEs and m/z 55 for monosaturated FAMEs. The regression curves were linear in the range of the FAME concentrations used for the analysis.

RNA extraction and real-time qPCR

RNA was isolated using Trizol reagent, cDNA was synthesized and quantitative real-time PCR (qPCR) performed in quadruplicate using 1x IQ™SybrGreen SuperMix and Chromo4™ System apparatus (Biorad, Milan, Italy) as previously described (Grasselli et al., 2016). The relative quantity of target mRNA was calculated by the comparative Cq method using glyceraldehyde 3-phosphate dehydrogenase (GAPDH) as housekeeping gene, and expressed as fold

induction with respect to controls (Vecchione et al., 2016). Primer pairs designed *ad hoc* starting from the coding sequences of R*attus norvegicus* (http://www.ncbi.nlm.nih.gov/Genbank/GenbankSearch.html) and synthesized by TibMolBiol (Genova, Italy) are listed in Table 1.

Expression of miRNA 122 (miR-122) was measured as described elsewhere (Baselga-Escudero et al., 2015). Briefly, reverse transcription was performed using the High capacity cDNA kit (ThermoFisher Scientific, Milan, Italy), following manufacturer's instructions, and the miRNA-specific reverse-transcription primers provided with the TaqMan MicroRNA Assay (ThermoFisher Scientific, Milan, Italy). Amplification was performed using the Stepone plus Real-Time PCR system (ThermoFisher Scientific) at 50 °C for 2 min and at 95 °C for 10 min followed by 40 cycles at 95 °C for 15 s and 60 °C for 1 min. Probe and primers for both miRNA-122-5p (4427975-002245) and miRNA U6 (4427975-001973) were purchased from ThermoFisher Scientific. The relative quantity of miRNA-122-5p was calculated by the comparative Cq method using miRNA U6 as housekeeping gene and expressed as fold induction with respect to controls.

Immunofluorescence of LC3 and AQP9

Cells grown on poly-L-lysine coated coverslips were rinsed with phosphate-buffered saline (PBS) at pH 7.4, fixed with 4% paraformaldehyde for 20 min and then permeabilized with 0.1% Triton X-100 for 15 min at room temperature (RT). After several washings (3 times for 5 min), slides were blocked with 0.1% gelatin in PBS for 15 min and incubated for 2 h at RT with rabbit polyclonal anti-LC3 (14600-1-AP; Proteintech, Manchester, UK) and/or anti-AQP9 affinity-purified antibodies (AQP9-1A; Alpha Diagnostics International, San Antonio, TX) at a concentration of 3 µg/mL and 4 µg/mL, respectively, in blocking solution (PBS added with 0.1% gelatin). Successively, slides were washed and incubated with fluorescein-isothiocyanate (FITC)-conjugated secondary antibody (Alexa Fluor 488; Thermo Fisher Scientific, Milano, Italy) diluted 1:1000 in blocking solution for 1h at RT. After staining, slides were washed thoroughly with PBS and mounted with an anti-fade medium containing DAPI (Vectashield, DBA, Segrate, Italy). Finally, slides were sealed and viewed with a Nikon Eclipse 600 photomicroscope equipped with a Nikon DMX 1200 camera (Nikon Instruments SpA, Calenzano, Italy).

Cytochrome C oxidase activity

Cytochrome C oxidase (COX) is the terminal enzyme complex in the respiratory chain. COX activity was assayed according to Moyes and coworkers (Moyes et al., 1997) following the decrease in absorbance at 550 nm. Briefly, 50 µM reduced cytochrome c was dissolved in 0.5% Tween-20 in 20 mM Tris-HCl (pH 8.0). Cytochrome c was reduced with ascorbate and dialyzed overnight to remove unreacted ascorbate. Then, the concentration of reduced cytochrome c was determined using an ε550=28.5 mM^{-l}. Immediately before the assay, cell extracts (about 3–10×10^4 cells) were added to the assay medium and incubated for 5 min. The reaction was started by adding 10 µM reduced cytochrome c and the change in absorbance was recorded at 550 nm for 3 min.

Western blotting

Immunoblotting analyses to assess the protein level of LC3α/β and of NF-kB were performed as previously described (Vecchione et al., 2017). For LC3α/β immunoblotting cells were lysed on ice in lysis buffer (NaCl 150 mM, Tris HCl pH 7.4, 50 mM, SDS 0.33%). For of NF-kB, nuclei were isolated by suspending the cellular pellet in 400 µL ice-cold Buffer A (20 mM Tris-HCl pH 7.8, 50 mM KCl, 10 µg/mL Leupeptin, 0.1 mM Dithiothreitol-DTT, 1 mM phenylmethanesulfonyl fluoride-PMSF); and 400 µL Buffer B (Buffer A plus 1.2% Nonindet P40). The suspension was vortex-mixed for 10 s, centrifuged, and washed. The nuclear pellet was resuspended in 100 µL Buffer B, mixed thoroughly in ice for 15 min and finally centrifuged. The supernatant containing the nuclear extracts was collected. About 30-50 µg proteins were electrophoresed on 10% sodium dodecyl sulfate polyacrylamide gel electrophoresis (SDS-PAGE) (Laemmli, 1970). Membrane was blocked in 5% fat-free milk/PBST (pH 7.4) and probed overnight at 4 °C using rabbit NF-kB p65 antibody (SC-109; Santa Cruz Biotechnology, DBA, Milan, Italy), or mouse anti-MAP LC3α/β p (SC-398822 Santa Cruz Biotechnology) in PBST buffer (PBS with 0.1% Tween 20) at 4°C (Towbin et al., 1979). Membranes were washed and incubated with horseradish peroxidase (HRP)-conjugated secondary antibody in PBST for 1 h at room temperature. Immune complexes were visualized using an enhanced chemiluminescence Western blotting analysis system (Bio-Rad ChemiDoc XRS System). Films were digitized and band optical densities were quantified against the actin band using a computerized imaging system and expressed as Relative Optical Density (ROD,

arbitrary units). ROD of each band was expressed as percentage respect to control and about 30-50 μg proteins of cellular homogenates were electrophoresed on SDS polyacrylamide gel electrophoresis (SDS-PAGE).

Measurement of extracellular glycerol

Glycerol content was measured in cellular medium after a brief centrifugation (14,000xg for 3 min at 4°C) after separation in chloroform:methanol (2:1). The water-soluble glycerol was determined by using the 'Triglycerides liquid' kit (Sentinel, Milan, Italy) (Vecchione et al., 2016). Varian Cary 50 spectrophotometer (Agilent, Milan, Italy) was used for spectrophotometric analysis. Data were expressed as percent glycerol content relative to controls.

Statistical analysis

Data were expressed as means ± standard deviation (S.D.) of at least three independent experiments in triplicate. Statistical analysis was performed using ANOVA with Tukey's post-hoc test (GraphPad Software, Inc., San Diego, CA, USA).

RESULTS

Effect of silybin on the fatty acid composition of LD

The cytosolic accumulation of TG in the different steatotic conditions, as visualized by ORO staining, was associated with a marked increase in LD number and size compared to control cells (Fig. 1A-C). Control FaO cells showed only few (about 72 LD/cell) and small (about 0.9 µm average diameter) LD, while both number and size of LD resulted significantly increased in SS and SH cells. While the number of LD was comparable between SS and SH cells (about 295 LD/cell), the average size of LD in SH was smaller than in SS cells (1.3 µm *vs* 1.5 µm, respectively). In SS cells silybin reduced the LD diameter to a value similar to that of control cells (1.1 µm), without effects on the number of LD. No change in LD diameter was seen in the SH cells exposed to silybin.

A

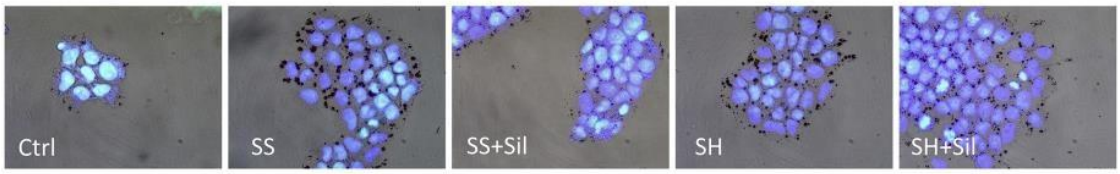

B

LDs number / cell

	Ctrl	SS	SS+Sil	SH	SH+Sil
Mean	72	294 *	248 *	296 *	328 *
Std. Deviation	1.41	161	24	58.7	9.19

* p≤0.001 vs Ctrl

C

LD diameter (µm)

	Ctrl	SS	SS+Sil	SH	SH+Sil
Mean	0.93	1.49	1.11 #	1.33 #	1.22 #
Std. Deviation	0.60	1.38	1.12	1.47	1.22

p≤0.001 vs SS

Figure 14. Effect of silybin on fatty acid accumulation

FaO cells were incubated in the presence of oleate/palmitate (SS), or oleate/palmitate and TNFα (SH), then treated for 24 h with 50 µM silybin (Sil). Untreated FaO cells were used as control (Ctrl). **(A)** Representative micrographs of FaO cells stained with DAPI and Oil-Red-O (ORO) (magnification 40x). **(B-C)** Average size of LDs and number of LDs/cells. Values are mean±S.D. from at least three independent experiments. Statistical significance between groups was assessed by ANOVA followed by Tukey's test. Symbols: Ctrl vs. all treatments *p≤0.001; SS vs. all treatments & p≤0.001.

Gas chromatography analysis of LD purified from steatotic cells (Fig. 2A) revealed an acyl composition of the TG in LD consistent with that typically found in mammalian cells in terms of both saturated (SFA) and unsaturated (UFA) fatty acids. The most abundant fatty acids

stored in LD included SFA such as myristic acid (MA, 14:0), palmitic acid (PA, 16:0), stearic acid (SA, 18:0), and UFA such as oleic acid (OA, 18:1) and linoleic acid (LA, 18:2). Analytically, the acyl profile in LD from SS cells showed a prevalence of PA (50.1%), followed by SA (27.4%), OA (10.8%), MA (7.4%) and LA (4.2%). SH cells exhibited an increase in PA content (65.6%) and a decrease in OA (6.4%), MA (1.1%) and LA (0.6%) contents, while SA did not change (26.2%). Silybin did not markedly modify the FA pattern in SS cells whereas in SH cells led to a reduction in PA (to 46.5%) and SA (to 20.2%) content and to an increase in OA (to 11.5%) and MA (to 13.8%) levels.

Of note, SH cells showed a marked increase in SFA/UFA ratio compared to SS cells (13.7 *vs* 5.7 in SH and SS cells, respectively), and a reduction in the content of short-medium chain FA (<C16) (4.3% *vs* 11.6% in SS and SH cells, respectively) (Fig. 2A, panel). Treatment with silybin rescued the altered FA profile since the SFA/UFA ratio decreased when SH cells were treated with silybin (from 13.6 to 7.0% in SH and SH+Sil cells). On the other hand, treatment with silybin increased the amount of FA <C16 that reached mean values of 15.9% and 18.6% in SS+Sil and SH+Sil conditions, respectively.

As shown in Figure 2B, both SS and SH cells showed a decrease in SCD-1 mRNA expression compared to control (0.39- and 0.62-fold induction, respectively; $p \leq 0.01$ and $p \leq 0.05$, respectively), while treatment with silybin increased SCD-1 mRNA level of +249% ($p \leq 0.05$) and +292% ($p \leq 0.001$) with respect to their counterpart SS and SH, respectively.

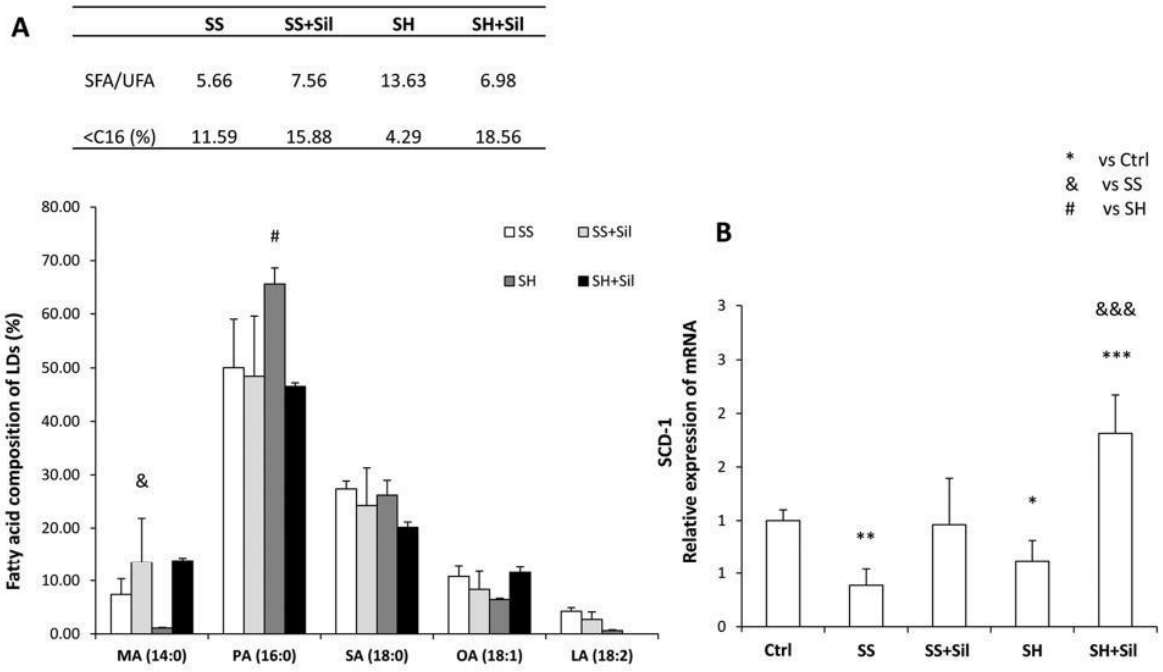

Figure 15. Effect of silybin on fatty acids composition of LDs

FaO cells were incubated in presence of oleate/palmitate (SS), or oleate/palmitate and TNFα (SH), then treated for 24 h with 50 µM silybin (Sil). Untreated FaO cells were used as control (Ctrl). **(A)** Acyl composition of LDs purified and analyzed by gas chromatography. **(B)** Real-time qPCR analysis of SCD-1 transcriptional expression. Values are mean±S.D. from at least three independent experiments. Statistical significance between groups was assessed by ANOVA followed by Tukey‟s test. Symbols: Ctrl vs. all treatments *p≤0.05, **p≤0.01, ***p≤0.001; SS vs. all treatments &p≤0.05, &&&p≤0.001; SH vs. all treatments # p≤0.05.

Effect of silybin on hepatocyte AQP9, glycerol uptake and autophagy of LD

Since liver steatosis *in vivo* has been reported to lead to AQP9 dysregulation (Gena et al., 2013; Cai et al., 2013; Rodriguez et al., 2014) and dysfunctional autophagy (Kwanten et al., 2016) we assessed the possible changes in AQP9 expression, glycerol import and autophagic process in FaO cells in the different experimental conditions.

By real-time qPCR, no differences in *AQP9* transcript levels occurred in both steatotic SS and SH cells compared to control (Fig. 3A), whereas marked upregulation of AQP9 was observed in SS and SH cells exposed to silybin (1.55- and 1.72-fold induction *vs* control cells, in SS and SH cells, respectively; $p \leq 0.001$) (Fig. 3A). In terms of protein, SS and SH cells showed a significant reduction of plasma membrane AQP9 immunoreactivity compared to control cells (Fig. 3B,C,E), and silybin restored the levels of AQP9 protein in SS and SH cells (Fig. 3D,F) to extents comparable to those of the control FaO cells. No changes in the transcript and protein levels of AQP9 were seen in control cells receiving silybin (data not shown).

Given the role of AQP9 in glycerol transport within hepatocytes, we measured the glycerol concentration in the culture medium in the attempt of correlating the levels of AQP9 with those of the glycerol influx. The extracellular level of glycerol for both SS and SH cells was similar to that of control cells, while it was significantly reduced by the treatment with silybin (-41% for SS+Sil *vs* SS; –46% for SH+Sil *vs*. SH; $p \leq 0.001$) (Fig. 3G).

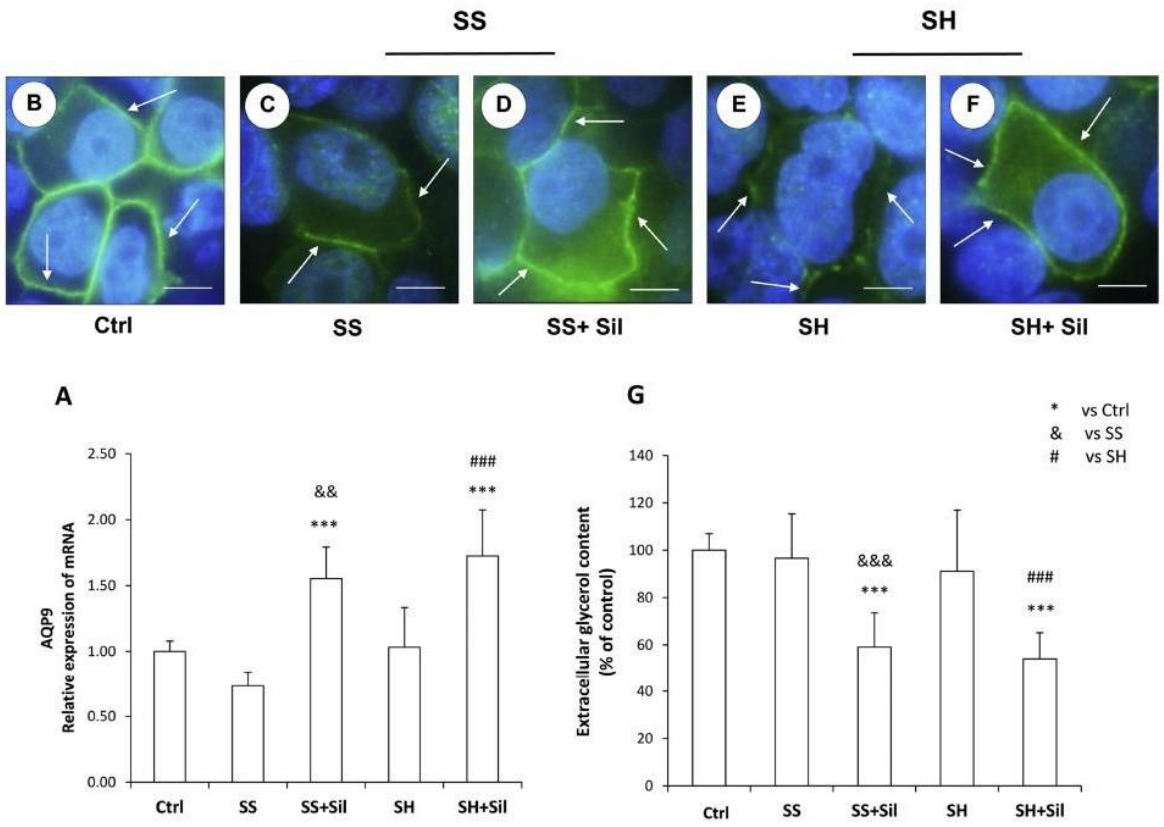

Figure 16. Effect of silybin on AQP9 expression and glycerol import

FaO cells were incubated with oleate/palmitate (SS), or oleate/palmitate and TNFα (SH), then treated for 24 h with 50 µM silybin (Sil). Untreated FaO cells were used as control (Ctrl). **(A)** Realtime qPCR analysis of AQP9 transcriptional expression. **(B-F)** Immunofluorescence analysis. AQP9 immunoreactivity (green fluorescence) is seen over the plasma membrane. Nuclei are stained by DAPI (blue fluorescence). **(G)** Glycerol content of culture medium. Values are mean±S.D. from at least three independent experiments. Statistical significance between groups was assessed by ANOVA followed by Tukey‟s test. Symbols: Ctrl vs. all treatments ***p≤0.001; SS vs. all treatments &&p≤0.01, &&&p≤0.001; SH vs. all treatments ### p≤0.001).

The possible effects of silybin on cell autophagy were investigated by assessing the intracellular expression and distribution of LC3-II, and by quantifying the LC3-II/LC3-I ratio (Tanida et al., 2004). In control conditions, only few punctuate structures, seen as green dots, were observed indicating LC3 recruitment on autophagosomes (Fig. 4A). Both SS and SH hepatocytes showed an increase in these cytosolic puncta (Fig. 4B, D), a profile indicating increased autophagy turnover accompanying NAFLD progression. The immunofluorescence was of wider diffusion when SS and SH were treated with silybin (Fig. 4C,E), resulting in a pattern more similar to that of the control cells (Fig. 4A). In line with these results, Western blot analysis (Fig. 4F) showed a significant increase in LC3-II/LC3-I ratio in both SS and SH cells

(+24% and +17%, respectively, *vs* control; $p \leq 0.001$ and $p \leq 0.05$), while silybin counteracted this increase in both steatotic conditions (−29% and -31%, respectively, *vs* their counterparts; $p \leq 0.001$). No changes in LC3-II/LC3-I ratio were seen in control FaO cells receiving silybin (data not shown).

In both steatotic conditions the Atg7 mRNA was overexpressed, but the increase was larger in SH cells compared to SS cells (2.84 vs 1.53-fold induction *vs* control, respectively; $p \leq 0.01$ and $p \leq 0.001$) (Fig. 4G). On the other hand, silybin was able to restore Atg7 expression near to control in SH hepatocytes (-60% *vs* SH; $p \leq 0.001$).

Since autophagy is known to activate NF-κB we assessed by immunoblotting the NF-κB activation as a downstream effect of autophagy stimulation (Fig. 4H). A significant decrease in NF-κB activation was seen when both SS and SH hepatocytes were treated with silybin (about -30% for both SS and SH; $p \leq 0.05$).

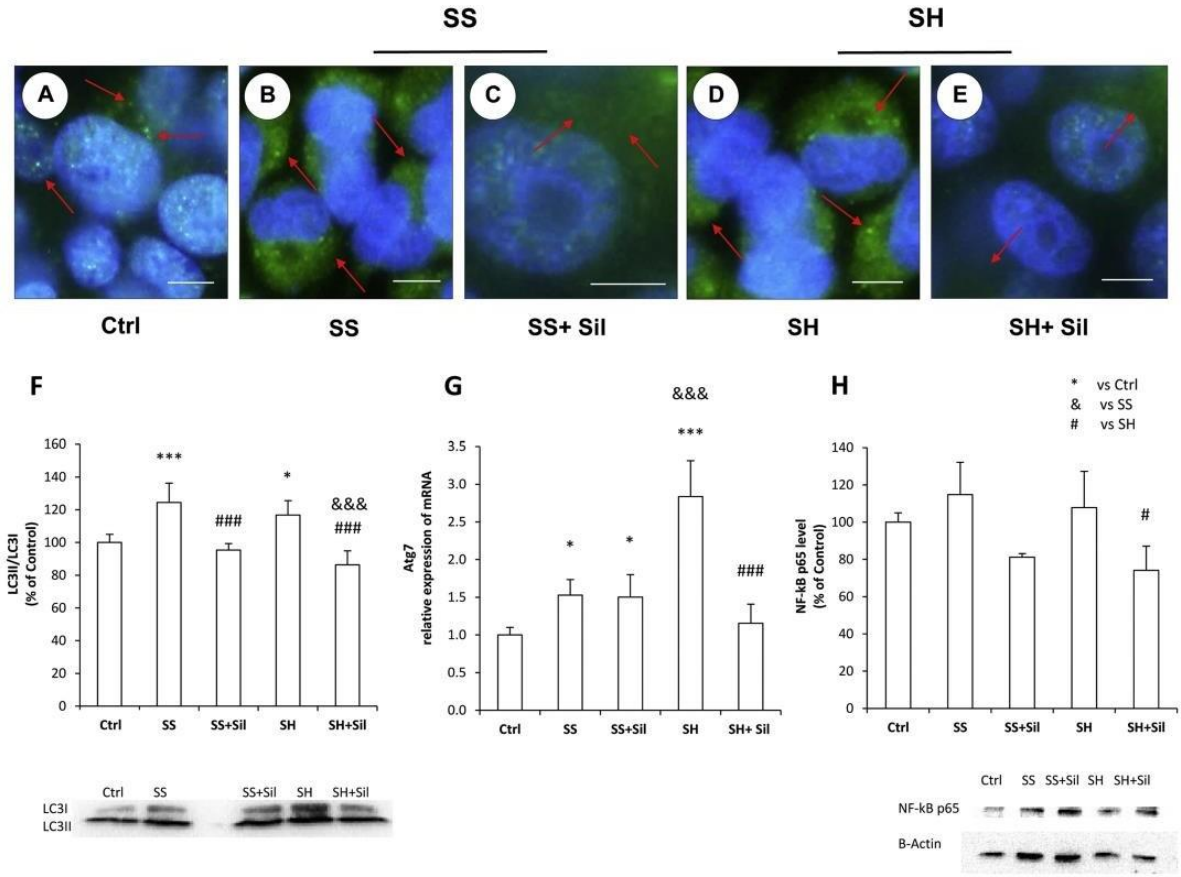

Figure 17. Effect of silybin on hepatocyte autophagy

(A-E) Immunofluorescence analysis. LC3-II immunoreactivity (green fluorescence) is seen over the plasma membrane. Nuclei are stained by DAPI (blue fluorescence). Control cells **(A)** show few punctuate structures (green dots) indicating LC3

recruitment on autophagosomes. Both SS **(B)** and SH **(D)** hepatocytes show an increase in these cytosolic puncta reflecting an increase in autophagy turnover. The immunofluorescence becomes more diffuse in SS and SH cells were treated with silybin **(C, E)**, resulting in a pattern more similar to that of control cells. F. Western blot analysis of LC3-II/LC3-I ratio. Both SS and SH cells show a significant increase in LC3-II/LC3-I ratio, while silybin counteracts this increase in both steatotic conditions. **(G)** Real-time qPCR analysis of Atg7 transcriptional expression. In both steatotic conditions, Atg7 mRNA results overexpressed, largely in SH cells compared to SS cells. The treatment with silybin restores the Atg7 expression near to control in SH hepatocytes. **(H)** Western blot analysis of NF-κB. A significant decrease in NF-κB activation is observed when both SS and SH hepatocytes are treated with silybin. Values are mean±S.D. from at least three independent experiments. Statistical significance between groups was assessed by ANOVA followed by Tukey‟s test. Symbols: Ctrl vs. all treatments *p≤0.05, ***p≤0.001; SS vs. all treatments &&&p≤0.001, SH vs. all treatments ###p≤0.001.

Effects of silybin on genes of hepatic lipid metabolism

Uptake of circulating FA by hepatocytes is also regulated by PCSK9. Analysis by qPCR showed that *PCSK9* mRNA expression was downregulated in both SS and SH cells, with respect to control (0.59- and 0.45-fold induction, respectively; $p \leq 0.001$), and silybin partially reversed this downregulation as *PCSK9* mRNA expression increased significantly in SH cells (+102% *vs* SH; $p \leq 0.01$) (Fig. 5A).

Mitochondria are the final destination of long chain FA for β-oxidation. In mitochondria, expression of VLCAD (Fig. 5B), the shuttle for FA, was up-regulated in SS and SH cells with respect to control (1.61- and 1.86-fold induction, respectively; $p \leq 0.05$), and it was further stimulated when cells were treated with silybin (2.21- and 4.47-fold induction *vs* control, respectively; $p \leq 0.01$). COX acting in the mitochondrial electron transport chain (Fig. 5D) increased significantly its activity only in SH cells (+97% *vs* control; $p \leq 0.001$), but not in SS cells, and silybin was able to stimulate COX activity in SS cells (+27% *vs* control), but not in SH cells (Fig. 5C). Expression of the uncoupling protein UCP2 (Fig. 5D) was also up-regulated in SS and SH cells with respect to control (1.72- and 2.97-fold induction *vs* control; $p \leq 0.01$ and $p \leq 0.0011$, respectively), and silybin counteracted this upregulation (-31% with respect to SH cells; $p \leq 0.01$). Silybin did not play any significant effect on the expression/activity of these proteins in control FaO cells (data not shown).

In hepatocytes miR-122 is recognised to be a major regulator of lipid metabolism (Tsai et al., 2009). A significant increase in miR-122 level was observed in SS cells upon treatment with silybin (2.01-fold induction *vs* control; $p \leq 0.001$) (Fig. 5E).

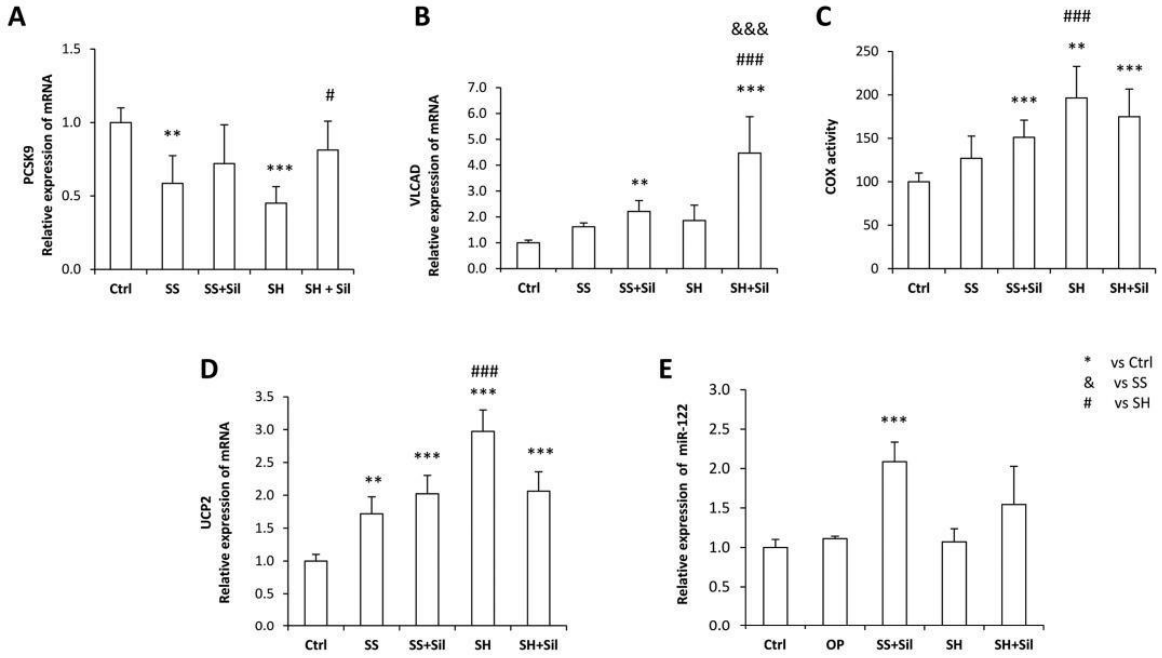

Figure 18. Effects of silybin on genes of hepatic lipid metabolism

FaO cells were incubated in the presence of oleate/palmitate (SS), or oleate/palmitate and TNFα (SH), then treated for 24 h with 50 µM silybin (Sil). Untreated FaO cells were used as control (Ctrl). **(A)** Real-time qPCR analysis of PCSK9 transcriptional expression. **(B)** Real-time qPCR analysis of VLCAD transcriptional expression. **(C)** Cytochrome C oxidase activity measured by enzymatic assay. **(D)** Real-time qPCR analysis of UCP2 transcriptional expression. **(E)** Real-time qPCR analysis of miR-122 transcriptional expression. The level of miR-122 is increased in SS cells upon treatment with silybin. Values are mean±S.D. from at least three independent experiments. Statistical significance between groups was assessed by ANOVA followed by Tukey‟s test. Symbols: Ctrl vs. all treatments ** p≤0.01, ***p≤0.001; SS vs. all treatments &&&p≤0.001; SH vs. all treatments ###p≤0.001.)

DISCUSSION

NAFLD is a worrisome health problem worldwide commonly encountered with the metabolic syndrome. No established therapy exists for NAFLD, and changes in lifestyles remain the most common approaches to treat overweight, obesity, insulin resistance, and liver steatosis. The nutraceutical silybin has shown beneficial effects in patients with NAFLD (Loguercio et al., 2012), and potential hepatoprotective effects in both animal and cellular models of NAFLD (Grasselli et al., 2019; Vecchione et al., 2017; Vecchione et al., 2016; Grattagliano et al., 2013).

In the present study, employing a cellular model of NAFLD progression widely employed in previous studies (Baldini et al., 2019), we found that the beneficial effect of silybin on hepatic steatosis involves amelioration of the FA profile of LD, stimulation of the mitochondrial oxidation and upregulation of miR-122 expression. Interestingly, silybin is also found to restore the levels of AQP9 and glycerol permeability while reducing the autophagy triggered by the ectopic accumulation of lipids. These results suggest a rather complex and pleiotropic role for silybin in the hepatic cells, involving several key molecular intracellular pathways active during liver steatosis.

The accuracy of the cellular model of NAFLD progression was verified by a series of morphometric and biochemical parameters. First of all, steatotic FaO cells showed an increase in number/size of LD compared to controls. However, the LD diameter was smaller in SH cells than in SS cells, suggesting that these conditions mimic microvesicular and macrovesicular steatosis, respectively. Of note, differences in type of histological steatosis might correlate with distinct phenotypic and prognostic manifestations of liver steatosis. For example, in drug-induced liver injury, acute steatosis is severe, and usually microvesicular because of disrupted mitochondrial beta-oxidation of lipids and oxidative energy production (Cullen, 2005). Also, acute liver failure of pregnancy occurs as microvesicular steatosis (Bacq, 1998). More chronic forms of liver damage, by contrast, occur with macrovesicular steatosis as (Ramachandran and Kakar, 2009). However, treatment with silybin was able to reduce the number of LD in both SS and SH cells and the diameter of LD in SS cells, while did not play detectable effects on the size of LD in SH cells. Another sign that silybin improves hepatic steatosis is the increase in miR-122 level in SS cells upon treatment with silybin according to

previous studies showing the involvement of miR-122 in NAFLD (Tsai et al., 2009). Indeed, *in vitro* studies showed downregulation of miR-122 in fatty hepatocytes, and reduced expression of major lipogenic genes upon upregulation of miR-122 in HepG2 cells (Cheung et al., 2008).

In terms of acyl composition, the LD of SS cells are rich in the saturated fatty acids PA and SA, and of the unsaturated OA. The PA content increases in SH cells (+15% *vs* SS cells) being partially balanced by a reduction in OA content (-4% *vs* SS cells). SH cells showed also a lower content of short-medium chain FA (<C16) compared to SS cells. The changes in SFA/UFA ratio might be a sign of more severe steatosis in SH cells compared to SS cells. Of note, the beneficial effect of silybin in SH cells was accompanied to a reduction in content of the saturated fatty acids PA and SA, and to an increase in content of the unsaturated OA, as well as to an increase in the amount of short-medium chain FA. In both SS and SH cells, the changes in the FA profile of LDs could be sustained by downregulation of the *SCD-1* mRNA expression. Interestingly, silybin was able to counteract the SCD-1 mRNA downregulation.

Uptake of FA by hepatocytes is regulated by PCSK9, and this effect is independent of its action on LDLR (Demers et al., 2015). Indeed, PCSK9 binds LDLR resulting in its internalization and degradation (Horton et al., 2009), but PCSK9 promotes also degradation of CD36, which is involved in FA uptake and TG storage/secretion. Indeed, *Pcsk9*$^{-/-}$ mice develop hepatic steatosis with liver sections showing accumulation of LD and marked increase in TG content (Demers et al., 2015). In the present experimental steatogenic setting, *PCSK9* mRNA was downregulated in both SS and SH cells. This condition would likely promote FA entry in hepatocytes, a mechanism potentially counteracting the excess of external FA. Notably, silybin significantly reversed *PCSK9* downregulation in SH cells, and apparently restored cellular function while reducing FA influx in the hepatocyte. The potential “double sword” effect of PCSK9 inhibition/activation in the hepatocyte, and the action of silybin, needs to be shortly commented, due to potential effects on systemic lipid metabolism. *In vivo* dysfunctional PCSK9 leads to persistently elevated serum LDL-cholesterol and increased risk of coronary heart disease (Lagace et al., 2006), nevertheless loss-of-function mutations are frequently associated with decreased LDL-cholesterol and low risk of heart disease (Cohen et al., 2006, Benn et al., 2010). Of note, statins, acting as hypolipemic drugs, lead to increased levels of PCSK9 resulting in a LDL-C-lowering effect *in vitro* (Dubuc et al., 2004), but clinical

studies do not confirm this effect (Huijgen et al., 2012). In this study, it appears that liver steatosis leads to dysregulation of PCSK9 (and possibly LDLR), while silybin restores at least in part the hepatocyte function. Furthermore, silymarin (and its main constituent silybin) are deemed as adjuvants in hyperlipoproteinemia (Skottova and Krecman, 1998) and reduce LDL lipid peroxidation. Silybin exerts an inhibitory effect on HMG-CoA reductase *in vitro* while, *in vivo*, reducing cholesterol synthesis (Cicero et al., 2017).

Together with the effect on other biomarkers of cardiovascular risk, the net effect of silymarin appears to be rather protective on the liver and on serum lipids (Voroneanu et al., 2016), although further studies need to investigate *in vivo* the effect of silybin on PCSK9-mediated effects during ongoing liver steatosis.

Mitochondria are the final destination of long chain FA for β-oxidation. In both SS and SH cells, UCP2 expression was upregulated in the attempt to avoid the excess synthesis of ATP. Moreover, as a response of toxic TG accumulation, SH cells stimulated the COX activity in the respiratory chain. The lipid lowering activity of silybin in both SS and SH cells was associated to increased long chain FA entering mitochondria through up regulation of VLCAD expression.

Our results suggest that the anti-steatotic action of silybin implies upregulation of AQP9 and increase of glycerol permeability in hepatocytes. This result is an important insight into the full understanding of the role played by this aquaglyceroporin in NAFLD/NASH. In humans, AQP9 is highly expressed in liver (Lindskog et al, 2016), where in post-prandial conditions it sustains the hepatic import of extracellular glycerol for the *ex-novo* synthesis of TG. Likely, silybin might increase the AQP9 levels through an epigenetic mechanism as most bioactive plant polyphenols do (Joven et al, 2014).

Moreover, silybin is found to diminish the fat-stimulated autophagy as demonstrated by the downregulation of the LC3-II and Atg7 expression in both SS and SH hepatocytes. Indeed, the autophagosome formation is regulated by Atg7 (Komatsu et al., 2005). The parallel reduction in NF-κB activation upon treatment with this phytocompound well fits with the role of NF-κB activation in promoting autophagic process (Trocoli and Djavaheri-Mergny, 2011).

The inverse correlation found between AQP9 levels and autophagy is compelling. Low levels of hepatocyte AQP9 were associated with the increased autophagy accompanying the TG

overaccumulation, whereas the opposite was observed after restoring the levels of AQP9. This finding is consistent with hepatocyte AQP9 expression being positively regulated by the mammalian target of rapamycin (mTOR) (Rodriguez et al, 2011), a paramount signaling pathway in the regulation of autophagy as the initiation of autophagosome formation by phosphorylating UNC51-like kinase 1 (ULK1) is inhibited by mTOR (Ravikumar et al., 2009; Rubinsztein et al., 2012). Of note, AQP9 might have good potentials as drug target in preventing or treating NAFLD/NASH (Calamita et al., 2018), and small compounds selectively and potently gating the AQP9 channel are already available (Jelen et al., 2011; Wacker et al., 2013; Sonntag et al., 2019). The present results lead to the attractive idea that pharmacological modulation of AQP9 may prevent or reduce TG over accumulation and consequent liver dysfunction through autophagy.

In summary, the beneficial effect of silybin on the *in vitro* model of NAFLD and NASH implied amelioration of the profile of FA stored in LD with an increase the short/medium chain FA ratio and a decrease of the saturated/monounsaturated FA ratio, (*ii*) stimulation of mitochondrial FA oxidation through upregulation of VLCAD and UCP2 and stimulation of COX activity, (*iii*) increase of the master regulator of hepatic lipid metabolism miR-122, (*iv*) increase of AQP9 expression and glycerol permeability, and (*iv*) diminution of fat-stimulated autophagy. Altogether, these results show that silybin has molecular effects on signaling pathways that were previously unknown and potentially protect the hepatocyte. These effects intersect TG metabolism, fat-induced autophagy and AQP9-mediated glycerol transport in hepatocytes.

8.Excess fructose and fatty acids trigger a model of non-alcoholic fatty liver disease progression in vitro: Protective effect of the flavonoid silybin

Elena Grasselli[1], Francesca Baldini[1], Giulia Vecchione[1], Paulo J Oliveira[2], Vilma A. Sardão[2], Adriana Voci[1], Piero Portincasa[3] and Laura Vergani[1]

[1]DISTAV-Department of Earth, Environment and Life Sciences, University of Genova, I-16132 Genova, Italy; [2]CNC-Center for Neuroscience and Cellular Biology, University of Coimbra, 3060-197 Cantanhede, Portugal; [3]division of Internal Medicine 'A. Murri', department of Biomedical Sciences and Human Oncology, University of Bari Medical School, I-70162 Bari, Italy

Int J Mol Med. 2019 Aug;44(2):705-712. doi: 10.3892/ijmm.2019.4234. Epub 2019 Jun 6.

ABSTRACT

Overconsumption of fats and sugars is a major cause of development of non-alcoholic fatty liver disease (NAFLD). The main objectives of the present study were to explore the pathways sustaining the interfering metabolic effects of excess fructose and fatty acids in hepatocytes, and to clarify the mechanisms through which the nutraceutical silybin rescues the functional and metabolic alterations that are associated with the NALFD progression. Cultured hepatocytes were exposed to fructose and fatty acids, alone or in combination, to induce different grades of steatosis in vitro. Cell viability, apoptosis, free radical production, lipid content, lipid peroxidation and activity of lipogenic enzymes were assessed by spectrophotometric assays. Oxygen consumption and mitochondrial respiration parameters were measured using a Seahorse analyzer. Expression of markers for liver steatosis and dysfunction were also evaluated by reverse transcription-quantitative polymerase chain reaction. The data revealed that fructose and fatty acid combination in vitro had a positive interference on lipogenic pathways, leading to more severe steatosis and liver dysfunction, reduced cell viability, increased apoptosis, oxidative stress and mitochondrial respiration.

Hepatic cell abnormalities were almost completely alleviated by silybin treatment. These findings suggest that silybin may serve as a novel and cost-effective dietary supplement for treatment and/or prevention of hepatosteatosis associated with NAFLD progression.

INTRODUCTION

Overnutrition plays a pivotal role in obesity and comorbidities including nonalcoholic fatty liver disease (NAFLD), type 2 diabetes mellitus and cardiovascular disease (CVD) (Vecchie et al., 2017). NAFLD is characterized by hepatic accumulation of fat, particularly triglycerides (TGs), and may range from simple steatosis to nonalcoholic steatohepatitis (NASH), cirrhosis and hepatocellular carcinoma (Mendez-Sanchez et al., 2018). In liver cells, excess TGs are stored in lipid droplets (LDs), and LD-associated proteins, such as the adipose differentiation-related protein (ADRP), regulate lipid packing and traffic (Listenberger et al., 2007). TG synthesis is a beneficial response against excess of potentially toxic fatty acids (FAs), leading to inflammation and reactive oxygen species (ROS) formation, particularly in mitochondria (Feldstein et al., 2004), which trigger lipid peroxidation of membranes acting in NAFLD progression (Neuschwander-Tetri, 2010). Fructose-enriched food may contribute to the development of NAFLD (Ter Horst and Serlie, 2017). Fructose can enter *de novo* FA synthesis in liver cells through the action of fatty acid synthase (FAS). However, the extent to which fructose contributes to the metabolic disorders remains unclear, as only a limited number of data reporting its direct effects on hepatocyte during NAFLD progression are available (Gnocchi et al., 2014). In liver cells, NAFLD is associated with alterations in lipogenic and lipolytic pathways, which are controlled by a number of transcription factors, such as peroxisome proliferator-activated receptor (PPAR) (Grasselli et al., 2017), and by microRNAs (miRNAs/miRs), including miR-122, which is the most abundant hepatic miRNA (Moore et al., 2011). Dysregulation of miRNA expression has been reported in rodent models of NAFLD, and in certain cases aligned with the changes observed in obese patients with steatosis (Dongiovanni et al., 2018).

A deeper understanding of the mechanisms underlying NAFLD progression would help identifying novel cost-effective therapeutic strategies. It has been reported that plant polyphenols are promising molecules for the management of NAFLD (Baselga-Escudero et al., 2017). Silybin, the most relevant flavonolignan extract from the seeds of milk thistle (*Silybum marianum*) (Loguercio et al., 2011), exhibited certain beneficial effects in a preliminary study on NAFLD patients (Loguercio and Festi, 2011).

In the present study, an *in vitro* model of NAFLD progression was established to identify the

pathways sustaining the interference between excess fructose and fatty acids on dysregulating lipid and radical metabolism in hepatocytes, and to verify the ability of silybin to reverse these alterations. The results may have an important translational value for possible therapy of hepatic steatosis associated with NAFLD.

MATERIALS AND METHODS

Cell treatments.

Rat hepatoma FaO cells (European Collection of Authenticated Cell Cultures, Salisbury, UK; cat. no. 89042701) were supplied as mycoplasma‐free and cultured in Coon's modified Ham's F12 with 10% fetal bovine serum (South American origin, EU‐approved; Euroclone, Milan, Italy). When 80% confluence was reached, the cells were incubated in starvation medium containing 0.25% bovine serum albumin (BSA). Subsequently, cells were treated with an oleate/palmitate mixture (2:1 molar ratio; final concentration, 0.75 mM) for 3 h (referred to as the FA treatment group), with 5.5 mM fructose for 72 h (Fru group), or with sequential combination of fructose for 72 h and FAs for 3 h (Fru/FA group). Cells in the Fru/FA group were then treated for 24 h with 50 µM silybin (stock solution, 10 mM in dimethyl sulfoxide). Silybin treatment was also performed on untreated FaO cells, which served as the control group.

Cell viability and apoptosis

The sulforhodamine B (SRB) assay, relying on the property of SRB to bind stoichiometrically to proteins, is used to determine cell density. Briefly, 1.5x104 cells/well were seeded in 96‐well culture plates and treated. Next, the cells were fixed and incubated with 0.5% SRB in 1% acetic acid for 1 h at 37˚C. The dye bound to proteins was extracted with 10 mM Tris‐HCl (pH 10), and quantified in a Varian Cary‐50 Bio spectrophotometer (Agilent Technologies, Inc., Milan, Italy) (Vichai and Kirtikara, 2006). Caspase 3‐like activity is a marker of apoptosis as it initiates DNA fragmentation (Wiechelman et al., 1988). Caspase activity was measured in cell extracts containing 25 µg proteins determined by the bicinchoninic acid method (Moreira et al., 2014). Following resuspension in 20 mM HEPES/NaOH (pH 7.5), 250 mM sucrose, 10 mM KCl, 2 mM MgCl2, 1 mM EDTA, 2 mM dithiothreitol (DTT) and 100 µM phenylmethylsulfonyl fluoride, the cell extracts were incubated for 1 h at 37˚C in 25 mM HEPES (pH 7.5), 10%

sucrose, 10 mM DTT, 0.1% CHAPS and 100 µM caspase substrate Ac-D EVD- pNA. The released pNA was measured spectrophotometrically, and the results are expressed as nmol of pNA released per µg of protein (Grasselli et al., 2011).

Lipid quantification and imaging

TGs were extracted from the different cell groups and spectrophotometrically quantified as previously described (Grasselli et al., 2010). Data are expressed as the percent TG content relative to the control group. For LD visualization, cells growing on coverslips were treated as aforementioned, rinsed with PBS, fixed with 4% paraformaldehyde, stained by Oil Red O (Goodridge, 1972) and then examined with a Leica DMRB light microscope equipped with a Leica CCD camera DFC420C (Leica, Wetzlar, Germany).

FAS activity

FAS activity in the different cell groups was measured according to Goodridge (Vecchione et al., 2016). Briefly, cell lysate was obtained by mixing cells with 0.1 M KPi (pH 7.0), 3 mM EDTA and 1 mM DTT via a syringe needle. Then 20 µg of lysate were mixed to 0.1 M KPi (pH 7.0), 0.025 mM acetyl coenzyme A (CoA), 0.2 mM NADPH, 3 mM EDTA, 1 mM DTT, 25 mg/ml BSA and 0.1 mM malonyl-CoA. NADPH disappearance was followed by spectrophotometric examination. FAS activity (nmol NADPH/min/mg protein) was expressed as the percentage relative to the control group.

ROS production and lipid peroxidation

ROS production was quantified through the oxidation of 2',7'-dichlorofluorescin diacetate (DCF-DA; Fluka, Germany) to 2',7'-dichlorofluorescein (DCF), which was measured using a LS50B fluorimeter (PerkinElmer, Inc., Waltham, MA, USA). Briefly, suspended cells were loaded with 10 µM DCF-DA at 37˚C in the dark, centrifuged (800 x g for 10 min at 4˚C) and resuspended in PBS (Iguchi et al., 1993). The fluorescent intensity was normalized to the protein content. Lipid peroxidation was then evaluated through the thiobarbituric acid reactive substance assay, as previously described (Pfaffl, 2001). Cells were incubated for 45 min at 95˚C with 2 vol thiobarbituric acid (TBA) solution, containing 0.375% TBA, 15% trichloroacetic acid and 0.25 N HCl. Subsequently, 1 vol N-butanol was added, and the absorbance of the organic phase was measured. Values [pmol of malondialdehyde (MDA)

per ml/mg protein] were expressed as the percentage relative to the controls.

RNA extraction and reverse transcription‑quantitative polymerase chain reaction (RT‑qPCR)

Total RNA was extracted using TRIzol reagent (Thermo Fisher Scientific, Inc., Milan, Italy) and quantified spectrophotometrically. Then, cDNA was synthesized by using RevertAid H Minus transcriptase according to manufacturer's instructions (Thermo Fisher Scientific, Inc.); qPCR was performed in quadruplicate using 1X IQ™ SYBR® Green SuperMix and a Chromo4™ system (Bio‑Rad Laboratories, Inc., Milan, Italy) (Baselga-Escudero et al., 2015). Primer pairs for the assessed genes were designed *ad hoc* starting from the coding sequences of *Rattus norvegicus* (http://www.ncbi.nlm.nih.gov/Genbank/GenbankSearch.html) and listed in TableI. The amplification conditions were as follows: 3 min at 95˚C, followed by 40 cycles consisting of 5 sec at 95˚C, 30 sec of annealing (temperatures listed in Table I), and 40 sec of extension at 72˚C. At the end, a melting curve ranging between 55 and 95˚C was measured. The relative quantity of target mRNA was calculated by using the comparative Cq method and was normalized for the expression of GAPDH gene (Vecchione et al., 2017). In order to measure miR‑122 expression, the High‑Capacity cDNA RT kit and the miRNA‑specific primers provided with the TaqMan MicroRNA Assay kit (Thermo Fisher Scientific, Inc.) were used. Amplification was performed using the StepOnePlus Real‑Time PCR system (Thermo Fisher Scientific, Inc.). Probe and primers for miR‑122‑5p (4427975‑002245) and miRNA U6 (4427975‑001973) were provided by Thermo Fisher Scientific, Inc. The relative expression of miR‑122 and mRNAs was calculated by the comparative Cq method using miRNA U6 and GAPDH as housekeeping genes (Vecchione et al., 2017).

Oxygen consumption

Oxygen consumption was measured using the Seahorse XFe96 Extracellular Flux analyzer (Agilent Technologies, Inc., Santa Clara, CA, USA) as previously described (Deus et al., 2015). Briefly, approximately 2x104 cells/well were seeded into 96-well plates. A final concentration of 3 µM oligomycin, 1 µM FCC P, and a mixture of 1 µM rotenone and 1 µM antimycin were added sequentially to cells. The sensor cartridge and the calibration plate were used for calibration. Three baseline rate measurements of oxygen consumption rate (OCR) were made using a 3-min mixing and 3-min measure cycle. The compounds were injected

pneumatically by the Seahorse XFe96 analyzer into each well and mixed, following which the OCR measurements were conducted using the 3-min mixing and 3-min measure cycle (Hudgins et al., 2011).

Statistical analysis

Data are expressed as the mean ± standard deviation of at least three independent biological experiments performed as technical triplicates. Statistical analysis was performed using analysis of variance with Tukey's post‑test (GraphPad Software, Inc., San Diego, CA, USA). Differences with $P \leq 0.05$ values were considered as statistically significant.

RESULTS

Excess FAs and fructose alter lipid metabolism and cell function

The extent of steatosis was assessed by ORO-staining and TG quantification. The steatosis features were assessed as accumulation of cytosolic LDs whose number and size markedly increases compared to control cells (Fig.1A). Quantification of intracellular TGs (Fig.1B) showed that both fructose and fatty acids alone increased the TG content (+57%, $p \leq 0.01$ and +87%, $p \leq 0.001$ vs control, respectively), and their combination (Fru/FA) led to a larger increase (+277% vs control; $p \leq 0.001$). As markers for LD accumulation and hepatic cell dysfunction we assessed mRNA expression of ADRP and IkBip, respectively (Fig.1C). ADRP expression was up-regulated by FAs alone (1.85-fold induction vs control; $p \leq 0.001$), and even more by Fru/FA combination (2.08-fold induction vs control; $p \leq 0.001$). IkBip expression was significantly up-regulated only by Fru/FA combination (1.61-fold induction vs control; $p \leq 0.001$). Fru alone, but not FAs, stimulated FAS activity (+125% vs control; $p \leq 0.05$), and Fru/FA combination reduced it (-59% vs Fru; $p \leq 0.05$). (Fig.1D). On the other hand, expression of the miR-122 showed a slight significant increase only in Fru/FA cells (1.52-fold induction vs control; $p \leq 0.05$) (Fig.1E).

Lipid peroxidation was assessed as a marker of oxidative stress. The MDA level increased in response to both FAs alone and Fru/FA combination (+89% and +67% vs control, respectively; $p \leq 0.001$) (Fig.1F). This oxidative imbalance was paralleled by changes in caspase 3-like activity which increased in cells exposed to both FAs alone and to Fru/FA combination (+142% and +145% vs control, respectively; $p \leq 0.001$) (Fig.1G). By contrast, cell viability did not change in FA cells, but it was s reduced in cells exposed to Fru alone (-13% vs control; $p \leq 0.01$) and further reduced by Fru/FA combination (-23% vs control; $p \leq 0.01$) (Fig.1H).

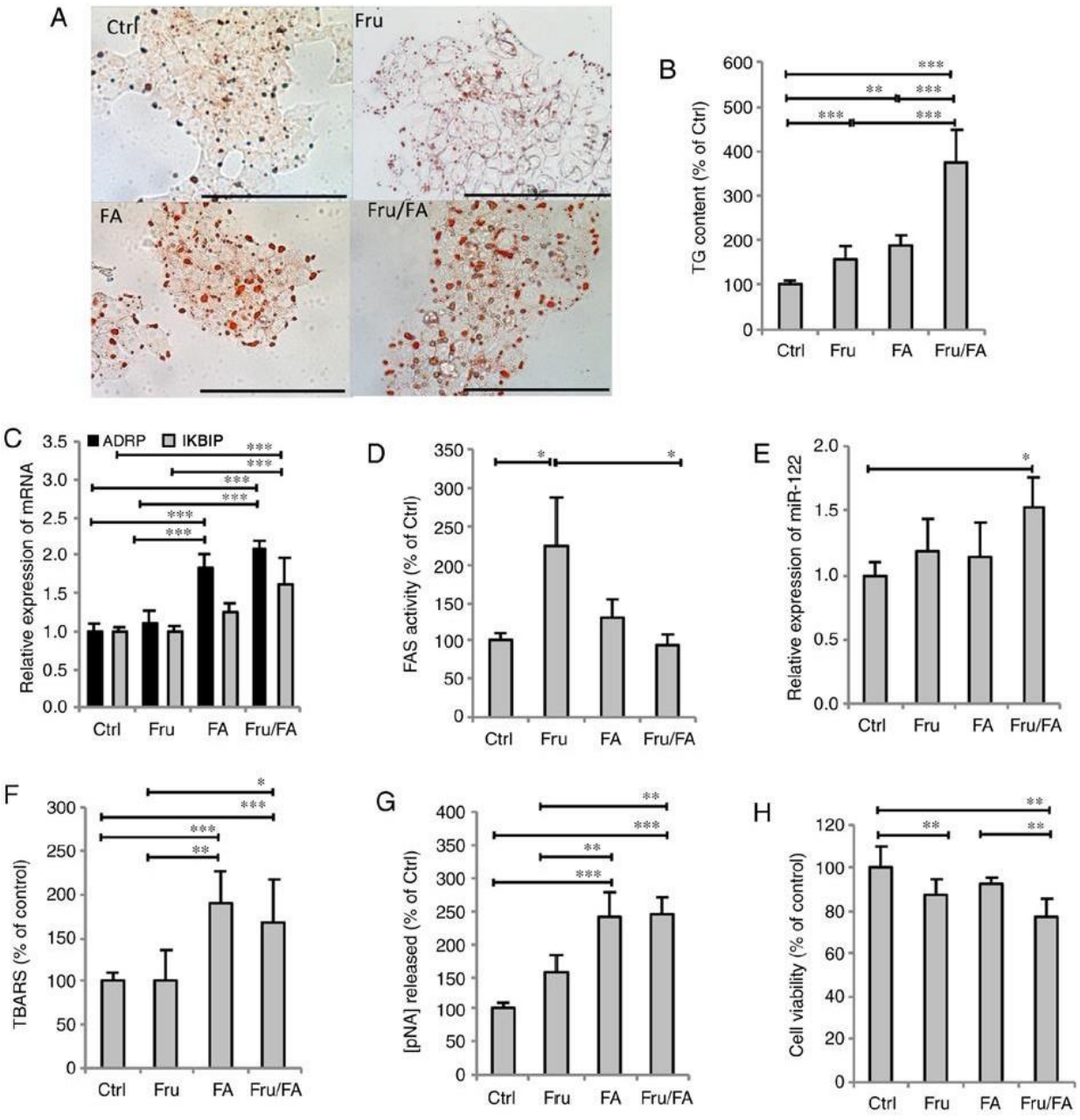

Figure 19. Steatogenic effects of Fru, FAs and their combination (Fru/Fa) in FaO cells

(A) Lipid droplet accumulation was visualized by Oil Red O staining (magnification, x40; bar, 100 µm). **(B)** TG content was quantified spectrophotometrically and normalized to total protein level. **(C)** Expression levels of AdRP and IKBIP mRNA were evaluated by RT-qPcR and expressed as the fold induction relative to the control. **(D)** FAS activity (nmol NAdPH/min/mg protein) was quantified spectrophotometrically. **(E)** miR-122 expression was evaluated by RT-qPCR using U6 as the internal control and is expressed as the fold induction relative to the control. **(F)** Malondialdehyde level (pmol MDA/ml/mg protein) was quantified by TBARS assay. **(G)** Activity of caspase 3 (nmol of pNA released/µg protein) was measured spectrophotometrically. **(H)** Metabolic activity was measured by sulforhodamine B assay (percentage relative to the controls). All values are expressed as the mean ± standard deviation from at least three independent experiments. *P≤0.05, **P≤0.01 and ***P≤0.001. Fru, fructose; FA, fatty acid; Ctrl, control; TG, triglyceride; ADRP, adipose differentiation-related protein; IKBIP, inhibitor of nuclear factor-κB kinase subunit β-interacting protein; RT-qPCR, reverse

transcription-quantitative polymerase chain reaction; FAS, fatty acid synthase; TBARS, thiobarbituric acid reactive substance.

Silybin counteracts the steatogenic effects of fructose and FAs

Exposure of Fru/FA cells to silybin 50µM for 24 h reduced markedly both the steatosis grade (-35% of TG ontent; p≤0.01), and the IkBip up-regulation (-32%; p≤0.001) compared to Fru/FA cells, whereas did not change the ADRP mRNA level (Fig.2A-C). Moreover, silybin led to changes in the lipogenic transcription factor PPARγ, whose expression was up-regulated in Fru/FA cells (1.55-fold induction vs control; p≤0.01) and reduced by silybin (-67% with respect to Fru/FA; p≤0.001), whereas both PPARα and PPARδ levels did not change (Fig.2D). Exposure to silybin further increased miR-122 expression (1.84-fold induction vs control; p≤0.001) in Fru/FA cells in which it was already over-expressed (Fig.2E). Treatment of control cells with silybin had no effects on expression of these genes.

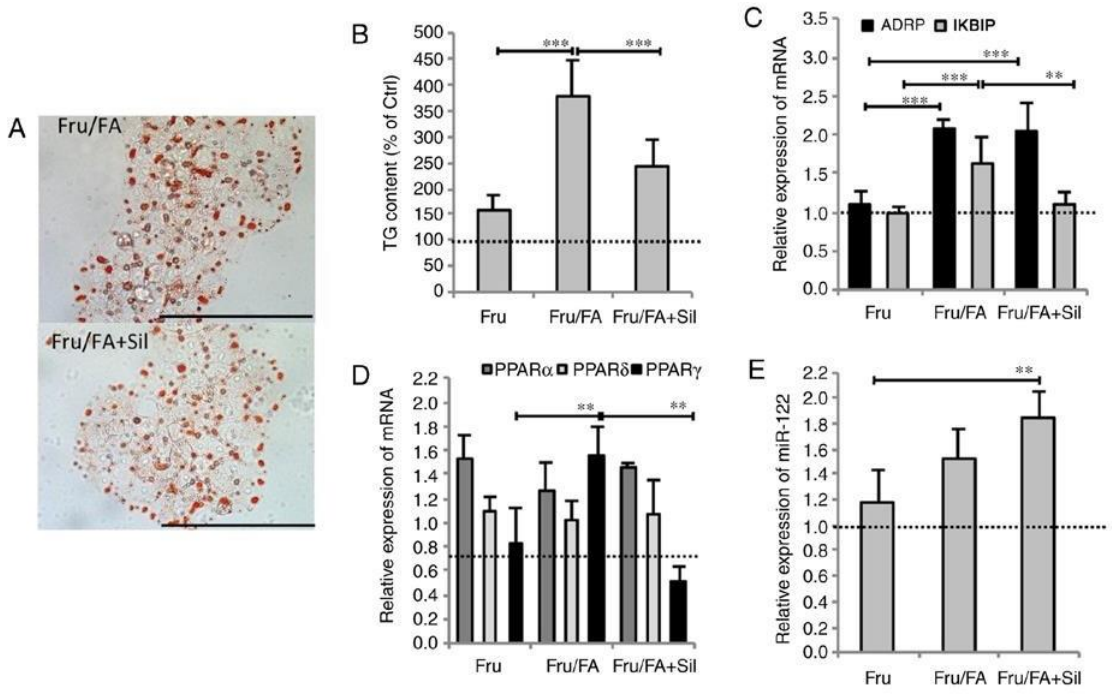

Figure 20. Silybin counteracts lipid metabolism dysregulation

Cells incubated with Fru/FA were then treated for 24 h with 50 µM silybin. **(A)** Microphotographs of Oil Red O-stained cells at a magnification of x40 (bar, 100 µm), and **(B)** histogram of TG content. **(C)** mRNA expression levels of ADRP and IKBIP, **(D)** mRNA expression levels of PPARα, γ and δ, and **(E)** miR-122 expression. All values are expressed as the mean ± standard deviation from at least three independent experiments. **P≤0.01 and ***P≤0.001. Fru, fructose; FA, fatty acid; TG,

triglyceride; ADRP, adipose differentiation-related protein; IKBIP, inhibitor of nuclear factor-κB kinase subunit β-interacting protein

Silybin counteracts apoptosis and mitochondrial dysfunction

Silybin did not rescue the reduction in cell viability caused by Fru/FA, but it played anti-apoptotic effects as indicated by the decrease in the caspase 3-like activity (-38% compared to Fru/FA cells; p≤0.001) (Fig.3A-B). Silybin was also able to counteract the lipid peroxidation (-30% compared to Fru/FA; p≤0.05) and the ROS levels (-50% with respect to Fru/FA; p≤0.001) (Fig.3C-D) being associated to excess fat in Fru/FA cells.

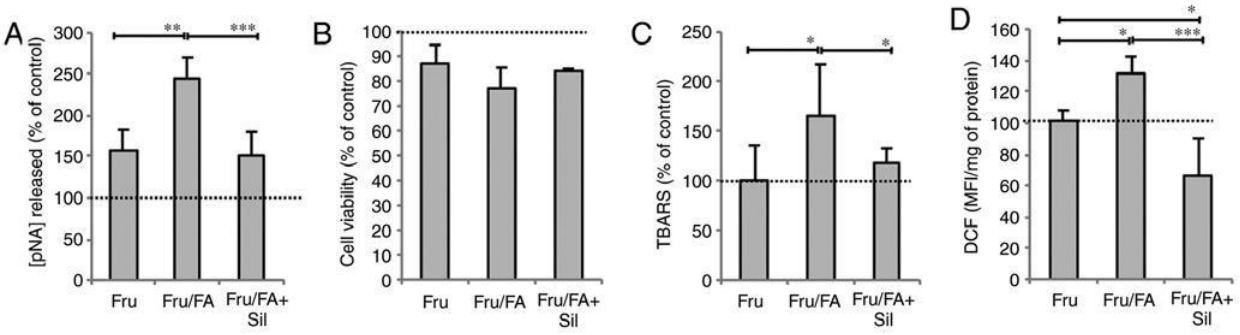

Figure 21. Silybin counteracts the cell viability and oxidative stress

Cells incubated with Fru/FA were then treated with silybin. **(A)** Activity of caspase 3. **(B)** Metabolic activity measured by sulforhodamine B assay, indicating the cell viability. **(C)** Malondialdehyde level was quantified by TBARS assay. **(D)** Intracellular level of reactive oxygen species was quantified fluorimetrically. All values are expressed as the mean ± standard deviation from at least three independent experiments. *P≤0.05, **P≤0.01 and ***P≤0.001. Fru, fructose; FA, fatty acid; TBARS, thiobarbituric acid reactive substance.

Steatotic hepatocytes typically stimulate respiration and ATP production in the attempt to counteract the excess TG (Vecchione et al., 2016). Silybin reduced basal respiration (-56%, p≤0.01), maximal respiration (-62%, p≤0.001) and ATP production (-60%, p≤0.001) in Fru/FA cells, without significant effects on proton leak (Fig.4A-D). Moreover, the expression of the mitochondrial proteins CPT-1 and UCP2, the main regulatory steps of mitochondrial FA oxidation, was increased in Fru/FA cells (2.29- and 1.74-fold induction, respectively, vs control; p≤0.001 and p≤0.01) and a further up-regulation was observed upon exposure to silybin (+68% and +50%, p≤0.001 for both (Fig.4E). Treatment of control cells with silybin had

no effects on apoptosis, lipid peroxidation, and mitochondrial respiration.

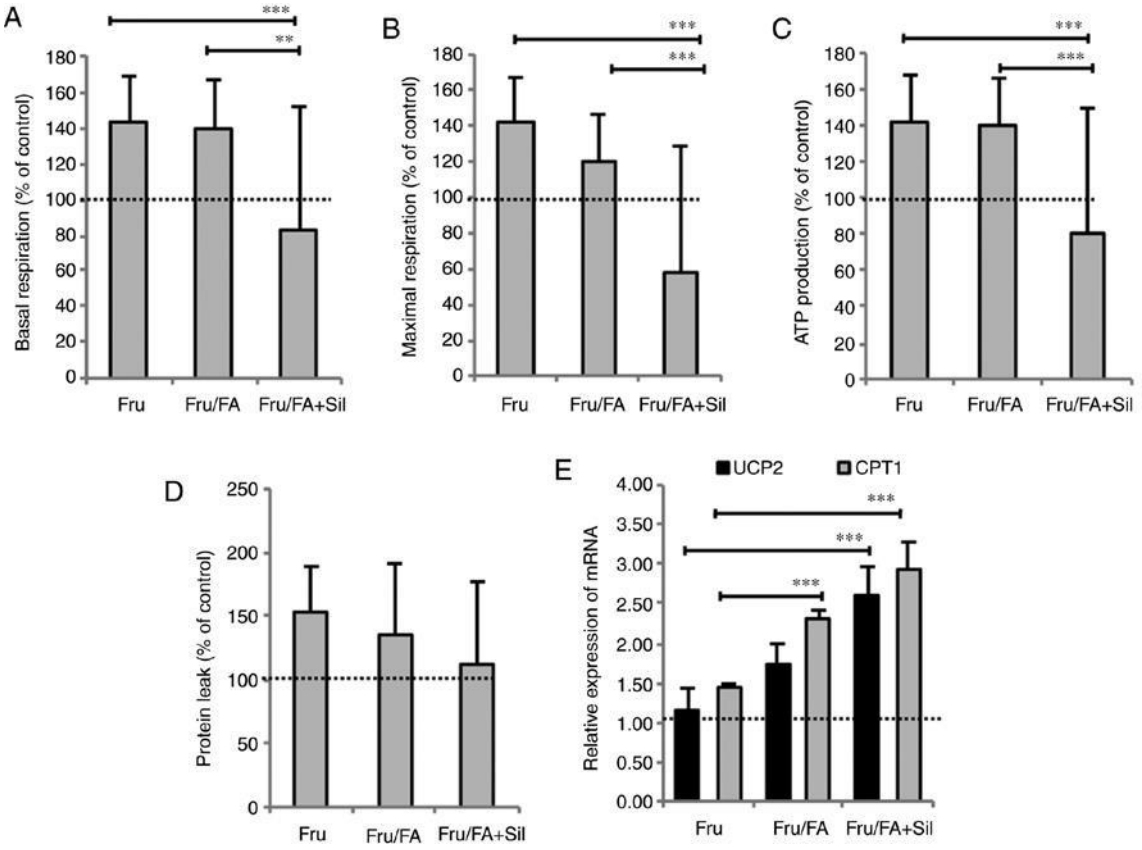

Figure 22. Silybin ameliorates mitochondrial dysfunction

Cells incubated with Fru/FA were then treated with silybin, and the following respiratory parameters were evaluated using the Seahorse XFe96 Extracellular Flux Analyzer: **(A)** cell basal respiration, **(B)** cell maximal respiration, **(C)** ATP production and **(D)** proton leak (all presented as the OcR pmol/min/SRB labeling). data are expressed as the mean ± standard deviation of 14 separate experiments (n=16). **(E)** mRNA expression levels of UcP2 and cPT1 were evaluated by reverse transcription-quantitative polymerase chain reaction. Values are expressed as the mean ± standard deviation from at least three independent experiments (n=16 for Seahorse experiments). **P≤0.01 and ***P≤0.001. Fru, fructose; FA, fatty acid; OCR, oxygen consumption rate; SRB, sulforhodamine B; CPT1, carnitine palmitoyltransferase 1; UCP2, uncoupling protein 2.

DISCUSSION

This study provided insights into the molecular mechanisms through which excess fructose impair the lipogenic pathways in hepatocytes. In the past, fructose was considered as a beneficial dietary component because it does not stimulate insulin secretion, but the harmful effects of fructose have recently gained mainstream attention. Studies reported that high fructose intake stimulates de novo lipogenesis (Hudgins et al., 2011), and mice fed fats and a high-fructose corn syrup equivalent developed severe NAFLD (Tetri et al., 2008). Our findings show that exposure of FaO cells to fructose/fatty acid combination led to larger TG synthesis and accumulation compared to the single agents, and that the more severe steatosis was associated to worsening of cell dysfunction parameters including cell viability, oxidative stress and mitochondrial respiration.

In our model, the sequential exposure of hepatocytes to high fructose and fatty acids mimics the NAFLD progression in vitro. Excess fructose alone stimulates FAS activity resulting in TG overproduction, and Fru/FA combination led to more severe cell dysfunction compared to single treatments as confirmed by: (i) larger steatosis; (ii) maximal up-regulation of ADRP and IkBip expression; (iii) enhanced lipid peroxidation, ROS production, and caspase 3-like activity, which are indexes of oxidative stress and apoptosis, respectively. The extensive damaging effect of Fru/FA combination was also evident looking at expression of miR-122 which seems to be involved in the onset/progression of NASH (Dongiovanni et al., 2018).

Mitochondria are the main site for FA degradation, and steatotic hepatocytes typically enhance mitochondrial β-oxidation to limit excess fat accumulation. Accordingly to this scenario, the mitochondrial proteins CPT-1 and UCP2 were overexpressed in cells treated with Fru/FA combination. Also basal and maximal mitochondrial respiration as well as ATP production were stimulated by Fru/FA combination in the attempt to compensate for the increased FA oxidation. Of note, the increase in oxidative stress due to the over-active β-oxidation may trigger proinflammatory pathways sustaining NAFLD progression.

The results of this in vitro study fit with those described in patients and animals. While a “high fat” diet results in obesity, insulin resistance, and hepatic steatosis with minimal inflammation and no fibrosis, the “Western cafeteria” diet being rich in fructose leads to steatosis associated to hepatic fibrosis, inflammation, oxidative stress and apoptosis.

The nutraceutical silybin is known as a general hepatoprotective, anti-steatotic agent (Vecchione et al., 2016; Vecchione et al., 2011), which has provided encouraging results in animal and cellular models of NAFLD (Vecchione et al., 2011; Rosso et al., 2015), and in clinical studies (Abenavoli et al., 2015; Federico et al., 2017; Wah Kheong et al., 2017). As further insight, we showed that silybin counteracted the metabolic dysfunctions caused by Fru/FA combination acting directly on hepatocytes. First, silybin reduced the largest TG accumulation resulting from Fru/FA combination by down-regulating the expression of PPARγ, the main transcription factor for lipogenic genes. The hepatoprotective action of silybin was able to counteract in vitro the Fru/FA-dependent increase in: (i) IkBip expression; (ii) intracellular ROS production and lipid peroxidation; (iii) apoptosis rate. However, silybin was no able to blunt the reduction in cell viability associated to exposure to Fru/FA combination. The action of silybin seems to be mainly dependent on its effects on mitochondria, with different mechanisms depending on the NAFLD grade (Vecchione et al., 2017). In our model mimicking a rather severe NAFLD, silybin exerts beneficial activity by inhibiting mitochondrial respiration which is stimulated in steatosis progression as a consequence of an increased oxidative metabolism due to stimulation of anabolic pathways (Satapati et al., 2015).

In conclusion, our model consisting of lipid-loaded hepatocytes mimicking in vitro the NAFLD progression offers new insights about the harmful steatogenic effects of fructose on liver cells, and supports the hepatoprotective activity of silybin. Further studies can translate these results into long-term beneficial effects, in the hope that onset, progression and worsening of NAFLD/NASH will be prevented/delayed in patients by using nutraceutical approaches

9.Biomechanics of cultured hepatic cells during different steatogenic hits

Francesca Baldini[1], Alice Bartolozzi[2], Martina Ardito[1], Adriana Voci[1], Piero Portincasa[3], Massimo Vassalli[2], Laura Vergani[1]

[1]Department of Earth, Environment and Life Sciences (DISTAV), University of Genova, Corso Europa 26, 16132, Genova, Italy; [2]Institute of Biophysics (IBF), National Research Council, Via De Marini 6, 16149, Genova, Italy; [3]Department of Biomedical Sciences and Human Oncology, University of Bari Medical School, Piazza Giulio Cesare 11, 70124, Bari, Italy

J Mech Behav Biomed Mater. 2019 Sep;97:296-305. doi: 10.1016/j.jmbbm.2019.05.036. Epub 2019 May 22.

ABSTRACT

Non-alcoholic fatty liver disease (NAFLD) is a chronic liver disease often associated with overnutrition. Number and morphometry of lipid droplets (LDs) define micro *vs* macrovesicular steatosis, influence the morphology and function of hepatocytes and possibly their stiffness. The link between grade and features of steatosis and biomechanical properties of single hepatocytes requires deeper investigations. *In vitro* NAFLD models with distinct steatosis conditions were set by exposing FaO hepatoma cells to single or combined fructose (Fru), fatty acids (FA), and tumor necrosis factor (TNF)α. Single Cell Force Spectroscopy and Quantitative Phase Microscopy quantified the single cell stiffness and a series of morphometric parameters; the mRNA expression of genes involved in lipid metabolism was quantified by real-time PCR. In our models, LD size and number increased with Fru and FA as single agents, and more with combined Fru/FA (macrovesicular steatosis), while FA/TNFα combination increased LD number with a reduction in their size (microvesicular steatosis). We found that the changes in LD size and number profoundly influenced cell stiffness and morphometry as follows: *(i)* single cell elasticity increased in macrovesicular steatosis (maximally with combined Fru/FA); *(ii)* FA-induced steatosis resulted in cells thinner and larger, whereas combined FA/TNFα shrunk the hepatocytes. Taken together the data on hepatocyte biomechanics show that, in addition to extent of lipid

accumulation, cell stiffness is mainly influenced by LD size, while cell morphometry directly relates to LD number. Our findings suggest that a novel mechanobiology perspective might provide future contributions in NAFLD research.

INTRODUCTION

The liver is not a primary fat storage depot and the steady state concentration of hepatic triglycerides (TGs) is rather low under physiological conditions. Excess TG accumulation in hepatocytes results in nonalcoholic fatty liver disease (NAFLD), the metabolic liver disease which attracts ever more attention in Western countries for its increasing prevalence as consequence of overnutrition (Brunt et al., 2015). NAFLD may encompass a spectrum of liver abnormalities ranging from the simple steatosis, to nonalcoholic steatohepatitis (NASH), to cirrhosis and hepatocarcinoma (Nagaya et al., 2008). Hepatic steatosis typically results from an imbalance in lipid metabolism network leading to excess TGs which derive from either excess fatty acid (FA) intake or *de novo* lipogenesis (Vergani, 2014). TGs are stored as cytosolic lipid droplets (LDs) (Sahini and Borlak, 2014; Gluchowski et al., 2017) which consist of a hydrophobic lipid core surrounded by a phospholipid monolayer and by LD-associated proteins which regulate lipid metabolism and traffic (Xu et al., 2018). Among them, the adipose differentiation-related protein (ADRP) is crucial for formation and structural maintenance of LDs and is a marker for the extent of lipid accumulation, as its overexpression stimulates lipogenesis and inhibits lipolysis (Grasselli et al., 2010). ADRP is mainly regulated by the peroxisome proliferator-activated receptors (PPARs), which are ligand-dependent transcription factors also involved in NAFLD progression (Wang et al., 2017; Silva et al., 2018).

In NAFLD patients, steatosis typically appears as macrovescicular steatosis (large LDs), which has rather good long-term prognosis with rare progression to fibrosis or cirrhosis. By contrast, microvescicular steatosis denotes a separate clinical entity with small LDs commonly associated with severe liver damage (i.e. by drugs) and worse prognosis (Tandra et al., 2010).

In hepatocytes, TG synthesis is a beneficial response against potentially dangerous FAs which are “aggressive” species leading to tumor necrosis factor (TNF)α and reactive oxygen species (ROS) production that act as early “inflammatory” hits and promote NAFLD progression (Bessone et al., 2018; Tilg and Moschen, 2010). Intracellular fat excess may damage mitochondrial and endothelial reticulum (ER) function (Lebaupin et al., 2018). The fat-dependent ER stress is associated with over-expression of the IκB kinase β (IKBKB)-interacting protein (IkBip), a marker for the progression of liver damage during NAFLD (Fromenty and

Pessayre, 1995).

Both excess fatty acids or fructose are steatosis-triggering agents. Our previous studies showed that sequential exposure of cultured hepatocytes to high concentrations of FAs and TNFα resulted in fat overload and oxidative stress which mimic *in vitro* the NAFLD progression (Vecchione et al., 2017). After 1960s, fructose consumption has increased worldwide and now represents more than 20% of total daily carbohydrate intake (10% of daily total energy intake) with effects on conditions such as insulin resistance and obesity (Gross et al., 2004). High-intake of fructose acts as a potent steatogenic agent in western- type diet (Tetri et al., 2008; Kohli et al., 2010).

Altered biomechanical properties of cells have been described in several diseases (Yarpuzlu et al., 2014). Our hypothesis is that fat accumulation should influence the biomechanics of single hepatocytes and trigger mechanosensitive processes. The progression of NAFLD *in vivo* is associated with an altered mechanical liver phenotype, in which the stiffness is strictly linked to organ dysfunction and used as a diagnostic marker (Singh et al., 2013). As LDs are stiffer than the surrounding cytosol, accumulation of LDs may mechanically distort the intracellular environment (Shoham et al., 2014). Nevertheless, a connection between changes in biomechanical properties and altered physiological functions of the cell has not been yet identified, and requires further investigations.

We hypothesize that the mechanical properties of single hepatocytes could depend on the steatosis grade and LD features. A detailed biophysical single cell study of different steatotic models mimicking NAFLD progression *in vitro* was performed by Single Cell Force Spectroscopy (SCFS) (Mescola et al., 2012) and high resolution Quantitative Phase Microscopy (QPM) (Barone-Nugent et al., 2002) to verify whether and how the cell elasticity and the morphometric features of steatosis could be associated with different steatotic conditions.

MATERIALS AND METHODS

Chemicals

All chemicals, unless otherwise indicated, were supplied by Sigma-Aldrich Corp. (Milan, Italy).

Cell culture and treatments

Rat hepatoma FaO cells were obtained from European Collection of Authenticated Cell Cultures (ECACC- Salisbury, Wiltshire ,UK). The cells were routinely checked for contaminants and screened for mycoplasma contamination. Cells were cultured in low glucose (1.8 gr/L) Coon's modified Ham's F12 supplemented with 2mM Glutamine and 10% Foetal Bovine Serum (FBS) (Euroclone Milan, Italy) at 37°C in a humidified atmosphere containing 5% CO_2 (Grasselli et al., 2011). For treatments, FaO cells were plated in plastic dishes and grown for 24h in high-glucose (4.5 gr/L) medium with 0.25% bovine serum albumin (BSA), and subjected to different treatments: Control (Ctrl) no treatment; Fructose (Fru) incubation with fructose 5.5 mM for 72 h; Fatty acids (FA) incubation with oleate/palmitate mixture (2:1 molar ratio, final concentration 0.75mM) for 3h; Fructose + Fatty acids (Fru/FA) sequential incubation with fructose for 72 h, then with FA for 3 h; Fatty acids + TNFα (FA/TNFα) sequential incubation with FA for 3 h and then with TNFα for 24 h [15].

Cell viability assessment

Cell viability in the different experimental conditions was assessed by Resazurin assay. Briefly, 1.5×10^4 cells/well were seeded in 96-well plates and treated as above described. At the end of treatment, medium was removed and cells were incubated for 30 min with 10μg/ml resazurin in fresh medium. The reduction of resazurin to resorufin, indicative of metabolic activity of the cells, was measured fluorimetrically (λ_{exc} 570nm; λ_{em} 600nm) in Biotek-Cytation 3 reader (Biotek Instruments, Winooski, VT, USA) (Voytik-Harbin et al., 1998).

Lipid droplet imaging

Cells grown on coverslips were rinsed with phosphate-buffered saline (PBS) pH 7.4 Neutral lipids were visualized by optical microscopy using the selective Oil-RedO (ORO) dye (Koopman et al., 2001). Briefly, after fixing in 4% paraformaldehyde for 20 min at room temperature, cells were washed with PBS, stained for 20 min with 0.3% ORO solution prepared from a stock 0.5% in isopropanol and diluted in water. After washing, slides wer

examined by Leica DMRB light microscope equipped with a Leica CCD camera DFC420C (Leica, Wetzlar, Germany) as previously described (Vecchione et al., 2017).

RNA extraction and real-time qPCR

RNA was isolated using Trizol reagent, cDNA was synthesized and quantitative real-time PCR (qPCR) performed in quadruplicate using 1x IQ™SybrGreen SuperMix and Chromo4™ System apparatus (Biorad, Milan, Italy). The relative quantity of target mRNA was calculated by the comparative Cq method using glyceraldehyde 3-phosphate dehydrogenase (GAPDH) as housekeeping gene, and expressed as fold induction with respect to controls (Vecchione et al., 2017). Primer pairs designed *ad hoc* starting from the coding sequences of *Rttus norvegicus* (http://www.ncbi.nlm.nih.gov/Genbank/GenbankSearch.html) and synthesized by TibMolBiol (Genova, Italy) are reported in previous papers (Vecchione et al., 2017).

Single cell force spectroscopy (SCFS)

SCFS allows to measure single cell elasticity using a nano-indentation device (Piuma Chiaro, Optics11, Amsterdam, NL) mounted on an inverted microscope. Living cells were measured in Petri dishes in the culture medium. The probe was brought in contact with the cell and the resulting interaction force was measured as a function of the cell deformation. The probe was a µm-sized glass sphere (radius of 9µm and stiffness of 0.2 N/m). After every experiment the probe was washed in ethanol 70% for 10 min. The probe was glued to an elastic cantilever which bends proportionally to the interaction force; the deflection was measured by a laser interferometer coupled to the instrument (Chavan et al., 2012). A grid of measurements was performed at room temperature for less than 2 h. For each experimental condition, about 50-70 curves were acquired over at least three different repeats. Single curves were acquired at the speed of 1 µm/s and the indentation of the cell evaluated up to a defined threshold of 400 nm. Before every experiment, the optical sensitivity and the geometrical factor were calibrated. The collected curves were analysed using a custom software programmed with Python 3 (Python Software Foundation, www.python.org) and the Numpy/Scipy Scientific Computing Stack (Jarrod et al., 2011). Every dataset was pre- filtered to eliminate irrelevant curves using a semi-automatic procedure.

To convert the curve in a reliable elasticity information, a further fitting step against a theoretical model is required. Among the many approaches proposed in literature (Chen et

al., 2014), the simplest and more accepted is based on the Hertzian dynamics (Johnson, 1985). The hypothesis behind the theoretical derivation of the Hertz formula (isotropy, homogeneity and pure elasticity of the sample) are fairly satisfied by a cellular system, and the corresponding Young's modulus does not provide a robust absolute indicator of the elasticity unless an extreme care is posed in the experimental procedure (probe selection, calibration, measurement protocol, data analysis) (Nataliia et al., 2014; Hermann et al., 2017). Given that cells show a largely viscous behavior (Trepat et al., 2007), special attention should be posed to the selection of the dynamical protocol (Fabry et al., 2001). In particular, if the indentation speed is maintained the same for all the experiments and it is kept under few µm/s, it is possible to obtain a robust effective elasticity indicator without explicitly accounting for viscosity (Guz et al., 2014).

Nevertheless, the use of the Hertz model provided to be effective in experimental designs in which the elasticity of single cells is used as a biomarker. Here a method is proposed to obtain relative elasticity that exploits the Hertz model but avoiding the main tricky steps of the standard implementations (see results).

Quantitative Phase Microscopy (QPM)

QPM aims at reconstructing the three dimensional (3D) shape of semi-transparent objects through recording the phase of the light. Cells grown on coverslips were fixed in 4% paraformaldehyde for 20 min and washed in PBS; then slides were mounted and observed. A home-made acquisition system equipped with a Nikon 40X infinity-corrected objective (NA 0.75; WD 0.66 mm), mounted on a motorized Z-axis with a 0.01 µm resolution step, allowed to integrate standard modular components (Optem FUSION, Qioptiq Photonics GmbH & Co KG). The sample was scanned using a motorized X-Y stage with a 0.5 µm resolution step. A modular stepper motor controller (phyMOTION™, Phytron, Gröbenzell, Germany) drives three motorized axes. A LED lamp is integrated for the illumination; a Gig-E DMK 23G274 camera (The Imaging Source, Bremen, Germany) equipped with a 1600×1200 pixels monochrome CCD is used. The control software was developed in LabVIEW [National Instruments, Austin, Texas] to automate all the microscope functions. An area of about $1cm^2$ was imaged, resulting in 80-100 stack per sample, each comprising 15 Z planes acquired with a 1µm step around the estimated best focal plane. Each Z-stack was transformed in a 3D phase map and, after calibration, in a thickness map where each pixel encodes for the optical

thickness of the sample (the product of the thickness times the refractive index) by implementing a method based on the Transport of Intensity Equation (TIE) (Petecchia et al., 2017). The reconstruction was performed inverting the TIE (Teague, 1983) using a strategy (Zuo et al., 2013) based on the Savitzky-Golay filters (Savitzky and Golay, 1964). The procedure was implemented in a custom software coded in Python 3 (Python Software Foundation, www.python.org) and based on the original Matlab source code provided by the authors. All the reconstructed maps were further processed in order to isolate (mask) single cells using a semi-automatic procedure implemented in the free software Gwyddion (Necas et al., 2011). A set of morphometric indicators was calculated for each cell, and a relevant subset was selected for comparison, as reported in Table 1 and sketched for visual reference in Fig. 4.

Statistical analysis

Data are expressed as means ± SD of at least three independent biological experiments performed as technical triplicates. Statistical analysis was performed using *ANOVA* with Tukey's post-test (GraphPad Software, Inc., San Diego, CA, USA). Multivariate linear regression analysis was used after testing of normal Gaussian distribution and logarithmic transformation. Statistical significance was assumed for p-values ≤ 0.05. In order to visually evaluate possible (direct or inverse) correlations among all parameters obtained from the experiments (biochemical, morphometric or mechanical) a full correlation matrix was calculated using the pandas Python package (https://pandas.pydata.org). Each cell of the matrix reports the pairwise correlation (Pearson's r coefficient) between two data sets.

RESULTS

Lipid accumulation pathways

The spectrophotometric quantification of TG content in hepatocytes showed that, compared to controls, lipid accumulation increased significantly (p≤0.05) with Fru (+57%), FA (+87%) and the increase was larger in cells exposed to Fru/FA combination (+277%); the effect of combined FA/TNFα was similar to FA alone (+90% *vs* control) (Fig. 1A). The microscopic analysis of cytosolic LDs in ORO-stained FaO cells showed a marked accumulation of LDs in all steatotic conditions as compared to controls (Fig. 1B). In control cells, the quantitative analysis showed only small (about 0.9±0.3 µm) and few (about 2 LDs/cell) droplets dispersed in the cytosol. LD size increased selectively in all steatotic conditions: about +39% with Fru, +214% with FA, +334% with Fru/FA, and +50% in FA/TNFα cells (Fig. 1C). LD number, by contrast, invariably increased to 10 (Fru), 13 (FA), 14 (Fru/FA), and 18 (FA/TNFα) LDs/cell (Fig. 1D). Interestingly, with respect to FA alone the exposure of cells to FA/TNFα combination decreased the LD size of about -52%, but increased the LD number from 13 to 18 LDs/cell.

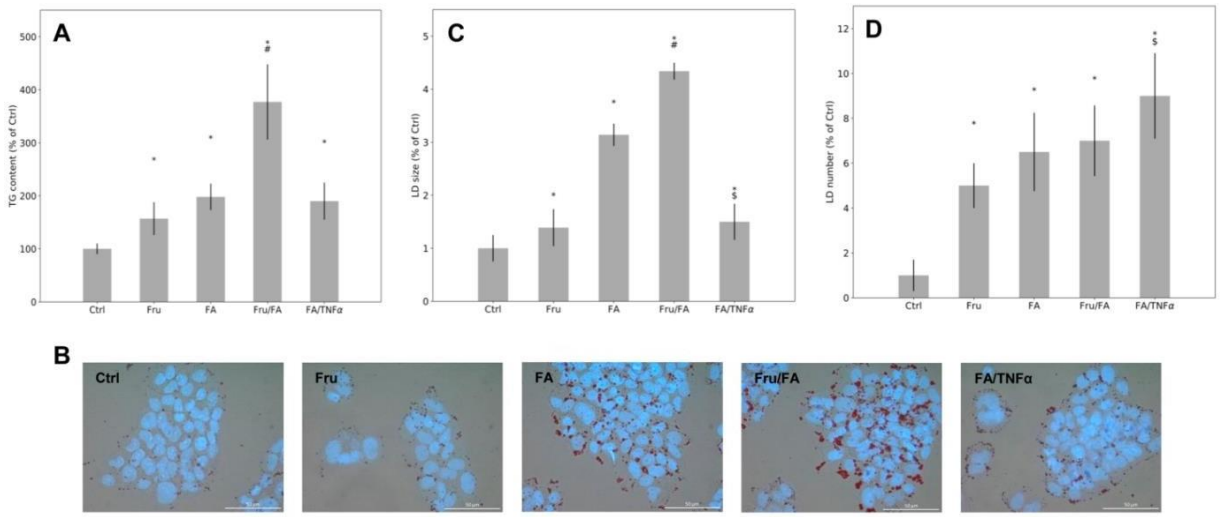

Figure 23. Lipid accumulation in different steatosis models

For FaO cells incubated in the absence (Ctrl) or in the presence of fructose (Fru), oleate/palmitate (FA), Fru/FA, FA/TNFα we show: **(A)** TG content expressed as percent TG content relative to controls, normalized for proteins determined with Bradford assay. **(B)** Microphotographes of cells stained with DAPI and Oil Red-O (ORO) (magnification 40x; Bar: 10 µm). **(C-D**) Average size of LDs. and number of LDs/cell. Values are mean±S.D. from at least three independent experiments. Statistical significance between groups was assessed by ANOVA followed by Tukey's test. Symbols: Ctrl *vs* all treatments *p≤0.05; FA *vs* all treatments #p≤0.05; Fru *vs* all treatments $ p≤0.05.

On the other hand, LD accumulation slightly affected cell viability: compared to control, a significant ($p \leq 0.05$) decrease was noted with Fru (-15%), Fru/FA (-27%) and FA/TNFα (-24%) but not with FA alone (Fig. 2A).

Hepatic lipid accumulation depends on the balance between lipolytic and lipogenic pathways which are under the master control of PPARα and PPAR γ (Varga et al., 2011), whose mRNA expression was assessed by qPCR (Fig. 2B). Fru alone increased PPARα mRNA expression (1.53-fold induction *vs* control; $p \leq 0.05$), without affecting PPARγ. On the other hand, FA, Fru/FA, and FA/TNFα up-regulated PPARγ expression (2.2-, 1.5- and 2.8-fold induction *vs* control, respectively; $p \leq 0.05$), but only FA/TNFα up-regulated also PPARα expression (1.8-fold induction *vs* control controls; $p \leq 0.05$).

Also ADRP mRNA expression, a marker for LD accumulation, changed differently in the different conditions. It was unchanged with Fru, significantly upregulated with FA and Fru/FA (1.85- and 2.08-fold induction *vs* control, respectively; $p \leq 0.05$), and again comparable to control with FA/TNFα (Fig. 2C). By contrast, IkBip mRNA expression, a marker for hepatic cell damage, was unaffected with Fru and FA,but became up-regulated with Fru/FA and greatly up-regulated with FA/TNFα (1.61-, and 4-6- fold induction *vs* control; $p \leq 0.05$) (Fig. 2C).

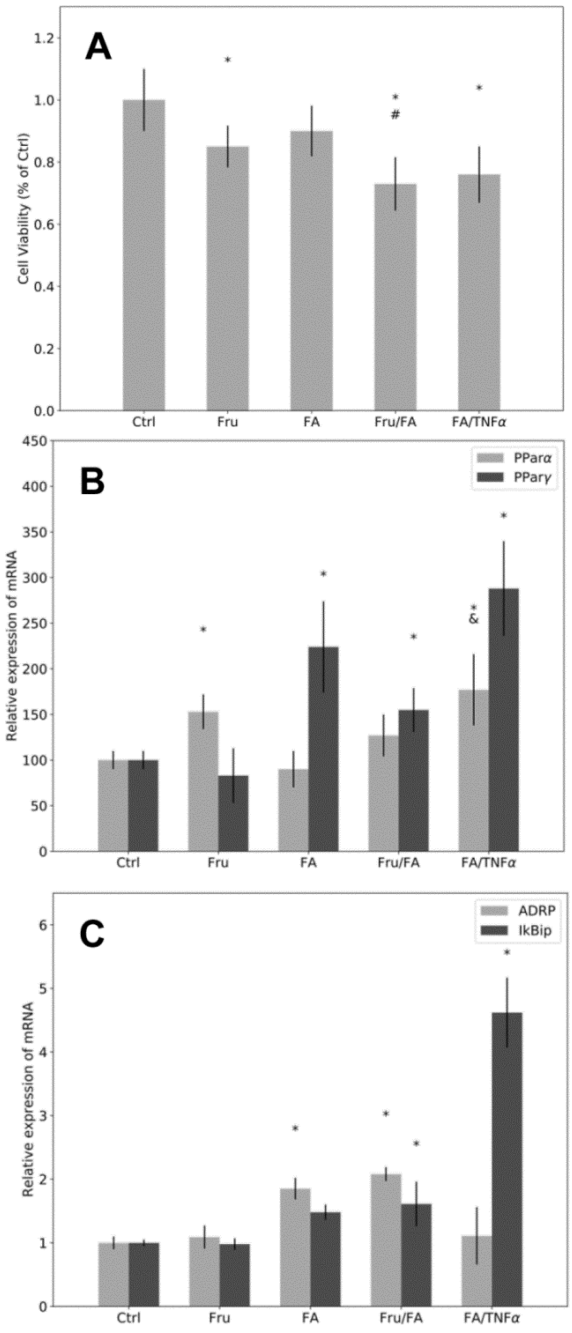

Figure 24. Modulation of cell function in different steatosis models

(A) The cell viability based on metabolic activity was assessed by resazurin assay; data are expressed as percentage values with respect to controls. The mRNA expression of PPARα and PPARγ **(B),** of ADRP and of IkBip **(C)** were evaluated by qPCR using GAPDH as the internal control. Data are expressed as fold induction with respect to controls. Bars represent SD. ANOVA followed by Tukey's test was used to assess the statistical significance between groups. Symbols: Ctrl *vs* all treatments *p≤0.05; FA *vs* all treatments #p≤0.05; Fru *vs* all treatments $ p≤0.05**.**

Lipid accumulation and single cell biomechanics

The elasticity of living cells in different steatotic conditions was assessed by SCFS through recording the force *vs* displacement curves (Fig. 3A-B). The curves require to be processed using a reliable a model. The simplest and more accepted approach is based on the Hertzian dynamics (Johnson, 1985). When an elastic sample is pushed using a rigid indenter of known geometry, the Hertz model predicts the behavior of the experienced force *F* as a function of the indentation depth δ (Puricelli et al., 2015; Abdelaziz et al., 2008) which, for a spherical indenter of radius *R*, can be written as (Johnson et al., 1971):

$$F = \frac{4\sqrt{R}}{3}\frac{E}{1-\nu}\delta^{\frac{3}{2}}$$

where *E* is the Young's modulus and *v* is the Poisson ratio of the sample. Fitting this formula to the collected curves supplies an estimate of the Young's modulus for single cell. This procedure is called direct fit (DFIT). When we are interested in a relative value of the elasticity to monitor its changes in different conditions, a more robust procedure can be introduced based on the so called Force Integration to Equal Limits (FIEL) method (A-Hassan et al., 1998). The FIEL approach evaluated the interaction work *w* (represented by the grey area in Fig. 3), rather than the interaction force. It makes possible to relate the change in the elasticity (relative stiffness E_r) of a sample to the ratio of the corresponding loading works:

$$E_r = \frac{E_2^*}{E_1^*} = \left(\frac{w_1}{w_2}\right)^{3/2}$$

thus, eliminating most of the tricky steps involved in the standard DFIT procedure. The relative elasticity $E_{r,n}$ of a sample *n* was calculated with respect to the average of the control dataset, such as:

$$E_{r,n} = \left(\frac{\langle w_{CTRL}\rangle}{w_n}\right)^{3/2}$$

The FIEL analysis, which has been specifically tuned for this study, guarantees an unprecedented sensitivity and robustness in the quantification of the mechanical properties, thus allowing to resolve small changes with statistical relevance.

Table 2 compares the main results obtained with the FIEL and the standard DFIT methods.

As depicted in Fig. 3C, the relative elasticity E_r values obtained with the DFIT approach are more broadly distributed (SD 2 to 4 folds larger than the one obtained with the FIEL method). Moreover, the FIEL distributions more closely resemble a Gaussian (Shapiro coefficient closer to 1) (Shapiro and Wilk, 1965).

The FIEL approach (Fig. 3D) showed that E_r significantly ($p \leq 0.05$) increased in cells exposed to either Fru or FAs as single agents (1.11 and 1.15 fold increase *vs* control, respectively), and a larger (1.17 fold increase *vs* control), but not statistically significant increase with respect to FAs and Fru occurred in cells exposed to Fru/FA combination. Conversely, the FA/TNFα combination led to an *Er* increase (1.09 fold increase *vs* control) similar to that observed for FAs alone.

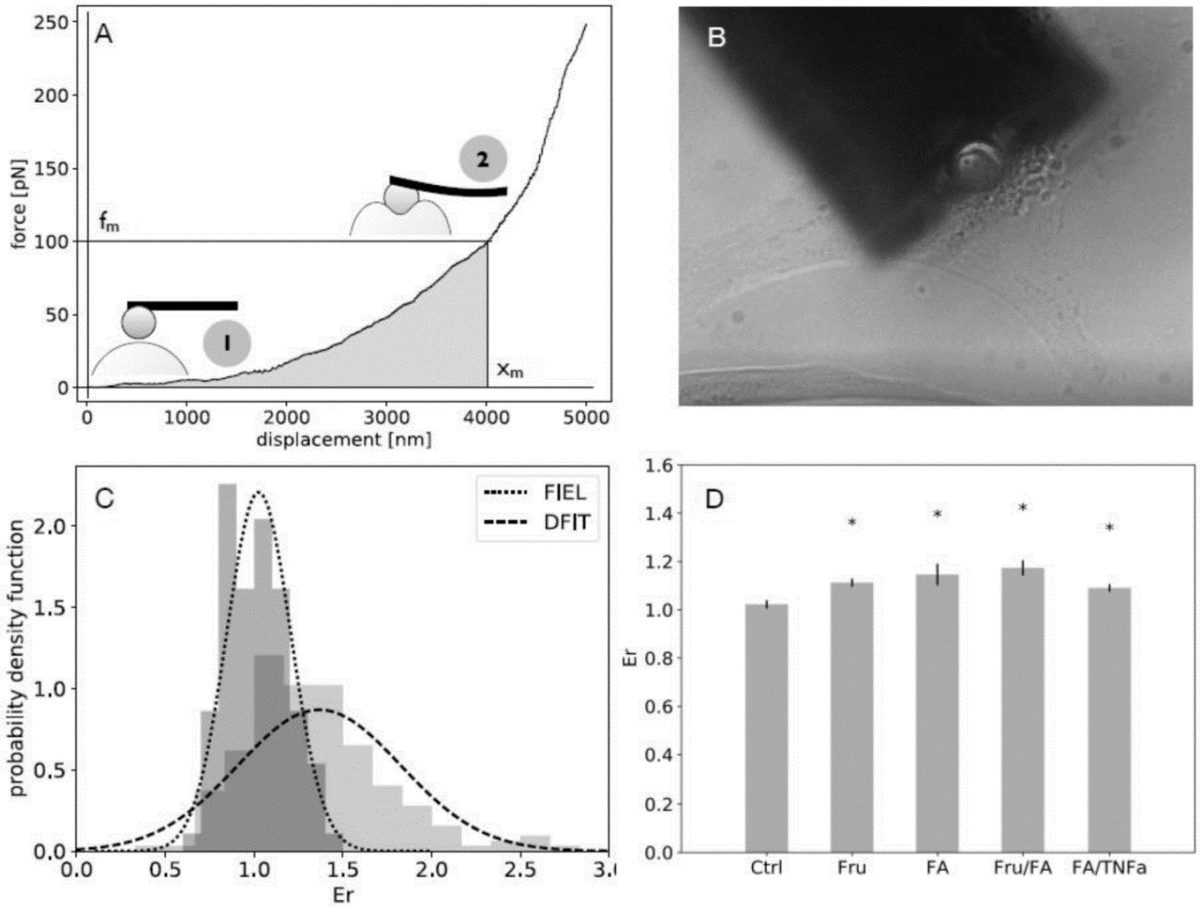

Figure 25. Effects of fatty acids, fructose and TNFα on single cell biomechanical properties

(A) Example of a force-displacement curve showing the two main steps: a no contact condition (1), indentation of the cell (2). The force value (the grey area under the curve) is computed in the FIEL procedure to derive elasticity. **(B)** Picture from a nano-indentation experiment: the spherical tip indenting a cell. **(C)** Probability density functions of both FIEL and DFIT methods. **(D)**

Relative Elasticity (*Er*) of single cell respect to the control, obtained through the FIEL method. Symbols: Ctrl *vs* all treatments *p≤0.05; FA *vs* all treatments #p≤0.05; Fru *vs* all treatments $ p≤0.05.

Lipid accumulation and single cell morphometry

The 3D shape of cells was reconstructed using QPM. In QPM images, each pixel encodes the physical thickness of the sample, providing a quantitative information related to several geometrical parameters. Fig. 4 provides an example of a reconstructed image of control cells represented with a 2D (Fig. 4A) or 3D (Fig. 4C) perspective, and summarizes the main 2D and 3D geometrical parameters of cells in different conditions (Fig.4B-D): cell roughness (R_C), cell height (H_C), surface extension (S_E), cell contact area (A_C) and radius of curvature (C_R).

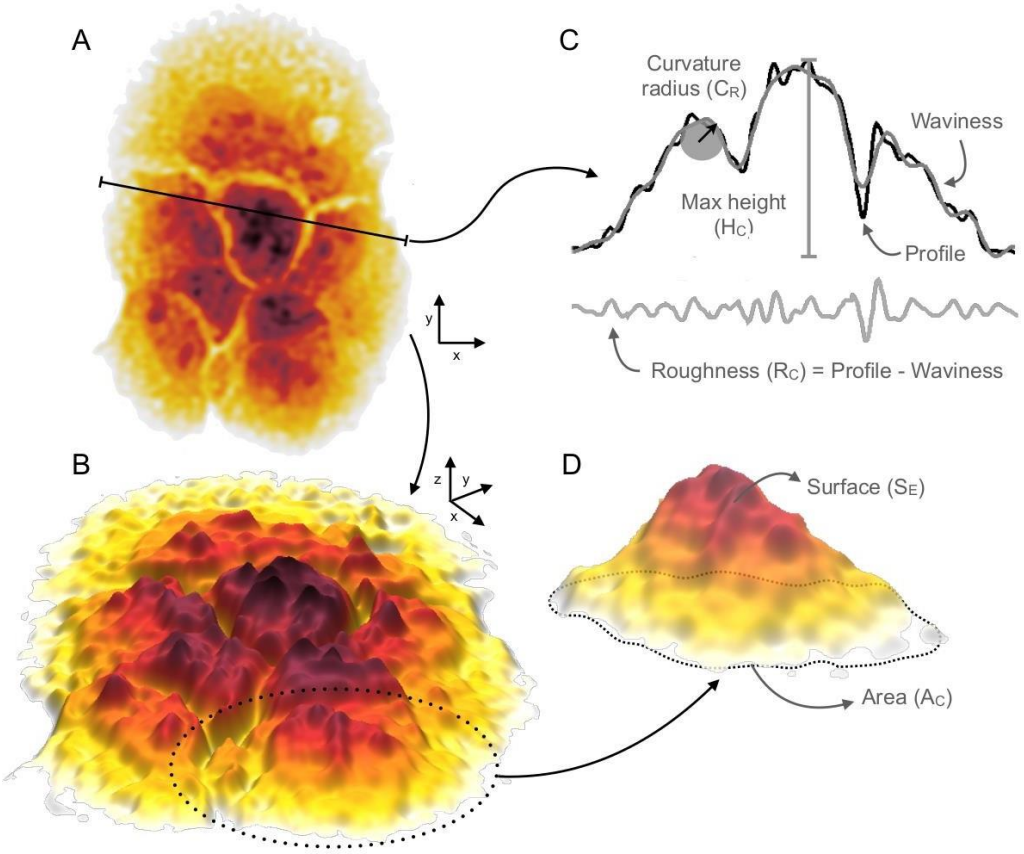

Figure 26. Single cell morphometry analysis in different steatosis models

Representative views of the reconstructed QPM images of control FaO cells represented with a 2D **(A)** or 3D **(B)** perspective. In the 2D perspective, the colour encodes the thickness of the cells; **(C)** and **(D)** graphic explanation of the morphometric parameters: radius of the curvature (C_R), cell height (H_C), cell roughness (R_C), surface extension (S_E), cell contact area (A_C).

While fructose alone did not significantly modify any of the morphometric parameters, FAs

alone led to significant ($p \leq 0.05$) alteration of almost all parameters (Fig. 5). In details, FAs make the cells thinner and larger than control cells as indicated by the marked reduction in H_C (-60% *vs* control) and the increase in A_C (+50% *vs* control) (Fig. 5B and D), and with a smoother surface and larger protrusions as indicated by the increase in C_R (+400% *vs* control) and the decrease in S_E (-60% *vs* control) (Fig. 5A and E). A similar trend was observed in Fru/FA cells, with a cell morphometry being intermediate between Fru and FA, nevertheless the highest grade of steatosis. By contrast, with FA/TNFα cells appeared peculiarly smaller compared to FA, and displayed a significant decrease in S_E (-20% *vs* control) (Fig. 5C).

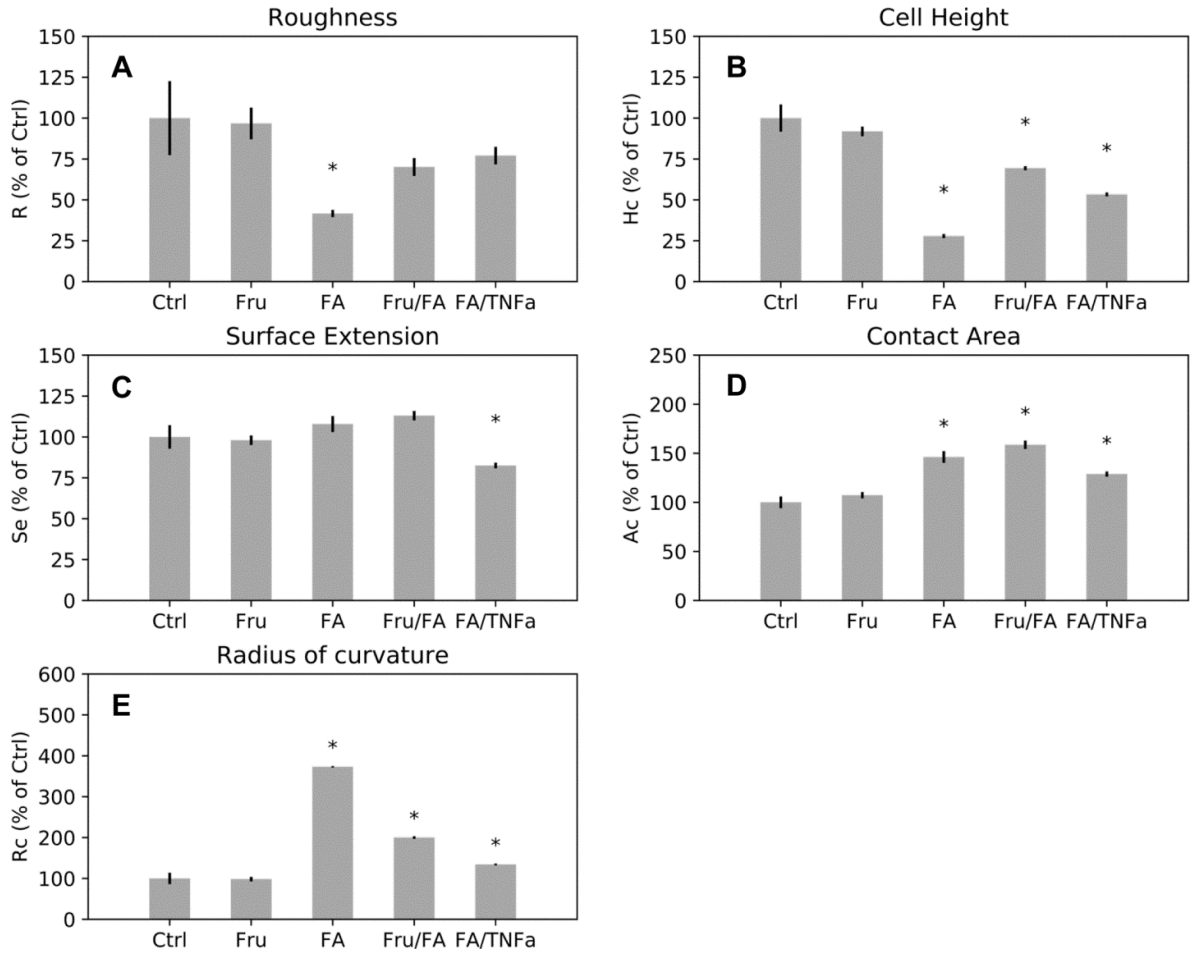

Figure 27. Single cell morphometric parameters in different steatosis models

The morphometric indicators computed for all the treatments are presented relative to the controls: **(A)** cell roughness (R_C); **(A)** cell height (H_C); **(C)** surface extension (S_E); **(D)** cell contact area (A_C); **(E)** radius of the curvature (C_R). Statistical significance respect to the control is marked when at least #$p \leq 0.05$.

Correlation among parameters

The possible correlations between the biochemical, functional and biomechanical parameters above discusses were assessed through the estimated correlation matrix (Fig. 6). Single cell elasticity E_f correlated positively ($p \leq 0.05$) with extent of TG accumulation, LD size, level of ADRP expression, and cell area (Ac) and negatively with cell viability (Fig. 2D). On the other hand, the level of IkBip expression, a marker for liver damage, correlated positively with number of LDs/cell and PPARα and PPARγ expression and correlated negatively with cell area (Ac). Intracellular TG content correlated positively with both LD size and ADRP expression, a marker for hepatic steatosis. Cell viability correlates negatively with TG content, LD number and size, and PPARα expression.

Figure 28 Correlation matrix of biochemical and mechanical parameters

Correlation matrix was computed among all the biochemical, mechanical and morphometric parameters. Statistical significance was assumed for correlation coefficients higher than 0.6 or lower than -0.6. Therefore, correlation coefficients within the interval $-0.6 \leq p \leq 0.6$ are not presented in the matrix. ### Values higher than 0.6 are represented in green, lower than -0.6 in pink. Along the diagonal every parameter is correlated with itself resulting in a correlation equal to 1.

DISCUSSION

Although NAFLD is raising dramatically worldwide, to date there are no sustainable treatments for this disease. The ongoing research focus on molecular steps that may mediate NAFLD onset and progression as potential therapeutic targets. This study provides new insights, at the single cell level, on the biomechanical and morphological changes of steatotic hepatocytes in response to distinct and relevant hits using *in vitro* models of NFALD. We found that lipid storage in LDs dramatically alters both the elasticity and the morphometry of the hepatic cells with variable effects depending on the structural features of LDs.

From a physical point of view, LDs protruding from the ER membrane are different from other vesicular organelles of the cell in that their core is highly hydrophobic and their shape is invariably spherical. In fact, while vesicular organelles have an aqueous lumen and flexible shape, LDs are always round to minimize the interface between hydrophobic core and cytosol. In NAFLD patients, we can find macrovesicular steatosis with large LDs and good long-term prognosis, or microvesicular steatosis with small LDs and more severe prognosis. Here, we adopted four different protocols to induce different kinds of hepatosteatosis consisting of excess fructose, excess fatty acids, a combination of both, and a combination of fatty acids and the pro-inflammatory cytokine TNFα. All conditions mimic valuable steps of a dysmetabolically-active context such as that occurring in *in vivo* when steatogenic factors are active.

The different grade and features of steatosis in the proposed *in vitro* models were firstly analyzed in terms of TG accumulation and LD number and size. TG accumulation increased in all steatotic conditions, but more markedly in cells treated with Fru/FA combination. LD size and number increased slightly in cells exposed to Fru, and more in cells exposed to FAs. Interestingly, Fru/FA combination markedly enlarged the LDs without changing their number, whereas FA/TNFα led to an increase in LD number with a reduction of their size with respect to FAs alone. The changes of LDs were paralleled with those of ADRP expression with increased passing from Fru to FAs and was maximal in Fru/FA cells, but decreased in FA/TNF cells. These findings indicate that Fru/FA combination mimics a condition of macrovesicular steatosis *in vitro*, while FA/TNFα combination induced a condition more similar to microvesicular steatosis. The correlation between *in vitro* macro- and microvesicular steatosis

with the ongoing cell dysfunction was confirmed by the changes in expression of IkBip, a marker for ER stress, and of PPARs. Both IkBip and PPARα expression was almost unaffected by Fru or FAs as single agents, while a marked up-regulation was caused by Fru/FA combination and an even larger up-regulation by FA/TNFα. Moreover, the up- regulation of PPAR in cells exposed to FA/TNFα indicates that microvesicular steatosis is a more damaging condition as PPARα activation is known to be associated with progression of steatosis, inflammation and fibrosis in pre-clinical models of non-alcoholic fatty liver disease (Silva and Peixoto, 2018).

Taken together these results indicate that: *(i)* level of ADRP expression was mainly dependent on LD size rather than on the grade of steatosis being quantified as intracellular TGs; *(ii)* up-regulation of IkBip expression, a marker of ER stress and cell damage, was dependent on the number of LDs/cell rather than on the steatosis grade. Therefore, the condition induced by FA/TNFα combination seems to be a reliable model of a microvesicular-like steatosis (Santhekadur et al., 2017).

To date, there is an increasing interest in studying the cell stiffness as a main driver of physiological regulation. Hepatocyte mechanical properties—at the single cell level—were not still investigated, and a limited number of studies were performed exclusively on adipocytes using AFM (Young-Nam et al., 2011). Here, we implemented an innovative approach to quantify the single cell stiffness in term of the relative elasticity *Er* measured by SCFS. We found that single cell stiffness was increased in cells exposed to either Fru or FAs as single agents, but the largest increase was induced by Fru/FA combination. Interestingly, the microvesicular-like steatosis induced by FA/TNFα combination showed a cell stiffness similar to that observed for FAs alone. This observation has practical and translational applications, in that it demonstrates that single cell stiffness depends on the steatosis grade rather than on LDs organization and distribution inside the cell.

In parallel, also the single cell morphometry assessed by QPM changed as a function of the steatosis grade and features. While a rather low grade of steatosis, such as that induced by fructose alone, did not alter the geometric parameters, the more marked steatosis induced by FAs made the cells thinner and larger than control cells and with a smoother surface and larger protrusions. On the other hand, Fru/FA cells showed a morphometry intermediate

between those of Fru and FA cells although the highest grade of steatosis. By contrast, cells with microvesicular-like steatosis induced by FA/TNFα appeared smaller compared to FA cells although they had a similar TG content. Therefore, we can conclude that geometric parameters do not depend exclusively on the total TGs accumulated in steatotic cells, but mainly on the number of LDs in cytosol.

We verified the possible correlations between the main biochemical, functional and biomechanical parameters recorded at the level of single cell. The TG content correlated positively with LD size and ADRP expression and negatively with cell viability and PPARα expression, thus indicating that, although TG synthesis is a protective response, an excess of intracellular fat leads to hepatic cell damages less or more severe depending on the extent of steatosis. We also found a positive correlation between E_r and the level of TG accumulation, ADRP expression, the LD size and the cell area; instead E_r correlated negatively with the cell viability. These results indicate that the single cell elasticity of hepatocytes increases along with the steatosis grade. On the other hand, the IkBip expression correlated positively with the number of LDs in the cytosol and the PPAR expression and correlated negatively with the cell area, thus suggesting that a higher number of small LDs damages the hepatocyte more than a small number of larger LDs, accordingly to what reported *in vivo* for microvesicular steatosis.

Taken together the present results suggest that at the single hepatocyte level: *(i)* the cell stiffness is directly influenced by the extent of TG accumulation and by the size of LDs and reflects negatively on cell viability; *(ii)* a condition of microvesicular steatosis (high number of LDs/cell) is associated to a more severe cell damage as indicated by the largest over expression of IkBip and PPARs, and the shrinking of the cell.

Therefore, our findings showing that *in vitro* hepatocytes stiffen with LD accumulation, point the attention to the potential role of mechanobiology in metabolic diseases, particularly those linked to overweight and obesity. Indeed, alterations of cell biomechanics might sustain the grade and speed of evolution of steatosis reflecting on liver stiffness in relation to the steatogenic inducer (e.g., dietary loads). The fine mechanisms relating the onset/progression of NAFLD to the morphological and mechanical phenotype of the hepatocyte are not yet completely understood, but our results show the existence of a link

between these aspects whose causality is worth investigating in future activity.

Moreover, this study paves the way to further experimental and translational applications. In fact, the link between physiopathological conditions and single cell elasticity might be exploited as a label-free biomarker of the disease progression, eventually opening for high throughput mechanical phenotyping approaches (Otto et al., 2015). In this view, it is envisaged that the effect of physical and chemical agents in counteracting/reducing liver steatosis might be monitored looking at the differential effect on the biomechanics of hepatocytes.

Table 1

Symbols and definitions of the main morphometric parameters used in the text; for additional details see the on-line documentation of the Gwyddion software [37, http://gwyddion.net/documentation/user-guide-en/statistical-analysis.html]

Parameter	**Symbol**	**Description**
Cell Roughness	R_C	RMS of the height after subtracting a smoothed shape obtained by low pass filtering the surface with a cut-off set to the 2% of the Nyquist frequency
Cell Height	H_C	Max height inside the region belonging to the selected region (cells)
Surface Extension	S_E	Surface area calculated upon triangulation of the height map
Cell Contact Area	A_C	Area in the plane occupied by the selected region (cells)
Radius of Curvature	C_R	Curvature radius at the max height (cell body) of the filtered surface (see Cell roughness)

Table 2

Mean and standard deviation of the gaussian probability density function, fitted on the relative Young's modulus distribution, are presented for both the DFIT and the FIEL methods. The result of the Shapiro normality test on the distributions are shown in the third column for each method.

	FIEL			DFIT		
	Mean	**SD**	**Shapiro**	**Mean**	**SD**	**Shapiro**
Ctrl	1,026	0,181	0,971	1,367	0,459	0,903
Fru	1,214	0,277	0,919	1,731	0,725	0,890
Fru/FA	1,318	0,331	0,949	1,608	0,668	0,903
FA	1,223	0,330	0,885	1,975	1,186	0,747
FA/TNFα	1,184	0,350	0,853	1,536	0,780	0,802

10.New Perspectives of S-Adenosylmethionine (SAMe) applications to attenuate fatty acid-induced steatosis and oxidative stress in hepatic and endothelial cells

Paper in preparation

ABSTRACT

S-Adenosyl-L-methionine (SAMe) is an endogenous pleiotropic molecule playing many functions, in the liver especially, including acting as a precursor for cysteine, one of amino acids of glutathione--the major physiologic defence mechanism against oxidative stress. SAMe is particularly important in opposing the toxicity of free oxygen radicals generated by various pathogens. SAMe also acts as the main methylating agent in the liver. Administration of SAMe as supernutrient results in many beneficial effects in various tissues, mainly in the liver, and especially in the mitochondria.

Keywords: SAMe; Non-alcoholic fatty liver disease; atherosclerosis; oxidative stress

INTRODUCTION

S-adenosylmethionine (SAMe) is an endogenous, pleiotropic amino acid metabolite involved in many crucial biochemical pathways, including biosynthesis of hormones and neurotransmitters (Cantoni, 1985; Bottiglieri, 2001). SAMe is synthesized mainly in the liver, and then distributed throughout the body (Friedel et al., 1989). SAMe acts as the main methyl donor in mammalian cells, where transfer of a methyl group to an acceptor molecule, such as DNA, proteins and phospholipids, modifies their structure and function (Mato, 2013). Indeed, DNA methylation switch on/off the gene transcription, protein methylation regulates the enzyme activity, phospholipid methylation modulates membrane fluidity. Moreover, SAMe is precursor for cysteine, one of the amino acids of glutathione, the major physiological defence against reactive oxygen species (ROS), thus it acts also as protection against oxidative stress.

SAMe has been involved in many liver diseases (Lu and Mato, 2012; Mato, 2013). Reduced hepatic SAMe levels were described in patients with alcoholic hepatitis resulting in decreased hepatic GSH levels (Lee et al., 2004), and SAMe administration has been shown to normalize the GSH levels (Vendemiale et al., 1989). Many studies done mostly in alcoholic liver disease, cholestasis of pregnancy, and primary biliary cirrhosis have shown significant improvement in liver test abnormalities during therapy with SAMe (Anstee and Day, 2012).

Non-alcoholic fatty liver disease (NAFLD) is the most common liver disease associated to obesity (Loomba and Sanyal, 2013; Huang et al., 2013), and is correlated with type 2 diabetes and cardiovascular risk (Anstee et al., 2013). Hepatic steatosis is the hallmark of NAFLD (Cohen et al., 2011) and free fatty acids (FAs) are the major mediators of steatosis; in fact, patients with NAFLD have elevated levels of circulating FAs. In the liver, FAs are esterified to TGs and stored in cytosolic lipid droplets (LDs) as protection against their toxicity, or alternatively, FAs are metabolized through β-oxidation in mitochondria and peroxisomes, and through β-oxidation in the endoplasmic reticulum (ER) with consequent ROS production. LDs (Cohen et al., 2011; Sahini, 2014) consist of a hydrophobic lipid core surrounded by a phospholipid monolayer and LD-associated proteins which regulate lipid metabolism and traffic (Xu et al., 2017). Among them, the adipose differentiation-related protein (ADRP) is crucial for formation and structural maintenance of LDs and is a marker for the extent of lipid

accumulation, as its overexpression stimulates lipogenesis and inhibits lipolysis (Grasselli et al., 2010).

NAFLD may encompass simple steatosis (NAFL), non-alcoholic steatohepatitis (NASH), cirrhosis, and even hepatocellular carcinoma (Cohen et al., 2011). Progression of NAFL to NASH is sustained by oxidative stress resulting from reactive oxygen species (ROS) deriving from fat catabolism (Day and James., 1998; Rolo et al., 2011). Oxidative stress, in fact, activates inflammatory signaling pathways such as that sustained by the nuclear factor kappa-B (NF-κB), a transcription factor of the inflammatory response also involved in liver diseases (Hoesel and Schmid, 2013).

Both hepatocytes and endothelial cells participate in progression of fatty liver disease, and obesity-related metabolic disorders cause endothelial dysfunction. Endothelium is a crucial blood–tissue interface controlling energy supply according to organ needs, as it is the first rate-limiting step in the utilization of long-chain FAs as fuels. Endothelial cells play regulatory functions through releasing various factors including nitric oxide (NO) and ROS (Shah et al., 1997). In the liver, the endothelial cells of sinusoids act in fibrosis development by sustaining wound healing response and inflammation (Braet and Wisse, 2002; Connolly et al., 2010). Wound healing process depends on endothelial cell migration which is mediated by the intercellular adhesion molecule-1 (ICAM-1) on the plasma membrane (Gay et al., 2011).

Here, we used rat hepatoma FaO cells exposed to a mixture of oleate/palmitate that represent a reliable *in vitro* model for hepatic steatosis widely employed in previous studies of our group (Grasselli et al., 2011; Grasselli et al., 2014). As FAs seem to play also direct effects on oxidative stress of vascular endothelium (Zhou et al., 2009), we used also human endothelial HECV cells exposed to FAs that could be compared to *in vivo* atherosclerosis, as endothelial damage is typically observed in metabolic syndrome (Szmitko et al., 2003).

The results showed that SAMe ameliorated lipid accumulation in hepatic cells and reduced lipid-dependent oxidative imbalance in both hepatic and endothelial cells thus showing potential applications as therapeutic agents.

MATERIALS AND METHODS

Chemicals

All chemicals, unless otherwise indicated, were supplied by Sigma-Aldrich Corp. (Milan, Italy).

Cell culture and treatments

FaO cells (European Collection of Authenticated Cell Cultures -ECACC- Salisbury, Wiltshire, UK) are a rat hepatoma cell line maintaining hepatocyte-specific markers (Lauris et al., 1986). Cells were grown in a humidified atmosphere with 5% CO_2 at 37°C in Coon's modified Ham's F12 medium supplemented with L-Glutamine and 10% foetal calf serum (FCS). HECV cells (Cell Bank and Culture - GMP-IST- Genoa, Italy) are a human endothelial cell line isolated from umbilical vein; they were grown at 37°C in Dulbecco's modified Eagle's medium High Glucose (D-MEM) supplemented with L-Glutamine and 10% FCS. For treatments, cells were grown until 80% confluence, then incubated overnight in serum-free medium with 0.25% bovine serum albumin (BSA). To mimic *in vitro* the effect of a high fat diet, cells were treated for 3 h with a mixture of oleate/palmitate at a final concentration of 0.75 mM (2:1 molar ratio). Thereafter, 'steatotic' cells (OP) were incubated for 24h in the absence or in the presence of SAMe (25, 50 and 100 M). Stock solution of SAMe 100 mM in HCl 0.1 M was diluted with the culture medium to the working concentration.

Protein quantification

The protein content was determined by the bicinchoninic acid (BCA) method using BSA as a standard (Wiechelman et al., 1988). All measurements were performed using a Varian Cary50 spectrophotometer.

Quantification of triglycerides

At the end of the treatments, FaO and HECV cells were scraped and centrifuged at 14,000xg for 3 min. After cell lysis, lipids were extracted in chloroform/methanol (2:1) then chloroform was evaporated (Grasselli et al., 2011). In each extract, TG content was determined by spectrophotometric analysis using the 'Triglycerides liquid' kit (Sentinel diagnostics, Milan, Italy). Values were normalized for the protein content determined by the bicinchoninic acid (BCA). Data are expressed as percent TG content relative to controls.

ROS production and lipid peroxidation measurement

The oxidation of the cell-permeant 2'-7' dichlorofluorescin diacetate (DCF-DA, Fluka, Germany) to 2'-7'dichlorofluorescein (DCF) is used for quantifying *in situ* the production of H_2O_2 and other ROS (Halliwell and Whiteman., 2004). Stock solution of DCF-DA (10mM in DMSO) was prepared and stored at -20°C in the dark. At the end of treatment, cells were scraped and gently spun down (600xg for 10 min at 4°C). After washing, cells were loaded with 10 µM DCF-DA in PBS for 30 min at 37°C in the dark. Then, cells were centrifuged, suspended in PBS and the fluorescence was measured fluorometrically (λex=495 nm; λem=525 nm). All measurements were performed in a LS50B fluorimeter (Perkin Elmer, USA) at 25°C using a water-thermostated cuvette holder.

Lipid peroxidation was determined spectrophotometrically through the thiobarbituric acid reactive substances (TBARS) assay which is based on the reaction of malondialdehyde (MDA; 1,1,3,3-tetramethoxypropane) with thiobarbituric acid (TBA) (Iguchi et al., 1993). Briefly, 1 vol. of cell suspension was incubated for 45 min at 95°C with 2 vol. of TBA solution (0.375% TBA, 15% trichloroacetic acid, 0.25 N HCl). Then, 1 vol. of N-butanol was added, and the organic phase was read at 532 nm in a Varian Cary 50 Bio UV-VIS spectrophotometer (Agilent, Milan, Italy) at 25°C using Peltier-thermostated cuvette holder. The MDA level was expressed as pmol MDA/mL/mg protein.

Oil-Red O staining

Neutral lipids were visualized using the selective Oil-RedO (ORO) dye (Grasselli et al., 2010). Briefly, after fixing in 4% paraformaldehyde, cells were washed with PBS, stained for 20 min with 0.3% ORO solution prepared from a stock 0.5% in isopropanol and diluted in water. After washing with distilled water, slides were examined by Leica DMRB light microscope equipped with a Leica CCD camera DFC420C (Leica, Wetzlar, Germany).

Measurement of Nitrite/Nitrate (NOx) Levels

NO production was measured by spectrophotometric measurement of the end products, nitrites and nitrates, using the Griess reaction (Green et al., 1982). After treatments, nitrite accumulation (µmol $NaNO_2$/mg sample protein) was calculated against a standard curve of sodium nitrite ($NaNO_2$). All spectrophotometric analyses were carried out at 25°C recording

absorbance at 540nm with a Varian Cary 50 spectrophotometer. Data are means ± S.D. of at least four independent experiments.

RNA extraction and real-time qPCR

RNA was isolated using Trizol reagent, cDNA was synthesized and quantitative real-time PCR (qPCR) was performed in quadruplicate using 1x IQTMSybrGreen SuperMix and Chromo4TM System apparatus (Biorad, Milan, Italy) (Grasselli et al., 2011). The relative quantity of target mRNA was calculated by the comparative Cq method using glyceraldehyde 3-phosphate dehydrogenase (*Gapdh*) as housekeeping gene and expressed as fold induction with respect to controls (Pfaffl, 2001). Primer pair sequences and efficiencies are reported in Tables S1 and S2.

Wound Healing assay

The migration of HECV was examined using the wound healing assay (Gay et al., 2011). The cells were seeded on 35×10mm tissue culture dishes and incubated for 24 h or until confluence was reached. After 3h of incubation with oleate/palmitate mixture, the cell monolayer was scraped with a p100 pipet tip making two crossing straight lines to create a ‘‘scratch’’ (Eppendorf AG, Hamburg, Germany). Then, two views on the cross were photographed on each well attached to the microscope at 4x magnification. The medium was replaced with fresh medium in the absence or presence of SAMe at different concentrations (25, 50 and 100 µM). Set of images were acquired at 3, 6 and 24 h. To determine the migration of HECV, the images were analysed using ImageJ free software (http://imagej.nih.gov/ij/). Percentage of the closed area was measured and compared with the value obtained before treatment. An increase of the percentage of closed area indicated the migration of cells. Data are means±S.D. of at least three independent experiments.

Statistical analysis

RNA and protein data are expressed as means ± S.D. of at least four independent experiments in triplicate. Statistical analysis was performed using ANOVA with Tukey’s post- test (GraphPad Software, Inc., San Diego, CA, USA).

RESULTS

Effects of SAMe on lipid accumulation in hepatic cells

Cells exposed to high concentrations of FAs mimic *in vitro* what is occurring *in vivo* in different tissues during high fat feeding and/or obesity. FaO cells were overloaded of lipids by exposure to oleate/palmitate mixture (0.75 mM) for 3h. Then, cells were treated for 24h with increasing concentrations of SAMe (25, 50 and 100 µM). No cytotoxic effects of the treatments were detected by MTT assay (data not shown).

The intracellular TG content was quantified in control (C) and steatotic cells incubated in the absence (OP) or in the presence of SAMe. In lipid-loaded FaO cells (Fig.1A), we observed a significant increase in TG content with respect to control (+113%; $p \leq 0.001$), and a significant decrease upon treatment with SAMe 25, 50 and 100 µM (-49%, -89% and -75%, respectively, compared to steatotic cells; $p \leq 0.001$). When the cytosolic LDs were visualized by ORO staining (Fig.1B), we observed that the number and size of LDs increased markedly in lipid-loaded cells (OP) compared to control and decreased upon incubation with SAMe. ADRP is the main LD-associated protein in the liver cells, and it regulates the TG traffic from/to LDs. ADRP mRNA level (Fig.1C) was significantly up-regulated in steatotic FaO cells (2.06-fold induction *vs* control; $p \leq 0.05$), and it was further up-regulated after exposure to SAMe (about 3-fold induction *vs* control; $p \leq 0.05$ for all SAMe concentrations).

The extent of lipid accumulation in liver cells depends on the balance between lipolytic and lipogenic pathways. Therefore, the lipid-lowering action of SAMe might be sustained by stimulation of oxidative and/or secretory pathways. Lipolytic pathways lead to the final FA oxidation, mainly in mitochondria. CPT1 is a mitochondrial protein acting as shuttle for FAs, so acting upstream to the mitochondrial FA oxidation. *CPT1* mRNA expression was up-regulated in steatoic FaO cells (1.83-fold induction *vs* control; $p \leq 0.001$) and it was further up-regulated exposure to SAMe (about 2.9-fold induction *vs* control; $p \leq 0.001$ for all SAMe concentrations) (Fig.1C). UCP2 is a mitochondrial uncoupling protein that separates oxidative phosphorylation from ATP synthesis resulting in energy dissipation as heat. Also, *UCP2* expression was significantly up-regulated upon lipid-loading (1.82-fold induction *vs* control; $p \leq 0.05$) (Fig.1C), but SAMe at all concentrations did not alter significantly *UCP2* expression.

As an attempt to reduce the TG accumulation, steatotic FaO cells stimulated the release of

TGs into the medium with respect to control (+29%; p≤0.05). Exposure to SAMe led to a significant reduction in TG release compared to steatotic cells (-35%, -58% and -52%, for SAMe 25, 50 and 100 µM respectively) (Fig.1D).

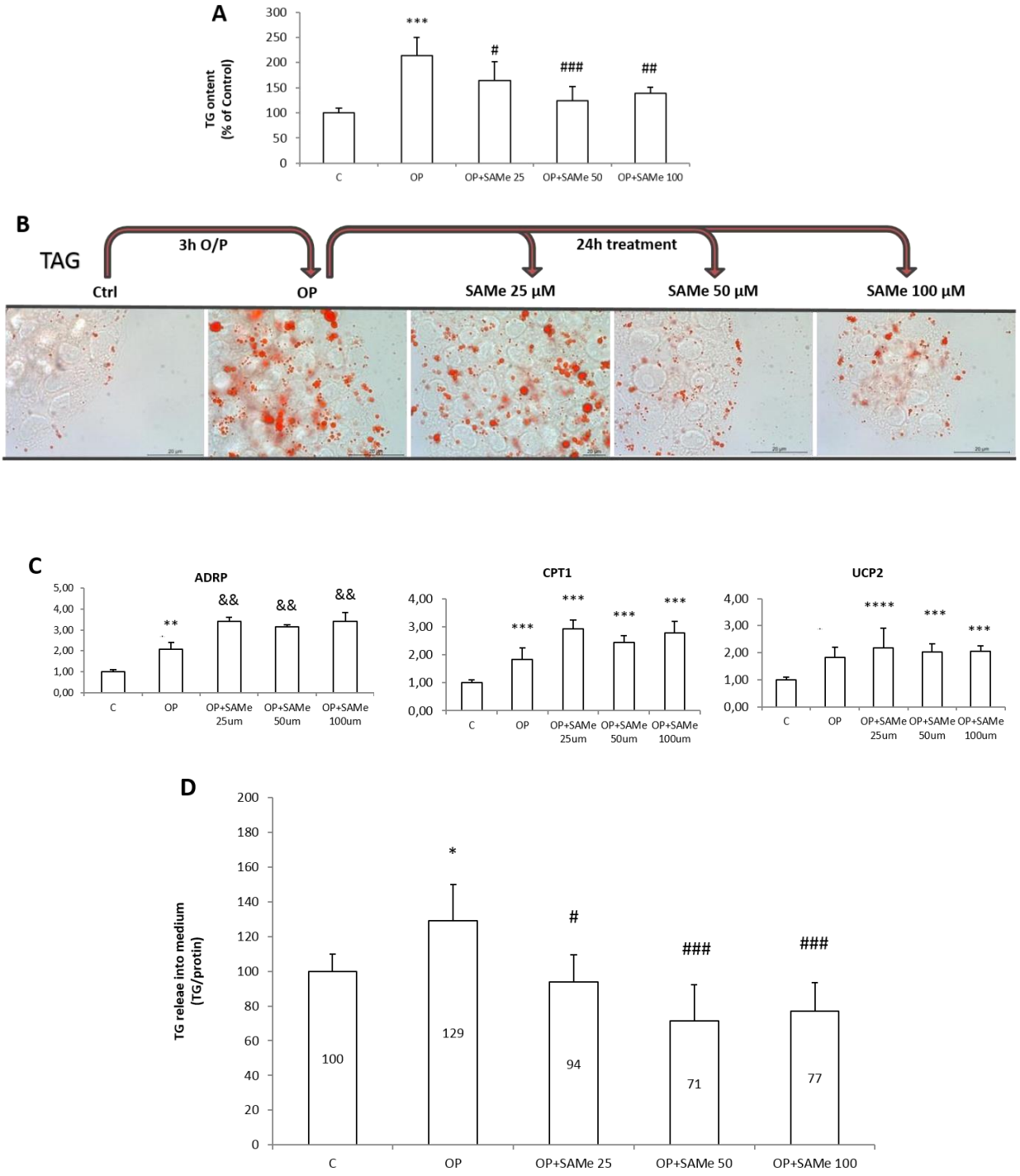

Figure 29. Effects of SAMe on lipid accumulation

For Fao cells incubated in the absence (C) or in the presence of oleate/palmitate (OP) alone or with different concentrations of SAMe 25, 50 and 100 µM (OP+SAMe 25, OP+SAMe 50, OP+SAMe 100) we show: **(A)** TG content expressed as percentage of TG content relative to control; normalized for proteins determinated with Bradford assay. **(B)** Microphotographes of cells

stained with Oil Red-O (ORO) (magnification 20x; Bar: 10 µm). **(C)** The mRNA expression of adipose differentiation-related protein (ADRP), carnitine palmitoyltransferase 1 (CPT-1) and uncoupling protein 2 (UCP-2) evaluated by quantitative PCR (qPCR); glyceraldehyde 3-phosphate dehydrogenase (GAPDH) was used as the internal control and data expressed as fold induction with respect to controls. **(D)** Extracellular TG content quantified in the medium by spectrophotometric assay. Statistical significance between groups was assessed by ANOVA followed by Tukey's test. Symbols: C *vs* all treatments *p≤0.05; **p≤0.01; ***p≤0.001; OP *vs* all treatments &p≤0.05, &&p≤0.01, &&&p≤0.001

Effects of SAMe on oxidative stress in hepatic cells

As a first indicator of the oxidative imbalance being potentially associated to lipid dysmetabolism we assessed lipid peroxidation by TBARS assay. As expected, the MDA level (Fig. 2A) increased in steatotic FaO cells (+63% compared to control; p≤0.001), and a dose-dependent decrease occurred upon exposure to SAMe compared to steatotic cells (-50%, -70% and -79%, for doses of 25, 50 and 100 µM, respectively; p≤0.05).

The lipid peroxidation is typically caused by higher levels of intracellular ROS, mainly hydrogen peroxide (H_2O_2), that we quantified by fluorimetric analysis (Fig. 2B). Steatotic FaO cells (OP) treated with SAMe showed a dose-dependent decrease in DCF florescence with respect to steatotic cells used as control (-9%, -24% and -34%, for doses of 25, 50 and 100 µM, respectively; p≤0.05 and p≤0.01, respectively).

The changes in H_2O_2 levels were paralleled by changes in the enzymatic activity of catalase, the main enzyme catalyzing the H_2O_2 decomposition (Fig. 2C). Catalase activity was stimulated in steatotic FaO cells (+61% compared to control; p≤0.001) and it was reduced upon exposure of steatotic cells to SAMe (-77%, -65% and -97%, for doses of 25, 50 and 100 µM, respectively; p≤0.05 and p≤0.01, respectively).

In control FaO cells, neither the MDA level, DCF signal and catalase activity were affected by SAMe (data not shown).

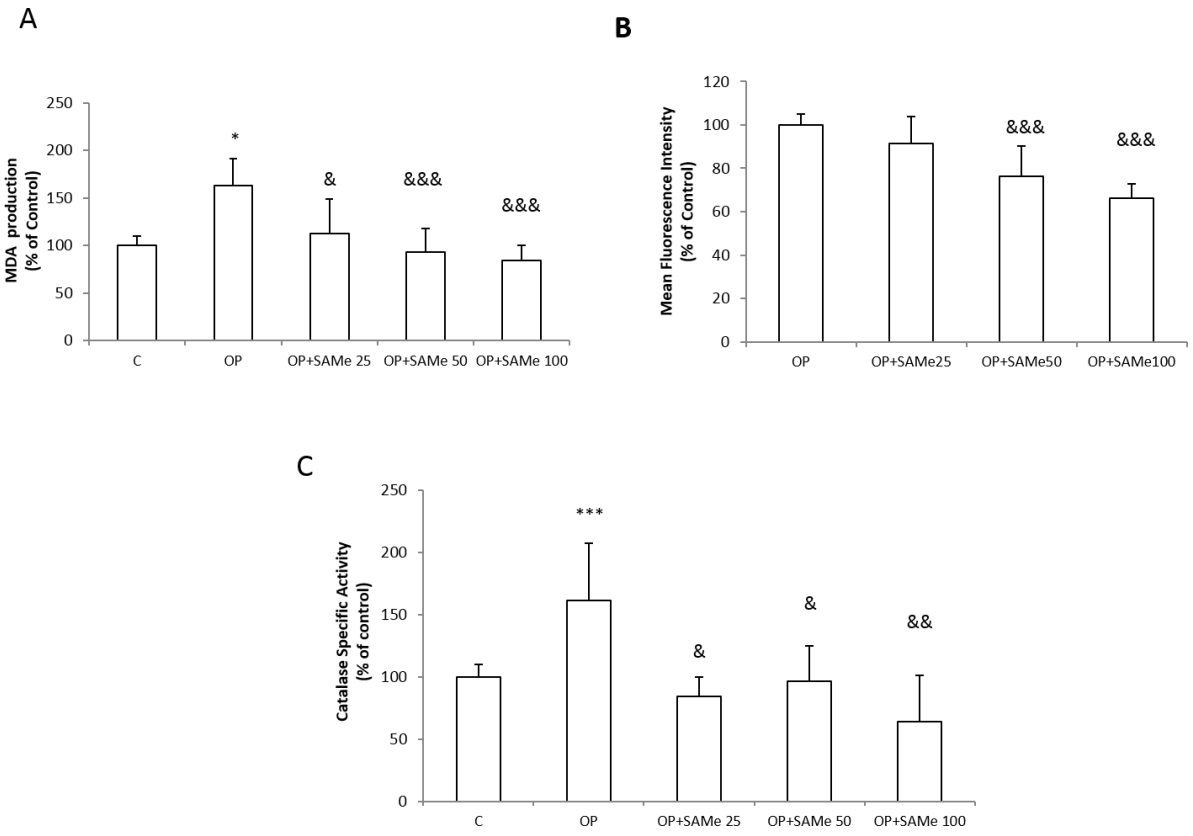

Figure 30. Effects of SAMe on oxidative stress

For Fao cells incubated in the absence (C) or in the presence of oleate/palmitate (OP) alone or with different concentrations of SAMe 25, 50 and 100 µM (OP+SAMe 25, OP+SAMe 50, OP+SAMe 100) we show: **(A)** The intracellular level of MDA (pmol MDA/mL x mg of sample protein) quantified by TBARS assay data are expressed as percentage values with respect to controls and normalized for total proteins; **(B)** The ROS level were also quantified by spectrofluorimeter assay of DCF-stained cells and data are expressed as percent mean fluorescence intensity (MFI) relative to steatotic cells and normalized for total proteins. **(C)** Catalase specific activity (micromoles of decomposed H2O2 per min/mg of sample protein) evaluated by spectrophotometric assay, data are expressed as percentage values with respect to controls and normalized for total proteins. Statistical significance between groups was assessed by ANOVA followed by Tukey's test. Symbols: C *vs* all treatments *p≤0.05; **p≤0.01; ***p≤0.001; OP *vs* all treatments &p≤0.05, &&p≤0.01, &&&p≤0.001

Effects of SAMe on lipid accumulation and function in endothelial cells

HECV cells were overloaded of lipids by exposure to oleate/palmitate mixture (0.75 mM) for 3h. Then, cells were treated for 24h with different doses of SAMe (25, 50 and 100 µM). MTT assay was performed to exclude toxic effects of the treatments (data not shown).

In lipid-loaded HECV cells (Fig.3A), we observed a significant increase in TG content with respect to control (+241%; p≤0.001), and a significant decrease upon treatment with SAMe 25 µM (-33%; p≤0.01) and 50 µM (-73%, p≤0.001) compared to steatotic cells.

NO is a major modulator of endothelial cell activity. In lipid-loaded HECV cells, we observed an increase in NO release with respect to control (+61%; $p \leq 0.001$), that was counteracted by SAMe at all concentrations of 25, 50 and 100 µM (-58%, -55% and -41% respectively, with respect to steatotic cells; $p \leq 0.001$) (Fig.3B).

Lipid-loading also resulted in oxidative stress in HECV cells. The MDA level (Fig.3C) increased in lipid-loaded HECV cells (+48% compared to control; $p \leq 0.01$), and decreased occurred upon exposure to SAMe compared to steatotic cells (-32%, -42% and -41%, for doses of 25, 50 and 100 µM, respectively; $p \leq 0.001$).

SAMe effects on migrating ability of HECV cells was evaluated using the Wound Healing assay (Fig.3D). No significant differences in cell migration rate were observed at all times after the scratch (for all doses of SAMe).

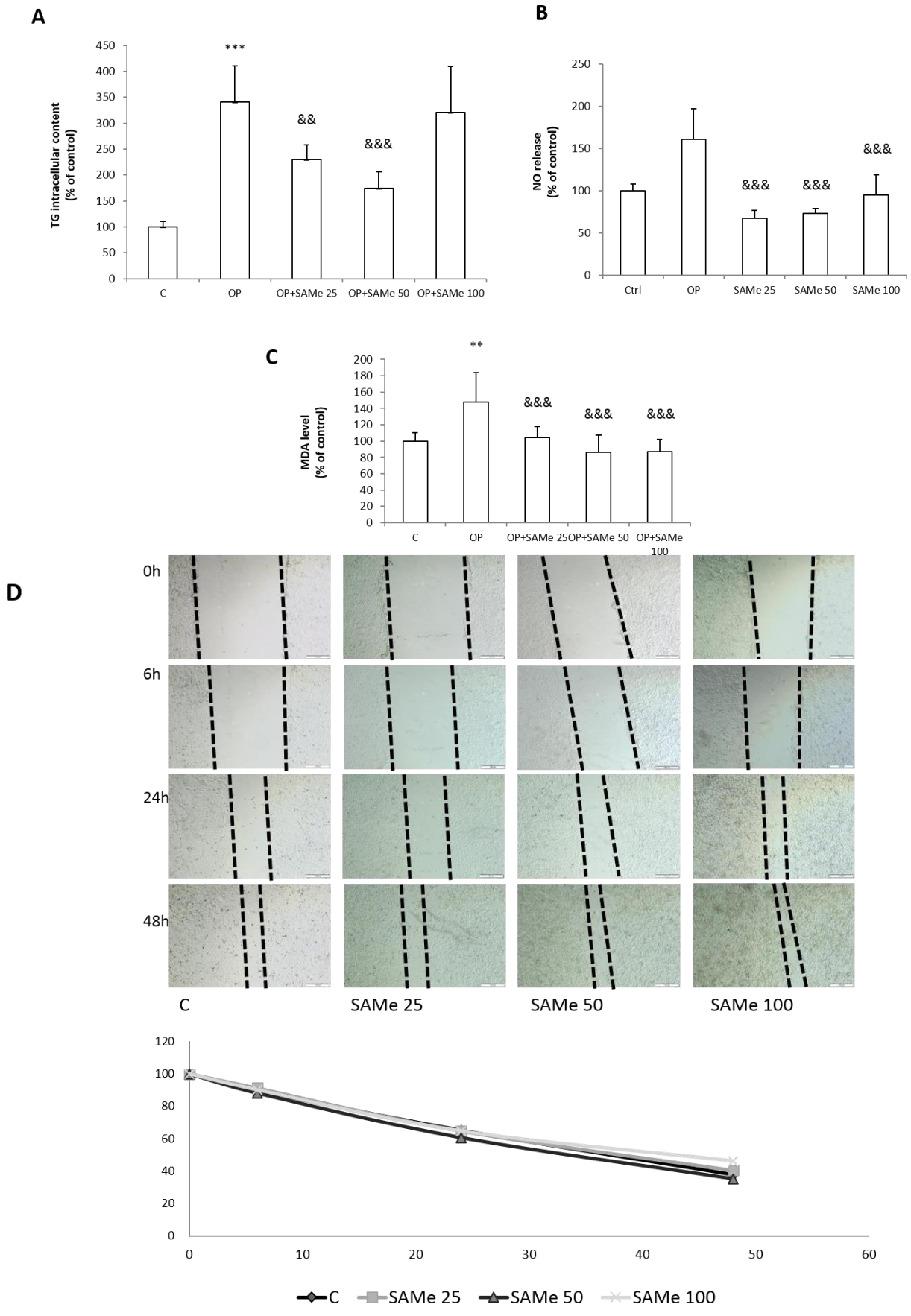
A
TG intracellular content (% of control)
450
400
350
300
250
200
150
100
50
0
***
&&
&&&
C
OP
OP+SAMe 25
OP+SAMe 50
OP+SAMe 100
B
NO release (% of control)
250
200
150
100
50
0
&&&
&&&
&&&
Ctrl
OP
SAMe 25
SAMe 50
SAMe 100
C
MDA level (% of control)
200
180
160
140
120
100
80
60
40
20
0
**
&&&
&&&
&&&
C
OP
OP+SAMe 25
OP+SAMe 50
OP+SAMe 100
D
0h
6h
24h
48h
C
SAMe 25
SAMe 50
SAMe 100
120
100
80
60
40
20
0
0
10
20
30
40
50
60
C
SAMe 25
SAMe 50
SAMe 100

Figure31. Effects of SAMe on lipid accumulation

For HECV cells incubated in the absence (C) or in the presence of oleate/palmitate (OP) alone or with different concentrations of SAMe 25, 50 and 100 µM (OP+SAMe 25, OP+SAMe 50, OP+SAMe 100) we show: **(A)** TG content expressed as percentage of TG content relative to control; normalized for proteins determinated with Bradford assay.; **(B)** NO release expressed as percentage of NO release relative to control; normalized for proteins **(C)** The intracellular level of MDA (pmol MDA/mL x mg of sample protein) quantified by TBARS assay data are expressed as percentage values with respect to controls and normalized for total proteins; **(D)** The migration of HECV was examined using the wound healing assay. Set of images were acquired at 3, 6 and 24 h. To determine the migration of HECV, the images were analysed using ImageJ free software (http://imagej.nih.gov/ij/). Percentage of the closed area was measured and compared with the value obtained before treatment. An increase of the percentage of closed area indicated the migration of cells. Data are means±S.D. of at least three independent experiments. Statistical significance between groups was assessed by ANOVA followed by Tukey's test. Symbols: C *vs* all treatments *p≤0.05; **p≤0.01; ***p≤0.001; OP *vs* all treatments &p≤0.05, &&p≤0.01, &&&p≤0.001

DISCUSSION

Hepatocytes and endothelial cells participate in progression of fatty liver disease, and obesity-related metabolic disorders cause endothelial dysfunction. Due to the increasing prevalence of obesity and obesity-related disorders worldwide, in the last decades there has been a growing interest in the discovery of promising molecule to treat these disorders.

SAMe represents the major physiological defence against ROS and previous study done in many liver diseases, such as alcoholic liver disease, cholestasis of pregnancy, and primary biliary cirrhosis, shown significant improvement in liver test abnormalities during therapy with SAMe. The present study provided insights into the effects and the molecular mechanisms through which SAMe, an endogenous molecule playing many functions, may ameliorate fatty acids-induced steatosis and oxidative stress in hepatic and endothelial cells.

In the cell models of the current study, the exposure of hepatocytes and endotheliocytes to fatty acids mimics, respectively, an *in vitro* model of NAFLD and atherosclerosis. Excess fatty acids on hepatocytes stimulates triglyceride intracellular accumulation and up-regulation of ADRP, CPT1 and UCP2 expression levels. Lipid peroxidation, ROS production and catalase activity were also enhanced in steatotic hepatocytes. Exposure of steatotic hepatocytes to different concentrations of SAMe led to a decrease in triglyceride content and lipid droplets size and number. CPT1, a mitochondrial protein acting as shuttle for FAs involved in mitochondrial FA oxidation, was up regulated in steatotic cells and furthermore after the exposure to SAMe, at all concentrations. In the light of that, the lipid-lowering action of SAMe might be sustained by stimulation of oxidative and/or secretory pathways. UCP2, a mitochondrial uncoupling protein, was significantly up-regulated upon lipid-loading but SAMe at all concentration did not change significantly its expression. Lipid peroxidation, ROS production and catalase activity were all significantly decreased upon treatment with SAMe.

On the other side, exposure of endothelial cells to oleate and palmitate, led to an increase in triglyceride content and lipid peroxidation. As a response to lipid-loading, endothelial cells released NO and produced ROS thus triggering proinflammatory events. The subsequent treatment with SAMe at different concentrations led to a decrease of triglyceride content and NO and ROS production.

We can conclude that SAMe is an efficacious lipid-lowering and antioxidant agent for steatotic hepatocytes and endotheliocytes. The anti-steatotic effect of the molecule seems to be sustained by an increase in catabolic pathways at mitochondrial level.

In conclusion, the beneficial effect of SAMe on the in vitro models of NAFLD and atherosclerosis suggests that the molecule possess a potential therapeutic benefit on these pathological conditions.

11.Cell model for adipogenic differentiation to investigate molecular events associated to adipocytes hypertrophy

Paper in preparation

ABSTRACT

Over the past several decades, there has been a significant change in lifestyle: the increase of a sedentary lifestyle and of the consume of calorie-dense and fat food leaded to an increase trend of obesity. The increase of obesity worldwide is accompanied by the increasing prevalence of many obesity-related disorders as cardiovascular diseases, diabetes, cancers. The epidemic of overweight and obesity worldwide represents one of the major challenges in chronic disease prevention; therefore, over the last years, the study of adipose tissue biology and the mechanisms involved in adipocyte hypertrophy has gained attention. Lipid droplets (LDs) hypertrophy in adipocytes is the main cause of energy metabolic system dysfunction and obesity: enlarged adipocytes are associated with insulin resistance and are an independent predictor of type 2 diabetes. Adipose tissue, apart from its classical role as an energy storage depot, is also a major endocrine organ secreting many factors, whose local and circulating levels are affected by the degree of adiposity.

To understand the molecular link between adipocyte hypertrophy and metabolic diseases we developed a procedure for inducing hypertrophy. To do this we used an *in vitro* model in which mature 3T3-L1 adipocytes were loaded with oleate/palmitate mixture, resulting in artificially hypertrophied mature adipocytes. Real-time RT-PCR analysis of PPARg and adiponectin expression in different adipocytes revealed higher expression in the hypertrophic adipocytes, respect to undifferentiated 3T3 cells.

In order to clarify the role of hypertrophic adipocytes in obesity, isolated from other factor, we investigated the cellular and molecular differences between mature and hypertrophic

adipocytes.

INTRODUCTION

Obesity is an important public health burden in both developed and developing countries, as it is associated with an increased risk of metabolic and cardiovascular diseases. The accumulation of excess fat in white adipose tissue (WAT) can occur through an increase in adipocyte volume (hypertrophy) and/or number (hyperplasia). Hypertrophic adipocytes are enlarged depending on the enlarging of cytosolic lipid droplets (LDs) storing the triglycerides (TGs).

During adipogenesis, fibroblast-like pre-adipocytes differentiate into mature adipocytes through a rearrangement of the molecular machinery and the peroxisome proliferator activated receptor gamma (PPAR γ is the major determinant of this process (Moset et al., 2016). PPARγ promotes primarily the lipogenic processes and contributes to FA uptake and TG accumulation during adipogenesis but also in mature adipocytes (Tamori et al., 2002; Brun et al., 1996). Mature adipocytes strictly regulate the balance between lipogenesis and lipolysis, and produce a panel of adipokines such as leptin, resistin, adiponectin, tumor necrosis factor-a (TNF-α), interleukin-1b (IL-1b) that modulate metabolism of the other tissues (Rajala and Scherer, 2003).

The 3T3-L1 cells are well-established murine preadipocytes displaying a fibroblast-like morphology that, under appropriate conditions, progress towards an adipocyte-like phenotype (Green and Meuth, 1974). A large body of articles have employed 3T3-L1 cells to investigate adipogenesis and obesity-related characteristics. One of the main advantages of this cell line is that provides a homogenous and reproducible system (Poulos et al., 2010).

In obesity conditions, hypertrophic adipocytes increase reactive oxygen species (ROS) production and inflammation and modulate the panel of released adipokines such as adiponectin and TNFα (Furukawa et al., 2004). Discrepant results about adiponectin production in hypertrophic adipocytes have been reported. While in human serum, high levels of adiponectin exerted anti-inflammatory, anti-atherogenic and anti-diabetic effects (Ouchi et al., 1999; Yamauchi et al., 2003), in mouse 3T3-L1 adiponectin over-expression led to increased cell size and TG content (Maeda et al., 2001). Adipose tissue of obese mice releases also TNFα, a proinflammatory cytokine which acts on peripheric tissues where it modulates degree of adiposity, impairs glucose and FA uptake and stimulates lipolysis leading

to hyperlipidaemic conditions.

Metallothioneins (MTs) are low-molecular-weight, cysteine-rich proteins acting in the metabolism of essential metals and protection against toxic heavy metals (Haq et al., 2003; Sato and Bremner, 1993, but they seem to be involved also in the regulation of WAT formation at earlier stages, are induced during the development of obesity (Sato et al., 2013). On the other hand, MTs have a potential to prevent obesity-related diseases, at least in part, through suppression of free radical generation and endoplasmic reticulum stress, in female mice (Sato et al., 2013). Moreover, MT-gene silencing led to enhanced lipid accumulation in 3T3-L1 cells (Kadota et al., 2017).

In the present study, we developed an adipocyte hypertrophy model to investigate differences between mature and hypertrophic adipocytes. 3T3-L1 pre-adipocytes were differentiated and then cultured for another 2 days with a mixture of long-chain fatty acids (oleate/palmitate 1 mM). Our findings suggest that adipocyte hypertrophy is enough to provoke changes at different cell levels: alterations of mitochondrial morphology and consequently activity, increase of oxidative stress.

MATERIALS & METHODS

Chemicals

All chemicals, unless otherwise indicated, were supplied by Sigma-Aldrich Corp. (Milan, Italy).

Cell culture and treatments

3T3-L1 mouse fibroblasts were purchased from the American Type Culture Collection (Manassas, VA, USA) and kindly provided by Prof. Bruzzone (University of Genoa). Cells were maintained in Dulbecco's modified Eagle medium (D-MEM) containing 25 mmol/l glucose and 10% Foetal Bovine Serum (FBS, Euroclone, Milan, Italy) under 5% CO_2 at 37°C. For adipocyte differentiation, cells were seeded at $2x10^5$ cells/mL in petri dishes. At 2-day post confluence, adipogenesis was induced by adding the differentiation mixture containing 1µM insulin, 1µM dexamethasone (DEX), and 500µM 3-isobuthyl-1-methylxanthine (IBMX) to the culture medium for 2 days. Then, cells were incubated with 100nM insulin for 7 days, changing the medium every 2–3 days. In all experiments, more than 90% of the cells were mature adipocytes after 10 days of incubation. Adipogenic differentiation was monitored at different days by lipid staining. To induce cellular hypertrophy, mature adipocytes were exposed to oleate/palmitate mixture (1 mM) for 2 days.

Protein quantification

The protein content was determined by the Bradford assay using bovine serum albumin (BSA) as a standard (Bradford, 1976).

Quantification of triglycerides

The TG content of 3T3-L1 cells in the different conditions was measured as previously described (Grasselli et al., 2011). Briefly, cells were scraped, centrifuged at 800xg for 10 min and lysed in phosphate buffered saline (PBS). Lipids were extracted in chloroform/methanol (2:1), and after chloroform evaporation TG were quantified using the 'Triglycerides liquid' kit (Sentinel diagnostic, Milan, Italy). The absorbance at 546 nm was recorded using a Varian Cary UV-VIS spectrophotometer 50 Bio (Agilent Technologies, Milan, Italy). Values were normalized for the protein content. Data are expressed as percent TG content relative to controls.

Lipid droplet staining and analysis

3T3-L1 cells were grown on collagen-coated glass slides. At the end of treatments cells were washed twice with PBS, fixed in 4% formaldehyde/PBS for 20 min, then washed in PBS. Neutral lipids of LDs were visualized using the selective Oil-RedO (ORO) dye as previously described (Baldini et al., 2019). Briefly, cells were stained for 30 min with 0.3% ORO solution which was freshly prepared from a stock solution of 0.5% in isopropanol, washed and mounted. LDs were also visualized using the fluorescent probe BODIPY 493/503 (Molecular Probes, Life Technologies, Monza, Italy) (Vecchione et al., 2017). After fixation and washing cells were incubated with 1 µg/mL BODIPY 493/503 in PBS for 30 min, washed and mounted with 4',6-diamidino-2-phenylindole (DAPI) (Sigma-Aldrich, Milan, Italy). Images were obtained using a Leica DMRB light microscope equipped with a Leica CCD camera DFC420C (Leica, Wetzlar, Germany). In each population, more than 500 cells were analyzed.

ROS production and lipid peroxidation measurement

The production of H_2O_2 and other ROS *in situ* was assessed through the oxidation of the cell-permeant 2′ -7′ dichlorofluorescin diacetate (DCF-DA, Fluka, Germany) to 2′ -7′ dichlorofluorescein (DCF) (Halliwell and Whiteman, 2004). Briefly, cells were scraped and gently spun down (600×g for 10 min at 4°C). After washing, cells were loaded with 10µM DCF-DA freshly prepared from a stock solution (10mM in DMSO) in PBS for 30 min at 37°C in the dark. Then, cells were centrifuged, suspended in PBS and the fluorescence signal (ex=495 nm; em=525 nm) was recorded using a Cary Eclipse Fluorescence Spectrophotometer (Agilent, Santa Clara, CA, United States) at 25 °C in water-thermostated cuvette holder. The fluorescence signal was expressed as MFI (mean fluorescence intensity)/mg of protein.

Lipid peroxidation was determined spectrophotometrically through the thiobarbituric acid reactive substances (TBARS) assay which is based on the reaction of malondialdehyde (MDA; 1,1,3,3-tetramethoxypropane) with thiobarbituric acid (TBA) (Iguchi et al., 1993). Briefly, 1 vol. of cell suspension was incubated for 45 min at 95°C with 2 vol. of TBA solution (0.375% TBA, 15% trichloroacetic acid, 0.25 N HCl). Then, 1 vol. of N-butanol was added and the organic phase was read at 532 nm in a UV-VIS spectrophotometer at 25°C using Peltier-thermostated cuvette holder. The MDA level was expressed as pmol MDA/mL/mg protein.

RNA extraction and Quantitative real-time polymerase chain reaction

Total RNA was isolated using Trizol reagent, according to the manufacturer's instructions. RNA concentration was quantified spectrophotometrically at 260 nm and purity was evaluated by measuring the ratio A260/A280. Total RNA (1.5 µg) was reverse transcribed using the RevertAid H Minus Reverse Trancriptase MULV (Thermo Fisher Scientific, Massachussets, USA), according to the manufacturer's suggestions, in a Master Cycler Personal (Eppendorf, Milan, Italy). Quantitative real-time PCR (qPCR) was performed in triplicate using iQ™ SYBR Green Supermix (Biorad, Monza, Italy) and CFX96™ Real-Time System (Biorad, Monza, Italy). All primer pairs were designed *ad hoc* starting from the coding sequences (http://www.ncbi.nlm.nih.gov/Genbank/GenbankSearch.html) and were synthesized by TibMolBiol custom oligosynthesis service (Genova, Italy). The relative quantity of target mRNA was calculated by using the comparative Cq method and was normalized for the expression of GAPDH gene, used as reference gene. The normalized expression of the target genes was thus expressed as relative quantity of mRNA (fold induction) with respect to controls (C). The data were analyzed using a Bio-Rad CFX manager software. Primer pairs designed *ad hoc* starting from the coding sequences of *Mus musculus* and synthesized by TibMolBiol (Genova, Italy) are listed in Table1.

Adiponectin Fwd	GCTCTCCTGTTCCTCTTAATCC	60	E9PWU4
Adiponectin Rev	GCAATCTCTGCCATCACG		
PPARγ Fwd	GGAATTAGATGACAGTGACTTGGC	60	P37238
PPARγ Rev	GGAGCACCTTGGCGAACAG		
TNFα Fwd	CATCTTCTCAAAATTCGAGTGACAA	60	P06804
TNFα Rev	TGGGAGTAGACAAGGTACAACCC		
UCP1 Fwd	GATGGTGAACCCGACAACTT	56	P12242
UCP1 Rev	CTGAAACTCCGGCTGAGAAG		
VLCAD Fwd	TGAATGACCCTGCCAAG	60	P50544
VLCAD Rev	CCACAATCTCTGCCAAGC		
GAPDH Fwd	GACCCCTTCATTGACCTCAAC	60	P16858
GAPDH Rev	CGCTCCTGGAAGATGGTGATGGG		

Mitochondrial Oxygen Consumption

Mitochondrial function was investigated by assessing respiration parameters using an

Oxygraph 2 k (O2K) high-resolution respirometer and processed with DatLab 6.2 software (Oroboros Instruments GmbH, Innsbruck, Austria). Aliquots of $2x10^6$ cells for each condition (pre-adipocytes, mature and hypertrophic adipocytes) were analysed by All the parameters were corrected for non-mitochondrial background oxygen consumption. Breifly, cells were collected and suspended in 2 mL of Mir05 buffer (0.5 mM EGTA, 3 mM $MgCl_2$, 60 mM K-lactobionate, 20 mM taurine, 10 mM H_2PO_4, 20 mM HEPES, 110 mM sucrose, 1 g/L BSA, pH=7.1) (Einer et al., 2019). For the measurement, cell suspension was injected in the in the oxygraph chamber and the oxygen consumption related to mitochondrial respiration was measured under continuous stirring, at 37°C. First, 10 µg/mL digitonin was added to permeabilize cells. Non-phosphorylating respiration was induced by adding the complex I-linked substrates glutamate (10 mM) and malate (2 mM). Subsequently, the OXPHOS-capacity of complex I-linked activity was measured after addition of a saturating concentration of ADP (2.5 mM). Then, succinate (10 mM) was added to evaluate OXPHOS-capacity of complex I&II-linked activity. The maximum oxygen consumption, which defines the electron transfer system capacity, was determined by adding the uncoupling compound carbonyl cyanide-4-(trifluoromethoxy)phenylhydrazone (FCCP) at 1 µM steps. At the end, 1 µM rotenone (complex I inhibitor) and 2.5 µM antimycin A (complex III inhibitor) were added. Data were corrected for non-mitochondrial background by subtraction of oxygen consumption level measured after addition of rotenone and antimycin A.

All the parameters were corrected for non-mitochondrial background by subtraction of oxygen consumption level measured after addition of rotenone and antimycin A (residual oxygen consumption non related to mitochondrial respiration).

Mitochondria content evaluation

The fluorescent probe MitoTracker Deep Red (Invitrogen, Thermo Fisher Scientific, Milan, Italy) was employed to label the membrane of intact mitochondria in living cells (Claus et al., 2011). At the end of treatment, cells were scraped and gently spun down (600×g for 10 min at 4 °C). After washing, cells were loaded with 0.1 µM MitoTracker in PBS freshly prepared from a stock solution (1.5 mM in DMSO) for 20 min at 37°C in the dark. Then, cells were centrifuged, suspended in PBS and the fluorescence (ex=644 ex=644 nm; em=665 nm) was measured in a Cary Eclipse Fluorescence Spectrophotometer at 25 °C using a water-thermostated cuvette holder. The fluorescence signal was expressed as MFI (mean

fluorescence intensity)/mg of protein.

Western Blot

Cells were collected by centrifugation and lysed in RIPA buffer (1% NP-40, 0.1% SDS, 50 mM Tris-HCl pH 7.4, 150 mM NaCl, 0.5% Sodium Deoxycholate, 1 mM EDTA). Lysates were centrifuged at 16,000 g/10 min at 4 °C. Equal amounts of protein (about 40 µg) were separated by SDS-PAGE and transferred to PVDF membranes (Bio-Rad, Munich, Germany). Membranes were blocked with 5% skim milk in Tris Buffered Saline with 0.1% Tween 20 (TBST and incubated overnight at 4°C using mouse anti-Hsp60 antibody (611562, BD Transduction Laboratories™, USA) or rabbit anti-citrate synthase (CS) antibody (16131-1-AP, Proteintech, United Kingdom) or rodent anti-OxPhos Complex Monoclonal Antibody (cocktail of multiple OxPhos antibodies: C-I-20, bovine complex I; C-II-30, bovine heart complex II; C- III-Core 2, bovine heart complex II, III; C-IV-I, human complex IV subunit I; C-V-alpha, bovine complex V; 45-8099, Thermo Fisher Scientific, Massachussets, United States). Appropriate secondary antibodies conjugated to horseradish peroxidase (HRP) and ECL solution were used to visualize proteins; the chemiluminescence signal was detected with the ChemiDoc™ Touch Imaging System (Bio-Rad, Munich, Germany).

Statistical analysis

Data are expressed as means ± S.D. of at least three independent experiments. GraphPad Prism 7.0 software was used for statistical evaluation. Statistical analysis was performed using ANOVA with Tukey's post-test (GraphPad Software, Inc., San Diego, CA, USA).

RESULTS

In vitro model of adipocyte hypertrophy

Differentiation of 3T3-L1 pre-adipocytes into mature adipocytes and then the progression towards hypertrophic adipocytes was assessed by cell morphology analysis and LD labelling. The spectrophotometric quantification of cellular TG content showed that lipid accumulation increased significantly in mature adipocytes (+110%; p≤0.001), and a larger increase was observed in hypetrophic cells (+225%; p≤0.001) compared to pre-adipocytes (Fig.1A). Changes in cell volume and LD enlargement typically occur *in vivo* during adipogenesis differentiation and hypertrophy. The morphometric analysis of ORO- and BODIPY-stained cells revealed that *in vitro* mature adipocytes were occupied by medium-sized LDs, while hypertrophic adipocytes contained very large or single LD (Fig.1B). The mean size and the size distribution of LDs were determined by computerized image analysis (Fig.1C). The average LD diameter in mature adipocytes was about 9.3±0.4 µm that increased to 16.2±2.6 µm in hypertrophic adipocytes.

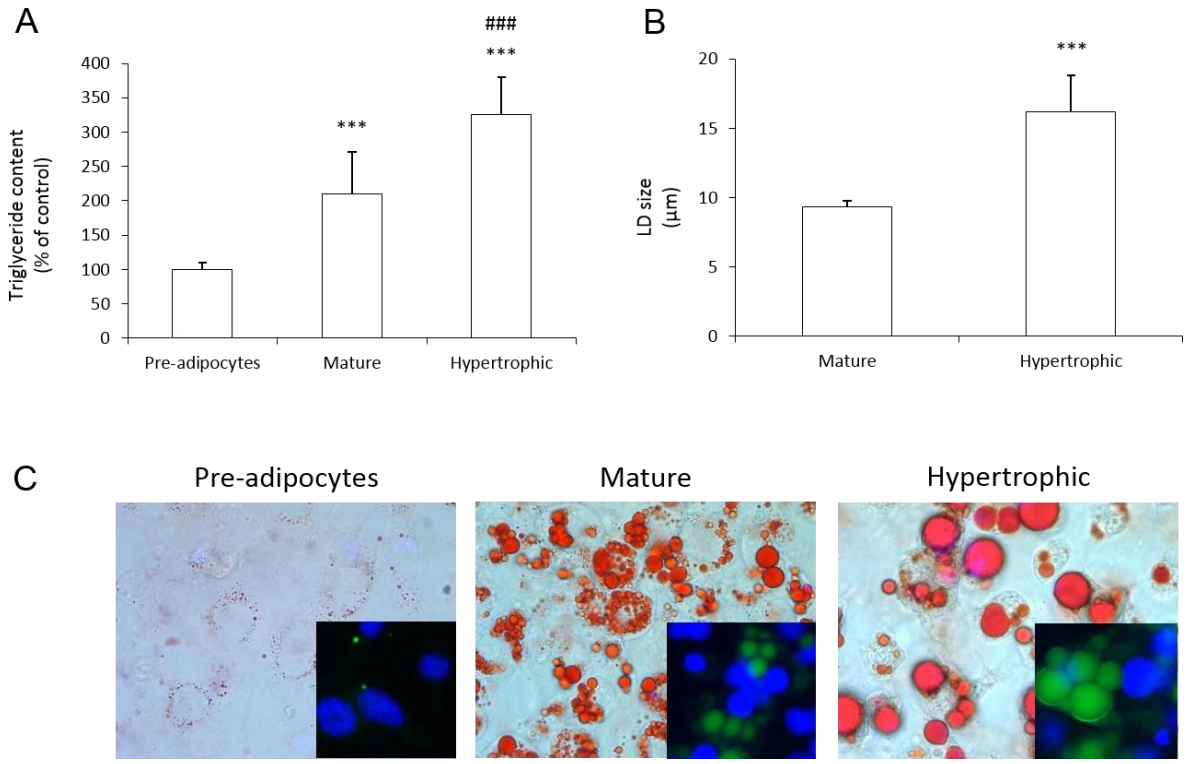

Figure 32. In vitro adipocyte hypertrophy

For 3T3L1 cells undifferentiated (pre-adipocytes), differentiated (mature) and hypertrophic we show: **(A)** TG content expressed as percent TG content relative to control, normalized for proteins determined with Bradford assay. **(B)**

Microphotographs of cells stained with ORO (magnification 40x). **(C and insert)** Microphotographs of cells stained with DAPI and BODIPY 493/503 (magnification 40x) and OilRedO; images were captured sequentially and then merged. For microscopy analysis a Leica DMRB light microscope equipped with a Leica CCD camera DFC420C was employed. Statistical significance between groups was assessed by ANOVA followed by Tukey's test. Symbols: Pre-adipocytes vs all treatments ***p ≤ 0.001; Mature vs all treatments ###p≤0.001.

As a response to increased intracellular TG, mature adipocytes released increased level of TGs into the culture medium (+237%; p≤0.05) with respect to control pre-adipocytes and the TG release was almost doubled in hypertrophic adipocytes (+491%; p≤0.001) (Fig.2C). As a marker for adipogenesis, PPARγ mRNA expression was assessed by qPCR (Fig.2A). In mature 3T3-L1 adipocytes, PPARγ overexpression accompanied the increase in the intracellular TG content (10.1-fold induction *vs* control; p≤0.001) and an even larger PPARγ overexpression was observed in hypertrophic cells (12.5-fold induction *vs* control controls; p≤0.001). On the other hand, although mature adipocytes showed a significant overexpression of adiponectin mRNA (2341-fold induction *vs* control; p≤0.001) compared to pre-adipocytes, no further increase in adiponectin mRNA was observed in hypertrophic adipocytes (2542-fold induction *vs* control; p≤0.001) (Fig.2B).

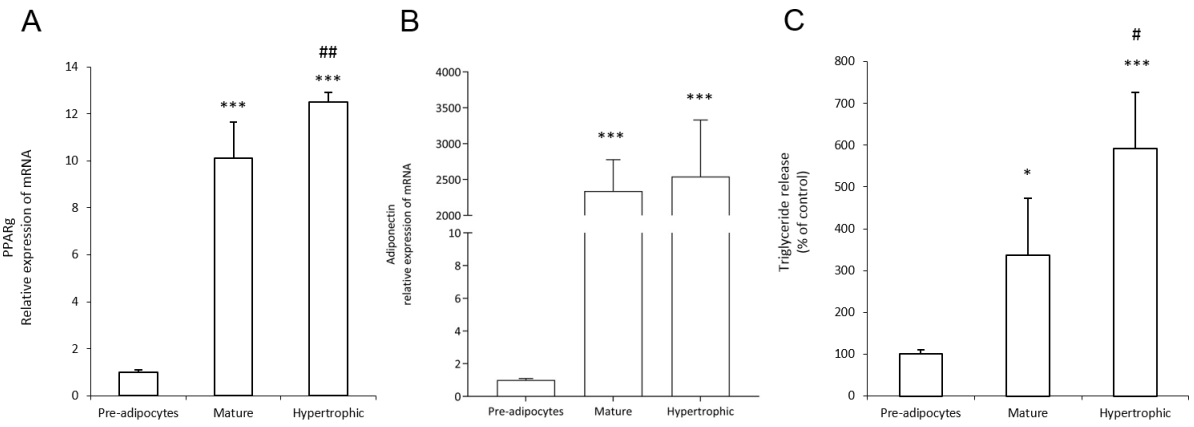

Figure 33. Markers for lipogenesis and adipocyte hypertrophy

For 3T3L1 cells undifferentiated (pre-adipocytes), differentiated (mature) and hypertrophic we show: The mRNA expression of PPARγ **(A)** and adiponectin **(B)** evaluated by qPCR using GAPDH as the internal control. Data are expressed as fold induction with respect to controls. **(C)** The extracellular TG content quantified in the medium by spectrophotometric assay; data are expressed as percent TG content relative to controls and normalized for total proteins. Anova followed by Turkey's test was used to assess the statistical significance between groups. Symbols: Pre-adipocytes vs all treatments, *p ≤ 0.05, ***p ≤ 0.001; Mature vs all treatments, #p ≤ 0.05, ##p≤0.01.

Adipocyte Hypertrophy and Oxidative Stress

Lipid accumulation typically results in increased fat oxidation producing excess of ROS which may damage important cellular components such as membranes (Seifert et al., 2010). When intracellular ROS production was quantified *in situ* by fluorimetric analysis of DCF-stained cells (Fig. 3A), we observed an increase in DCF signal in hypertrophic adipocytes with respect to mature adipocytes (+38% vs control, p≤0.01).

Excess ROS may result in oxidative stress condition which trigger lipid peroxidation of membranes that we assessed by TBARS assay. We found increased MDA levels in mature adipocytes (+98% *vs* control; p≤0.01) and a larger increase in hypertrophic adipocytes (+161% *vs* control; p≤0.01) (Fig.3B) which are sign of fat-dependent oxidative stress.

In the attempt to counteract oxidative stress mature adipocytes overexpressed the antioxidant peptides MT-1 and MT-2 (4.69- and 1,97-fold induction, *vs* control respectively; p≤0.01). However, no further increase in MT expression was observed in hypertrophic adipocytes (4,82- and 2.31-fold induction, *vs* control respectively; p≤0.001) (Fig.3C).

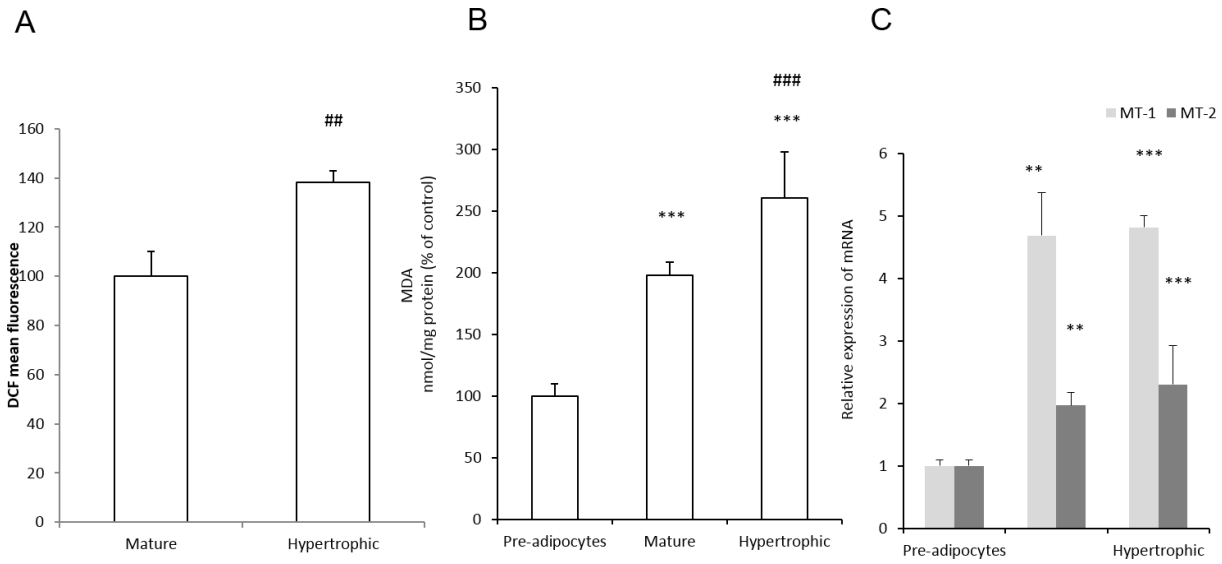

Figure 34. Adipocyte hypertrophy increased ROS production and oxidative stress

In 3T3L1 cells undifferentiated (pre-adipocytes), differentiated (mature) and hypertrophic we assessed: **(A)** The ROS level were quantified by spectrofluorimeter assay of DCF-stained cells and data are expressed as percent mean fluorescence intensity (MFI) relative to mature adipocytes and normalized for total proteins; **(B)** The intracellular level of MDA (pmol MDA/mL x mg of sample protein) quantified by TBARS assay. Data are expressed as percentage values with respect to controls and normalized for total proteins. **(C)** The mRNA expression of MT1 and MT2 evaluated by qPCR using GAPDH as

the internal control. Data are expressed as fold induction with respect to controls. Anova followed by Turkey's test was used to assess the statistical significance between groups. Symbols: Pre-adipocytes vs all treatments, *p ≤ 0.05, ***p ≤ 0.001; Mature vs all treatments, ##p≤0.01.

Adipocyte Hypertrophy and mitochondrial activity

Assessing mitochondrial function typically relies on respiration investigation, and here we employed an intact cell approach using the Oxygraph 2 k (O2K) high-resolution respirometer (Fig.4A). Both the routine respiration and the non-phosphorylating respiration linked to complex I activity [N(GM)L] were rather constant in all conditions (about 50 pmol/s and 25 pmol/s, respectively). By contrast, both the OXPHOS-capacity of complex I-linked activity [N(GM)P] and of complex I&II-linked activity [NS(GMS)P], as well as the maximum oxygen consumption [NS(GMS)ET] were significantly reduced in hypertrophic condition. In details, [N(GM)P] in pre- and mature adipocytes was about 70 pmol/s and decreased to 45.91 pmol/s in hypertrophic adipocytes (-27%; p≤0.05 *vs* mature). [NS(GMS)P] decreased from about 100 pmol/s in pre- and mature adipocytes to 66.23 pmol/s in hypertrophic adipocytes (-33%, p≤0.05 *vs* mature adipocytes), and [NS(GMS)ET] from about 162 pmol/s in both pre- and mature adipocytes to 92.39 pmol/s in the hypertrophic cells (-43%, p≤0.01 *vs* mature adipocytes).

The levels of OXPHOS proteins in all the above conditions were assessed by western blotting. The protein level of all the complexes was similar in pre-adipocytes and mature adipocytes; only the complex IV showed a slight reduction in mature adipocytes (-18%, p≤0.05, with respect to control). By contrast, a significant reduction in the protein level of all the complexes was observed in hypertrophic adipocytes with respect to mature adipocytes: -30%, for complex I (p≤0.001), -16% for complex II (p≤0.01), -24% for complex III (p≤0.001), -40% for complex IV (p≤0.001) and -33% for complex V (p≤0.001) (Fig.4B).

In order to verify if the differences in mitochondrial respiration could depend on a loss of mitochondria in hypertrophic adipocytes we assessed the expression of citrate synthase (CS) and heat shock protein 60 (HSP60), which are frequently used as biomarkers for mitochondrial content (Larsen et al., 2012). Although, both the CS and HSP60 levels decreased during adipogenesis process passing from pre- to mature adipocytes, no differences were observed between mature and hypertrophic adipocytes (Fig.4C). Also the mitotracker fluorescence, a probe selective for intact mitochondria, did no show changes in

hypertrophic adipocytes respect to mature adipocytes (data not shown).

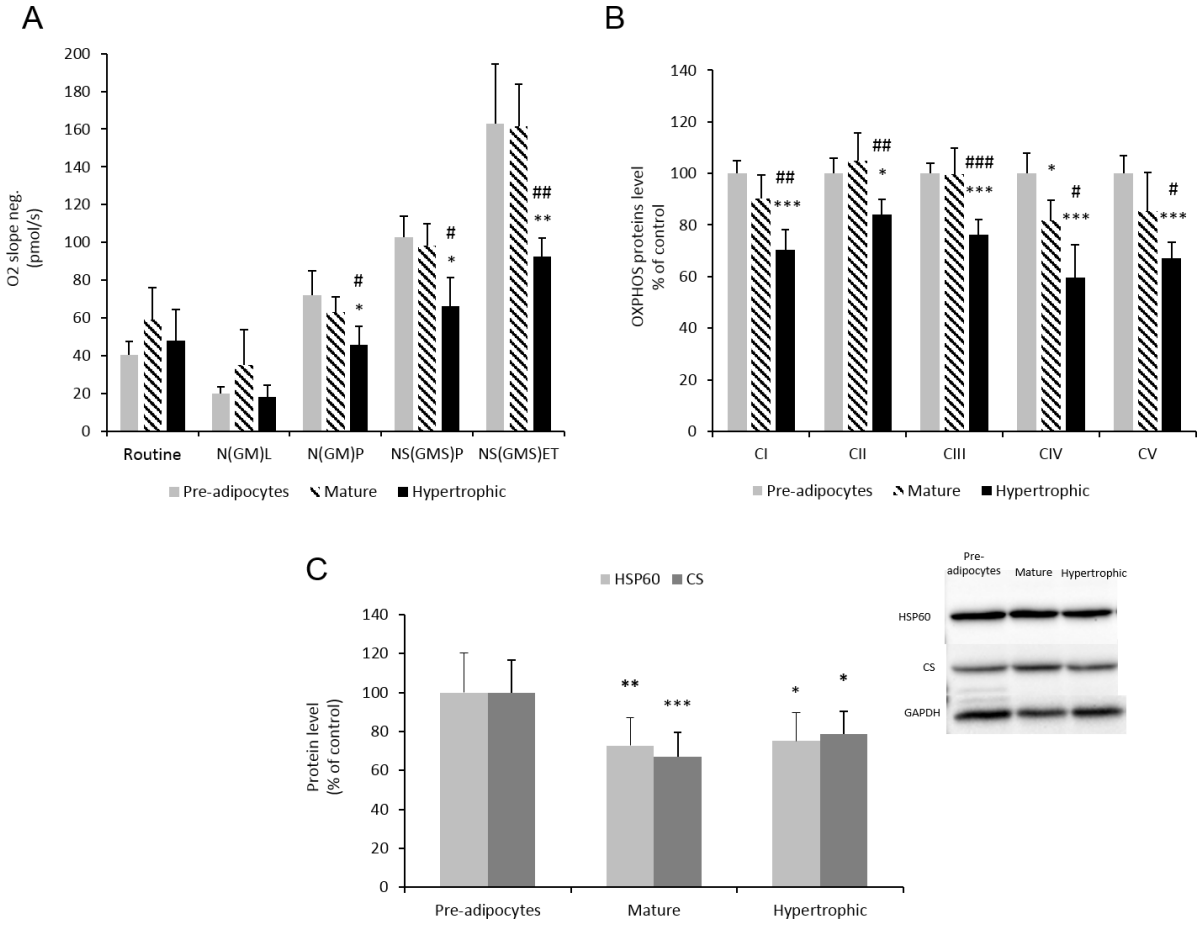

Figure 35. Adipocyte hypertrophy impaired mitochondrial respiration

In 3T3-L1 cells mimicking pre-adipocyte, mature and hypertrophic adipocyte condition the mitochondria function and integrity were assessed. **(A)** Oxygen consumption related to mitochondrial respiration was assessed by using the Oxygraph 2 k (O2K) high-resolution respirometer. The following parameters were measured: routine respiration, non-phosphorylating respiration linked to complex I activity [N(GM)L], OXPHOS-capacity of complex I-linked activity [N(GM)P], OXPHOS-capacity of complex I&II-linked activity [NS(GMS)P], maximum oxygen consumption [NS(GMS)ET]. Data are expressed as pmol/s. **(B)** Protein level of the individual OXPHOS complexes was assessed by Western blotting and densitometric analysis. (C-I-20, bovine complex I; C-II-30, bovine heart complex II; C-III-Core 2, bovine heart complex II, III; C-IV-I, human complex IV subunit I; C-V-alpha, bovine complex V). (**C)** Protein expression of HSP60 and Citrate Synthase (CS) were evaluated by Western blotting and densitometric analysis. GAPDH was the protein loading control used as housekeeping gene. Data are expressed as percentage values with respect to controls. Anova followed by Turkey's test was used to assess the statistical significance between groups. Symbols: Pre-adipocytes vs all treatments, *p ≤ 0.05, **p ≤ 0.01, ***p ≤ 0.001; Mature vs all treatments, #p≤0.05, ##p≤0.01, ###p≤0.001.

DISCUSSION

Obesity is a pandemic condition that leads to health impairment by increasing the risk of developing several diseases such as T2DM, MetS, CVDs and several types of cancer. The molecular mechanisms connecting obesity to onset and progression of these diseases need to be clarified, but it is well recognized that fat accumulation in adipose tissue results in an altered expression of several hormones, growth factors, and adipokines.

Obesity depends on adipocyte hypertrophy which is an adaptive response to nutrient excess and correlates directly with metabolic disease (Rydén et al., 2014). When the hypertrophic threshold is reached the adipocyte buffering capacity is exceeded leading to ectopic lipid deposition in peripheral tissues. Previous studies showed that adipocyte and LD size influence several metabolic functions (Margareta et al., 2006).

To promote hypertrophy, after differentiation 3T3-L1 adipocytes were challenged for 2 days with a mixture of oleate (C18:1), and palmitate (C16:0), the fatty acids most abundant in the diet and in the body. As a first result we could observe, as expected, an increase in triglyceride content in mature adipocytes and a further increase in the hypertrophic condition. Lipid droplets average size was increased in differentiated adipocytes exposed to oleate and palmitate, thus confirming the induction of the hypertrophic condition. As a response to increased intracellular fat content, mature adipocytes released increased level of triglycerides into the culture medium and this released was almost doubled in hypertrophic condition.

As a marker for adipogenesis, we assessed PPARγ expression: in mature cells, PPARγ overexpression accompanied the increase in the intracellular triglyceride content and an even larger overexpression was observed in hypertrophic cells.

Once preadipocytes have committed to the adipogenesis program, a transcriptional cascade is activated and induces the expression of metabolic genes and adipokines associated with the adipocyte phenotypes, such as leptin, adiponectin, TNF-α, and IL-6. Indeed, we observed an increased adiponectin expression in mature adipocytes and hypertrophic ones.

Lipid accumulation typically results in increased fat oxidation and consequent ROS production which may damage important cellular components. We observed an increase in

ROS production upon differentiation and an even larger increase in the hypertrophic model. Excess ROS may damage cellular membranes, leading to lipid peroxidation: MDA levels in mature adipocytes were increased and a larger increase in hypertrophic adipocytes, which are sign of fat-dependent oxidative stress. The levels of the antioxidant proteins MT1 and MT2 are known to be increased during the development of obesity in the attempt to counteract oxidative stress in mature adipocytes. MT-1 and MT-2 were overexpressed in both mature and hypertrophic adipocytes; however, no further increase in MT expression was observed in hypertrophic adipocytes.

Furthermore, we investigated the effects at mitochondrial level of the exposure of mature adipocytes to fatty acids. Employing an O2K high-resolution respirometer, we evaluated different parameters of mitochondrial respiration. Taken together, the results clearly indicate that the hypertrophic condition in vitro led to a general reduction in the mitochondrial oxygen consumption, although the routine respiration, which is controlled by basal energy demand of the cells, was unchanged. The reduction in activity of both complex I and II in hypertrophic adipocytes was paralleled by a marked decrease in the capacity of the electron transfer system (ETS) measured from the noncoupled state of maximum respiration.

In order to investigate the reason of the mitochondrial respiration decrease in hypertrophic adipocytes, we measured ss the levels of OXPHOS proteins of all the five respiratory complexes. The results obtained suggested that the lower mitochondrial oxygen consumption that we observed in hypertrophic adipocytes seems to be depend on the reduction in the amount of the mitochondrial complexes.

With the intention to clarify whether the decrease in mitochondrial oxygen consumption and OXPHOS proteins level in hypertrophic cells is due to a decrease in mitochondria content or mitochondria morphology, we assessed the expression of citrate synthase (CS) and heat shock protein 60 (HSP60), which are frequently used as biomarkers for mitochondrial content. Although, both the CS and HSP60 levels decreased during adipogenesis process passing from pre- to mature adipocytes, no differences were observed between mature and hypertrophic adipocytes. As a confirm, the mitotracker fluorescence, a probe selective for intact mitochondria, did no show changes in hypertrophic adipocytes respect to mature adipocytes. Therefore, we can conclude that the decrease in mitochondrial oxygen

consumption and OXPHOS proteins level which in hypertrophic adipocytes does not depend on a reduced mitochondrial content, but on alteration of mitochondria morphology and integrity.

12.Conclusions

The prevalence of obesity has increased worldwide in the past 50 years, reaching pandemic levels. Obesity represents a major health challenge because it substantially increases the risk of diseases such as type 2 diabetes mellitus, fatty liver disease, hypertension, myocardial infarction, stroke, and several cancers, thereby contributing to a decline in both quality of life and life expectancy. Obesity prevention and treatments frequently fail in the long term (for example, behavioral interventions aiming at reducing energy intake and increasing energy expenditure) or are not available or suitable (bariatric surgery) for the majority of people affected. For all these reasons, in the last decades, many studies have been performed to elucidate the molecular mechanisms involved in obesity progression and therapy, and often cellular models have been developed for the experimental investigations.

In the light of that, the aim of my thesis project was *(i)* to investigate the cellular and molecular changes determined by overnutrition and overweight at different organ levels using *in vitro* models of metabolic disorders and *(ii)* to assess the possible effects of natural and synthetic compounds to counteract these conditions. Below we summarized the main results of my research activities.

12.1 Effects of steatogenic compounds on hepatocytes as a model of hepatic steatosis

Overconsumption of fats and sugars is a major cause of development of non-alcoholic fatty liver disease (NAFLD). My studies explored the pathways sustaining the interfering metabolic effects of different steatogenic agents in hepatocytes and provided new insights, at the single cell level, on the biomechanical and morphological changes of steatotic cells using an *in vitro* model of NAFLD.

Cells were exposed alone or in combination to excess of oleate and palmitate (0.75 mM), of fructose (5.5 mM) or of TNFα (10 ng/ml). The different grade and features of steatosis were firstly analyzed in terms of triglycerides (TG) accumulation and lipid droplets (LD). Our results showed that the intracellular TG content increased more markedly in cells treated with fructose and fatty acids in combination. Interestingly, the combination of fructose and fatty acids, markedly enlarged the LD without changing their number, whereas fatty acids and

TNFα in combination led to an increase in LD number with a reduction of their size with respect to fatty acids alone. ADRP expression level mirrored the changes in lipid droplets. All these finding together suggests that the combination of sugar and fat mimics a condition of macrovesicular steatosis *in vitro*, while fatty acids in combination with TNFα induced a condition more similar to microvesicular steatosis. The correlation between *in vitro* macro- and microvesicular steatosis with the ongoing cell dysfunction was confirmed by the changes in expression of IkBip, a marker for ER stress, and of PPARs.

In parallel, in the same cellular steatotic models, we quantified the single cell stiffness in term of relative elasticity measured by single cell force spectroscopy (SCFS) by using an innovative approach. Single cell stiffness was increased in cell exposed to either fructose or fatty acids as single agents, but the largest increase was induced by the combination of the two steatogenic agents, which mimics a macrovesicular steatosis *in vitro*. Interestingly, the microvesicular-like steatosis showed a cell stiffness similar to the one observed for fatty acids alone. This observation demonstrated that single cell stiffness depends on the steatosis grade rather than on lipid droplets organization and distribution inside the cell.

Moreover, we reconstructed the three-dimensional shape of steatotic cells by quantitative phase microscopy (QPM) in order to obtain information about the single cell morphometry, which changed as a function of the steatosis grade and features. While a rather low grade of steatosis, such as that induced by fructose alone, did not alter the geometric parameters, the more marked steatosis induced by fatty acids made the cells thinner and larger than control cells and with a smoother surface and larger protrusions. On the other hand, cells mimicking the macrovesicular condition showed a morphometry intermediate between those treated with fructose and fatty acids as single agents, although the highest grade of steatosis. By contrast, cells with microvesicular-like steatosis appeared smaller compared to cells exposed to fatty acids alone, although they had a similar triglyceride content. Therefore, we can conclude that geometric parameters do not depend exclusively on the total triglycerides content in steatotic cells, but mainly on the number of lipid droplets in cytosol. Therefore, our findings point the attention to the potential role of mechanobiology in metabolic diseases, particularly those linked to overweight and obesity.

12.2 Molecular events associated to adipocyte hypertrophy

Obesity depends on adipocyte hypertrophy which is an adaptive response to nutrient excess and correlates directly with metabolic disease. The aim of the present study was to compare mature and hypertrophic adipocytes at molecular and cellular level.

To promote hypertrophy, after differentiation 3T3-L1 mouse adipocytes were challenged for 2 days with a mixture of oleate and palmitate. As a first result we could observe, as expected, an increase in triglyceride content in mature adipocytes and a further increase in the hypertrophic condition. Lipid droplets average size was increased in differentiated adipocytes exposed to oleate and palmitate, thus confirming the induction of the hypertrophic condition. As a response to increased intracellular fat content, mature adipocytes released increased level of triglycerides into the culture medium and this released was almost doubled in hypertrophic condition.

As a marker for adipogenesis, we assessed PPARγ and adiponectin expression. In adipocytes, increased PPARγ expression accompanied the increase in fat content and the largest overexpression was observed in hypertrophic cells. By contrast, we observed an increased adiponectin expression during adipogenesis but without differences between mature and hypertrophic adipocytes.

Lipid accumulation typically results in increased fat oxidation and consequent ROS production which may damage important cellular components. We observed an increase in ROS production during adipogenesis and the largest increase occurred in the hypertrophic adipocytes. Excess ROS may lead to lipid peroxidation, and in fact MDA levels were increased in mature adipocytes and a larger increase in hypertrophic adipocytes, which are sign of fat-dependent oxidative stress.

Furthermore, we investigated the effects at mitochondrial level of adipocyte differentiation and hypertrophy. Employing an O2K high-resolution respirometer, we evaluated different parameters of mitochondrial respiration. Taken together, the results clearly indicated that the hypertrophic condition *in vitro* led to a general reduction in the mitochondrial oxygen consumption, although the routine respiration, which is controlled by basal energy demand of the cells, was unchanged. The reduction in activity of both complex I and II in hypertrophic adipocytes was paralleled by a marked decrease in the capacity of the electron transfer system (ETS) measured from the *noncoupled* state of maximum respiration. For a better

understanding we assessed also the levels of OXPHOS proteins of all the five respiratory complexes. The results obtained suggested that the lower mitochondrial oxygen consumption that we observed in hypertrophic adipocytes might depend on the reduction in the amount of the mitochondrial complexes.

In order to verify the mitochondria content, we assessed the expression of citrate synthase (CS) and heat shock protein 60 (HSP60), which are frequently used as biomarkers for mitochondrial content. Although, both the CS and HSP60 levels decreased during adipogenesis process passing from pre- to mature adipocytes, no differences were observed between mature and hypertrophic adipocytes. As a confirm, the mitotracker fluorescence, a probe selective for intact mitochondria, did no show changes in hypertrophic adipocytes respect to mature adipocytes. Therefore, we can conclude that the decrease in mitochondrial oxygen consumption and OXPHOS proteins level which in hypertrophic adipocytes does not depend on a reduced mitochondrial content, but on alteration of mitochondria morphology and integrity.

12.3 Effects of natural and synthetic compounds on lipid accumulation and inflammation

12.3.1 Silybin

Silybin is the major active constituent of silymarin, an extract of the milk thistle seeds *(Silybum marianum* L. Gaertner, Compositae). It exhibits pharmacological effects, particularly in the liver by exerting antioxidant, anti-inflammatory and antifibrotic properties. The present study provides a deeper characterization of some patho-physiologically relevant mechanisms of action of silybin administered at dose of 50 µmol/L directly to fatty hepatocytes.

As a first result we observed a significant reduction in TG accumulation, and this lipid lowering activity seems to be promoted by activation of lipid catabolism pathways, as suggested by up-regulation of PPARα and PPARδ, and by inhibition of lipogenic pathways, as suggested by the downregulation of PPARγ. The stimulation of catabolism of fatty acids by silybin was confirmed by the up-regulation of CPT-1, the first component and rate-limiting step of mitochondrial β-oxidation, of CYP2E1, involved in microsomal oxidation, and of AOX,

involved in peroxisomal α-oxidation.

Another sign that silybin ameliorate hepatic steatosis was the increase in miR-122 level in steatotic cells upon treatment with silybin. Moreover, our results suggested that the anti-steatotic action of silybin implies upregulation of AQP9 and increase of glycerol permeability in hepatocytes. As well as a reduction of the fat-stimulated autophagy as demonstrated by the downregulation of the LC3-II and Atg7 expression in steatotic cells.

Uptake of fatty acids by hepatocytes is regulated by PCSK9, and this effect is independent of its action on LDL receptor. Indeed, PCSK9 promotes degradation of CD36, which is involved in fatty acids uptake and triglyceride storage/secretion. Our data showed that PCSK9 mRNA was downregulated in steatotic cells, and silybin significantly reversed PCSK9 downregulation in steatotic cells, and apparently restored cellular function while reducing fatty acids influx in the hepatocyte.

Silybin was also able to modify the lipid droplets composition, with a reduction in content of the saturated fatty acids and an increase in content of the unsaturated ones, as well as with an increase in the amount of short-medium chain fatty acids.

Silybin shown also effects at the mitochondrial level leading to a significant increase in mitochondria size, improvement of the organization of mitochondrial cristae, and reduction in both basal and maximal.

The reduction in fat accumulation exerted by silybin in the steatotic hepatocytes is associated with the improvement of the oxidative unbalance as demonstrated by the reduction in lipid peroxidation (MDA levels, namely), catalase activity, NF-κB activation and the oxidative DNA damage measured as extracellular levels of 8-OHdG. Looking at all these results together, the present study suggests that the antioxidant capacity of silybin effectively counteracts the possible damaging effects of a high rate of fat catabolism which is stimulated in the attempt to reduce excess FA accumulation.

All these results suggest together a complex and pleiotropic role for silybin in the hepatic cells, involving several key molecular intracellular pathways active during liver steatosis and indicate the molecule as a promising treatment for NAFLD.

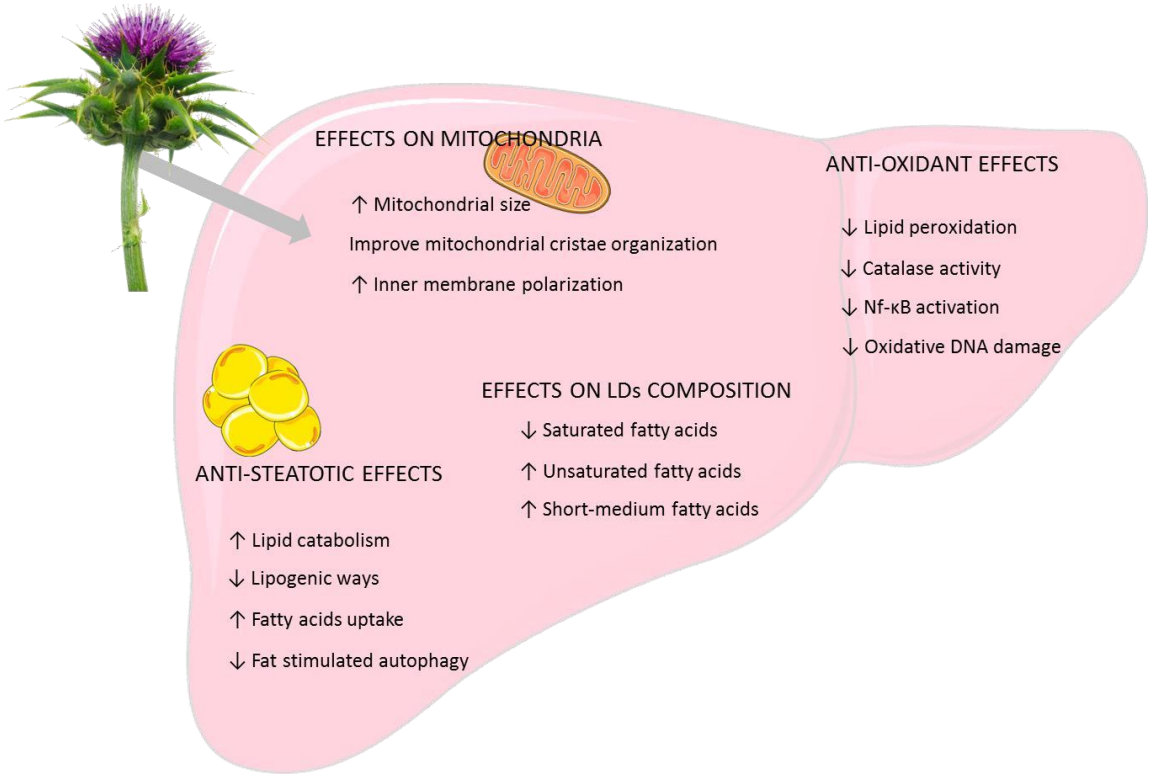

Figure 36 Effects of silybin on liver: scheme of the effects of the nutraceutic silybin on liver

11.3.2SAMe

SAMe, an endogenous molecule playing many functions, is an important physiological defence against excess of ROS and previous studies described a potential role for treatment of liver abnormalities. The present study provided insights into the effects and the molecular mechanisms through which SAMe, may ameliorate fatty acids-induced steatosis and oxidative stress in hepatic and endothelial cells.

In the cell models of the current study, the exposure of hepatocytes and endotheliocytes to fatty acids mimics, respectively, an *in vitro* model of NAFLD and atherosclerosis. Exposure of steatotic hepatocytes to different concentrations of SAMe led to a decrease in triglyceride content and lipid droplets size and number. CPT1, a mitochondrial protein acting as shuttle for FAs involved in mitochondrial FA oxidation, was up regulated in steatotic cells and furthermore after the exposure to SAMe, at all concentrations. In the light of that, the lipid-lowering action of SAMe might be sustained by stimulation of oxidative and/or secretory pathways. UCP2, a mitochondrial uncoupling protein, was significantly up-regulated upon

lipid-loading but SAMe at all concentration did not change significantly its expression. Lipid peroxidation, ROS production and catalase activity were all significantly decreased upon treatment with SAMe.

On the other side, exposure of endothelial cells to oleate and palmitate, led to an increase in triglyceride content and lipid peroxidation. As a response to lipid-loading, endothelial cells released NO and produced ROS thus triggering proinflammatory events. The subsequent treatment with SAMe led to a decrease of triglyceride content and NO and ROS production.

We can conclude that SAMe is an efficacious lipid-lowering and antioxidant agent for steatotic hepatocytes and endotheliocytes. The anti-steatotic effect of the molecule seems to be sustained by an increase in catabolic pathways at mitochondrial level. In conclusion, the beneficial effect of SAMe on the in vitro models of NAFLD and atherosclerosis suggests that the molecule possess a potential therapeutic benefit on these pathological conditions.

13. Summary of major findings and future perspectives

The presents PhD thesis has been focused on two different aims:

1. To study the molecular mechanisms associated with excess fat accumulation in different tissues involved in a condition of obesity: liver, vascular endothelium and adipose tissue.

To this aim, three cellular models of NAFLD, atherosclerosis and adipocyte hypertrophy were developed and employed.

Our studies demonstrated, first of all, that the *in vitro* model of NAFLD, that we developed, well mimics *in vitro* the onset and progression of NAFLD from simple steatosis to steatohepatitis. My studies explored, in particular, the pathways sustaining the interfering effects of different steatogenic agents such as fatty acids, fructose and TNFα on hepatocytes. The main findings of these studies demonstrated the metabolic interference among these compounds at the level of the hepatic cells leading to a more severe steatosis with respect to the single agents (Chapter 5; Chapter 6). Treatment with different steatotic agents alone or in combination, led to different grade and features of steatosis. Analysis of triglyceride content, lipid droplet morphology and different molecular markers, suggests that the combination of sugar and fat mimics a condition of macrovesicular steatosis, while fatty acids in combination with TNFα induced a condition more similar to microvesicular steatosis. Interestingly, our studies provided also new insights, at the single cell level, on the biomechanical and morphological changes associated with more or less sever steatosis depending mainly on the size of the lipid droplets (Baldini et al., 2019). Single cell stiffness analysis demonstrated that all the steatotic conditions shown an increase in cell stiffness with respect to control cells and that the macrovesicular steatosis was associated with the largest increase in single cell stiffness. The results obtained demonstrated that the stiffness at single cell level depends on the grade of steatosis rather than on lipid droplets organization and distribution inside the cell (Chapter 9).

In parallel, my research investigated endothelium dysfunction being associated with NAFLD and

obesity. My results obtained using an *in vitro* model of endothelial dysfunction showed that treatment with long chain fatty acids induced fat accumulation and oxidative stress also in human endothelial cells thus well mimicking a condition of atherosclerosis *in vitro* (Chapter 10).

FInaly, the most recent part of my activity was focused on an *in vitro* model of adipocyte hypertrophy, represented by mouse pre-adipocytes treated with an adipogenic mixture allowed to clarify the molecular and cellular changes involved in adipocyte maturation and hypertrophy (Chapter 11). After a preliminary characterization of the model in term of triglyceride content, lipid droplet morphology and molecular markers, I proceeded evaluating the oxidative stress and the mitochondria function and integrity. The hypertrophic condition shown a larger increase in fat accumulation and a consequent increase in free radical production and oxidative stress. The most important finding of this study was that the hypertrophic condition *in vitro* led to a general reduction in the mitochondrial oxygen consumption and in the amount of the mitochondrial OXPHOS proteins, although mitochondrial content was unchanged compared to mature adipocyte.

2. To identify and investigate some natural compounds that may be employed as nutraceuticals:

- ***Silybin.*** Silybin was used to treat FaO cells with different grade of steatosis (Chapter 5; Chapter 6; Chapter 7; Chapter 8). We found that the beneficial effects of silybin on hepatic steatosis involved: (*i*) increase in lipid catabolism pathways, (*ii*) inhibition of lipogenic pathways, (*iii)* reduction of lipid peroxidation, catalase activity and NF-κB activation, (*iv*) amelioration of the profile of fatty acids (FA) stored in lipid droplets with an increase in the short/medium chain FA ratio, and a decrease in the saturated/monounsaturated FA ratio, (*v*) stimulation of mitochondrial FA oxidation, (*vi*) increase in the level of miR-122, the master regulator of hepatic lipid metabolism; (*vii*) increase in AQP9 expression and glycerol permeability, (*viii*) diminution of fat-stimulated autophagy. At mitochondrial level, silybin led to a significant increase in mitochondria size, improved the organization of mitochondrial cristae, increased the polarization of the inner membrane of mitochondria and the ATP production.

In conclusion, my studies provided new insights about the protective effects of silybin administered directly to hepatocytes mimicking *in vitro* the NAFLD progression. Further studies are on the way to translate such promising results into long-term beneficial effects, in the hope that onset, progression and worsening of NAFLD/NASH will be prevented/delayed in human being by using more natural nutraceutic approaches led to a decrease in triglyceride content being associated with an average reduction in lipid droplet size and number, and an increase in mitochondria fatty acid oxidation

- **S-Adenosylmethionine (SAMe).** Our studies (Chapter 10) provided insights into the effects and the molecular mechanisms through which SAMe, an endogenous molecule playing many functions as methyl donor, may ameliorate fatty acid-induced steatosis and oxidative stress in hepatic and endothelial cells, respectively. We demonstrated that SAMe in steatotic hepatocytes played significant anti-steatotic and protective effects. Indeed, on steatotic hepatocytes SAMe led to a decrease in triglyceride content. The anti-steatotic effect of the molecule seems to be sustained by an increase in catabolic pathways at mitochondrial level. Moreover, SAMe was also efficacious on stressed endothelial cells. Treatment of dysfunctional endothelial cells with SAMe at different concentrations led to a decrease of nitric oxide and ROS production.

  In conclusion, the beneficial effect of SAMe on the in vitro models of NAFLD and atherosclerosis suggests that the molecule possess a potential therapeutic benefit on these pathological conditions that should be investigated even more in the future, also in other *in vitro* and *in vivo* models

.

14.Bibliography

- Abdelaziz Sameur, Honoré P. Yin, Denis Duhamel, Vladimir Vilke. A simple model for elastic and viscoelastic punch indentation problems with experimental validation. 2008. <hal-00232791>
- Abenavoli L, Greco M, Nazionale I, et al.: Effects of Mediterranean diet supplemented with silybin-vitamin E-phospholipid complex in overweight patients with non-alcoholic fatty liver disease. Expert Rev Gastroenterol Hepatol 9: 519-527, 2015.
- Aebi H. Catalase in vitro. Methods Enzymol (1984) 105:121–6. doi:10.1016/ S0076-6879(84)05016-3
- Aharoni-Simon M, Hann-Obercyger M, Pen S, Madar Z, Tirosh O. Fatty liver is associated with impaired activity of PPARγ-coactivator 1α (PGC1α) and mitochondrial biogenesis in mice. Lab Invest (2011) 91:1018–28. doi:10.1038/ labinvest.2011.55
- Alkhouri N, Dixon LJ, Feldstein AE. Lipotoxicity in nonalcoholic fatty liver disease: not all lipids are created equal. Expert Rev Gastroenterol Hepatol 2009; 3: 445-451 [PMID: 19673631 DOI: 10.1586/egh.09.32]
- Ambros V. The functions of animal microRNAs. Nature. 2004 Sep 16;431(7006):350-5. Review. doi:10.1038/nature02871
- Ament Z, West JA, Stanley E, Ashmore T, Roberts LD, Wright J, Nicholls AW, Griffin JL. PPAR-pan activation induces hepatic oxidative stress and lipidomic remodelling. Free Radic Biol Med 2016; 95: 357-368 [PMID: 26654758 DOI: 10.1016/j.freeradbiome d.2015.11.033]
- Anstee QM, Day CP. S-adenosylmethionine (SAMe) therapy in liver disease: a review of current evidence and clinical utility. J Hepatol. 2012 Nov;57(5):1097- 109. doi: 10.1016/j.jhep.2012.04.041. Epub 2012 May 30.
- Anstee QM, Targher G, Day CP. Progression of NAFLD to diabetes mellitus, cardiovascular disease or cirrhosis. Nat Rev Gastroenterol Hepatol 2013;10:330–44. doi:10.1038/nrgastro.2013.41.
- Aragno M, Tomasinelli CE, Vercellinatto I, Catalano MG, Collino M, Fantozzi R, Danni O, Boccuzzi G. SREBP-1c in nonalcoholic fatty liver disease induced by Western-type high-fat diet plus fructose in rats. Free Radic Biol Med 2009; 47: 1067-1074 [PMID: 19616615 DOI:10.1016/j.freeradbiomed.2009.07.016]
- Atshaves BP, Storey SM, McIntosh AL, Petrescu AD, Lyuksyutova OI, Greenberg AS, Schroeder F. Sterol carrier protein-2 expression modulates protein and lipid composition of lipid droplets. J Biol Chem 2001;276:25324-25335. doi:10.1074/jbc.M100560200
- Bacq Y. Acute fatty liver of pregnancy. Semin Perinatol. 1998 Apr;22(2):134-40. doi: 10.1016/s0146-0005(98)80045-1
- Baffy G, Brunt EM, Caldwell SH. Hepatocellular carcinoma in non-alcoholic fatty liver disease: an emerging menace. J Hepatol (2012) 56:1384–91. doi:10.1016/j.jhep.2011.10.027
- Baffy G. Uncoupling protein-2 and non-alcoholic fatty liver disease. Front Biosci 2005;10:2082-2096. doi: 10.2741/1683
- Baldini F, Bartolozzi A, Ardito M, Voci A, Portincasa P, Vassalli M, Vergani L. Biomechanics of cultured hepatic cells during different steatogenic hits. J Mech Behav Biomed Mater. 2019 Sep;97:296-305. doi: 10.1016/j.jmbbm.2019.05.036. Epub 2019 May 22.

- Barone-Nugent ED, Barty A, Nugent KA. Quantitative phase-amplitude microcopy I: optical microscopy. J Microsc, 2002 Jun;206(Pt 3):194-203 doi: 10.1046/j.1365- 2818.2002.01027.x
- Baselga-Escudero L, Pascual-Serrano A, Ribas-Latre A, et al.: Long-term supplementation with a low dose of proanthocyanidins normalized liver miR-33a and miR-122 levels in high-fat diet-induced obese rats. Nutr Res 35: 337-345, 2015.
- Baselga-Escudero L, Souza-Mello V, Pascual-Serrano A, Rachid T, Voci A, Demori I, et al. Beneficial effects of the mediterranean spices and aromas on non-alcoholic fatty liver disease. Trends Food Sci Technol (2017) 61:141–59. doi:10.1016/j.tifs.2016.11.019
- Begriche K, Massart J, Robin M-A, Borgne-Sanchez A, Fromenty B. Druginduced toxicity on mitochondria and lipid metabolism: mechanistic diversity and deleterious consequences for the liver. J Hepatol (2011) 54:773–94. doi:10.1016/j.jhep.2010.11.006
- Bekaert M, Verhelst X, Geerts A, Lapauw B, Calders P. Association of recently described adipokines with liver histology in biopsy-proven non-alcoholic fatty liver disease: a systematic review. Obese Rev. 2016 Jan;17(1):68-80. doi: 10.1111/obr.12333.
- Benn M, Nordestgaard BG, Grande P, Schnohr P, Tybjaerg-Hansen A. PCSK9 R46L, low- density lipoprotein cholesterol levels, and risk of ischemic heart disease: 3 independent studies and meta-analyses. J Am Coll Cardiol. 2010 Jun 22;55(25):2833- 42. doi: 10.1016/j.jacc.2010.02.044.
- Berlanga A, Guiu-Jurado E, Porras JA, Auguet T. Molecular pathways in non- alcoholic fatty liver disease. Clin Exp Gastroenterol (2014) 7:221–39. doi:10.2147/ CEG.S62831
- Bernardino RL, Marinelli RA, Maggio A, Gena P, Cataldo I, Alves MG, Svelto M, Oliveira PF, Calamita G. Hepatocyte and Sertoli Cell Aquaporins, Recent Advances and Research Trends. Int J Mol Sci. 2016 Jul 9;17(7). pii: E1096. doi: 10.3390/ijms17071096.
- Bessone F, Razori MV, Roma MG. Molecular pathways of nonalcoholic fatty liver disease development and progression. Cell Mol Life Sci. 2018 Oct 20. doi: 10.1007/s00018-018-2947-0. [Epub ahead of print]
- Black RA, et al. A metalloproteinase disintegrin that releases tumour-necrosis factor-alpha from cells. Nature. 1997; 385:729–733. [PubMed: 9034190)
- Bottiglieri T. S-Adenosyl-L-methionine (same): From the bench to the bedside- molecular basis of a pleiotrophic molecule. Am J Clin Nutr. 2002;76:1151S–7S
- Boyle, J. J., Wilson, B., Bicknell, R., Harrower, S., Weissberg, P. L., and Fan, T. P. (2000) J. Pathol. 192, 234–242
- Bradbury MW, Berk PD. Lipid metabolism in hepatic steatosis. Clin Liver Dis. 2004 Aug;8(3):639-71, xi.
- Bradford MM (1976) A rapid and sensitive method for the quantitation of microgram quantities of protein utilizing the principle of protein-dye binding. Analyt. Biochem 72:248-254. https://doi.org/10.1016/0003-2697(76)90527-3
- Braet F, Wisse E. Structural and functional aspects of liver sinusoidal endothelial cell fenestrae: a review. Comp Hepatol 2002;1:1.
- Brun RP, Tontonoz P, Forman BM, Ellis R, Chen J, Evans RM, Spiegelman BM: Differential activation of adipogenesis by multiple PPAR isoforms. Genes Dev 10:974–984, 1996
- Brunt EM, Wong VW, Nobili V, Day CP, Sookoian S, Maher JJ, Bugianesi E, Sirlin CB, Neuschwander-Tetri BA, Rinella ME. Nonalcoholic fatty liver disease. Nat Rev Dis Primers 2015; 1: 15080 [PMID: 27188459 DOI: 10.1038/nrdp.2015.80]

- Bruzzone S, Ameri P, Briatore L, Mannino E, Basile G, Andraghetti G, Grozio A, Magnone M, Guida L, Scarfì S, Salis A, Damonte G, Sturla L, Nencioni A, Fenoglio D, Fiory F, Miele C, Beguinot F, Ruvolo V, Bormioli M, Colombo G, Maggi D, Murialdo G, Cordera R, De Flora A, Zocchi E. The plant hormone Abscisic acid increases in human plasma after hyperglycemia and stimulates glucose consumption by adipocytes and myoblasts. 2012 FASEB J. PMID: 22075645. DOI: 10.1096/fj.11-190140.
- Cai C, Wang C, Ji W, Liu B, Kang Y, Hu Z, Jiang Z. Knockdown of hepatic aquaglyceroporin-9 alleviates high fat diet-induced non- alcoholic fatty liver disease in rats. 2013 Mar;15(3):550-6. doi: 10.1016/j.intimp.2013.01.020.
- Calamita G and Portincasa P. Present and future therapeutic strategies in non- alcoholic fatty liver disease. Expert Opin Ther Targets. 2007 Sep;11(9):1231-49. doi:10.1517/14728222.11.9.1231
- Calamita G, Delporte C, Marinelli RA (2015). Hepatobiliary, salivary glands and pancreas aquaporins in health and disease In: G. Soveral, A. Casini and S. Nielsen Ed. Int Immunopharmacol.Aquaporins in health and disease: new molecular targets for drug discovery. CRC Press Taylor & Francis Group, ISBN: 9781498707831; Cat# K24910. Chapter 9, pages 183-205.
- Calamita G, Perret J, Delporte C. Aquaglyceroporins: Drug Targets for Metabolic Diseases? Front Physiol. 2018 Jul 10;9:851. doi: 10.3389/fphys.2018.00851.
- Calamita, G, Gena P, Ferri D, Rosito A, Rojek A, Nielsen S, Marinelli RA, Frühbeck G, Svelto M. Biophysical assessment of aquaporin-9 as principal facilitative pathway in mouse liver import of glucogenetic glycerol. Biol Cell. 2012 Jun;104(6):342-51. doi: 10.1111/boc.201100061.
- Cantoni GL. The role of s-adenosylhomocysteine in the biological utilization of s-adenosylmethionine. Prog Clin Biol Res. 1985;198:47–65
- Chang J. Medicinal herbs: drugs or dietary supplements? Biochem Pharmacol 2000; 59: 211-219 [PMID: 10609549 DOI: 10.1016/ S0006-2952(99)00243-9]
- Chavan D, T. C. van de Watering, G. Gruca, J. H. Rector, K. Heeck, M. Slaman, and D. Iannuzzi; Review of Scientific Instruments 83, 115110 (2012) doi: 10.1063/1.4766959
- Chen Q, Marsh J, Ames B, Mossman B. Detection of 8-oxo-2'-deoxyguanosine, a marker of oxidative DNA damage, in culture medium from human mesothelial cells exposed to crocidolite asbestos. Carcinogenesis (1996) 17:2525–7. doi:10.1093/carcin/17.11.2525
- Cheung O, Puri P, Eicken C, Contos MJ, Mirashahi F, Maher JW, Kellum JM, Min H, Luketic VA, Sanyal AJ. Nonalcoholic steatohepatitis is associated with altered hepatic microRNA expression. *Hepatology*. 2008;48(6):1810–1820. doi: 10.1002/hep.22569.
- Choi AM, Ryter SW, Levine B. Autophagy in human health and disease. N Engl J Med. 2013;368:651–662. doi:10.1056/NEJMra1205406
- Choi R-Y, Ham JR, Lee M-K. Esculetin prevents non-alcoholic fatty liver in diabetic mice fed high-fat diet. Chem Biol Interact (2016) 260:13–21. doi:10.1016/j.cbi.2016.10.013
- Cicero, A.F.G.; Colletti, A.; Bajraktari, G.; Descamps, O.; Djuric, D.M.; Ezhov, M.; Fras, Z.; Katsiki, N.; Langlois, M.; Latkovskis, G., et al. Lipid-lowering nutraceuticals in clinical practice: position paper from an International Lipid Expert Panel. Nutrition reviews 2017, 75, 731-767. doi:10.1093/nutrit/nux047.
- Claus C, Chey S, Heinrich S, Reins M, Richrdt B, Pinkert S, Fechner H, Gaunitz F, Schäfer I, Seibel P, Liebert UG. Involvement of p32 and Microtubules in Alteration of Mitochondrial Functions by Rubella Virus. J Virol. 2011 Apr; 85(8): 3881–3892 doi: 10.1128/JVI.02492-10

- Clayton DF, Weiss M, Darnell JE, Jr. Liver-specific RNA metabolism in hepatoma cells: variations in transcription rates and mRNA levels. Mol Cell Biol 1985;5:2633-2641.
- Cnop M, Foufelle F, Velloso LA. Endoplasmic reticulum stress, obesity and diabetes. Trends Mol Med 2012; 18: 59-68 [PMID: 21889406 DOI: 10.1016/j.molmed.2011.07.010]
- Cohen JC, Boerwinkle E, Mosley TH Jr, Hobbs HH. Sequence variations in PCSK9, low LDL, and protection against coronary heart disease. N Engl J Med. 2006 Mar 23;354(12):1264-72. doi:10.1056/NEJMoa054013
- Cohen JC, Horton JD, Hobbs HH. Human Fatty Liver Disease: Old Questions and New Insights. Science (80-) 2011;332:1519–23. doi:10.1126/science.1204265.
- Connolly MK, Bedrosian AS, Malhotra A, Henning JR, Ibrahim J, Vera V, et al. In hepatic fibrosis, liver sinusoidal endothelial cells acquire enhanced immunogenicity. J Immunol 2010;185:2200–8. doi:10.4049/jimmunol.1000332.
- Crespo J, Cayón A, Fernández-Gil P, Hernández-Guerra M, Mayorga M, Domínguez-Díez A, et al. Gene expression of tumor necrosis factor alpha and TNF- receptors, p55 and p75, in nonalcoholic steatohepatitis patients. Hepatology (2001) 34:1158–63.10.1053/jhep.2001.29628
- Criollo A, Chereau F, Malik SA, Niso-Santano M, Mariño G, Galluzzi L, Maiuri MC, Baud V, Kroemer G. Autophagy is required for the activation of NFκB. Cell Cycle. 2012 Jan 1;11(1):194-9. doi: 10.4161/cc.11.1.18669.
- Cullen JM. Mechanistic classification of liver injury. Toxicol Pathol. 2005;33(1):6-8. doi:10.1080/01926230590522428
- Day CP, James OF. Steatohepatitis: a tale of two “hits”? Gastroenterology 1998;114:842–5.
- Day CP. Non-alcoholic steatohepatitis (NASH): where are we now and where are we going? Gut 2002; 50: 585-588 [PMID: 11950797 DOI: 10.1136/gut.50.5.585]
- Day P, James OF. Steatohepatitis: a tale of two ‘hits’? Gastroenterology, vol. 114, no. 4 I, pp. 842–845, 1998. Gastroenterology. 1998 Apr;114(4):842-5.
- Demers A, Samami S, Lauzier B, Des Rosiers C, Ngo Sock ET, Ong H, Mayer G. PCSK9 Induces CD36 Degradation and Affects Long-Chain Fatty Acid Uptake and Triglyceride Metabolism in Adipocytes and in Mouse Liver. Arterioscler Thromb Vasc Biol. 2015 Dec;35(12):2517-25. doi: 10.1161/ATVBAHA.115.306032.
- Deus CM, Zehowski C, Nordgren K, Wallace KB, Skildum A, Oliveira PJ. Stimulating basal mitochondrial respiration decreases doxorubicin apoptotic signaling in H9c2 cardiomyoblasts. Toxicology (2015) 334:1–11. doi:10.1016/ j.tox.2015.05.001
- Di Sario A, Bendia E, Taffetani S, Omenetti A, Candelaresi C, Marzioni M, De Minicis S, Benedetti A. Hepatoprotective and antifibrotic effect of a new silybin- phosphatidylcholine-Vitamin E complex in rats. Dig Liver Dis. 2005 Nov;37(11):869-76. Epub 2005 Oct 5
- Dongiovanni P, Meroni M, Longo M, Fargion S and Fracanzani AL: miRNA Signature in NAFLD: A Turning Point for a Non-Invasive Diagnosis. Int J Mol Sci 19, 2018.
- Donnelly KL, Smith CI, Schwarzenberg SJ, Jessurun J, Boldt MD, Parks EJ. Sources of fatty acids stored in liver and secreted via lipoproteins in patients with nonalcoholic fatty liver disease. J Clin Invest 2005; 115: 1343-1351 [PMID: 15864352 DOI: 10.1172/ JCI23621]
- Donnelly KL, Smith CI, Schwarzenberg SJ, Jessurun J, Boldt MD, Parks EJ. Sources of fatty acids stored in liver and secreted via lipoproteins in patients with nonalcoholic fatty liver disease. The Journal of clinical investigation 2005; 115(5): 1343-51. doi:10.1172/JCI23621

- Donnelly KL, Smith CI, Schwarzenberg SJ, Jessurun J, Boldt MD, Parks EJ. Sources of fatty acids stored in liver and secreted *via* lipoproteins in patients with nonalcoholic fatty liver disease. *J. Clin. Invest.*, 2005, *115*(5),1343-1351. doi.org/10.1172/JCI23621
- Dubuc G, Chamberland A, Wassef H, Davignon J, Seidah NG, Bernier L, Prat A. Statins upregulate PCSK9, the gene encoding the proprotein convertase neural apoptosis- regulated convertase-1 implicated in familial hypercholesterolemia. Arterioscler Thromb Vasc Biol. 2004 Aug;24(8):1454-9. Epub 2004 Jun 3. doi:10.1161/01.ATV.0000134621.14315.43
- Eaton S. Control of mitochondrial beta-oxidation flux. Prog Lipid Res 2002; 41: 197- 239 [PMID: 11814524 DOI: 10.1016/ S0163-7827(01)00024-8]
- Eberlé D, Hegarty B, Bossard P, Ferré P, Foufelle F. SREBP transcription factors: master regulators of lipid homeostasis. Biochimie 2004; 86: 839-848 [PMID: 15589694 DOI: 10.1016/ j.biochi.2004.09.018]
- Eckel RH, Alberti KG, Grundy SM, Zimmet PZ. The metabolic syndrome. Lancet 2010; 375(9710): 181-3. doi:10.1016/S0140-6736(09)61794-3.
- Einer C, Leitzinger C, Lichtmannegger J, Eberhagen C, Rieder T, Borchard S, Wimmer R, Denk G, Popper B, Neff F, Polishchuk EV, Polishchuk RS, Hauck SM, von Toerne C, Müller JC, Karst U, Baral BS, DiSpirito AA, Kremer AE, Semrau J, Weiss KH, Hohenester S, Zischka H. A High Calorie Diet Aggravates Mitochondrial Dysfunction and Triggers Severe Liver Dama ge in Wilson Disease Rats. Cell Mol Gastroenterol Hepatol. 2019;7(3):571-596. doi: 10.1016/j.jcmgh.2018.12.005. Epub 2018 Dec 23.
- Emad A-Hassan, William F. Heinz, Matthew D. Antonik, Neill P. D'Costa, Soni Nageswaran, Cora-Ann Schoenenberger and Jan H. Hoh. Biophysical Journal, 1998, 74, doi:10.1016/S0006-3495(98)77868-3
- Fabry B, Maksym GN, Butler JP, Glogauer M, Navajas D, Fredberg JJ. Scaling the microrheology of living cells..Phys Rev Lett. 2001 Oct 1;87(14):148102. Epub 2001 Sep 13
- Federico A, Conti V, Russomanno G, et al.: A Long-term Treatment with Silybin in Patients with Non-alcoholic Steatohepatitis Stimulates Catalase Activity in Human Endothelial Cells. In Vivo 31: 609-618, 2017.
- Federico A, Trappoliere M, Tuccillo C, de Sio I, Di Leva A, Del Vecchio Blanco C, et al. A new silybin-vitamin E-phospholipid complex improves insulin resistance and liver damage in patients with non-alcoholic fatty liver disease: preliminary observations. Gut (2006) 55:901–2. doi:10.1136/ gut.2006.091967
- Feldstein AE, Werneburg NW, Canbay A, et al.: Free fatty acids promote hepatic lipotoxicity by stimulating TNF-alpha expression via a lysosomal pathway. Hepatology 40: 185-194, 2004.
- Fernández-Alvarez A, Alvarez MS, Gonzalez R, Cucarella C, Muntané J, Casado M. Human SREBP1c expression in liver is directly regulated by peroxisome proliferator- activated receptor alpha (PPARalpha). J Biol Chem 2011; 286: 21466-21477 [PMID: 21540177 DOI:10.1074/jbc.M110.209973]
- Ferré P, Foufelle F. Hepatic steatosis: a role for de novo lipogenesis and the transcription factor SREBP-1c. Diabetes Obes Metab 2010; 12 Suppl 2: 83-92 [PMID: 21029304 DOI: 10.1111/ j.1463-1326.2010.01275.x]
- Folch J, Less M, Sloane Stanely GH. A simple method for the isolation and purification of total lipides from animal tissues. J Biol Chem 1957;226:497-509.
- Friedel HA, Goa KL, Benfield P. S-adenosyl-L-methionine. A review of its pharmacological properties and therapeutic potential in liver dysfunction and affective disorders in relation to its physiological role in cell metabolism. Drugs 1989; 38: 389

- Fromenty B, Pessayre D. Inhibition of mitochondrial beta-oxidation as a mechanism of hepatotoxicity. Pharmacol Ther (1995) 67:101–54. doi:10.1016/ 0163-7258(95)00012- 6
- Furukawa S, Fujita T, Shimabukuro M, Iwaki M, Yamada Y, Nakajima Y, Nakayama O, Makishima M, Matsuda M, Shimomura I. Increased oxidative stress in obesity and its impact on metabolic syndrome. J Clin Invest 114: 1752–1761, 2004
- G. Marchesini, M. Brizi, A.M. Morselli-Labate, G. Bianchi, E. Bugianesi, A.J. McCullough, et al. Association of non-alcoholic fatty liver disease to insulin resistance Am J Med, 107 (1999), pp. 450-455
- Gao J, Serrero G. Adipose differentiation related protein (ADRP) expressed in transfected COS-7 cells selectively stimulates long chain fatty acid uptake. J Biol Chem (1999) 274:16825–30. doi:10.1074/jbc.274.24.16825
- García-Ruiz I, Solís-Muñoz P, Fernández-Moreira D, Muñoz-Yagüe T, Solís-Herruzo JA. In vitro treatment of HepG2 cells with saturated fatty acids reproduces mitochondrial dysfunction found in nonalcoholic steatohepatitis. Dis Model Mech (2015) 8:183–91. doi:10.1242/dmm.018234
- Gay AN, Mushin OP, Lazar DA, Naik-Mathuria BJ, Yu L, Gobin A, Smith CW OO. Wound healing characteristics of ICAM-1 null mice devoid of all isoforms of ICAM-1. J Surg Res 2011:1–7. doi:10.1016/j.jss.2011.06.053.
- Gazák R, Walterová D, Kren V. Silybin and silymarin--new and emerging applications in medicine. Curr Med Chem. 2007;14(3):315-38
- Gena P, Buono ND, D'Abbicco M, Mastrodonato M, Berardi M, Svelto M, Lopez L, Calamita G. Dynamical modeling of liver Aquaporin-9 expression and glycerol permeability in hepatic glucose metabolism. Eur J Cell Biol. 2017 Jan;96(1):61-69. doi: 10.1016/j.ejcb.2016.12.003.
- Gena P, Mastrodonato M, Portincasa P, Fanelli E, Mentino D, Rodríguez A, Marinelli RA, Brenner C, Frühbeck G, Svelto M, Calamita G. Liver glycerol permeability and aquaporin-9 are dysregulated in a murine model of Non-Alcoholic Fatty Liver Disease. PLoS One. 2013 Oct 30;8(10):e78139. doi: 10.1371/journal.pone.0078139.
- Gluchowski NL, Becuwe M, Walther TC, Farese RV Jr. Lipid droplets and liver disease: from basic biology to clinical implications. Nat Rev Gastroenterol Hepatol, 2017 Jun;14(6):343-355 doi: 10.1038/nrgastro.2017.32. Epub 2017 Apr 21.
- Gnocchi D, Massimi M, Alisi A, Incerpi S and Bruscalupi G: Effect of fructose and 3,5-diiodothyronine (3,5-T(2)) on lipid accumulation and insulin signalling in non-alcoholic fatty liver disease (NAFLD)-like rat primary hepatocytes. Horm Metab Res 46: 333- 340, 2014.
- Goodridge AG: Regulation of the activity of acetyl coenzyme A carboxylase by palmitoyl coenzyme A and citrate. J Biol Chem 247: 6946-6952, 1972.
- Grandl M, Schmitz G. Fluorescent high-content imaging allows the discrimination and quantitation of E-LDL-induced lipid droplets and Ox-LDLgenerated phospholipidosis in human macrophages. Cytometry A (2010) 77:231–42. doi:10.1002/cyto.a.20828
- Grasselli E, Baldini F, Vecchione G, Oliveira PJ, Sardão VA, Voci A, Portincasa P, Vergani L. Excess fructose and fatty acids trigger a model of non-alcoholic fatty liver disease progression in vitro: Protective effect of the flavonoid silybin. Int J Mol Med. 2019 Aug;44(2):705-712. doi: 10.3892/ijmm.2019.4234.
- Grasselli E, Canesi L, Portincasa P, Voci A, Vergani L and Demori I: Models of non- Alcoholic Fatty Liver Disease and Potential Translational Value: the Effects of 3,5-L- diiodothyronine. Annals of Hepatology 16: 0-0, 2017.

- Grasselli E, Cortese K, Fabbri R, Smerilli A, Vergani L, Voci A, Gallo G, Canesi L. Thyromimetic actions of tetrabromobisphenol A (TBBPA) in steatotic FaO rat hepatoma cells. Chemosphere 2014; 112:511-8.
- Grasselli E, Cortese K, Voci A, Vergani L, Fabbri R, Barmo C, Gallo G, Canesi L. Direct effects of Bisphenol A on lipid homeostasis in rat hepatoma cells. Chemosphere 2013; 91: 1123-1129 [PMID: 23399309 DOI: 10.1016/j.chemosphere.2013.01.016]
- Grasselli E, Voci A, Canesi L et al (2011) Non-receptor-mediated actions are responsible for the lipid-lowering effects of iodothyronines in FaO rat hepatoma cells. J Endocrinol 210:59-69. https://doi.org/10.1530/JOE-11-0074
- Grasselli E, Voci A, Canesi L, Goglia F, Ravera S, Panfoli I, Gallo G, Vergani L. Non- receptor-mediated actions are responsible for the lipid-lowering effects of iodothyronines in FaO rat hepatoma cells. J Endocrinol 2011; 210: 59-69 [PMID: 21508094 DOI: 10.1530/JOE-11-0074]
- Grasselli E, Voci A, Canesi L, Salis A, Damonte G, Compalati AD, Goglia F, Gallo G, Vergani L. 3,5-diiodo-L-thyronine modifies the lipid droplet composition in a model of hepatosteatosis. Cell Physiol Biochem 2014; 33: 344-356 [PMID: 24525903 DOI: 10.1159/000356674]
- Grasselli E, Voci A, Demori I, Vecchione G, Compalati AD, Gallo G, Goglia F, De Matteis R, Silvestri E, Vergani L. Triglyceride Mobilization from Lipid Droplets Sustains the Anti-Steatotic Action of Iodothyronines in Cultured Rat Hepatocytes. Front Physiol. 2016 Jan 12;6:418. doi: 10.3389/fphys.2015.00418.
- Grasselli E, Voci A, Pesce C, Canesi L, Fugassa E, Gallo G et al (2010) PAT protein mRNA expression in primary rat hepatocytes: effects of exposure to fatty acids. Int J Mol Med 25:505–512
- Grattagliano I, Diogo CV, Mastrodonato M, de Bari O, Persichella M, Wang DQ, Liquori A, Ferri D, Carratù MR, Oliveira PJ, Portincasa P. A silybin-phospholipids complex counteracts rat fatty liver degeneration and mitochondrial oxidative changes. World J Gastroenterol. 2013 May 28;19(20):3007-17. doi: 10.3748/wjg.v19.i20.3007.
- Green LC, Wagner DA, Glogowski J, Skipper PL, Wishnok JS TS. Analysis of nitrate, nitrite, and [15N]nitrate in biological fluids. Anal Biochem 1982;126:131–8.
- Green, H.; Meuth, M. An established pre-adipose cell line and its differentiation in culture. Cell 1974, 3,127–133
- Greenspan P, Mayer EP, Fowler SD. Nile red: a selective fluorescent stain for intracellular lipid droplets. J Cell Biol 1985; 100: 965-973 [PMID: 3972906]
- Grell M. Tumor necrosis factor (TNF) receptors in cellular signaling of soluble and membrane-expressed TNF. J. Inflamm. 1995; 47:8–17. [PubMed: 8913925]
- Gross LS, Li L, Ford ES, Liu S. Increased consuption of refined carbohydrates and the epidemic of type 2 diabetes in the united states: an ecologic assessment. Am J Clin Nutr, 2004 May;79(5):774-9 doi: 10.1093/ajcn/79.5.774
- Guz N, Dokukin M, Kalaparthi V, Sokolov I. If cell mechanics can be described by elastic modulus: study of different models and probes used in indentation experiments. Biophys J. 2014 Aug 5;107(3):564-575. doi: 10.1016/j.bpj.2014.06.033
- H. Cortez-Pinto, M.E. Camilo, A. Baptista, A.G. De Oliveira, M.C. De Moura Non- alcoholic fatty liver: another feature of the metabolic syndrome? Clin Nutr, 18 (1999), pp. 353-358
- Halliwell B, Whiteman M. Measuring reactive species and oxidative damage in vivo and in cell culture: how should you do it and what do the results mean? Br J Pharmacol. 2004 May;142 (2):231-55.

- Haq F, Mahoney M, Koropatnick J. Signaling events for metallothionein induction. Mutat Res. 2003 Dec 10;533(1-2):211-26.
- Heiska, L., Alfthan, K., Gronholm, M., Vilja, P., Vaheri, A., and Carpen, O. (1998) J. Biol. Chem. 273, 21893–21900
- Hennig EE, Mikula M, Goryca K, Paziewska A, Ledwon J, Nesteruk M, et al. Extracellular matrix and cytochrome P450 gene expression can distinguish steatohepatitis from steatosis in mice. J Cell Mol Med (2014) 18:1762–72. doi:10.1111/jcmm.12328
- Hermann Schillers, Carmela Rianna, Jens Schäpe, Tomas Luque, Holger Doschke, Mike Wälte, Juan José Uriarte, Noelia Campillo, Georgios P. A. Michanetzis, Justyna Bobrowska, Andra Dumitru, Elena T. Herruzo, Simone Bovio, Pierre Parot, Massimiliano Galluzzi, Alessandro Podestà, Luca Puricelli, Simon Scheuring, Yannis Missirlis, Ricardo Garcia, Michael Odorico, Jean-Marie Teulon, Frank Lafont, Malgorzata Lekka, Felix Rico, Annafrancesca Rigato, Jean-Luc Pellequer, Hans Oberleithner, Daniel Navajas & Manfred Radmacher; Standardized Nanomechanical Atomic Force Microscopy Procedure (SNAP) for Measuring Soft and Biological Samples; Scientific Reports 7, Article number: 5117 (2017) doi:10.1038/s41598-017- 05383-0
- Hoesel B, Schmid JA. The complexity of NF-κB signaling in inflammation and cancer. Mol Cancer 2013;12:86. doi:10.1186/1476-4598-12-86.
- Horton JD, Cohen JC, Hobbs HH. PCSK9: a convertase that coordinates LDL catabolism. J Lipid Res. 2009 Apr;50 Suppl:S172-7. doi: 10.1194/jlr.R800091-JLR200. Epub 2008 Nov 19.
- Hotamisligil GS, Arner P, Caro JF, Atkinson RL, Spiegelman BM. Increased adipose tissue expression of tumor necrosis factor-alpha in human obesity and insulin resistance. J Clin Invest (1995) 95:2409–15. doi:10.1172/JCI117936
- Huang YY, Gusdon AM, Qu S. Nonalcoholic fatty liver disease: molecular pathways and therapeutic strategies. Lipids Health Dis 2013; 12: 171 [PMID: 24209497 DOI: 10.1186/1476-511X-12-171]
- Hudgins LC, Parker TS, Levine DM and Hellerstein MK: A dual sugar challenge test for lipogenic sensitivity to dietary fructose. The Journal of Clinical Endocrinology & Metabolism 96: 861-868, 2011.
- Huijgen R, Boekholdt SM, Arsenault BJ, Bao W, Davaine JM, Tabet F, Petrides F, Rye KA, DeMicco DA, Barter PJ, Kastelein JJ, Lambert G. Plasma PCSK9 levels and clinical outcomes in the TNT (Treating to New Targets) trial. J Am Coll Cardiol. 2012 May 15;59(20):1778-84. doi: 10.1016/j.jacc.2011.12.043.
- Iguchi H, Kojo S, Ikeda M (1993) Lipid peroxidation and disintegration of the cell membrane structure in cultures of rat lung fibroblasts treated with asbestos. J Appl Toxicol 13:269–75. https://doi.org/10.1002/jat.2550130409
- Jarrod Millman K and Michael Aivazis; Python for Scientists and Engineers, Computing in Science & Engineering, 13, 9-12 (2011), doi:10.1109/MCSE.2011.36 J. Chen; Nanobiomechanics of living cells: a review. Interface Focus. 2014 Apr 6; 4(2): 20130055. doi:10.1098/rsfs.2013.0055
- Jelen, S, Wacker S, Aponte-Santamaría C, Skott M, Rojek A, Johanson U, Kjellbom P, Nielsen S, de Groot BL, Rützler M. Aquaporin-9 protein is the primary route of hepatocyte glycerol uptake for glycerol gluconeogenesis in mice. J Biol Chem. 2011 Dec 30;286(52):44319-25. doi: 10.1074/jbc.M111.297002.
- Jenkins Y, Sun T-Q, Markovtsov V, Foretz M, Li W, Nguyen H, et al. AMPK activation through mitochondrial regulation results in increased substrate oxidation and improved metabolic

parameters in models of diabetes. PLoS One (2013) 8:e81870. doi:10.1371/journal.pone.0081870

- Jin JC, Zhang X, Jin XL, Quian CS, Jjang H, Ruan Y. MicroRNA-122 regulation of the morphology and cytoarchitecture of hepatoma carcinoma cells. Mol Med Rep. 2014 Apr;9(4):1376-80. doi: 10.3892/mmr.2014.1930.
- Johnson K, K. Kendall, A. Roberts; Surface energy and the contact of elastic solids; Proc. R. Soc. London. A. Math. Phys. Sci., 324 (1971), pp. 301-313 doi: 10.1098/rspa.1971.0141
- Johnson KL.; 1985. Contact mechanics. Cambridge, UK: Cambridge University Press
- Joshi-Barve S, Barve SS, Amancherla K, Gobejishvili L, Hill D, Cave M, et al. Palmitic acid induces production of proinflammatory cytokine interleukin-8 from hepatocytes. Hepatology (2007) 46:823–30. doi:10.1002/hep.21752
- Joven, J, Micol, V, Segura-Carretero, A, Alonso-Villaverde, C, Menéndez, JA (2014). Bioactive food components platform. Crit Rev Food Sci Nutr 54(8):985-100. doi: 10.1080/10408398.2011.621772
- Kadota Y, Toriuchi Y, Aki Y, Mizuno Y, Kawakami T, Nakaya T, Sato M, Suzuki S. Metallothioneins regulate the adipogenic differentiation of 3T3-L1 cells via the insulin signaling pathway. PLoS One. 2017 Apr 20;12(4):e0176070. doi: 10.1371/journal.pone.0176070. eCollection 2017
- Kandaswami C, Middleton E. Free radical scavenging and antioxidant activity of plant flavonoids. Adv Exp Med Biol 1994; 366: 351-376 [PMID: 7771265 DOI: 10.1007/978- 1-4615-1833-4_ 25]
- Kevil, C. G. (2003) Pathophysiology 9, 63–74
- Khalil M, Khalifeh H, Baldini F, Salis A, Damonte G, Daher A, Voci A, Vergani L. Antisteatotic and antioxidant activities of Thymbra spicata L. extracts in hepatic and endothelial cells as in vitro models of non-alcoholic fatty liver disease. J Ethnopharmacol. 2019 Jul 15;239:111919. doi: 10.1016/j.jep.2019.111919.
- Kohli R, Kirby M, Xanthakos SA, Softic S, Feldstein AE, Saxena V, Tang PH, Miles L, Miles MV, Balistreri WF, Woods SC, Seeley RJ. High-fructose, medium chain trans-fat diet induces liver fibrosis and elevates plasma coenzyme Q9 in a novel murine model of obesity and nonalcoholic steatohepatitis. Hepatology. 2010 Sep;52(3):934-44. doi: 10.1002/hep.2379
- Koliaki C, Szendroedi J, Kaul K, Jelenik T, Nowotny P, Jankowiak F, et al. Adaptation of hepatic mitochondrial function in humans with non-alcoholic fatty liver is lost in steatohepatitis. Cell Metab (2015) 21:739–46. doi:10.1016/ j.cmet.2015.04.004
- Komatsu M, Waguri S, Ueno T, Iwata J, Murata S, Tanida I, Ezaki J, Mizushima N, Ohsumi Y, Uchiyama Y, Kominami E, Tanaka K, Chiba T. Impairment of starvation- induced and constitutive autophagy in Atg7-deficient mice. J Cell Biol 2005;169:425- 34 PMID: 15866887 doi: 10.1083/jcb.200412022.
- Kong L, Zhu J, Han W, Jiang X, Xu M, Zhao Y, Dong Q, Pang Z, Guan Q, Gao L, Zhao J, Zhao L. Significance of serum microRNAs in pre-diabetes and newly diagnosed type 2 diabetes: a clinical study. Acta Diabetol. 2011 Mar;48(1):61-9. doi: 10.1007/s00592- 010-0226-0.
- Koopman R., Schaart G., Hesselink M. K. (2001). Optimisation of oil red O staining permits combination with immunofluorescence and automated quantification of lipids. Histochem. Cell Biol. 116, 63–68 doi:10.1007/s004180100297
- Krawczyk M, Bonfrate L, Portincasa P. Nonalcoholic fatty liver disease. Best Pract Res Clin Gastroenterol. 2010 Oct;24(5):695-708. doi: 10.1016/j.bpg.2010.08.005.
- Kwanten, WJ, Martinet, W, Francque, SM (2016). Chapter: Authophagy in non- alcoholic fatty

liver disease (NAFLD). Intech 455-483. Book: Autophagy in Current Trends in Cellular Physiology and Pathology. Edited by Nikolai V. Gorbunov and Marion Schneider. doi: 10.5772/64534. http://dx.doi.org/10.5772/64534

- Laemmli UK. Cleavage of structural proteins during the assembly of the head of bacteriophage T4. Nature 1970; 227: 680-685 [PMID: 5432063 DOI: 10.1038/227680a0]
- Lagace TA, Curtis DE, Garuti R, McNutt MC, Park SW, Prather HB, Anderson NN, Ho YK, Hammer RE, Horton JD. Secreted PCSK9 decreases the number of LDL receptors in hepatocytes and in livers of parabiotic mice. J Clin Invest. 2006 Nov;116(11):2995- 3005. doi:10.1172/JCI29383
- Lang CH, Dobrescu C, Bagby GJ. Tumor necrosis factor impairs insulin action on peripheral glucose disposal and hepatic glucose output. Endocrinology (1992) 130:43– 52. doi:10.1210/endo.130.1.1727716
- Larsen A, Nielsen J, Hansen Neigaard C, Nielsen LB, Wibrand F, Stride N, Schroder HD, Boushel R, Helde JW, Dela F, Hey-Mogensen M. Biomarkers of mitochondrial content in skeletal muscle of healthy young human subjects. J Physiol. 2012 Jul 15; 590(Pt 14): 3349–3360. Published online 2012 May 14. doi: 10.1113/jphysiol.2012.230185
- Lauris V, Crettaz M, Kahn CR. Coordinate roles of insulin and glucose on the growth of hepatoma cells in culture. Endocrinology 1986;118:2519–24. doi:10.1210/endo-118- 6-2519.
- Lebeaupin C, Vallée D, Hazari Y, Hetz C, Chevet E, Bailly-Maitre B. Endoplasmic reticulum stress signaling and the pathogenesis of non-alcoholic fatty liver disease. J Hepatol. 2018 Oct;69(4):927-947 doi: 10.1016/j.jep.2018.06.008. Epub 2018 Jun 27
- Lee TD, Sadda MR, Mendler MH, Bottiglieri T, Kanel G, Mato JM, Lu SC. Abnormal hepatic methionine and glutathione metabolism in patients with alcoholic hepatitis. Alcohol Clin Exp Res 2004; 28: 173
- Lesmana CRA, Hasan I, Budihusodo U, Gani RA, Krisnuhoni E, Akbar N, et al. Diagnostic value of a group of biochemical markers of liver fibrosis in patients with non-alcoholic steatohepatitis. J Dig Dis (2009) 10:201–6. doi:10.1111/j.1751-2980.2009.00386.x
- Liao JK. Linking endothelial dysfunction with endothelial cell activation. J Clin Invest. 2013 Feb;123(2):540-1. doi: 10.1172/JCI66843. Epub 2013 Feb 1
- Lindskog C, Asplund A, Catrina A, Nielsen S, Rützler M. A Systematic Characterization of Aquaporin-9 Expression in Human Normal and Pathological Tissues. J Histochem Cytochem. 2016 May;64(5):287-300. doi: 10.1369/0022155416641028.
- Listenberger LL, Ostermeyer-Fay AG, Goldberg EB, Brown WJ and Brown DA: Adipocyte differentiation-related protein reduces the lipid droplet association of adipose triglyceride lipase and slows triacylglycerol turnover. J Lipid Res 48: 2751- 2761, 2007.
- Loguercio C, Andreone P, Brisc C, Brisc MC, Bugianesi E, Chiaramonte M, Cursaro C, Danila M, de Sio I, Floreani A, Freni MA, Grieco A, Groppo M, Lazzari R, Lobello S, Lorefice E, Margotti M, Miele L, Milani S, Okolicsanyi L, Palasciano G, Portincasa P, Saltarelli P, Smedile A, Somalvico F, Spadaro A, Sporea I, Sorrentino P, Vecchione R, Tuccillo C, Del Vecchio Blanco C, Federico A. Silybin combined with phosphatidylcholine and vitamin E in patients with nonalcoholi c fatty liver disease: a randomized controlled trial. Free Radic Biol Med. 2012 May 1;52(9):1658-65. doi: 10.1016/j.freeradbiomed.2012.02.008.
- Loguercio C and Festi D: Silybin and the liver: from basic research to clinical practice. World J Gastroenterol 17: 2288-2301, 2011.
- Loguercio C, Tiso A, Cotticelli G, et al.: Management of chronic liver disease by general practitioners in southern Italy: unmet educational needs. Dig Liver Dis 43: 736-741, 2011.

- Loomba R, Sanyal AJ. The global NAFLD epidemic. Nat Rev Gastroenterol Hepatol 2013;10:686–90. doi:10.1038/nrgastro.2013.171.
- Lu SC, Mato JM. S-adenosylmethionine in liver health, injury, and cancer. Physiol Rev 2012; 92: 1515
- Luca Puricelli, Massimiliano Galluzzi, Carsten Schulte, Alessandro Podestà, and Paolo Milani; Nanomechanical and topographical imaging of living cells by atomic force microscopy with colloidal probes; Review of Scientific Instruments 86, 033705 (2015) doi:10.1063/1.4915896
- Maeda N, Takahashi M, Funahashi T, Kihara S, Nishizawa H, Kishida K, Nagaretani H, Matsuda M, Komuro R, Ouchi N, Kuriyama H, Hotta K, Nakamura T, Shimomura I, Matsuzawa Y. PPAR_ ligands increase expression and plasma concentration of adiponectin, an adipose-derived protein. Diabetes 50: 2094 –2099, 2001
- Margareta Jernås Jenny Palming Kajsa Sjöholm Eva Jennische Per-Arne Svensson Britt G. Gabrielsson Max Levin Anders SjögrenMats Rudemo Theodore C. Lystig Björn Carlsson Lena M. S. Carlsson , and Malin Lönn Published Separation of human adipocytes by size: hypertrophic fat cells display distinct gene expression FASEB J 5 Jun 2006 https://doi.org/10.1096/fj.05-5678fje
- Mato JM, Martinez-Chantar ML, Lu SC. S-adenosylmethionine metabolism and liver disease. Ann Hepatol 2013; 12: 183–9.
- Mendez-Sanchez N, Cruz-Ramon VC, Ramirez-Perez OL, Hwang JP, Barranco-Fragoso B and Cordova-Gallardo J: New Aspects of Lipotoxicity in Nonalcoholic Steatohepatitis. Int J Mol Sci 19, 2018.
- Mescola, S. Vella, M. Scotto, P. Gavazzo, C. Canale, A. Diaspro, A. Pagano, M. Vassalli; Probing cytoskeleton organisation of neuroblastoma cells with single-cell force spectroscopy; J. Molecular Recognition 25, 270-277 (2012) doi: 10.1002/jmr.2173
- Mizushima N, Ohsumi Y, Yoshimori T. Autophagosome formation in mammalian cells. Cell Struct Funct 2002; 27: 421-429 [PMID: 12576635 DOI: 10.1247/csf.27.421]
- Molina-Molina E, Lunardi Baccetto R, Wang DQ, de Bari O, Krawczyk M, Portincasa P. Exercising the hepatobiliary-gut axis. The impact of physical activity performance. Eur J Clin Invest. 2018 Aug;48(8):e12958. doi: 10.1111/eci.12958.
- Moore KJ, Rayner KJ, Suarez Y and Fernandez-Hernando C: The role of microRNAs in cholesterol efflux and hepatic lipid metabolism. Annu Rev Nutr 31: 49-63, 2011.
- Moreira AC, Branco AF, Sampaio SF, Cunha-Oliveira T, Martins TR, Holy J, et al. Mitochondrial apoptosis-inducing factor is involved in doxorubicin- induced toxicity on H9c2 cardiomyoblasts. Biochim Biophys Acta (2014) 1842:2468–78. doi:10.1016/j.bbadis.2014.09.015
- Morrison WR and Smith LM. Preparation of fatty acid methyl esters and dimethylacetals from lipids with boron fluoride. J Lipid Res 1964;5:600-608.
- Moseti, D.; Regassa, A.; Kim,W.K. Molecular Regulation of Adipogenesis and Potential Anti-Adipogenic Bioactive Molecules. Int. J. Mol. Sci. 2016, 17
- Moyes CD, Mathieu-Costello OA, Tsuchiya N, Filbur C, Hansford RG. Mitochondrial biogenesis during cellular differentiation. Am. J. Physiol. 272 (1997) Cl345-Cl351. doi:10.1152/ajpcell.1997.272.4.C1345
- Nagaya T, Tanaka N, Komatsu M, Ichijo T, Sano K, Horiuchi A, et al. Development from simple steatosis to liver cirrhosis and hepatocellular carcinoma: a 27-year follow-up case. Clin J Gastroenterol (2008) 1:116–21. doi:10.1007/s12328-008-0017-0
- Nagaya T, Tanaka N, Suzuki T, Sano K, Horiuchi A, Komatsu M, et al. Downregulation of SREBP-

1c is associated with the development of burned-out NASH. J Hepatol (2010) 53:724–31. doi:10.1016/j.jhep.2010.04.033

- Nakamura MT, Yudell BE, Loor JJ. Regulation of energy metabolism by long-chain fatty acids. Prog Lipid Res 2014; 53: 124-144 [PMID: 24362249 DOI: 10.1016/j.plipres.2013.12.001]
- Nataliia Guz, Maxim Dokukin, Vivekanand Kalaparthi, and Igor Sokolov; If Cell Mechanics Can Be Described by Elastic Modulus: Study of Different Models and Probes Used in Indentation Experiments; Biophys J. 2014 Aug 5; 107(3): 564–575. doi:10.1016/j.bpj.2014.06.033
- Necas D, Klapetek P. Gwyddion: an open-source software for SPM data analysis. Cent Eur J Phys. 10(1), 2012, 181-188 doi:10.2478/s11534-011-0096-2
- Neuschwander-Tetri BA: Hepatic lipotoxicity and the pathogenesis of nonalcoholic steatohepatitis: the central role of nontriglyceride fatty acid metabolites. Hepatology 52: 774-788, 2010.
- Okuda S, Nishiyama N, Saito H, Katsuki H. Hydrogen peroxidemediated neuronal cell death induced by an endogenous neurotoxin, 3-hydroxykynurenine. Proc Natl Acad Sci USA 1996; 93: 12553-12558 [PMID: 8901620 DOI: 10.1073/pnas.93.22.12553]
- Otto O, Rosendahl P, Mietke A, Golfier S, Herold C, Klaue D, Girardo S, Pagliara S, Ekpenyong A, Jacobi A, Wobus M, Töpfner N, Keyser UF, Mansfeld J, Fisher-Friedrich E, Guck J. Real-time deformability cytometry: on-the-fly cell mechanical phenotyping. Nat Methods, 2015 Mar;12(3):199-202, 4 p following 202 doi: 10.1038/nmeth.3281. Epub 2015 Feb
- Ouchi N, Kihara S, Arita Y, Maeda K, Kuriyama H, Okamoto Y, Hotta K, Nishida M, Takahashi M, Nakamura T, Yamashita S, Funahashi T, Matsuzawa Y. Novel modulator for endothelial adhesion molecules: adipocyte-derived plasma protein adiponectin. Circulation 100: 2473–2476, 1999.
- Paton CM, Ntambi JM. Biochemical and physiological function of stearoyl-CoA desaturase. American Journal of Physiology. Endocrinology and Metabolism. 297 (1). PMID 19066317 Am J Physiol Endocrinol Metab. 2009 Jul;297(1):E28-37. doi: 10.1152/ajpendo.90897.2008.
- Paul A, Chang BH-J, Li L, Yechoor VK, Chan L. Deficiency of adipose differentiation- related protein impairs foam cell formation and protects against atherosclerosis. Circ Res (2008) 102:1492–501. doi:10.1161/CIRCRESAHA. 107.168070
- Pessayre D, Fromenty B. NASH: a mitochondrial disease. J Hepatol (2005) 42:928–40. doi:10.1016/j.jhep.2005.03.004
- Petecchia L, Viti F, Sbrana F, Vassalli M, Gavazzo P. A biophysical approach to quantify skeletal stem cells trans-differentiation as a model for the study of osteoporosis. Biophys Chem, 2017 Oct;229:84-92. doi:10.1016/j.bpc.2017.05.011. Epub 2017 May 26
- Pfaffl MW. A new mathematical model for relative quantification in real-time RT-PCR. Nucleic Acids Res 2001; 29: e45 [PMID: 11328886 DOI: 10.1093/nar/29.9.e45]
- Portincasa P, Grattagliano I, Lauterburg BH, Palmieri VO, Palasciano G, Stellaard F. Liver breath tests non-invasively predict higher stages of non- alcoholic steatohepatitis. Clin Sci (Lond) (2006) 111:135–43. doi:10.1042/ CS20050346
- Portincasa P, Grattagliano I, Palmieri VO, Palasciano G. Nonalcoholic steatohepatitis: recent advances from experimental models to clinical management. Clin Biochem 2005; 38: 203-217 [PMID: 15708540 DOI: 10.1016/j.clinbiochem.2004.10.014]
- Portincasa P, Palasciano G, Svelto M, Calamita G (2008). Aquaporins in the hepatobiliary tract. which, where, what they do in health and disease. Eur J Clin Invest, 38(1):1-10. doi: 10.1111/j.1365-2362-2007.01897.x.

- Poulos, S.P.; Dodson, M.V.; Hausman, G.J. C ell line models for differentiation: Preadipocytes and adipocytes.Exp. Biol. Med. 2010, 35, 1185–1193
- Primassin S, Tucci S, Spiekerkoetter U. Hepatic and muscular effects of different dietary fat content in VLCAD deficient mice. Mol Genet Metab. 2011 Dec;104(4):546- 51. doi: 10.1016/j.ymgme.2011.09.011.
- Rajala MW, Scherer PE. Minireview: The adipocyte--at the crossroads of energy homeostasis, inflammation, and atherosclerosis. Endocrinology. 2003 Sep;144(9):3765-73
- Ramachandran R, Kakar S. Histological patterns in drug-induced liver disease. J Clin Pathol. 2009 Jun;62(6):481-92. doi: 10.1136/jcp.2008.058248.
- Ramsay RR, Gandour RD, van der Leij FR. Molecular enzymology of carnitine transfer and transport. Biochim Biophys Acta 2001; 1546: 21-43 [PMID: 11257506 DOI: 10.1016/ S0167-4838(01)00147-9]
- Ravikumar B1, Sarkar S, Davies JE, Futter M, Garcia-Arencibia M, Green-Thompson ZW, Jimenez-Sanchez M, Korolchuk VI, Lichtenberg M, Luo S, Massey DC, Menzies FM, Moreau K, Narayanan U, Renna M, Siddiqi FH, Underwood BR, Winslow AR, Rubinsztein DC. Regulation of mammalian autophagy in physiology and pathophysiology Physiol Rev. 2010 Oct;90(4):1383-435. doi: 10.1152/physrev.00030.2009.
- Reina M, Martínez A. Silybin and 2,3-Dehydrosilybin Flavonolignans as Free Radical Scavengers. J Phys Chem B 2015; 119: 11597-11606 [PMID: 26259041 DOI: 10.1021/acs. jpcb.5b06448]
- Ricchi M, Odoardi MR, Carulli L, Anzivino C, Ballestri S, Pinetti A, Fantoni LI, Marra F, Bertolotti M, Banni S, Lonardo A, Carulli N, Loria P. Differential effect of oleic and palmitic acid on lipid accumulation and apoptosis in cultured hepatocytes. J Gastroenterol Hepatol 2009; 24: 830-840 [PMID: 19207680 DOI: 10.1111/j.1440- 1746.2008.05733.x]
- Ricchi M, Odoardi MR, Carulli L, Anzivino C, Ballestri S, Pinetti A, Fantoni LI, Marra F, Bertolotti M, Banni S, Lonardo A, Carulli N, Loria P. Differential effect of oleic and palmitic acid on lipid accumulation and apoptosis in cultured hepatocytes. J Gastroenterol Hepatol. 2009 May;24(5):830-40. doi: 10.1111/j.1440- 1746.2008.05733.x.
- Rinella ME. Nonalcoholic fatty liver disease: a systematic review. JAMA 2015; 313: 2263-2273 [PMID: 26057287 DOI: 10.1001/ jama.2015.5370]
- Rodríguez A, Moreno NR, Balaguer I, Méndez-Giménez L, Becerril S, Catalán V, Gómez-Ambrosi J, Portincasa P, Calamita G, Soveral G, Malagón MM, Frühbeck G. Leptin administration restores the altered adipose and hepatic expression of aquaglyc eroporins improving the non-alcoholic fatty liver of ob/ob mice. Sci Rep. 2015a Jul 10;5:12067. doi: 10.1038/srep12067.
- Rodríguez A, Gena P, Méndez-Giménez L, Rosito A, Valentí V, Rotellar F, Sola I, Moncada R, Silva C, Svelto M, Salvador J, Calamita G, Frühbeck G. Reduced hepatic aquaporin-9 and glycerol permeability are related to insulin resistance in non- alcoholic fatty liver disease. Int J Obes (Lond). 2014 Sep;38(9):1213-20. doi: 10.1038/ijo.2013.234.
- Rodríguez A, Marinelli RA, Tesse A, Frühbeck G, Calamita G. Sexual Dimorphism of Adipose and Hepatic Aquaglyceroporins in Health and Metaboli c Disorders. Front Endocrinol (Lausanne). 2015b Nov 5;6:171. doi: 10.3389/fendo.2015.00171.
- Rodríguez A1, Catalán V, Gómez-Ambrosi J, García-Navarro S, Rotellar F, Valentí V, Silva C, Gil MJ, Salvador J, Burrell MA, Calamita G, Malagón MM, Frühbeck G. Insulin- and leptin-mediated control of aquaglyceroporins in human adipocytes and hepatocytes is mediated via the PI3K/Akt/mTOR signaling cascade. J Clin Endocrinol Metab. 2011 Apr;96(4):E586-97. doi: 10.1210/jc.2010-1408.

- Rolo AP, Teodoro JS, Palmeira CM. Role of oxidative stress in the pathogenesis of nonalcoholic steatohepatitis. Free Radic Biol Med 2012;52:59–69. doi:10.1016/j.freeradbiomed.2011.10.003.
- Rosso N, Marin V, Giordani A, Persiani S, Sala F, Cavicchioli L, et al. The pros and the cons for the use of silybin-rich oral formulations in treatment of liver damage (NAFLD in particular). Curr Med Chem (2015) 22:2954–71. doi:10.2174/0929867322666150729114235
- Ruart M, Chavarria L, Campreciós G, Suárez-Herrera N, Montironi C, Guixé-Muntet S, Bosch J, Friedman SL, Garcia-Pagán JC, Hernández-Gea V. Impaired endothelial autophagy promotes liver fibrosis by aggravating the oxidative stress response during acute liver injury. J Hepatol. 2019 Mar;70(3):458-469. doi: 10.1016/j.jhep.2018.10.015. Epub 2018 Oct 25.
- Rubí B, Antinozzi PA, Herrero L, Ishihara H, Asins G, Serra D, Wollheim CB, Maechler P, Hegardt FG. Adenovirus-mediated overexpression of liver carnitine palmitoyltransferase I in INS1E cells: effects on cell metabolism and insulin secretion. Biochem J 2002; 364: 219-226 [PMID: 11988095 DOI: 10.1042/bj3640219]
- Rubinsztein DC, Codogno P, Levine B. Autophagy modulation as a potential therapeutic target for diverse diseases. Nat Rev Drug Discov. 2012 Sep;11(9):709-30. doi: 10.1038/nrd3802
- Rydén M, Andersson DP, Bergström IB, Arner P. Adipose tissue and metabolic alterations: regional differences in fat cell size and number matter, but differently: a cross-sectional study. J Clin Endocrinol Metab. 2014;99(10):
- Sahini N BJ. Recent insights into the molecular pathophysiology of lipid droplet formation in hepatocytes. Progr Lipid Res 2014:86–112. doi:10.1016/j.plipres.2014.02.002.
- Sahini N, Borlak J. Recent insights into the molecular pathophysiology of lipid droplet formation in hepatocytes. Prog Lipid Res, 2014, Apr;54:86-112 doi: 10.1016/j.plipres.2014.02.002. Epub 2014 Mar 6
- Saller R, Meier R, Brignoli R. The use of silymarin in the treatment of liver diseases. Drugs 2001; 61: 2035-2063 [PMID: 11735632 DOI: 10.2165/00003495-200161140- 00003]
- Saller R, Meier R, Brignoli R. The use of silymarin in the treatment of liver diseases. Drugs (2001) 61:2035–63. doi:10.2165/00003495-200161140-00003
- Santhekadur PK, Kumar DP, Sanyal AJ. Preclinical models of non-alcholic fatty liver disease. J Hepatol. 2018 Feb;68(2):230-237. doi: 10.1016/j.jhep.2017.10.031. Epub 2017 Nov 9
- Satapati S, Kucejova B, Duarte JA, et al.: Mitochondrial metabolism mediates oxidative stress and inflammation in fatty liver. The Journal of clinical investigation 125: 4447- 4462, 2015.
- Satapati S, Kucejova B, Duarte JAG, Fletcher JA, Reynolds L, Sunny NE, et al. Mitochondrial metabolism mediates oxidative stress and inflammation in fatty liver. J Clin Invest (2015) 125:4447–62. doi:10.1172/JCI82204
- Sato M, Bremner I. Oxygen free radicals and metallothionein. Free Radic Biol Med. 1993 Mar;14(3):325-37.
- Sato M, Kawakami T, Kadota Y, Mori M, Suzuki S. Obesity and metallothionein. Curr Pharm Biotechnol. 2013;14(4):432-40.
- Savitzky A, Golay JE. Smoothing and differentiation of data by simplified least squares procedures. Anal Chem, 1964, 36(8), pp 1627-1639 doi:10.1021/ac60214a047
- Scaduto RC, Grotyohann LW. Measurement of mitochondrial membrane potential using fluorescent rhodamine derivatives. Biophys J (1999) 76:469–77. doi:10.1016/S0006-3495(99)77214-0

- Schlottmann S, Buback F, Stahl B, Meierhenrich R, Walter P, Georgieff M, Senftleben
- Sciacqua A, Perticone M, Miceli S, Laino I, Tassone EJ, Grembiale RD, Andreozzi F, Sesti G, Perticone F. Endothelial dysfunction and non-alcoholic liver steatosis in hypertensive patients. Nutr Metab Cardiovasc Dis. 2011 Jul;21(7):485-91. doi: 10.1016/j.numecd.2009.11.015. Epub 2010 Mar 12
- Seifert EL, Estey C, Xuan JY, Harper M-E. Electron transport chain-dependent and - independent mechanisms of mitochondrial H2O2 emission during long-chain fatty acid oxidation. J Biol Chem (2010) 285:5748–58. doi:10.1074/ jbc.M109.026203
- Serviddio G, Bellanti F, Sastre J, Vendemiale G, Altomare E. Targeting mitochondria: a new promising approach for the treatment of liver diseases. Curr Med Chem. 2010;17(22):2325-37
- Serviddio G, Giudetti AM, Bellanti F, Priore P, Rollo T, Tamborra R, et al. Oxidation of hepatic carnitine palmitoyl transferase-I (CPT-I) impairs fatty acid beta-oxidation in rats fed a methionine-choline deficient diet. PLoS One (2011) 6:e24084. doi:10.1371/journal.pone.0024084
- Shah V, Haddad FG, Garcia-Cardena G, Frangos JA, Mennone A, Groszmann RJ, et al. Liver sinusoidal endothelial cells are responsible for nitric oxide modulation of resistance in the hepatic sinusoids. J Clin Invest 1997;100:2923–30. doi:10.1172/JCI119842.
- Shapiro SS, M.B.Wilk, An analysis of variance test for normality (complete samp1es) Biometrika, 1965, 52 doi: 10.2307/2333709
- Shimano H. Sterol regulatory element-binding proteins (SREBPs): transcriptional regulators of lipid synthetic genes. Prog Lipid Res 2001; 40: 439-452 [PMID: 11591434 DOI: 10.1016/ S0163-7827(01)00010-8]
- Shoham N, Girshovitz P, Katzengold R, Shaked NT, Benayahu D, Gefen A. Adipocyte stiffness increases with accumulation of lipid droplets. Biophys J, 2014 Mar 18;106(6):1421-31 doi: 10.1016/j.bpj.2014.01.045
- Silva AKS, Peixoto CA. Role of peroxisome proliferator-activated receptors in non- alcoholic fatty liver disease inflammation. Cell Mol Life Sci. 2018 Aug;75(16):2951- 2961. doi: 10.1007/s00018-018-2838-4. Epub 2018 May 22.
- Singh S, Fujii LL, Murad MH, Wang Z, Asrani SK, Ehman RL, Kamath PS, Talwalkar JA. Liver Stiffness Is Associated With Risk of Decompensation, Liver Cancer, and Death in Patients With Chronic Liver Diseases: A Systematic Review and Meta-analysis. 2013 Dec;11(12):1573-84.e1-2; quiz e88-9 doi: 10.1016/j.cgh.2013.07.034. Epub 2013 Aug 15
- Skottová N, Krecman V. Silymarin as a potential hypocholesterolaemic drug. Physiol Res. 1998;47(1):1-7.
- Solhi H, Ghahremani R, Kazemifar AM, Hoseini Yazdi Z. Silymarin in treatment of non- alcoholic steatohepatitis: A randomized clinical trial. Caspian J Intern Med 2014; 5: 9- 12 [PMID: 24490006]
- Solhi H, Ghahremani R, Kazemifar AM, Hoseini Yazdi Z. Silymarin in treatment of non- alcoholic steatohepatitis: a randomized clinical trial. Caspin J Intern Med (2014) 5:9– 12.
- Sonntag Y, Gena P, Maggio A, Singh T, Artner I, Oklinski MK, Johanson U, Kjellbom P, Nieland JD, Nielsen S, Calamita G, Rützler M. Identification and characterization of potent and selective aquaporin-3 and aquaporin-7 inhibitors. J Biol Chem. 2019 May 3;294(18):7377-7387. doi: 10.1074/jbc.RA118.006083
- Sturla L, Mannino E, Scarfì S; Bruzzone S, Magnone M, Sociali G, Booz V, Guida L, Vignarolo T,

Fresia C, Ermionite L, Buschiazzo A, Marini C, Sambuceti G, De Flora A, Zocchi E. Abscisic acid enhances glucose disposal and induces brown fat activity in adipocytes in vitro and in vivo. Biochim Biophys Acta Mol Cell Biol Lipids. 2007. 1862 (2), 131-144. PMID: 27871880. doi: 10.1016/j.bbalip.2016.11.005

- Szmitko PE, Wang C-H, Weisel RD, Jeffries GA, Anderson TJ, Verma S. Biomarkers of vascular disease linking inflammation to endothelial activation: Part II. Circulation 2003;108:2041–8. doi:10.1161/01.CIR.0000089093.75585.98.
- Tamori Y, Masugi J, Nishino N, Kasuga M. Role of peroxisome proliferator- activated receptor-_ in maintenance of the characteristics of mature 3T3-L1 adipocytes. Diabetes 51: 2045–2055, 2002.
- Tandra S, Yeh MM, Brunt EM, Vuppalanchi R, Cummings OW, Ünalp-Arida A, Wilson LA, Chalasani N. Presence and significance of microvesicular steatosis in nonalcoholic fatty liver disease. J Hepatol. 2011 Sep;55(3):654-659. doi: 10.1016/j.jhep.2010.11.021. Epub 2010 Dec 21
- Tanida I, Ueno T, Kominami E. LC3 conjugation system in mammalian autophagy. Int J Biochem Cell Biol. 2004 Dec;36(12):2503-18. doi:10.1016/j.biocel.2004.05.009
- Teague MR. Deterministic phase retrieval: a Green's function solution. Journal of the Optical Society of America. Vol.73, Issue 11, pp.1434-1441 (1983) doi:10.1364/JOSA.73.001434
- Teissier E, Nohara A, Chinetti G, Paumelle R, Cariou B, Fruchart JC, Brandes RP, Shah A, Staels B. Peroxisome proliferatoractivated receptor alpha induces NADPH oxidase activity in macrophages, leading to the generation of LDL with PPAR-alpha activation properties. Circ Res 2004; 95: 1174-1182 [PMID: 15539630 DOI: 10.1161/01.RES.0000150594.95988.45]
- Ter Horst KW and Serlie MJ: Fructose Consumption, Lipogenesis, and Non-Alcoholic Fatty Liver Disease. Nutrients 9, 2017.
- Tesse A, Grossini E, Tamma G, Brenner C, Portincasa P, Marinelli RA, Calamita G. Aquaporins as Targets of Dietary Bioactive Phytocompounds. Front Mol Biosci. 2018 Apr 18;5:30. doi: 10.3389/fmolb.2018.00030.
- Tetri LH, Basaranoglu M, Brunt EM, Yerian LM and Neuschwander-Tetri BA: Severe NAFLD with hepatic necroinflammatory changes in mice fed trans fats and a high- fructose corn syrup equivalent. American journal of physiology. Gastrointestinal and liver physiology 295: G987-995, 2008.
- Tetri LH, Basaranoglu M, Brunt EM, Yerian LM, Neuschwander-Tetri BA. Severe NAFLD with hepatic necroinflammatory changes in mice fed trans fats and a high-fructose corn syrup equivalent. Am J Physiol Gastrointest Liver Physiol, 2008 Nov;295(5):G987- 95 doi: 10.1152/ajpgi.90272.2008. Epub 2008 Sep 4
- Tilg H, Moschen AR. Evolution of inflammation in nonalcoholic fatty liver disease: the multiple parallel hits hypothesis. Hepatology (2010) 52:1836–46. doi:10.1002/hep.24001
- Towbin H, Staehelin T, Gordon J. Electrophoretic transfer of proteins from polyacrylamide gels to nitrocellulose sheets: procedure and some applications. Proc Natl Acad Sci USA 1979; 76: 4350-4354 [PMID: 388439]
- Trappoliere M, Caligiuri A, Schmid M, Bertolani C, Failli P, Vizzutti F, Novo E, di Manzano C, Marra F, Loguercio C, Pinzani M. Silybin, a component of sylimarin, exerts anti-inflammatory and anti-fibrogenic effects on human hepatic stellate cells. J Hepatol 2009; 50: 1102-1111 [PMID: 19398228 DOI: 10.1016/ j.jhep.2009.02.023]
- Trepat X, Deng L, An SS, Navajas D, Tschumperlin DJ, Gerthoffer WT, Butler JP, Fredberg JJ. Universal physical responses to stretch in the living cell. Nature. 2007 May 31;447(7144):592-

- Trocoli A, Djavaheri-Mergny M. The complex interplay between autophagy and NF-κB signaling pathways in cancer cells. Am J Cancer Res. 2011;1(5):629-49.
- Trunkey DD. Priorities in trauma management. Mil Med 1990; 155: 217-219 [PMID: 2114583 DOI: 10.1016/j.jhep.2010.09.027]
- Tsai WC, Hsu MT, Lai TC, Chau GY, Lin CW, Chen CM, Lin CD, Liao YL, Wang JL, Chau YP, Hsu MT, Hsiao M, Huang HD, Tsou AP. MicroRNA-122, a tumor suppressor microRNA that regulates intrahepatic metastasis of hepatocellular carcinoma. Hepatology. 2009 May;49(5):1571-82. doi: 10.1002/hep.22806.
- U. Prolonged classical NF-kappaB activation prevents autophagy upon E. coli stimulation in vitro: a potential resolving mechanism of inflammation. Mediators Inflamm. 2008;2008:725854. doi: 10.1155/2008/725854.
- Vanni E, Bugianesi E, Kotronen A, De Minicis S, Yki-Järvinen H, Svegliati-Baroni G. From the metabolic syndrome to NAFLD or vice versa? Dig Liver Dis 2010; 42: 320- 330 [PMID: 20207596 DOI: 10.1016/j.dld.2010.01.016]
- Varga T, Czimmerer Z, Nagy L. PPARs are a unique set of fatty acid regulated transcription factors controlling both lipid metabolism and inflammation. Biochim Biophys Acta, 2011 Aug;1812(8):1007-22 doi: 10.1016/j.bbadis.2011.02.014. Epub 2011 Mar 5
- Vecchie A, Dallegri F, Carbone F, et al.: Obesity phenotypes and their paradoxical association with cardiovascular diseases. European journal of internal medicine, 2017.
- Vecchione G, Grasselli E, Compalati AD, Ragazzoni M, Cortese K, Gallo G, Voci A, Vergani L. Ethanol and fatty acids impair lipid homeostasis in an in vitro model of hepatic steatosis. Food Chem Toxicol. 2016 Apr;90:84-94. doi: 10.1016/j.fct.2016.02.004. Epub 2016 Feb 5.
- Vecchione G, Grasselli E, Cioffi F, Baldini F, Oliveira PJ, Sardão VA, Cortese K, Lanni A, Voci A, Portincasa P, Vergani L. The Nutraceutic Silybin Counteracts Excess Lipid Accumulation and Ongoing Oxidative Stress in an In Vitro Model of Non-Alcoholic Fatty Liver Disease Progression. Front Nutr, 2017 Sep 19;4:42 doi: 10.3389/fnut.2017.00042. eCollection 2017
- Vendemiale G, Altomare E, Trizio T, Le Grazie C, Di Padova C, Salerno MT, Carrieri V, Albano O. Effects of oral S-adenosyl-L-methionine on hepatic glutathione in patients with liver disease. Scand J Gastroenterol 1989; 24: 407–15
- Vergani L, Vecchione G, Baldini F, Grasselli E, Voci A, Portincasa P, Ferrari PF, Aliakbarian B, Casazza AA, Perego P. Polyphenolic extract attenuates fatty acid- induced steatosis and oxidative stress in hepatic and endothelial cells. Eur J Nutr. 2018 Aug;57(5):1793-1805. doi: 10.1007/s00394-017-1464-5.
- Vergani L. Fatty acids and effects on in vitro and in vivo models of liver steatosis. Curr Med Chem. 2019;26(19):3439-3456. doi: 10.2174/0929867324666170518101334.
- Vergani L. Lipid lowering effects of iodothyronines: in vivo and in vitro studies on rat liver. World J Hepatol (2014) 6:169–77. doi:10.4254/wjh.v6.i4.169
- Vichai V, Kirtikara K. Sulforhodamine B colorimetric assay for cytotoxicity screening. Nat Protoc (2006) 1:1112–6. doi:10.1038/nprot.2006.179
- Villanova N, Moscatiello S, Ramilli S, Bugianesi E, Magalotti D, Vanni E, et al. Endothelial dysfunction and cardiovascular risk profile in nonalcoholic fatty liver disease. Hepatology 2005; 42:473e80
- Voroneanu L, Nistor I, Dumea R, Apetrii M, Covic A. Silymarin in Type 2 Diabetes Mellitus: A Systematic Review and Meta-Analysis of Randomized Controlled Trials. J Diabetes Res.

2016;2016:5147468. doi: 10.1155/2016/5147468.

- Voytik-Harbin SL, Brightman AO, Waisner B, Lamar CH, Badylak SF. Application and evaluation of the alamarBlue assay for cell growth and survival of fibroblasts. In Vitro Cell Dev Biol Anim (1998) 34:239–46. doi:10.1007/ s11626-998-0130-x
- Wacker SJ, Aponte-Santamaría C, Kjellbom P, Nielsen S, de Groot BL, Rützler M. The identification of novel, high affinity AQP9 inhibitors in an intracellular binding site. Mol Membr Biol. 2013 May;30(3):246-60. doi: 10.3109/09687688.2013.773095.
- Wah Kheong C, Nik Mustapha NR and Mahadeva S: A Randomized Trial of Silymarin for the Treatment of Nonalcoholic Steatohepatitis. Clin Gastroenterol Hepatol 15: 1940-1949 e1948, 2017.
- Wang CW. Lipid droplets, lipophagy, and beyond. Biochim Biophys Acta. 2016 Aug;1861(8 Pt B):793-805. doi: 10.1016/j.bbalip.2015.12.010.
- Wang N, Kong R, Luo H, Xu X, Lu J. Peroxisome proliferator-activated receptors associated with nonalcoholic fatty liver disease. PPAR Res, 2017;2017:6561701 doi: 10.1155/2017/6561701. Epub 2017 Dec 5
- Wiechelman KJ, Braun RD and Fitzpatrick JD: Investigation of the bicinchoninic acid protein assay: identification of the groups responsible for color formation. Anal Biochem 175: 231-237, 1988.
- Williams SB, Cusco JA, Roddy MA, Johnstone MT, Creager MA. Impaired nitric oxide-mediated vasodilation in patients with non-insulin-dependent diabetes mellitus. J Am Coll Cardiol 1996;27:567e74.
- Xu S, Zhang X, Liu P. Lipid droplet proteins and metabolic diseases. Biochim Biophys Acta Mol Basis Dis. 2018 May;1864(5 Pt B):1968-1983 doi: 10.1016/j.bbadis.2017.07.019. Epub 2017 Jul 21
- Yamaguchi K, Yang L, McCall S, Huang J, Yu XX, Pandey SK, Bhanot S, Monia BP, Li YX, Diehl AM. Inhibiting triglyceride synthesis improves hepatic steatosis but exacerbates liver damage and fibrosis in obese mice with nonalcoholic steatohepatitis. Hepatology 2007; 45(6): 1366-74. doi:10.1002/hep.21655.
- Yamauchi T, Kamon J, Waki H, Imai Y, Shimozawa N, Hioki K, Uchida S, Ito Y, Takakuwa K, Matsui J, Takata M, Eto K, Terauchi Y, Komeda K, Tsunoda M, Murakami K, Ohnishi Y, Naitoh T, Yamamura K, Ueyama Y, Froguel P, Kimura S, Nagai R, Kadowaki T. Globular adiponectin protected ob/ob mice from diabetes and ApoE-deficient mice from atherosclerosis. J Biol Chem 278: 2461–2468, 2003.
- Yarpuzlu B, Ayyildiz M, EnisTok O, Gulhan Aktas R, Basdogan C. Correlation between the mechanical and histological properties of liver tissue. J Mech Behav Biomed Mater. 2014 Jan;29:403-16. doi: 10.1016/j.jmbbm.2013.09.016. Epub 2013 Oct 10.
- Yki-Järvinen H. Non-alcoholic fatty liver disease as a cause and a consequence of metabolic syndrome. Lancet Diabetes Endocrinol (2014) 2:901–10. doi:10.1016/S2213-8587(14)70032-4
- Young-Nam K, Won KK, Kwang-Hee B. Monitoring of adipogenic differentiation of single-cell level using atomic force microscopic analysis. Spectrosc, 26(2011) 329-335 329 doi:10.3233/SPE-2012-0566
- Zhang W, Kudo H, Kawai K, Fujisaka S, Usui I, Sugiyama T, Tsukada K, Chen N, Takahara T. Tumor necrosis factor-alpha accelerates apoptosis of steatotic hepatocytes from a murine model of non-alcoholic fatty liver disease. Biochem Biophys Res Commun. 2010 Jan 22;391(4):1731-6. doi: 10.1016/j.bbrc.2009.12.144.

- Zhou H, Liu X, Liu L, Yang Z, Zhang S, Tang M, et al. Oxidative stress and apoptosis of human brain microvascular endothelial cells induced by free fatty acids. J Int Med Res. 2009 Nov-Dec;37(6):1897-903.
- Zhou H, Liu X, Liu L, Yang Z, Zhang S, Tang M, Tang Y, Dong Q, Hu R. Oxidative stress and apoptosis of human brain microvascular endothelial cells induced by free fatty acids. J Int Med Res. 2009 Nov-Dec;37(6):1897-903.
- Zimmermann R, Lass A, Haemmerle G, Zechner R. Fate of fat: the role of adipose triglyceride lipase in lipolysis. Biochim Biophys Acta (2009) 1791: 494–500. doi:10.1016/j.bbalip.2008.10.005
- Zuo C, Chen Q, Yu Y, Asundi A. Transport-of-intensity phase imaging using Savitzky- Golay differentiation filter-theory and applications. Opt Express, 2013 Mar 11;21(5):5346-62 doi:10.1364/OE.21.005346

15.Curriculum vitae

PERSONAL INFORMATION

Francesca Baldini

Via dei Pilastri 85, 19125 La Spezia (SP) Italia

+39 339 5306655

baldinifrancesca92@gmail.com

Date of birth: 11/06/1992 Nationality: Italian

EDUCATION

November 2016 – October 2019: PhD student in the course of "Sciences and Technologies for the environment and the territory (STAT)"–at DISTAV (Department. of Earth, Environ, and Life Sciences), University of Genoa (Italy). Thesis title: **"**Evaluation of the effects of natural and synthetic compounds on lipid accumulation and inflammation in hepatocytes, endotheliocytes and adipocytes"

October 2014 – July 2016: Master's degree in Molecular and Health Biology cum laude, University of Genoa (Italy). Thesis title: "Hepatoprotective and antioxidant effects of polyphenolic compounds extracted from olive pomace"

September 2011 – November 2014: Bachelor's degree in Biology cum laude, University of Genoa (Italy). Thesis title: "Analysis of the activation of endothelial cells exposed to quartz dust"

PROFESSIONAL EXPERIENCE

1/11/16 – 31/10/19: PhD student in Sciences and Technologies for the environment and the territory (STAT) at DISTAV, University of Genoa (Italy).

Supervisor: Prof. Laura Vergani e Prof. Adriana Voci

15/04/19 – 15/07/19: Visiting PhD Researcher

Institut für Toxikologie und Umwelthygiene - Technical University (TUM) of Munich (Germany)

Local Advisor: Prof. Hans Zischka

1/07/17 – 31/03/18: Visiting PhD Researcher

Institute of Biophysics – National Research Council (CNR) – Genoa (Italy)

Local Advisor: Dr. Massimo Vassalli

10/01/17 – 10/03/17: teaching support activities

Teaching support activities for the "Scientific degree project", university of Genoa (Italy).

Scientific activity

Professional skills

Spectrophotometric assays for quantification of proteins and nucleic acids**.** Cell culture and treatments to mimic in vitro hepatic steatosis, adipocyte hypertrophy and endothelial disfunction. Spearation of cellular fractions and isolation of lipid droplets.

Spectrophotometric assays for the evaluation of lipid peroxidation (TBARs assay), of nitric oxide production (Griess method), of triglycerides content. Analysis of enzyme activity. Evaluation of cell proliferation (MTT assay) and cell migration (Wound Healing assay). Fluorimetric assays for the evaluation of free radical production.

Molecular biology techniques: DNA/RNA extraction from cells and tissues, agarose gel electrophoresis , RNA retro-transcription, semi quantitative PCR, real-time PCR, Western Blot. Data analysis and interpretation.

Skills in sample preparation for advanced microscopic techniques: optical, fluorescence, confocal microscopy, Single Cell Force Microscopy (SCFS) to measure single cell elasticity, Quantitative Phase Microscopy (QPM) for cell tridimensional reconstruction.

Determination of oxygen consumption due to mitochondrial respiration in permeabilized cells using Oroborus, O2k-FluoRespiromiter.

Personal skills

Mother tongue: Italian

Other language: English (Good level of oral expression, writing and reading)

Digital skills

Optimal use of Microsoft Office™ (Excel, Word, PowerPoint), of other program (ImageJ), statistic software (R, GraphPad Prism) and specific programs for molecular biology (Primer-BLAST), database on line (GeneBank, Pubmed).

Involvement in teaching, supervision or mentoring

- 2018/2019: co-supervisor of 2 Master students in Molecular and Health Biology (University of Genoa)
- 2018/2019: co-supervisor of 1 Bachelor student in Environmental and Natural Sciences (University of Genoa)
- 2017/2018: co-supervisor of 1 Bachelor student in Biological Sciences (University of Genoa)

Other activities

Peer reviewer for international journals (Journal of Functional Foods).

Participation to scientific courses and workshop

- Courses and practical for PhD students in DISTAV and seminar during the whole PhD doctoral school registration (2016-2019)
- ISSUGE lessons (2017): The Extraordinary Microscope: multimodal and correlative approaches in nanomedicine, Prof. Alberto Diaspro; Role of polychromatic flow cytometry in clinical and translational medicine, Dott. Daniela Fenoglio; May the Force be with you: exploiting atomic force microscopy to image and probe cells and molecules, Dr. Massimo Vassalli
- Practical workshop on advanced microscopy (3rd NIC@IIT) (Genoa, Italy - 13-16 Dec. 2016)

- Course of Statistic applied to Experimental Research, University of Genoa (November-December 2015)

Scientific production

ORCID: https://orcid.org/0000-0002-6284-436X

Publications

1. **Baldini F**, Grasselli E, Damonte G, Salis A, Serale N, Voci A, Portincasa P, Gena P, Vergani L, Calamita G. Aquaporin-9 is involved in the lipid-lowering activity of the nutraceutical silybin on hepatocytes through modulation of autophagy and lipid droplets composition. Biochim Biophys Acta Mol Cell Biol Lipids 2020 Mar;1865(3):158586. doi: 10.1016/j.bbalip.2019.158586. Epub 2019 Dec 6.
2. Grasselli E, **Baldini F**, Vecchione G, Oliveira PJ, Sardão VA, Voci A, Portincasa P, Vergani L. Excess fructose and fatty acids trigger a model of non-alcoholic fatty liver disease progression in vitro: Protective effect of the flavonoid silybin. Int J Mol Med. 2019 Aug;44(2):705-712. doi: 10.3892/ijmm.2019.4234. Epub 2019 Jun 6.
3. **Baldini F**, Bartolozzi A, Ardito M, Voci A, Portincasa P, Vassalli M, Vergani L. Biomechanics of cultured hepatic cells during different steatogenic hits. J Mech Behav Biomed Mater. 2019 Sep;97:296-305. doi: 10.1016/j.jmbbm.2019.05.036. Epub 2019 May 22.
4. Khalil M, Khalifeh H, **Baldini F**, Salis A, Damonte G, Daher A, Voci A, Vergani L. Antisteatotic and antioxidant activities of *Thymbra spicata* L. extracts in hepatic and endothelial cells as in vitro models of non-alcoholic fatty liver disease. J Ethnopharmacol. 2019 Jul 15;239:111919. doi: 10.1016/j.jep.2019.111919. Epub 2019 Apr 25.
5. Amaroli A, Ravera S, **Baldini F**, Benedicenti S, Panfoli I, Vergani L. Photobiomodulation with 808-nm diode laser light promotes wound healing of human endothelial cells through increased reactive oxygen species production stimulating mitochondrial oxidative phosphorylation. Lasers Med Sci. 2019 Apr;34(3):495-504. doi: 10.1007/s10103-018-2623-5. Epub 2018 Aug 25.
6. Vecchione G, Grasselli E, Cioffi F, **Baldini F**, Oliveira PJ, Sardão VA, Cortese K, Lanni A, Voci A, Portincasa P, Vergani L. The Nutraceutic Silybin Counteracts Excess Lipid Accumulation and Ongoing Oxidative Stress in an In Vitro Model of Non-Alcoholic Fatty Liver Disease

Progression. Front Nutr. 2017 Sep 19;4:42. doi: 10.3389/fnut.2017.00042. eCollection 2017.

7. Vergani L, Vecchione G, **Baldini F**, Grasselli E, Voci A, Portincasa P, Ferrari PF, Aliakbarian B, Casazza AA, Perego P. Polyphenolic extract attenuates fatty acid-induced steatosis and oxidative stress in hepatic and endothelial cells. Eur J Nutr. 2018 Aug;57(5):1793-1805. doi: 10.1007/s00394-017-1464-5. Epub 2017 May 19.
8. Vecchione G, Grasselli E, Voci A, **Baldini F**, Grattagliano I, Wang DQ, Portincasa P, Vergani L. Silybin counteracts lipid excess and oxidative stress in cultured steatotic hepatic cells. World J Gastroenterol. 2016 Jul 14;22(26):6016-26. doi: 10.3748/wjg.v22.i26.6016.
9. Khalil M, Khalifeh H, **Baldini F**, Serale N, Parodi A, Voci A, Vergani L, Daher A. Antitumor activity of ethanolic extract from Thymbra spicata L. aerial parts: effects on cell viability and proliferation, apoptosis induction, STAT3 and NFkB signaling. Journal of Functional Foods. ***Under review***
10. Vergani L, **Baldini F**, Khalil M, Ardito M, Molina-Molina E, Portincasa P. Effects of deoxycholic acid and ursodeoxycholic acid on fatty-acid induced hepatic steatosis and oxidative stress. Elsevier Editorial System(tm) for Arab Journal of Gastroenterology. ***Under review***

Oral presentation

1. 53rd Annual Scientific Meeting of the European Society for Clinical Investigation (ESCI). Coimbra (Portugal), 22-24 May 2019. Steatosis in hepatocytes impairs endothelial cell function by promoting lipid accumulation and oxidative stress in a manner depending on the grade of hepatic steatosis. **Baldini F**, Khalil M, Fabbri R, Serale N, Voci A, Portincasa P, Vergani L.
2. 52nd Annual Scientific Meeting of the European Society for Clinical Investigation (ESCI). Barcelona (Spain), 30 May-1 June 2018. Extent of lipid accumulation affects biochemical, mechanical, and functional parameters of cultured hepatic cells. **Baldini F**, Bartolozzi A, Vassalli M, Khalil M, Grasselli E, Voci A, Portincasa P, Vergani L.
3. 68th Italian Physiological Society National Congress (SIF). Pavia (Italy), 6-8 September 2017. The nutraceutic silybn counteracts the excess lipid accumulation in a cellular model of NAFLD progression by affecting lipolytic pathways. **Baldini F**, Grasselli E, Demori I, Voci A, Vecchione G, Khalil M, Cortese K, Portincasa P, Gena P, Calamita G, Vergani L.

Poster presentation

4. *Joint Meeting of the Federation European Physiological Societies and the Italian Physiological Society-FEPS-SIF*. Bologna (Italy), 10-13 September 2019. Lipid accumulation in hepatocytes impairs endothelial cell function in a manner dependent on the grade of hepatic steatosis. **Baldini F**, Khalil M, Fabbri R, Serale N, Voci A, Portincasa P, Vergani L.
5. *Joint Meeting of the Federation European Physiological Societies and the Italian Physiological Society-FEPS-SIF*. Bologna (Italy), 10-13 September 2019. Aquaporin-9 (AQP9) is involved in the lipid-lowering activity of the nutraceutical silybin on hepatocytes through modulation of autophagy. Vergani L, **Baldini F**, Grasselli E, Voci A, Khalil M, Portincasa P, Gena P. Calamita G.
6. *Joint Meeting of the Federation European Physiological Societies and the Italian Physiological Society-FEPS-SIF.* Bologna (Italy), 10-13 September 2019. Investigation of the possible antiproliferative and hepatoprotective effects of an alcoholic extract from *Thymbra spicata* (Lamiaceae) aerial parts. Khalil M, Khalifeh H, **Baldini F**, Daher A, Voci A, Vergani L.
7. *12th World Congress on Polyphenols Applications*. Bonn (Germany), 25-28 September 2018. Polyphenolic extracts of T. spicata play antitumor, antioxidant and antisteatotic activity in dfferent tumoral cell lines. Khalil M, **Baldini F**, Voci A, Mariotti M, Khalifeh H, Daher A, Vergani L.
8. *69th Italian Physiological Society National Congress (SIF).* Firenze (Italy), 19-21 September 2018. Accumulation of lipid droplets in multiple steatogenic models of cultured hepatocytes affects cell stiffness in the single cell biomechanic model. **Baldini F**, Bartolozzi A, Vassalli M, Khalil M, Voci A, Portincasa P, Vergani L.
9. *3rd Nanoengineering for mechanobiology symposium*. Camogli (Italy), 25-28 March 2018. A robust approach from nano indentation experiments. Bartolozzi A, **Baldini F**, Barbieri M, Vergani L, Vassalli M.
10. *51st Annual Scientific Meeting of the European Society for Clinical Investigation (ESCI).* Genova (Italy), 17-19 May 2017. Dietary plant polyphenols tune down hepatosteatosis and atherosclerosis in cellular models of disease. **Baldini F**, Vecchione G, Grasselli E, Voci A, Portincasa P, Ferrari PF, Aliakbarian B, Casazza AA, Perego P, Vergani L.

11. *51st Annual Scientific Meeting of the European Society for Clinical Investigation (ESCI).* Genova (Italy), 17-19 May 2017. In vitro models of fatty liver for the study of lipid homeostasis in health and disease. Voci A, Grasselli E, Vecchione G, **Baldini F**, Demori I, Portincasa P, Vergani L.
12. *51st Annual Scientific Meeting of the European Society for Clinical Investigation (ESCI)*. Genova (Italy), 17-19 May 2017. Silybin-vitamin E phytosome complex counteracts lipid excess and oxidative stress in an in vitro model of non-alcoholic steatohepatitis (NASH). Vecchione G, Grasselli E, Oliveira PJ, Sardao VA, Cioffi F, **Baldini F**, Cortese K, Voci A, Portincasa P, Vergani L.
13. *51st Annual Scientific Meeting of the European Society for Clinical Investigation (ESCI).* Genova (Italy), 17-19 May 2017. Combined actions of fructose and fatty acids induce steatohepatitis in vitro. Grasselli E, Demori I, Vecchione G, Oliveira PJ, Sardão VA, **Baldini F**, Voci A, Portincasa P, Vergani L.
14. *67° Italian Physiological Society National Congress (SIF).* Catania (Italy), 20-22 September 2016. Hepatic lipid homeostasis in health and disease: in vitro and in vivo models of fatty liver. Vecchione G, Grasselli E, Demori I**, Baldini F**, Voci A, Cortese K, Portincasa P, Vergani L
15. *5th International Conference on Industrial Biotechnology, The Italian Association of Chemical Engineering (AIDIC).* Bologna (Italy), 10-13 April 2016. Antioxidant and hepatoprotective potential of phenolic compounds from olive pomace. Vergani L, Vecchione G, **Baldini F**, Voci A, Ferrari PF, Aliakbarian B, Casazza AA, Perego P.
16. *66° Italian Physiological Society National Congress (SIF).* Genova (Italy), 16-18 September 2015. Induction of oxidative stress and inflammation in human vascular endothelial cells by fine quartz particles. Ragazzoni M, **Baldini F**, Grasselli E, Gallo G, Scarfì S, Giovine M, Voci A, Vergani L.

16.Ringraziamenti

Chi mi conosce bene sa quanto io sia negata nell'imprimere su carta emozioni: non sono mai stata brava ad esprimere a parole tutto quello che sento dentro, ma oggi desidero provarci con tutte le mie forze per dire grazie a tutte le persone che costellano la mia vita e che mi hanno dato forza lungo questo percorso.

Eccomi giunta alla fine di questa tesi e di questi splendidi tre anni di Dottorato nei quali credo di essere maturata sia lavorativamente sia, soprattutto, come persona. Sono tante le conoscenze che ho fatto durante questi anni, i rapporti che ho stretto e le persone che desidero ringraziare profondamente e senza le quali non sarei qui oggi.

Dopo tre anni di tirocinio e altrettanti di Dottorato, il laboratorio di Fisiologia è stato ben più che un semplice luogo di lavoro. Vorrei iniziare ringraziando la Prof.ssa Vergani e la Prof.ssa Voci, relatrici di questa tesi di Dottorato, oltre che per l'aiuto fornitomi in tutti questi anni e la grande conoscenza che mi hanno donato, per la disponibilità e la gentilezza sempre dimostratemi: senza di loro questo lavoro non avrebbe preso vita e non avrei avuto la possibilità di inseguire i miei sogni.

Un grazie di cuore a Rita e Michele per il loro sostegno, la loro amicizia e per avermi sempre aiutata nei momenti di bisogno.

Un ringraziamento sincero va alla Boss Balbi: grazie per tutte le risate, le defibrillazioni, l'aiuto costante, i tuoi ingressi a passo di moonwalk che mi hanno strappato un sorriso anche nelle giornate più storte! Sei sempre stata una fonte di ispirazione che mi ha dato il coraggio di credere nel percorso che ho intrapreso.

Grazie a Khalil, il miglior compagno di percorso, collega ed amico che potessi desiderare: grazie per le risate, per tutto l'aiuto e per i caffè condivisi durante questi anni!

A Manon, compagna di avventure ed amica sempre presente nei momenti di bisogno, posso solo dire *merci beaucoup*! Grazie per tutte le risate, il sostegno reciproco nei momenti di difficoltà e per aver condiviso tantissime avventure che mi hanno aiutata a crescere come persona.

Un ringraziamento che viene dal cuore va ai ragazzi del laboratorio di Microbiologia. Grazie a

Giovanni per tutte le volte che ha saputo ascoltarmi e strapparmi un sorriso nei momenti difficili e per esserci sempre stato ogni qualvolta ne avessi bisogno. Grazie ad Alessio per la gentilezza e l'altruismo che mi ha sempre dimostrato e per aver sempre trovato una parola di conforto nelle giornate storte. *Muchas gracias* Aide per tutte le risate, le chiacchiere e le birrrrre condivise.

A Peter, una delle persone più dolci che io conosca, che mi ha insegnato quanto possa essere grande un cuore, posso solo dire grazie *biscuit*!

Non posso non spendere alcune righe per ringraziare le ragazze con cui ho condiviso questo percorso: Nadia, Chiara, Angelica e Martina, non solo colleghe fantastiche e piene di passione ma soprattutto amiche speciali, al mio fianco durante questi anni e senza il cui aiuto (e la cui pazienza!) non sarei certamente arrivata fin qui oggi.

Un pensiero alla fine di questo percorso va certamente a Giulia e Matteo, compagni di vita universitaria, membri dello SMAD group e amici insostituibili. Grazie per esserci sempre stati fin dal primo giorno di Università, nei momenti belli e anche in quelli un po' più difficili.

Vorrei ringraziare dal profondo del cuore la mia famiglia per essermi sempre stata accanto ed avermi amata incondizionatamente. Un grazie speciale lo voglio dedicare a mio padre, Alessandro, per la sua incapacità di lamentarsi (che vorrei aver ereditato un po' di più), il suo inguaribile ottimismo e la sua energia positiva, che mi hanno dato forza anche nei momenti più impervi di questo percorso. Grazie a mia madre, Annalisa, che mi ha trasmesso la forza, il coraggio e l'indipendenza di cui vado fiera e perché, anche se ogni tanto ti faccio arrabbiare, mi perdoni sempre. Grazie ad entrambi per avermi insegnato la contagiosità di un sorriso, l'importanza dell'umiltà e per aver creduto in me anche quando io stessa non ci riuscivo. Grazie perché siete, per me, i genitori migliori del mondo. A mia cugina Giada, una delle persone più belle, pure ed altruiste che io conosca; con la rara capacità di emozionarsi e partecipare con trasporto ai traguardi altrui, come fossero propri. Grazie di esserci sempre. A tutti e quattro i miei nonni che, anche se non ci sono più, hanno sempre fatto il tifo per me e mi hanno amata al di sopra di ogni cosa. Sono stata la nipote più fortunata del mondo.

Ultimo ma non certo per importanza. Con tutto l'amore di cui sono capace, voglio ringraziare Alberto, per così tanti motivi che mi è impossibile ricordarli ed elencarli tutti. Grazie per tutte le quotidiane dimostrazioni di amore: per il bucato pulito, la pasta al forno rincasando la sera, gli

abbracci a fine giornata e per aver reso Casa ogni luogo in cui ci trovassimo. Grazie per esserci sempre, in prima linea, all'apice della gioia e, soprattutto, nei momenti più difficili; per le risate più vere, l'amore più profondo e per aver creduto in noi anche quando io non l'ho reso per nulla facile. Per avermi sempre sostenuta in tutte le mie scelte, accettando tutti i miei lati, anche quelli un po' più spigolosi, senza mai chiedere niente in cambio. Grazie.